ABSTRACT

THE ROLE OF SDF-1α AS A VASCULOGENIC CHEMOKINE AND ENDOTHELIUM-ASSOCIATED CELL ADHESION MOLECULE FOR THE RECRUITMENT OF BONE MARROW-DERIVED PROGENITOR CELLS TO DEVELOPING TUMORS

By Molishree Umesh Joshi

June 2010

Director: Dr. Kathryn M. Verbanac

DEPARTMENT OF SURGERY, Interdisciplinary Program in Biological Sciences

Tumor vascularization is an important control point in cancer progression and its inhibition is a promising approach to cancer therapy. Stromal-derived factor-1α (SDF-1α or CXCL12) is a chemoattractant for lymphocytes, hematopoietic progenitor cells, and vascular endothelial cells. SDF-1α binds to the CXCR4 receptor on cell surfaces and to heparan sulfate in cell membranes and the extracellular matrix. We hypothesized that SDF-1α is an important mediator of tumor vasculogenesis, recruiting bone marrow-derived endothelial progenitor cells to tumors. We evaluated the role of SDF-1α in the adhesion of bone marrow-derived lineage-negative cells (Lin^- BMC) to the murine Lewis lung adenocarcinoma (LLCaB subclone), both *in vitro* and *in vivo*. LLCaB lung and liver metastases expressed significantly elevated levels of SDF-1α compared to normal tissue from naïve controls and primary tumors. SDF-1α expression inversely correlated with tumor size, implicating involvement in early tumor development. SDF-1α was detected on ~30% of blood vessels in primary and metastatic tumors by double immunocytochemistry staining and on endothelial cells within primary cultures of dissociated LLCaB tumors (DTC). Lin^- BMC enriched for $Sca1^+cKit^+$ (LSK) cells, including endothelial progenitors and $CXCR4^+$ cells, were used for subsequent adhesion studies. LSK cells

preferentially adhered *in vitro* to DTC, compared to other target cell types. Pre-incubation with anti-CXCR4 antibody or the CXCR4 antagonist AMD3100 decreased adhesion of LSK cells by 50%. Biolocalization of adoptively-transferred *EGFP*-Lin^- BMC in tumor-bearing wild-type mice was evaluated by qPCR for the *egfp*-transgene. A significantly greater number of Lin^- BMC localized to metastases 2-3 days after intravenous injection than to adjacent healthy tissue, normal organs, or primary tumors. Control $CXCR4^-$ *EGFP*-dermal fibroblasts showed significantly less tumor localization. One-week post-injection, Lin^- BMC were still detected in every metastasis, suggesting that BMC were retained and/or had replicated. These data support the hypothesis that the biolocalization of circulating Lin^- BMC to tumors is SDF-1α-mediated. We have also put forth the novel proposal that SDF-1α promotes early tumor vasculogenesis as a tumor endothelium-associated adhesion molecule for circulating $CXCR4^+$ Lin^- BMC. These findings may aid our understanding of the mechanism of tumor vascularization and the design of tumor-targeted therapy.

THE ROLE OF SDF-1α AS A VASCULOGENIC CHEMOKINE AND ENDOTHELIUM-ASSOCIATED CELL ADHESION MOLECULE FOR THE RECRUITMENT OF BONE MARROW-DERIVED PROGENITOR CELLS TO DEVELOPING TUMORS

A Dissertation

Presented To

The Faculty of the Department of

Interdisciplinary PhD Program in Biological Sciences

East Carolina University

In Partial Fulfillment

Of the Requirements for the Degree

Doctor of Philosophy in Biological Sciences

By

Molishree Umesh Joshi

June 2010

THE ROLE OF SDF-1α AS A VASCULOGENIC CHEMOKINE AND ENDOTHELIUM-ASSOCIATED CELL ADHESION MOLECULE FOR THE RECRUITMENT OF BONE MARROW-DERIVED PROGENITOR CELLS TO DEVELOPING TUMORS

By

Molishree Umesh Joshi

APPROVED BY:
DIRECTOR OF DISSERTATION: _____
Kathryn M. Verbanac, Ph.D.

COMMITTEE MEMBER: _____
Shaw M. Akula, Ph.D.

COMMITTEE MEMBER: _____
Timothy Gavin, PhD.

COMMITTEE MEMBER: _____
Alexander Murashov, Ph.D.

COMMITTEE MEMBER: _____
Roberta Johnke-Tracy, Ph.D.

INTERIM PROGRAM DIRECTOR DONALD R. HOFFMAN:

_____
Donald R. Hoffman, Ph.D.

DEAN OF THE GRADUATE SCHOOL:

_____
Paul J. Gemperline, Ph.D.

ACKNOWLEDGEMENT

I would like to take this opportunity to thank the many people who have generously provided guidance and support throughout my time at East Carolina University, made these years intellectually stimulating, and full of fond memories. I wish to thank my thesis advisor and mentor Dr. Kathryn M. Verbanac for allowing me to perform this research in her laboratory, and for her patience and guidance. She has motivated me to be critical thinker, writer, and orator, and to passionately pursue the field of bio-medical sciences. I owe my deepest gratitude to my committee members: Dr. Akula, Dr. Gavin, Dr. Murashov, and Dr. Johnke-Tracy, for their encouragement, critique, and valuable suggestions. I would like to express my deepest appreciation to Dr. Carl Haisch for his advice and support. I am also grateful to Keith Pittman for being an amazing teacher, supporter, and friend. I would like to thank Jianfen Lu, Ann Mannie, Jered Meyers, Dare Imes, and other members of Verbanac research group for their enormous assistance, companionship and for making Greenville my home away from home. I am thankful to my fellow graduate students for their friendship, and the many faculty and staff members from every Department at Brody School of Medicine. I am grateful to the Interdisciplinary PhD Program in Biological Science and Department of Surgery for providing financial and administrative support that has made this research possible.

I am thankful to my family for their encouragement and for making life fun and adventurous. I dedicate this dissertation research to my parents: To my father Dr. Umesh Chandra Joshi for instilling in me the never-ending curiosity and love for science and to my mother Deepa Joshi for her undying love and support.

TABLE OF CONTENTS

APPENDIX

LIST OF TABLES

LIST OF FIGURES

LIST OF ABBREVIATIONS

aFGF	Acidic Fibroblast Growth Factor
ANG-1/2	Angiopoietins
bFGF	Basic Fibroblast Growth Factor
BM	Bone Marrow
BMC	Bone Marrow Cells
bEnd.3	Brain Endothelioma Cell Line
CEC	Circulating Endothelial Cells
CEP	Circulating Endothelial Progenitors
CD	Cluster of Differentiation
cDNA	Complementary Deoxyneucleic Acid
CXCR	CXC Chemokine Receptor
cKit	Cytokine Receptor
DNA	Deoxyneucleic Acid
DTC	Dissociated Tumor Cells
EC	Endothelial Cells
eNOS	Endothelial Nitric Oxide Synthatase
EPC	Endothelial Progenitor Cells
Eph	Ephrin Receptor
EGFP	Enhanced Green Fluorescent Protein
ELISA	Enzyme Linked ImmunoSorbent Assay
ECM	Extracellular Matrix
FGF	Fibroblast Growth Factor
GAG	Glycoamine Glycans
HSC	Hematopoietic Stem Cells
Actb*EGFP*	Hemizygous Enhanced Green Fluorescent Protein Transgene under Chicken Beta Actin Promoter
HS	Heparane Sulphate
HGF	Hepatocyte Growth Factor
Actb^{+}*EGFP*	Homozygous Enhanced Green Fluorescent Protein Transgene under Chicken Beta Actin Promoter
Ubq*EGFP*	Homozygous Enhanced Green Fluorescent Protein Transgene under Ubiquitin Promoter
HUVEC	Human Vascular Endothelial Cell Line
HIF	Hypoxia Induced Factor
ICAM	Inter-Cellular Adhesion Molecule
Id-1	Inhibitor of differentiation
IL	Interleukin
LLCaB	Lewis Lung Adenocarcinoma Cell Line
Lin^{-} BMC	Lineage-negative Bone Marrow Cells
LSK	Lin^{-} Sca1^{+}cKit^{+} Bone Marrow Cells
LPS	Lipopolysaccaride
MMP	Matrix Metalloproteinase
PB	Peripheral Blood

PMNC	Peripheral Mononuclear Cells
PlGF	Platelet Growth Factor
3T3-L1	Pre-Adipocyte Cell Line
PH	Propyl Hydroxylase
PSGL-1	P-selectin Glycoprotein Ligand
qPCR	Quantitative Polymerase Chain Reaction
RTK	Receptor Tyrosine Kinase
RT-PCR	Reverse Transcriptase Polymerase Chain Reaction
RNA	Ribonucleic Acid
Sca1	Stem Cell Antigen
SDF-1	Stromal Derived Factor
TEC	Tumor Endothelial Cell
TGF-β	Tumor Growth Factor-beta
TNF-α	Tumor Necrosis Factor-alpha
VEC	Vascular Endothelial Cells
VCAM	Vascular Cell Adhesion Molecule
VEGF	Vascular Endothelial Growth Factor
VEGFR	Vascular Endothelial Growth Factor Receptor
vWF	Von Willebrand Factor

CHAPTER I: INTRODUCTION

Cancer is a disease in which cells undergo *uncontrolled proliferation*, leading to *invasion* into adjacent tissues and *metastasis* to other organs in the body via the circulatory system (1-3;3). In the 1970's Dr. Judah Folkman pioneered the idea that angiogenesis was an important point in the control of cancer progression and that its inhibition would be a valuable new approach in cancer therapy (4;5). This is now a widely accepted theory and there has been considerable focus on designing therapies that could potentially target developing blood vessels. Despite significant advances in cancer research, the mechanism by which tumor cells metastasize and acquire angiogenic phenotypes is not fully understood. Although there has been substantial progress in the field of cancer treatment and improvement in survival and quality of life for some patients, cancer can remain a devastating diagnosis. Hence, it is important to enhance our understanding about the important mediators involved in the process of tumor vascularization and growth that may aid in the design of superior therapy.

General Properties of Tumors

All cancers arise gradually as the cells are unable to correct mutations that arise. These errors could be due to several factors including, but not limited to, exposure to chemical carcinogens, ionizing radiation, viral or bacterial infection, genetic mutations, hormonal imbalance, immune-system dysfunction, and/or hereditary factors. Such factors could lead to mutations in tumor suppressor genes, proto-oncogenes and DNA repair genes and cause the cells to undergo uncontrolled cell division and lose their capacity for apoptosis and senescence. Tumorous cell clusters rely on the diffusion of oxygen and other essential nutrients for growth; this process is inadequate once tumors become 1-2 mm^2 in size (4;5). The growth of these

micro-tumors is restored if they undergo angiogenesis i.e. *formation of new vasculature*. Thus, tumor vascularization constitutes an important control point in cancer progression and its inhibition has been suggested to be a valuable approach to cancer therapy.

Many groups have reported that tumor blood vessels are morphologically and physiologically heterogeneous; with abnormal arterio-venous architecture, irregular diameter and aberrant branching (6;7). Tumor blood vessels are devoid of a complete basement membrane, smooth muscle cells, and pericytes, and are leaky. This abnormal vascular architecture is thought to be responsible for the high intra-tumor pressure, erratic blood shunting, and hypoxia present in tumors (7). Several hypoxia-induced genes and proteins that are expressed or upregulated in tumors have also been identified.

Most tumors are hypoxic in nature (7-9). Tumors rapidly outgrow their blood supply, creating regions where the oxygen concentration is significantly lower than in healthy tissues. Hypoxia is likely a result of the uncontrolled cell proliferation, creating a higher cell density, and thus taxing the local oxygen supply. Hypoxic zones within tumors are usually resistant to radiotherapy and chemotherapy and can ultimately contribute to recurrence (7;9). Hypoxia and hypoxia-regulating proteins have been demonstrated to be associated with a worse prognosis (10-12), making it a determining factor of cancer progression and therapeutic response (7;9;13;14) .

Hypoxia-induced factor (HIF) is a dimer of α and β subunits, each of which has three isoforms. HIF-1 is the best studied among these. In normoxic conditions the enzyme prolyl-hydroxylase (PH) is active and causes hydroxylation of HIF-1α. A component of E3 ubiquitin ligase complex binds the hydroxylated HIF-1α and earmarks it for degradation. In contrast, under hypoxic conditions PH is inactive, which leads to the accumulation of HIF-1α. This leads to the

dimerization of HIF-1β with HIF-1α and the active dimer binds to the hypoxia-response element (DNA binding site) resulting in the transcription and synthesis of downstream proteins (7).

HIF-1 is reported to be over expressed in numerous human tumors (7;15) and is recognized as an important regulator of tumor proliferation. Its expression influences several downstream signaling pathways that affect cell proliferation, survival and migration, matrix physiology, and angiogenesis. Vascular endothelial growth factor (VEGF), stromal-derived factor (SDF-1), matrix metalloproteinase (MMP), insulin growth factor (IGF-2), and tumor growth factor (TGF) are among the well-studied target genes of HIF-1 and influence angiogenesis, anaerobic metabolism, vasodilatation, respiration, erythropoesis and apoptosis. These events ultimately lead to malignant progression and increased tumor aggressiveness (Review in (7).

Hypoxia is the most potent stimulator of VEGF, which is a well studied growth factor in tumor biology (8). VEGF is an important regulator of blood vessel growth and permeability, and is upregulated in many human and experimental tumors. Many anti-VEGF and anti-VEGF receptor (VEGFR) monoclonal antibodies and small-molecule inhibitors are in clinical development for use as cancer therapeutic agents (16). VEGF in turn induces the expression of SDF-1α (14;17); SDF-1α and its receptor CXCR4, have been implicated in tumor angiogenesis and organ-specific metastasis. Low oxygen tension also regulates angiopoietins (ANG-1 and ANG-2) and their receptor (Tie-2), which have wide-ranging effects on tumor angiogenesis, inflammation, and vascular extravasation of cells. Although the role of angiopoietins in tumor angiogenesis is controversial, ANG-2 is reported to be pro-angiogenic and ANG-1 is thought to be a stabilizing factor for tumor vasculature (18;19). ANG-1 has also been demonstrated to bind integrins, which are strongly implicated in cancer progression. Integrin α5β1 is expressed mainly

on vascular endothelial cells and is upregulated along with fibronectin in tumor neovasculature. Integrins αvβ3 and αvβ5 are involved in angiogenesis, and are expressed in malignancies such as melanomas, gliomas, and breast, prostate, and colon cancers (16). VEGF and hypoxia also directly influence the expression of integrins on endothelial cells (20). The expression of certain ephrins by endothelial cells is also influenced by hypoxia (21-23). It has been shown that HIF-2α plays an important role in vascular remodeling during tumor vascularization through activation of ephrin A1 on endothelial cells (21). The receptors for ephrins (Eph receptors) have been correlated with the growth of solid tumors. Eph receptors have been shown to be overexpressed in a wide range of cancers including melanoma, breast, prostate, pancreatic, gastric, and esophageal and colon cancer as well as hematopoietic tumors (24). E-selectin (25) and its carbohydrate ligands (Sialyl Lewis-a, and Sialyl Lewis-x) have also been shown to be induced by hypoxia. Expression of Sialyl Lewis-a/x is reported to be elevated during hypoxia-induced cancer progression in locally advanced cancers (26;27). Thus, hypoxia contributes significantly to the invasive, metastatic and angiogenic phenotypes of aggressive cancers.

Tumor Vascularization

It is generally accepted that there are two main processes by which new blood vessels are created in tumors: 1) angiogenesis and 2) vasculogenesis. Several researchers are of the opinion that the two processes occur either concomitantly or sequentially (28;29). Vascular co-option and vasculogenic mimicry have also been suggested to give rise to tumor vasculature (30).

Tumor Angiogenesis

Angiogenesis is defined as the physiological process involving the formation of new blood vessels from pre-existing vessels (19;31-33). It is a normal process in embryonic growth

and development, wound healing, and the menstrual cycle. As aforementioned, it is now well-established that tumors require angiogenesis to grow and metastasize to secondary sites in the body (5). The basic process involved in angiogenesis is proliferation of existing, activated vascular endothelial cells (VEC) culminating in the formation of tube-like structures for blood flow.

Tumors secrete angiogenic factors that activate VEC in the blood vessels in adjacent tissue. The activated VEC proliferate and release proteases and other enzymes, which modify the basement membrane and extracellular matrix (ECM). Integrins on the surface of VEC interact with their respective ligands in the ECM, which leads to their assisted and directional migration towards the tumor-derived chemotactic signal. Additional enzymes, such as matrix metalloproteinase, remodel the surrounding ECM for the "sprouting" vessel. The developing blood vessels roll up to form tube-like structures and finally the individual conduits connect to form blood vessel loops. These blood vessels are stabilized by smooth muscle cells (SMC) or pericytes, and the blood flow begins (34).

Many proteins like acidic and basic fibroblast growth factors (aFGF, bFGF), transforming growth factor (TGF-β), hepatocyte growth factor (HGF), VEGF, angiogenin, angiopoietins, interleukin-8 (IL-8), SDF-1α, integrins, selectins, and ephrins have been implicated as positive regulators of angiogenesis in tumors (35-37). These proteins are produced by various cell types including fibroblasts, endothelial cells, tumor cells, and immune cells in the microenvironment, and cause proliferation and recruitment of VEC from adjacent blood vessels towards neo-vasculature in tumors (38).

The major signaling pathway in tumor angiogenesis is thought to involve VEGF and its receptors. Suppression of tumor growth and angiogenesis have been demonstrated clinically by

blocking VEGF and VEGFR2 in approaches including an anti-VEGF antibody (Avastin®), VEGFR2 mutant, anti-VEGFR2 antibodies, small molecule inhibitors of VEGF receptor tyrosine kinase (RTK), and soluble VEGF receptors (39-41).

The CXC chemokine family consists of ligands and receptors that interact to produce pro-angiogenic and angiostatic effects (42). Activation of the chemokine receptor CXCR2 by pro-angiogenic ligands or triggering of CXCR4 by ligand CXCL12/SDF-1 has been reported to promote angiogenesis. Blocking the function of CXCR2 by specific antibodies has been shown to inhibit pancreatic cancer cell-induced angiogenesis (43). In contrast, engagement of CXCR3 by angiostatic chemokines has been demonstrated to inhibit vascularization.

Inhibitor of differentiation-1 (Id-1) gene has been demonstrated to confer angiogenic property like migration and capillary-like tube/cord formation on fully differentiated human umbilical vein endothelial cells (HUVEC). In the in vivo experiments in ischemic limb injury model, Id1-overexpressing HUVEC increased capillary density and improved limb salvage compared to control HUVEC. Thus Id-1 has been shown to contribute to therapeutic angiogenesis (44). Id-1 has also been reported to regulate angiogenesis through the transcriptional repression of thrombospondin-1, a potent inhibitor of angiogenesis (45).

Several investigators have demonstrated that sprouting angiogenesis in tumors could also be negatively regulated to restrict tumor growth by using naturally occurring angiostatic agents like thrombospondin-1, prolactin, platelet factor-4, interferon-α, interferon-γ inducible protein-10, angiostatin, endostatin, tumstatin, etc. Although the receptors for several of these angiostatic proteins have been indentified, their mode of action is not clearly understood (Reviewed in (45-47). Sprouting angiogenesis in tumors remains an attractive point of control in tumor progression.

Tumor Vasculogenesis

Vasculogenesis is defined as the process by which the primary vascular network (primitive plexus) is created by hematopoietic stem cells (HSC) and endothelial progenitor cells (EPC) in the developing embryo. The process is initiated by the formation of blood islands containing precursors called hemangioblasts. The fusion of these blood islands forms the primary capillary plexus and their elongation leads to generation of blood vessels. The role of post-natal vasculogenesis has been recently recognized and is a topic of much debate.

Asahara's group was the first to isolate endothelial progenitor cells (EPC) from bone marrow (BM) and demonstrate the mobilization and contribution of EPC to neo-vascularization in an ischemic injury model (48;49). This initiated the exploration of the involvement of BM-derived EPC in tumor vascularization via post-natal vasculogenesis. When this project was started in 2006, there were 3 out of a total of 9 reports that demonstrated the incorporation of BM-EPC in developing vasculature. Tumor-localization of EPC was shown to be mediated by VEGFR-1/2 and Selectins (50-52). Since then many investigators have implicated the importance of hypoxia-induced proteins in localization of BMC to tumors (Table 1). There are conflicting reports about the contribution of BM-derived EPC to tumor vascularization: only 12/28 (43%) reports have demonstrated BMC-mediated vasculogenesis, (Table 1). In addition, the mechanism by which BM-derived cells might be mobilized from bone marrow, recruited, and retained in tumors is not clearly understood. Recently Nolan *et al.* demonstrated that BM-derived cells contributed to tumor vascularization in early tumors, but as tumors progressed these cells were gradually replaced by tissue-derived EC (53). Other reports indicate that the BM-derived EPC acted as the angiogenic switch and were responsible for the advancement of micro-metastases (28;54). Nevertheless, several other reports have indicated that although bone

Table 1: Literature Summary of the Contribution of Bone marrow-derived Endothelial Progenitor Cells in Tumor Vasculogenesis

YEAR	AUTHOR	REF	TUMOR	RESULTS	BMC in tumors	EPC in tumor BV
2001	Lyden	(50)	B6RV2, LLC	Anti-VEGFR1 and VEGFR2 antibodies ablated tumor growth	+	+
2003	Vajkoczy	(51)	C6	Selectins and PSGL-1-mediated localization of embryonic EPC	+	+
2003	De Palma	(55)	TS/A, N202.1A, B15/BL, LLC/3LL	BM-EPC not detected in tumor vasculature	+	–
2003	Capillo	(56)	Namalwa, Granta 519	EPC were mobilized in tumor bearing mice	?	–
2004	Göthert	(57)	LLC, B6RV2	BMC did not contribute to tumor endothelium	–/+	–
2004	Li	(52)	TMA 1202	BMC-mediated vascularization in poorly differentiated adenocarcinoma	+	+
2005	Bagley	(58)	MDA-MB-231	EPC and pericytes stabilized tumor vasculature but did not initiate vasculogenesis	+	?
2005	Jodele	(59)	SK-N-BE	MMP9-mediated recruitment of BMC to tumors	+	?
2005	Patil	(60)	LLC	LSK localized to tumors did not incorporate into tumor BV	+	–
2006	Santarelli	(61)	RT-2	$GFP^+CD34^+Flk1^+$ cells incorporated into tumor vasculature	+	+
2006	Aghi	(62)	KR158, GL261	SDF-1α-mediated localization of EPC to glioma	+	+
2006	Li	(63)	N202, LLC	α4β1-mediated homing to Lin^- cells to tumor vasculature	+	+
2006	Emerson	(64)	B16F10	VEGF and PlGF mediated vasculogenesis	+	+
2007	Nolan	(53)	B6RV2, LLC, B16F0, PyMT	BM-EPC recruited to the periphery of tumors	+	+
2008	Tabatabai	(65)	SMA-560	Anti-Eselectin antibody the number of LSK cells in tumor decreased by 85%	+	?
2008	Gao	(28)	LLC, PyMT	BM-EPC recruited to micro-metastases and acted as angiogenic switch for tumor progression	+	+
2008	Mahler	(66)	hNB, MPNST	Decrease in BM-EPC in HSV-treated tumors	+	?
2008	Suriano	(67)	TG1-1	BM-EPC detected in tumors in presence of estrogen	+	?
2008	Purhonen	(68)	B16F10	$VEGFR2^+$ cells not mobilized from BM in presence of tumor	+	–
2008	Ahn	(69)	MT1A2, TG1-1, B16F1, LLC	BMC infiltrating tumors were not EPC	+	–
2008	Reddy	(70)	Ewings Sarcoma	SDF-1 stimulated migration of $CD34^+$ to functional vessels	+	–
2008	Du	(71)	Glioblastoma	HIF1 recruited BMC to tumors	+	?
2009	Chan	(72)	HCT1116, SU.86.86, HT29, RKO	PHD2-mediated infiltration of BM-derived $CD11b^+$ and $CD45^+$ cells	+	?
2009	Wickersheim	(73)	LLC, B16, TRAMP C1	BMC recruitment in poorly differentiated tumors	+	+
2009	Folkins	(74)	C6	VEGF and SDF-1 dependent localization of BMC	+	?
2009	Murakami	(75)	3LL	Chemotherapy increased circulating EPC	+	?
2009	Madlambayan	(76)	LLC, B16, Pan-02, EL4	$CD31^+$ BM-derived cells in tumor-associated vasculature	+	+
2010	Kioi	(77)	U251, U87MG	Inhibition of HIF-1 and SDF-1/CXCR4 prevented influx of $CD11b^+$ BMC and post irradiation tumor vascularization	+	+

BMC (Bone Marrow Cells), EPC (Endothelial Progenitor Cells), BV (Blood Vessels); B6RV2 lymphoma , C6 glioma, MCA/120 fibrosarcoma,B16F1 murine melanoma, TS/A mammary carcinoma, N202.1A mammary carcinoma, B15/BL melanoma, LLC/3LL Lewis lung carcinoma, Namalwa, Granta 519, B6RV2 Lymphoma, RT-2 Rat glioblastoma, KR158 astrocytoma, GL261 glioma,N202 breast carcinoma, B16F10 murine melanoma, PyMT spontaneous tumor, SMA-560 glioma, hNB Human neuroblastoma, MPNST Malignant peripheral nerve sheath tumor, TG1-1 mammary tumor, B16F10 murine melanoma, MT1A2 mammary carcinoma, SK-N-BE Human neuroblastoma, TMA 1202 human prostate adenocarcinoma, Pan-O2 pancreatic, EL4 lymphoma, U251 and U87MG glioblastoma; PHD2 prolyl hydroxylases

marrow-derived cells localized to tumors they did not contribute to tumor vasculature (Table 1).

Overall, based on current literature, the detection of EPC in tumor blood vessels ranges from < 1% to ~33% of tumor vasculature (51;61;73;78). This disagreement is thought to be due to the lack of universal consensus for EPC phenotype. Tumor type, and the stage and location of tumor have also been suggested to contribute to this debate (Reviewed in (54;79;80). Nonetheless, several growth factors, chemokines, protein receptors, proteases, and signaling pathways have been demonstrated to be instrumental in mobilizing EPC into circulation and mediated their tumor-localization. In particular, key modulators of angiogenesis such as VEGF/VEGFR, SDF-1/CXCR4, selectin/selectin ligands and hypoxia-regulating proteins have been implicated in tumor vasculogenesis.

Inhibitor of differentiation-1 (Id-1) is thought to be important in modulating the role of EPC in tumor development. Id-1 is reported to be a repressor of thrombospondin, regulator of ECM remodeling, angiogenesis and vasculogenesis (81). It was recently reported that angiogenic defects in Id mutant mice inhibited the growth of tumor xenografts (82). Inducible ribonucleic interference (RNAi)-mediated suppression of Id-1 in BM was reported to reduce the level of circulating EPC ($ckit^{+}VEGFR2^{+}CD11b^{-}$) and impair the formation of pulmonary macro-metastases (28).

Despite the controversy, bone marrow-derived cells and post-natal vasculogenesis appear to be important in certain aspects of tumor growth and progression of the metastatic disease.

Vascular Co-Option

Co-opt vascularization is thought to occur when tumor cells localize to a well-vascularized host organ and progress by co-opting with the host blood vessel. Hence, these tumors develop as blood vessel-dependent tumors as opposed to initiating tumor angiogenesis

(46;83). Vascular co-option was first observed in C6 glioma in rat brains, where small tumors were well vascularized and the vasculature displayed characteristics of normal brain vessels. Vascular co-option has now been reported in several tumor types like murine Lewis lung carcinoma and ovarian cancer, human melanoma and Kaposi Sarcoma (46). The vessel that initially supported tumor growth later regressed in the glioma model. This was thought to be due to VEC apoptosis. Finally, the expression of Angiopoietin-2 and VEGF-mediated angiogenesis at the periphery of tumor mass was demonstrated to rescue tumor growth (46;83). Anti-VEGF therapies, that target developing tumor vasculature, are believed to inhibit maturation of vessels in the process of vessel co-option.

Vascular Mimicry

Vascular mimicry is defined as the formation of fluid-channels lined with tumor cells without the participation of VEC, BMC and independent of vascularization (6;46;84). This is also referred to as 'pseudo-vasculogenesis' (6;46;84). This has been observed in several aggressive tumors like melanoma, ovarian, prostatic and breast carcinomas (6;46;84). Although the detailed mechanism of vascular mimicry is not known, it was suggested that special microenvironments caused tumor cells to dedifferentiate into a pluripotent embryonic phenotype and transdifferentiate into an endothelial cell-like phenotype. These tumor cells have been shown to express endothelial cell markers like CD34, CD105 and VE-Cadherin (85).

Anti-angiogenic Strategies

As discussed earlier, tumor vascularization is a critical point of control in tumor proliferation and numerous clinically translatable anti-angiogenic therapies that target specific steps in tumor vascularization are under investigation. Anti-angiogenic therapies hold great

therapeutic potential for several reasons: 1) easy accessibility, 2) specificity, 3) low toxicity, 4) tumor cells drug resistance surmountability, and 5) applicability to a wide array of tumors (47;86;87).

One possibility for vascular targeting is the use of antibodies and immunotoxins to kill tumor endothelial cells (TEC). Tumor endothelium is more easily accessible to targeting antibodies than tumor antigens, which require antibody extravasation. However, this approach is constrained by the incomplete knowledge of antigens specific to TEC. Nonetheless, several small molecules and monoclonal antibodies that target various steps involved in tumor vascularization. Some of these therapeutic inhibitors include epidermal growth factor inhibitors (Cetuximab, Erlotinib), anti-HER-2 antibody (Herceptin), receptor tyrosine kinase inhibitors (Sunitinib, Sorafenib, Axitinib, Pazopanib, Lapatinib), TNF-α inhibitors (Lenaliomide, Thalidomide) and inhibitors of VEGF/VEGFR (Bevacizumab, Aflibercept, Cediranib, Apatinib), are being currently tested in combination with radiotherapy and/or chemotherapy in Phase III clinical trials for different types of cancers. Tumors can also be targeted by the local or systemic introduction of genetically modified cells that specifically localize to tumors and continually release anti-angiogenic factors. Lal *et al.* were the first to report the implantation and survival of systemically injected endothelial cells (EC) within mouse gliomas in 1994 (31). Later, in a mouse 4T1 mammary tumor model Zweibel *et al.* intravenously administrated EC that were genetically modified for recombinant human IL-2. These EC were reported to incorporate into tumor vasculature and significantly reduced the metastatic burden (88;89). Thus, the use of genetically modified EC was an attractive potential treatment strategy for delivering therapeutic agents to tumors. This approach has not been vigorously pursued in part because of the set backs in clinical gene therapy and limited availability of syngeneic human endothelial cells.

Bone marrow-derived hematopoietic stem cells (HSC) or endothelial precursors / progenitor cells (EPC) may offer an alternate option for tumor targeting using gene therapy (87;90). Wei *et al.* systemically injected embryonic EPC that were transfected with a suicide construct to convert the prodrug 5-fluorocytosine (5-FC) to its active form 5-fluorouracil (5-FU) into mice with tumors. They saw an improvement in survival in the mice that also received 5-FC fusion protein, the substrate for the suicide gene (78). Thus, understanding the mechanism by which EPC localize to tumors and contribute to tumor vascularization could be exploited to 1) control vasculogenesis by arresting tumor growth, and 2) use genetically-modified autologus EPC as a therapeutic Trojan horse(91).

Endothelial Cells

The innermost layer of all blood and lymphatic vessels consists of a single layer of specialized squamous epithelial cells called endothelial cells (EC)(92). They are typically flat, with a cobblestone morphology, and their long axes are oriented parallel to the direction of blood flow. The tight junctions and gap junctions help EC cells form epithelial sheets that restrict the extravasation of fluid, proteins, and cells from vasculature. Yamashita summarized molecular markers that distinguished the murine vascular (i.e. arterial and venous) and lymphatic endothelial cells (93). This group also showed that all EC differentiate from common progenitors. VEGF is thought to guide the differentiation of $VEGFR2^{+}$ progenitors into $CD31^{+}$ VE-$Cadherin^{+}$ endothelial cells. VEGF is also implicated in the maturation of $ephrinB2^{-}EphB4^{+}$ venous EC. On the other hand, Notch signaling in the presence of VEGF, TGF-β, mechano-chemical stimuli like shear stress and high oxygen concentration in arterial blood were reported to be responsible for the differentiation of arterial EC. CXCR4 and ephrinB2 were two of the

markers shown to be expressed by arterial EC. VEGF-C and angiopoietins have been reported to be important for the generation of lymphatic EC ($Prox1^{+}LYVE1^{+}VEGFR3^{+}$) (93).

Vascular Endothelial Cells

Vascular endothelial cells (VEC) line the lumen of all blood vessels in the circulatory system and are quiescent under normal physiological conditions. They function in maintenance of the selective barrier between circulating molecules and tissue, thrombosis, vasodilatation and vasoconstriction, and in inflammation and angiogenesis. This heterogeneity in function is due to the variation in morphology and protein expression in VEC in different organs and vascular beds. Additionally, this disparity is suggested to be due to cellular functions like nutrient uptake, waste removal, blood pressure regulation and neighboring cells arising under physiological and pathological conditions (92). Small molecules, water, and soluble proteins are transported across the endothelium by pinocytosis, while VEC in organs such as kidney and brain have fenestrations to perform functions like filtration and transportation of larger molecules (92). The anti-coagulants and anti-thrombogenic substances, like *von Willebrand* factor (vWF also called coagulating factor VIII), produced by VEC maintain a non-thrombogenic barrier between platelets and sub-endothelial tissue (92). Damage to the endothelium causes the release of pro-thrombic agents that result in platelet aggregation and clot formation. Blood flow in vasculature is modulated by secretion of vasoconstrictors (endothelin, angiotensin, etc.) and vasodilators (nitric oxide, prostacyclin, etc.). Immune responses are controlled by regulating the interaction of lymphocytes with cell adhesion molecules on VEC. Several cytokines, chemokines, interleukins (IL-6, IL-8), and cell adhesion molecules (integrins, ICAM-1, ICAM-2, VCAM, L-selectin, E-selectin, etc) have been established as important immune-modulators. It has also been reported that VEC uptake Ulex europaeus lectin 1(UEA-1) and acetylated low density lipoprotein (Ac-

LDL) (94-96). Finally, when endothelium is damaged in response to tissue injury or during neo-vascularization, as in embryonic development, menstruation, and tumor growth, the activated VEC enable and participate in formation of new blood vessels. Several unique proteins have been shown to be expressed by VEC *in vivo* and in *ex vivo* cultures. Some markers that are routinely used to identify VEC are listed in Table 2 (97).

Circulating Endothelial Cells

Circulating endothelial cells (CEC) were first detected in 1970 in blood smears based on their morphology from patients with vascular injury. On average, 99% of EC are quiescent and very few (~5 cells / mL) are detected in healthy individuals (98-100). Although the mechanism by which VEC detach from blood vessels is poorly understood, it is thought to be mediated by neutrophil attack, cytokines, and proteases activated by vascular injury. Thus, it is generally agreed that the number of CEC is correlated with the degree of endothelial injury (98-100). Cell adhesion proteins such as cadherins, integrins, and their ligands are also thought to be involved in this process. Although there is a lack of consensus on phenotypic identification, CEC are suggested to express vWF, CD146, and VE-Cadherin in the absence of CD45, CD14, and CD133. Similar to vascular endothelial cells, CEC uptake Ulex europaeus lectin 1(UEA-1) and acetylated low-density lipoprotein (Ac-LDL).

Elevated numbers of CEC have been described in patients diagnosed with several different types of cancers. In this scenario it is not clear whether CEC are simply markers of altered vascular integrity or actually contribute to neoplastic progression (Reviewed by (99). In addition to VEC shed from activated tumor vessels, the increase in CEC could also be attributed to bone marrow-derived circulating endothelial progenitors (CEP) differentiating into CEC. It is suggested that CEC can be distinguished from CEP, by the expression CD133 (primitive stem

Table 2: Endothelial Cell Specific Markers

Cell Surface Marker	Cluster of Differentiation (CD)	Cells that Express the Markers
Endoglin	CD105	EC, fibroblasts, and SMC
E-selectin	CD62E	Activated EC
PECAM-1	CD31	EC, and certain tumors
P-selectin	CD62P	EC, platelets
VCAM	CD106	EC
VE-Cadherin	CD144	EC
VEGFR1	-	EC, Hematopoietic cells
VEGFR2	CD309	EC, EPC
vWF	-	EC, megakaryocytes

cell marker) on CEP (101). However, there is a need for further analysis of sorted and functionally tested CEC/CEP to identify specific markers recognizing individual cell types.

Endothelial Progenitor Cells

Endothelial progenitor cells (EPC) are a sub-population of BM-derived cells that have the potential to differentiate into mature EC and contribute to the process of re-endothelialization and neo-vascularization (Figure 1) (48;63;64;83;90;102-110). These cells have generated much interest since they were proposed to have the potential for treating human vascular disease and to be a possible target to restrict tumor vascularization. However, there have been conflicting reports about the accurate identity, characteristics, and function of EPC. The majority of EPC are thought to reside in bone marrow in close association with HSC and BM stromal cells. This association is hypothesized to provide the optimal environment for survival and growth of progenitor cells. Several cell surface proteins on HSC have been identified as putative markers to define progenitor cells that have the capability to differentiate into EC. Some of these proteins have been reported to be expressed by other cell populations (Table 3). The EPC and HSC have been suggested to arise from common precursor as they share common markers like CD34, CD133, and CD117 (Table 4). In addition, defining the identity of EPC is further complicated by the presence of circulating endothelial progenitors and circulating endothelial cells.

Characteristics of Endothelial Progenitor Cells

The putative cell surface markers for EPC from multiple studies are shown in Table 5 (Adapted from (105). Several research groups have analyzed the phenotypic expression of endothelial cell specific markers on viable $CD34^+$ and $CD34^+FGFR^+$ cells collected from BM, umbilical cord blood (UCB), and cytokine mobilized peripheral blood (PB) from human donors.

The $CD34^+$ $FGFR1^+$ cell were reported to co-express the primitive hematopoietic cell antigen, AC133/CD133 (aka Prominin-1 or PROM-1) and like the EC (1) grew slowly in culture, (2) were stimulated by fibroblast growth factor-2 (FGF-2) and VEGF, (3) gave rise to cells that express von Willebrand factor (vWF) and VE-Cadherin and (4) incorporated acetylated low-density lipoprotein (Ac-LDL). This cell population was also reported to express EC-specific proteins like CD34, FGFR, CD38, VE-Cadherin, ckit, CD31, VEGFR2, and CD133. Thus, it was concluded that the $CD34^+FGFR^+$ population contained ECP (111). Human $CD34^+$ cells from different hematopoietic sources have been reported to express CD133 and VEGFR2. These cells when incubated with VEGF and FGF-2 on collagen were shown to differentiate into $CD133^-$ $VEGFR2^+$ mature EC (112). $CD133^+$ cells isolated from PB and cultured in VEGF and stem cell growth factor were also reported to express the markers for mature EC: CD31, CD34, VE-Cadherin, VEGFR2, Tie-2 and vWF (113). It has also been demonstrated that the BM-derived EPC were $CD133^+$, $CD34^+$, $VEGFR2^+$ and VE-$Cadherin^-$. EPC isolated from PB lost CD133 and gradually differentiated into mature EC in culture. A small sub-fraction of mononuclear cells of PB-derived EPC became $CD133^{+/-}$, $CD34^+$, $VEGFR2^+$, $CD14^-$, VE-$Cadherin^-$, and $eNOS^-$ after 4-7 days in culture. These cells, within several weeks in culture, acquired a mature EC phenotype: $CD133^-$, $CD34^{+/-}$, $VEFGR2^+$, $CD14^-$, VE-$Cadherin^+$, $eNOS^+$, and vWF^+ (48;49;83;102-104;106;114). Similar to progenitor cells from bone marrow and peripheral blood, tissue resident progenitor cells are also thought to be able to differentiate to EC (104). The most widely accepted phenotype used to define the human EPC appears to be $CD34^+CD133^+VEGFR2^+$. These markers are used to characterize the early functional human angioblast and EPC. However, $CD34^+CD133^+VEGFR2^+$ cells isolated from human PB and UCB

Figure 1: Endothelial Progenitor Cells are a Subpopulation of the Bone Marrow Cells not Committed to any Specific Lineage (Lin^- BMC) (Adapted from(48;115)

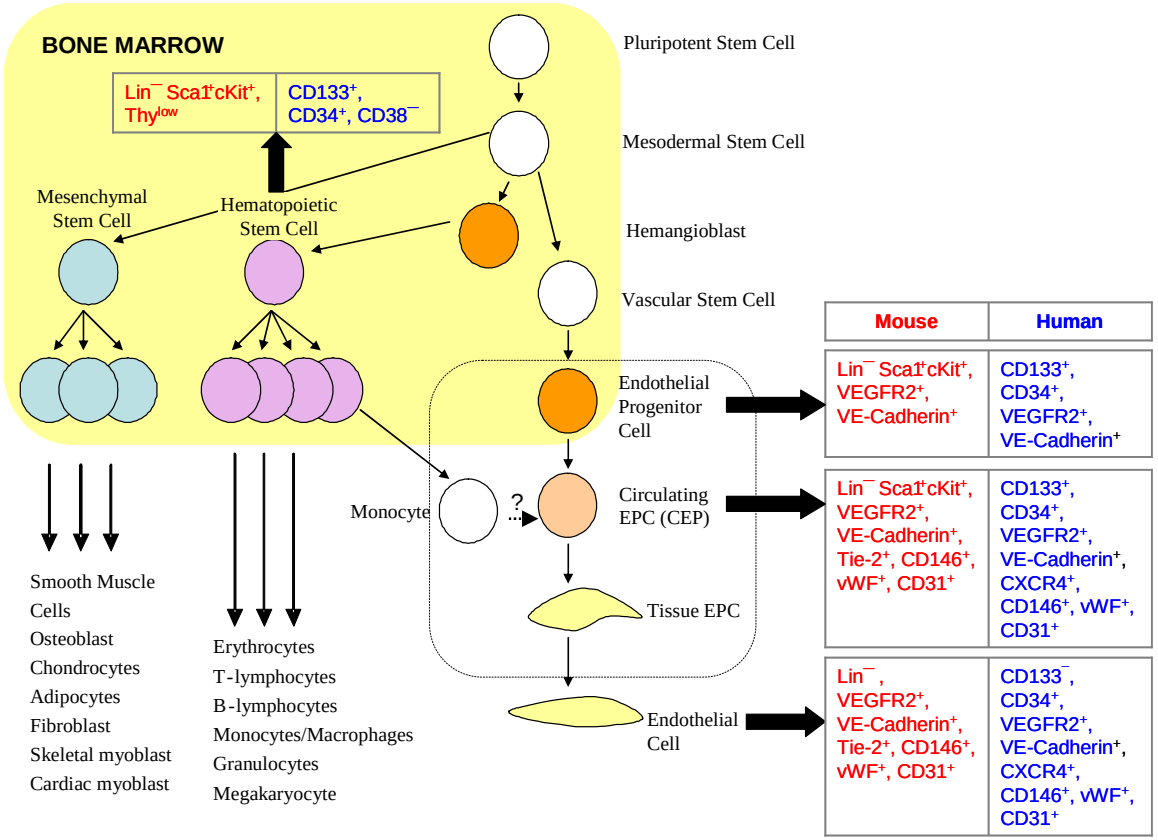
BONE MARROW
Lin⁻ Sca1⁺cKit⁺, Thy^low
CD133⁺, CD34⁺, CD38⁻
Pluripotent Stem Cell
Mesodermal Stem Cell
Mesenchymal Stem Cell
Hematopoietic Stem Cell
Hemangioblast
Vascular Stem Cell
Endothelial Progenitor Cell
Monocyte
?
Circulating EPC (CEP)
Tissue EPC
Endothelial Cell
Smooth Muscle Cells
Osteoblast
Chondrocytes
Adipocytes
Fibroblast
Skeletal myoblast
Cardiac myoblast
Erythrocytes
T-lymphocytes
B-lymphocytes
Monocytes/Macrophages
Granulocytes
Megakaryocyte
Mouse
Human
Lin⁻ Sca1⁺cKit⁺, VEGFR2⁺, VE-Cadherin⁺
CD133⁺, CD34⁺, VEGFR2⁺, VE-Cadherin⁺
Lin⁻ Sca1⁺cKit⁺, VEGFR2⁺, VE-Cadherin⁺, Tie-2⁺, CD146⁺, vWF⁺, CD31⁺
CD133⁺, CD34⁺, VEGFR2⁺, VE-Cadherin⁺, CXCR4⁺, CD146⁺, vWF⁺, CD31⁺
Lin⁻, VEGFR2⁺, VE-Cadherin⁺, Tie-2⁺, CD146⁺, vWF⁺, CD31⁺
CD133⁻, CD34⁺, VEGFR2⁺, VE-Cadherin⁺, CXCR4⁺, CD146⁺, vWF⁺, CD31⁺

Table 3: Endothelial Progenitor Markers Shared by Cells of other Lineages

CD Number	Common name and Synonyms	Expression
CD11b	Integrin α_M, Mac-1, CR3	Monocytes, granulocytes, macrophages, NK- cells
CD13	Alanine aminopeptidase	Epithelial cells, macrophages, granulocytes, synaptic membranes from the CNS
CD14	LPS-R, Mo2	Macrophages, monocytes
CD31	PECAM-1, GPIIa	Platelets, monocytes, granulocytes, B-cell
CD34	Mucosialin	Hematopoietic progenitor cells, capillary endothelial cells, bone marrow stromal, mast cells
CD38	Cyclic ADP ribose hydrolase	Activated T-cells, Plasma cell, NK-cells
CD45	Protein tyrosine phosphatase, receptor type, C	All hematopoietic cells except erythrocytes and plasma cells
CD62L	L-selectin,	B-cells, T-cells, monocytes, neutrophils, eosinophils, NK- cells, bone marrow myeloid cells
CD105	Endoglin	Endothelial cell, bone marrow cell subset
CD117	SCF-receptor, c-kit	Progenitor cells
CD133	Prominin-1, AC133	Stem cell subset
CD144	VE-Cadherin	Endothelial cell
CD146	MUC18, P1H12	Endothelial cell
CD309	VEGFR2, Flk-1	Endothelial cell
CD331	FGFR1, Flt-2	
	Sca1, Ly6A/E, Ly6D	HSC, liver sinusoid cells

Table 4: Classification of Human Hematopoietic Stem Cells (HSC), Endothelial Progenitor Cells (EPC), and Circulating Endothelial Cells (CEC) Based on Source of Origin and Protein Markers

Cell type	Source of origin	Phenotypic marker
HSC	Bone marrow	CD34, CD133, CD117
EPC	Bone marrow, peripheral blood, umbilical cord blood, parenchyma and tissue specific EPC	CD34, CD133, CD117, VEGFR2, VE-Cadherin, FGFR
CEP	Bone marrow	CD31, CD34, CD133, VEGFR2, VE-Cadherin, CXCR4, CD146, vWF
CEC	Mature Endothelium	CD34, VEGFR2, VE-Cadherin, CD146, vWF

did not differentiate into EC *in vitro* (Reviewed in (105). Thus, the debate about EPC identity is far from over.

Currently human EPC are being isolated using 3 general approaches: 1) Peripheral mononuclear cells (MNC) cultured on fibronectin-coated tissue culture plates, 2) $CD34^+$ cells cultured on fibronectin, reportedly giving rise to $CD34^+VEGFR2^+$ endothelial progenitor cells, and 3) MNC cultured in the colony forming unit-Hill (CFU-Hill) and endothelial colony forming cell (ECFC) assays. Although the CFU-Hill cells had characteristic properties and protein expression similar to EC, they neither formed capillaries nor proliferated extensively *in vitro*. The ECFC, on the other hand, have been shown to express antigens similar to endothelium and formed capillaries *in vitro* and *in vivo* (Reviewed in (105;116-118).

The bone marrow is comprised of the lineage-committed cells and the lineage-negative pluripotent stem / progenitor cells. The lineage-committed cells include mature blood cells like erythrocytes, monocytes, macrophages, dendritic cells, natural killer cells, and B- and T-cells. Studies in mouse models have shown that endothelial progenitors are a subset of the lineage-negative BMC (Lin^- BMC) (49). It is also reported that $Lin^-cKit^+Flk1^+$ express the stem cell marker Sca-1 and have endothelial properties (53;119). Additionally, bone marrow-derived $Lin^-Sca1^+cKit^+$ (LSK) are a good source of EPC (119) and have been reported to possess therapeutic potential for angiogenesis (80;115;120). The expression of CD133 on mouse EPC has not been absolutely confirmed, but like human EPC they have been shown to be $CD34^+$, $VEGFR2^+$, and $CD45^-$ (Figure 1 and Table 5). The murine EPC also express CD31 (PECAM) and von Willebrand Factor (vWF), and have the capacity to uptake Ac-LDL or bind lectins. Some of these properties are shared by HSC, CEP, and CEC. The expressions of VEGFR2 and VE-Cadherin have been recommended to be more specific for murine EPC (48;104;105;118).

Table 5: Surface Immunophenotype of Endothelial Progenitor Cells (Adapted from 105)

Human		Mouse	
Cell surface Markers	**Number of reports**	**Cell surface Markers**	**Number of reports**
$CD34^+$	14	$VEGFR2^+$	5
$CD133^+$	8	$cKit^+$	5
$VEGFR2^+$	6	Lin^- BMC^+	3
$CD45^+$	4	$Sca1^+$	2
$CD31^+$	2	$CD34^+$	2
$CD14^+$	2	$CD13^+$	2
$CD45^-$	2	$CD45^-$	0
Other markers		**Other markers**	
$CD11b^+$, $CD62L^+$, $FGFR1^+$, $CD146^+$, VE-$Cadherin^+$, $CD3^-$		$CD133^+$, $CXCR4^+$, VE-$Cadherin^+$	

Overall, $Lin^{-}Sca1^{+}cKit^{+}$ cells constitute a very minuscule proportion of total bone marrow cells. Their percentage in BM has been reported to range from 0.1 - 3% in wild-type mice (121-124). Bone marrow-derived Lin^{-} cells from healthy C57Bl/6 mice were reported to contain 5%, 23% and 5% of $Sca1^{+}$, $cKit^{+}$ and $Sca1^{+}cKit^{+}$ cells respectively (125;126). Similarly, Koike *et al.* also reported that 4% of Lin^{-} bone marrow cells were double-positive for Sca1and cKit (120). Friedlander demonstrated that Lin^{-} BMC expressed Sca1 (4%), cKit(70%), VEGFR2 (2%), CD31 (81%) and Tie-1 (1%). They also showed that the Lin^{-} BMC cell participated in neo-vascularization by incorporating into the developing blood vessel in a mouse cornea assay (63;108;110). Ikehara *et al.* described the differentiation of Lin^{-} BMC into EPC. Lin^{-} BMC when cultured in presence of granulocyte colony stimulating factor (GCSF) and monocyte colony stimulating factor (MCSF) had elevated numbers of $Flk1^{+}CD45^{-}$, $Sca1^{+}CD45^{-}$, $CD31^{+}CD45^{-}$ or $CD146^{+}CD45^{-}$ cells. When these cultured Lin^{-} cells were intravenously injected into ischemic hind limbs of mice, the number of intramuscular capillaries in the ischemic leg increased substantially (120). The expression of CXCR4 on murine Lin^{-} BMC has also been reported and the presence of CXCR4 has been demonstrated to cause their migration in response to SDF-1α (127).

Mobilization of Endothelial Progenitor Cells

Current literature indicates that coronary artery bypass surgery, myocardial infarction, burn injuries, hypoxia, exercise, and cancerous pathology lead to an increase in circulating endothelial progenitors in man (83;102;103;114). Involvement of EPC is thought to be essential for regeneration and repair of injured tissue and for vasculogenesis in tumors (48;83;103;128). EPC recruitment to the sites of neoangiogenesis is triggered by the increased availability of angiogenic growth factors and chemokines like VEGF, angiopoietin, and SDF-1α. It is thought

that early infiltrating EPC recruit additional EPC by secreting VEGF, HGF, G-CSF and GM-CSF (48). Furthermore, it has been shown that tumor-derived VEGF and PlGF, and possibly angiopoietin, activate matrix metalloproteinase-9 (MMP-9) within the bone marrow microenvironment. This results in the cleavage of membrane-bound kit-ligand (aka stem cell factor or SCF) from BM stromal cells. The increased level of soluble kit-ligand within the BM promoted the mobilization of stem and progenitors, including EPC and HSC. The mobilized EPC and HSC translocated from the osteoblastic zone to the vascular zone, where they proliferated, differentiated and were launched into the peripheral circulation (80;129;130). Several cytokines like IL-2, IL-3, IL-6, IL-8, IL-1β, erythropoietin, and stem cell factor (SCF) have been implicated in the mobilization of HSC and the increase in circulating EPC (38;83;90).

Recent evidence suggests that hypoxic environments, such as in tumors, regulate the angiogenic properties of BM-derived vascular progenitors. As mentioned earlier, expression of VEGF is regulated by hypoxia. Recently, the hypoxia-responding integrins were shown to be involved in regulating the expression of SDF-1α and recruiting $CXCR4^+$ EPC to ischemic tissue (131). Hordijk *et al.* described that in response to SDF-1α there was a loss of VE-Cadherin-mediated endothelial cell-cell adhesion. This loss of cell-cell adhesion was considered to be responsible for the increased permeability of BM endothelium and for the mobilization of human $CD34^+$ cells from bone marrow (132). *In vitro*, transmigration of $CD34^+$ cells across the human umbilical cord vascular endothelial cells (HUVEC) and the bone marrow endothelial cell (BMEC) monolayer in response to all CXC, CC and CX3C chemokines, except MIP-1α, has also been reported. The maximum effect was observed in response to SDF-1α (133). The $CD34^+$ circulating hematopoietic progenitor cells have been shown to express CXCR4 and are chemoattracted to SDF-1α (110;134;135). Additionally, *in vitro* assays have demonstrated an

additive effect of VEGF on SDF-1α-mediated trans-endothelial migration of $CD34^+$ progenitor cells (134). In conclusion, VEGF and SDF-1α appear to be most critical in mobilization of hematopoietic stem cells and endothelial progenitors *in vitro* and *in vivo*.

Endothelial Progenitor Cells and Tumor Neo-vascularization

Lyden published the first report in 2001 indicating that EPC localized to new blood vessels in tumors. They reported that Id-mutant mice had significantly fewer $VEGFR2^+$ bone marrow-derived circulating endothelial progenitor cells. Additionally, compared to the wild-type mice, the tumor growth was demonstrated to be severely impaired in these Id-mutant mice. They concluded that VEGF-responsive BM-derived precursors were necessary for tumor angiogenesis and growth (50;53;136). Since then several conflicting reports, that either refuted or supported the theory of tumor vasculogenesis, have been published.

There have been a few reports that indicated that BM-derived cells localized to tumors, but that these cells were not EPC and that they did not incorporate into the vasculature (Table 1) (56;57;60;68-70;137). Shinde-Patil *et al.* injected the Indium oxide-labeled Lin^- $Sca1^+cKit^+$ BMC mice with heterotopic Lewis lung tumor. Biolocalization of EPC was detected by radioactivity. Most cells were detected in liver at both 24- and 72-hours post-injection. Less than 2.5% of the injected cells localized to tumors. Immunohistological analysis revealed that most EPC detected in tumors were located perivascularly (60). Purhonen *et al.* did not observe an increase in BM-derived circulating $VEGFR2^+$ cells in the presence of tumor. $VEGFR2^+$ BMC were used as EPC in these experiments. Most BM-derived cells in tumors were once again observed in the perivascular space (68). Another group suggested that tumor infiltrating BM-derived cells were predominantly $CD11b^+$. CD11b is integrin alpha M and is routinely used as a marker for the macrophages-monocyte lineage. These $CD11b^+$ cells were demonstrated as a

major source of MMP-9, which remodeled the ECM and assisted in the sprouting of blood vessels. Genetic ablation of MMP-9 was shown to significantly decrease tumor growth and vascularization (69). In a separate account, SDF-1α was reported to stimulate the migration of $CD34^+$ BMC *in vivo*. Although these cells were recruited to tumors, they were found in close proximity of functional blood vessels and supporting pericytes (70).

In contrast, there are about eleven reports that have shown the incorporation of EPC into developing tumor vasculature and their significant contribution to the process of vasculogenesis. Vajkocky *et al.* transplanted *ex vivo*-cultured embryonic EPC (eEPC) into tumor-bearing athymic mice. They observed approximately 43% of the injected eEPC to be arrested in tumors. Of these tumor-localized cells, approximately 55% eEPC were observed to have extravasated into the tumor interstitium and nearly 33% contributed to the functional tumor blood vessels. This homing of eEPC was shown to be mediated by selectins and PSGL-1 (one of the ligands for selectins, Table 7); and blocking these receptor-ligand interactions reduced the homing of eEPC by 77% (51). Santarelli *et al.* observed that 12% of $CD34^+VEGFR2^+$ cells in tumors were derived from BM. They also found these cells to be incorporated into the blood vessels, contributing 4.2% to tumor vasculature (61). Another group demonstrated that integrin α4β1 mediated the homing to human $CD34^+$ and murine Lin^- BMC to tumor vasculature (63). Emerson *et al.* implicated VEGF and PlGF in mediating vasculogenesis. They reported that the recruitment of EPC to tumors was mediated by VEGFR1, but blocking VEGFR2 prevented EPC-mediated vessel formation (64). Kaplan also reported a similar observation. However, they suggest that BM-derived $VEGFR1^+$ cells created the 'pre-metastatic niche' that enabled the establishment of tumor cells in specific organs. $VEGFR2^+$ BMC later infiltrated into the developing tumor and contributed to vascularization. Thus, blocking both VEGFR1 and

VEGFR2 has been proposed to be important to prevent the BMC-mediated contribution to the development and vascularization of metastases (138).

As tumors grow, the core is devoid of blood supply and becomes necrotic. The actively developing tumor vasculature is described to be at the periphery of the tumors. Several investigators have shown that EPC were preferentially recruited to the tumor periphery (53;63). This was shown to be mediated by elevated expression of α4β1 ligand at the periphery (139). Additionally, higher numbers of BM-derived cells have been shown to be recruited to poorly differentiated tumors (52;73). Although, it was initially thought that EPC stabilized tumor vasculature rather than initiate vasculogenesis (28), newer reports suggest otherwise. It was recently described that tumor-localized EPC matured into endothelial cells and incorporated into tumor vessels, and that this contribution of BM-derived EPC to tumor vasculature was diluted as tumor progressed. Supporting this theory, selective ablation of EPC showed a substantial delay in tumor growth (140). Moreover, BM-EPC recruited to micro-metastases have been suggested to act as the 'angiogenic switch' for tumor progression (28). This report suggested that EPC contributed in the early phase of tumor development and were instrumental in initiation of tumor vascularization.

In conclusion, a significant amount of research has been carried out to understand the mechanism of post-natal vasculogenesis in tumors, but much of the information remains controversial. Two reasons for the disagreement concerning vasculogenesis in tumors are inconsistency in the phenotype of endothelial progenitors and the type, stage, and location of tumors under investigation.

Endothelial Cell Adhesion Molecules

The cell adhesion molecules (CAM) are cell surface proteins that are involved in cell-cell and cell-ECM interactions. They are composed of an intracellular domain that interacts with the cytoskeleton, a transmembrane domain, and an extracellular domain that binds to ligands. They are broadly classified into calcium-independent (Integrin and Immunoglobulin super family) and calcium-dependent (Cadherin and Selectins) CAMs. Endothelial cells use cell adhesion molecules, such as integrins and cadherins to attach themselves to each other and to the vascular ECM, and selectins to arrest circulating leukocytes.

Integrins

Integrins are a group cell-surface heterodimeric proteins, composed of α and β subunits that interact with the ECM and play important role in signal transduction. In mammals, 19 α and 8 β subunits have been characterized; these subunits combine to generate 24 unique integrins (141). Endothelial cells express a subset of integrins including vitronectin receptors (αvβ3 and αvβ5), fibronectin receptors (α4β1, α5β1), collagen receptors (α1β1, α2β1), laminin receptors (α3β1, α6β1, and α6β4), and osteopontin receptor (α9β1). Reports from several laboratories have shown that genetic ablation or blocking of certain integrin subunits resulted in defective vasculature development, embryonic lethality, and reduced tumor angiogenesis (Reviewed in (33;141-144). Integrins αvβ3, αvβ5, and α4β1 have been implicated in tumor growth, vascularization, and metastasis. Several integrin-targeted therapeutic agents are currently in clinical trials for cancer therapy (16;143).

Immunoglobulin Super Family (IgSF)

The immunoglobulin super family (IgSF) is a large family of proteins that is involved in numerous functions including ligand recognition, binding, and adhesion. Members of this family

primarily involved in adhesion are ICAM-1 (intracellular cell adhesion molecule aka CD54), VCAM-1 (vascular cell adhesion molecule aka CD106), PECAM-1 (Platelet-endothelial cell adhesion molecule aka CD31), and NCAM (neural cell adhesion molecule aka CD56). Both ICAM-1 and VCAM-1 have been shown to be upregulated in EC in response to TNF-α and IL-1 (145). VCAM-1, on endothelial cells, is reported to be a ligand for integrin VLA-4 (very late antigen-4 or α4β1). The overexpression of VCAM-1 has been associated with oncogenesis, tumor angiogenesis, and metastasis in gastric carcinoma (146). PECAM-1 or CD31 is expressed by EC and is routinely used as a marker for endothelial cells.

Cadherin

Cadherins mediate calcium-dependent interactions between neighboring cells. Different members of the cadherin family are found in different organs. E-cadherins are found in epithelial tissue, N-cadherins are found in neurons, and P-cadherins are found in the placenta. VE-Cadherin is expressed on EC and is believed to provide the mechanical barrier to inter-endothelial leakage. VE-Cadherin was reported to be expressed on non-endothelial cells *in vitro* and on blood conduits made of tumor cells implicated in vascular mimicry (85). Recent reports have revealed that BM-derived EPC participating in tumor vascularization expressed VE-Cadherin (28;53) and has been suggested to be a superior marker for identifying EPC and EC. Additionally, there are few studies implicating VE-cadherin as a possible target for inhibiting angiogenesis in tumors, although mostly in combination with other chemo- and anti-angiogenic therapy (147).

Selectins

Selectins are a group of calcium-dependent type I single-chain transmembrane proteins. There are three selectins based on the cell type in which they are predominantly expressed: E-

selectin (endothelial cells), L-selectin (leukocytes), and P-selectin (platelets and endothelial cells). All selectins consist of an N-terminal lectin-like domain, an epidermal growth factor like domain, six consensus repeats, a single transmembrane domain, and a short cytoplasmic domain. Selectins bind sialylated and fucosylated oligosaccharides such as Sialyl Lewis-x (sLe-x); these sugar moieties make up the terminal components of glycans attached to glycoproteins and glycolipids (148;149).

L-selectin and Tumor Biology

L-selectin also known as CD62L, leukocyte adhesion molecule (LAM-1), lectin adhesion molecule (LECAM-1), is expressed by leukocytes, and is responsible for leukocyte trafficking. Several activating factors including GM-CSF, interferon-α, IL-8, adrenalin, and shear stress influence L-selectin expression. Soluble L-selectin (sL-selectin) is reported to be functionally active and thought to be involved in obstructing the adhesion of leukocytes to endothelium (149). L-selectin and sL-selectin have been reported to be elevated in several diseases including meningeal leukemia and lymphoma (149;150). Furthermore, L-selectin has also been reported to be involved in metastasis of tumor cell (151).

Some ligands that bind L-selectin include GlyCAM-1, MadCAM-1, CD34, PSGL-1, Sialyl Lewis-x and sulfated molecules like 6-sulfo-sLe-x, heparin, and sulfatides. Some of these ligands have been found to be expressed on certain tumor cells and implicated in the metastatic process (151).

P-selectin and Tumor Biology

Platelets and endothelial cells express P-selectin (CD62P, LECAM-3). It is constitutively expressed in α-granules in platelets and Weibel-Palade bodies in endothelial cells. Histamine, thrombin, activated complement, and certain viruses lead to the rapid mobilization of P-selectin

to the cell surface, and cytokines like IL-4, IL-13, and oncostatin M cause an upregulation in P-selectin mRNA and protein synthesis. Some of the ligands that bind P-selectin include PSGL-1, sLe-x, heparin, and sulfatides. In two independent studies, Borsig and Garcia demonstrated that metastasis of colon cancer cells was mediated by binding of sulfatides on colon cancer cells to P-selectin on endothelium. In the presence of sulfatase or heparin the metastatic burden was significantly reduced (151;152).

E-selectin

E-selectin (CD62E, LECAM-2) is a well-studied endothelial leukocyte adhesion molecule (ELAM) that is selectively expressed on activated endothelium during inflammatory responses and during tumor development. E-selectin is usually absent from resting endothelium (34;145;149;153-155). It has a molecular weight of 64 kDa, but has detected between 107-115 kDa by western blotting. This disparity in molecular weight is most likely due to variable glycosylation of E-selectin. It was reported to be transiently expressed in endothelial cells in response to TNFα, IL-1β, NF-κB, and activator protein. E-selectin mRNA has been reported to have a short half-life of 2 hours (156). The synthesized protein was shown to be directly delivered to plasma membrane (157). In response to IL-1β treatment, E-selectin was detected on cell surface of human umbilical vein endothelial cells as early as 30 minutes, peaked by 4 hours, and subsequently declined to basal levels by 24 hours (158). Surface E-selectin is slowly endocytosed and degraded by lysosomes. A VEGF-mediated induction of E-selectin on endothelial cells has also been reported (159). In addition, Tabatabai *et al.* demonstrated that upregulation of E-selectin in tumors was mediated by VEGF (65). E-selectin has been reported to bind to several glycoproteins and glycolipids. Some of the E-selectin ligands are sLe-x, Sialyl

Lewis- a (sLe-a), E-selectin ligand (ESL-1), Leukosialin/CD43, CD44, LAMP-1, P-selectin glycoprotein (PSGL-1) and even L-selectin (Table 6).

E-selectin and tumor biology

The contribution of E-selectin to tumor growth and metastasis was recognized in early the 1990's. In an early experiment, murine endothelial cells (EC) expressing E-selectin were co-transplanted with tumor cells that expressed sLe-x and sLe-a. It was demonstrated that the initial adhesion of tumor cells and EC was mediated by the interaction of E-selectin on endothelium and sLe-x and sLe-a on tumor cells. These results indicated that the interaction of tumor cells and EC was highly dependent on the interaction of the cell adhesion molecule mediating the adhesion of cancer cells to EC. Blocking sLe-x and sLe-a remarkably retarded tumor growth and angiogenesis (32). In a separate report, E-selectin mRNA was shown to be induced in the lungs of B16 tumor bearing wild-type mice. E-selectin expression was significantly reduced in B16 tumors in $p38a^{+/-}$ mice, suggesting that expression of E-selectin was mediated by p38a (160;161). Other studies, similar to the ones mentioned above, have suggested the involvement of E-selectin in adhesion and growth of metastatic tumor cells.

E-selectin and Metastasis

There is strong evidence for the involvement of E-selectin in tumor development. However, the precise relationship between E-selectin expression, cell adhesion, tumor invasion, and metastasis remains unclear. Several metastatic tumors isolated from human subjects with cancers of the colon, prostrate, breast, pancreases, and lung were reported to express functional ligands of E-selectin and adhered to an endothelial cell monolayer expressing E-selectin. It is believed that tumor cells might harness and exploit the selectin-dependent mechanism, commonly used by leukocytes, for metastasis (162). The efficiency of E-selectin-mediated

Table 6: E-selectin Ligands

CD number	Common Name		Cell Type
CD208	CLA	Cutaneous lymphocyte antigen *(modification of PSGL-1)*	T-cells, endothelial cells, B cells, NK , DC, Langerhans cells in the skin
-	ESL-1	E-selectin Ligand	Endothelial cell, fibroblast, neutrophil, colon carcinoma, lymphoma,
CD107a	LAMP-1	Lysosomal-associated membrane protein	Keratinocytes, Melanocytes, Microglial cells, Platelets
CD147	Basigin		EC, Pericytes, T-cells, follicular dendritic cells, Mesenchymal stem cell, Keratinocytes,
CD15s	sLe-x	Sialyl Lewis x	Tumor cells
CD162	PSGL-1	P-selectin glycoprotein ligand-1	WBC, EC
CD43	Leukosialin	Sialophorin	Basophils, B-cells, DC, Enterocytes, Macrophage, Mast cells, Microglial cells, Mast Cells, Neutrophils, Osteoblast, Platelets, T-cells, HSC
CD44	HCELL	Phagocytic Glycoprotein 1 (pgp 1) and HCAM	Adipocytes, Astrocytes, Basophils, B-cells, Chondrocytes, DC, EC, Enterocytes, Eosinophils, Fibroblasts, Keratinocytes, Mast cells, Macrophage, Melanocytes, Monocytes, Osteoblasts, Osteoclasts, Schwann cells, T-cells, Thyrocytes,
CD62-L	L-selectin		Basophils, DC, Eosinophils, Keratinocytes, Macrophages, Megakaryocytes, Monocytes, Neutrophils
CD65	VIM-2	Ceramide Dodecasaccharide	Myeloid cells, Monocytes

binding of colon carcinoma cells to endothelial cells has been demonstrated to correlate with their metastatic potential. It was thus proposed that soluble forms of E-selectin ligand, LAMP-1 and leukosialin (CD43), would be useful therapeutic agent to prevent metastases (163). Elevated levels of E-selectin have been often reported on blood vessels close to or within tumor metastasis. This notion that E-selectin on activated endothelium facilitated tumor cell seeding was validated by Uotani's report. They observed an elevation in E-selectin in livers after partial hepatectomy. They observed an increase in the incidences of liver metastases when tumor cells were injected after hepatectomy. Furthermore, a significant decrease in metastatic burden was reported in the presence of E-selectin neutralizing antibodies. This experiment confirmed the role of E-selectin in establishing metastases in their model (164). Insug *et al.* intravenously administered the Sialy Lewis-a expressing B16 tumor cells mixed with Sialy Lewis-a-mimicking antagonizing peptide or unrelated peptide into healthy mice or E-selectin$^{-/-}$ mice. They observed that colonization of tumor cells was blocked by the antagonizing peptide in wild-type mice and was completely abolished in E-selectin knockout mice (165;165). Another group of investigators showed that the metastatic process in the lung was almost completely abrogated in the genetically manipulated mice that lacked the expression of E-selectin, regardless of sLe-x/a expression on tumor cells (165-168). Consequently, Thurin *et al.* proposed that the interaction of tumor cells, via the carbohydrate determinant, and E-selectin constituted an important step in the metastatic process, and that carbohydrate antigen mimetic could potentially be used for anti-adhesive tumor therapeutics (165;168;169). Our laboratory has obtained similar results supporting the function of E-selectin in colonization and growth of Lewis lung tumor cells. Besides contributing to tumor cell metastasis, E-selectin appears to be involved in tumor vascularization (170;171) (Verbanac laboratory, manuscript in preparation).

E-selectin and Tumor Vascularization

There are over seven hundred reports on the subject of 'E-selectin and Cancer', found in a PubMed search, but less than a handful of these have fully explored the role of E-selectin in tumor vascularization. Nonetheless, E-selectin expression in tumor endothelium is theorized to be important and soluble E-selectin is thought to be an important angiogenic growth factor. E-selectin expression was reported to be elevated in proliferating EC in blood vessels in hemangiomas. It was concluded that E-selectin was instrumental in angiogenesis and a plausible marker for proliferating endothelium (172). Compared to benign mucosa, the *in situ* E-selectin expression in tumor-associated vessels in gastric carcinomas was reported to be 34% higher. In addition, E-selectin positive vessels were more frequently observed in regions that were densely vascularized and this overexpression of E-selectin was shown not to be associated with the inflammatory infiltrate (173). These studies suggest that E-selectin expression is in all probability elevated in tumors that acquire actively proliferating vasculature. Our laboratory has observed expression of E-selectin on tumor-derived EC. Additionally, results from *in vivo* biolocalization studies showed a 70% decrease in adhesion of adoptively-transferred vascular endothelial cells to tumor endothelium in the presence of E-selectin blocking antibody (170) (Verbanac laboratory, manuscript in preparation). These reports suggest that E-selectin might be involved in tumor vascularization.

Soluble E-selectin

Circulating soluble E-selectin (sE-selectin) is thought to be released by enzymatic degradation or due to shedding from damaged endothelial cells. It is considered to be evidence of endothelial activation. Similar to patients with inflammatory conditions, sE-selectin has been reported to be elevated in serum and plasma of patients with breast, ovarian, gastrointestinal

cancers as well as multiple myelomas compared to healthy controls (162;174;175). Level of circulating E-selectin has been correlated with the severity of certain cancers (176;177) and is suggested to have a role in pathogenesis and prognosis of cancer patients (178;179).

Selectin Ligands in Tumor Biology and Metastasis

The ligands that bind E-selectin are listed in Table 6. Some of these glycoproteins have also been shown to bind L- and P-selectin, and have been implicated in tumor biology. Tumor cells, in particular carcinoma and leukemic cells have been reported to express sLe-x structures in abundance. Carcinoma cells are also enriched with sLe-a structure, which is the isomer of sLe-x. This supports the hypothesis that blood-borne disseminated tumor cells use the selectin-carbohydrate interaction to adhere to endothelial cells at metastatic sites (180).

Lysosomal-associated membrane protein (LAMP-1, CD107a) is expressed on the luminal side of the lysosomal membrane of most normal cells. It is glycosylated with N- and O-linked carbohydrate chains. Sialyl Lewis-x (sLe-x) is most abundantly present on N-glycans of LAMP-1 and constitutes 12% of the total terminal structure; LAMP-1 contains around 12 N-glycans. In comparison to LAMP-1, sialophorin (Leukosialin, gpL115, CD43) is a major sialoglycoprotein on the surface of human T cells, monocytes, granulocytes, some B cells, pluripotent hematopoietic stem cells and bone marrow derived-$Lin^{-}Sca1^{+}cKit^{+}$ cells. Sialyl Lewis-x is present in O-glycans on CD43 and constitutes 1% of total terminal structure but leukosialin contains about 80 O-glycans. Thus, despite the differential glycosylation on LAMP-1 and CD43, both bind E-selectin with equal affinity and have been proposed as potential inhibitors for E-selectin-mediated adhesion (163).

Elevated expression of LAMP-1 and sLe-x has been reported on colon carcinoma cells with high metastatic potential compared to carcinoma cells that are poorly metastatic (180-182).

LAMP-1 was also shown to be important for the adhesion of human ovarian cancer cells to the extracellular matrix (183). Expression of LAMP-1 was demonstrated in human melanoma, fibrosarcoma, and colon-adenocarcinoma cells. The authors strongly proposed the LAMPs as a family of adhesive glycoproteins that participated in the complex process of tumor invasion and metastasis (184). Similarly, CD43 has been shown to be important in the growth of melanoma tumors. A significant retardation in the growth of B16F10 melanomas and development of metastatic foci was observed in $CD43^{-/-}$ mice compared with wild-type control mice (185). Other E-selectin ligands, PSGL-1 and ESL-1, have been reported to be expressed on human prostate tumor cells and in prostate tumor cells in bone metastases (186).

The glycosyl residues, like sLe-x and sLe-a, on the terminals of glycoproteins that bind selectins are most likely responsible for mediating the adhesion of tumor cells to activated EC, platelets, and ECM. The synthesis of these sialylated glycosyl residues requires specialized enzymes – glycosyltransferases. Thus, several investigators are evaluating the expression of specific glycosyltransferases in different metastatic cancer cells. Recently it was demonstrated that fucosyltransferase-3, -6, and/or -7 were important in synthesis of Sialyl Lewis-x and ESL-1 on metastatic prostate cancer cells (162). Thus, selectin ligands, specific glycosyl residues, and glycosyltransferases play a very important role in tumor biology and metastasis.

Pharmacological Targeting of Selectin

Currently no clinical trials investigating selectin or selectin-targeting agents are being conducted. However, theoretically anti-E-selectin, anti-PSGL-1, soluble PSGL-1-Ig, and glycosylation inhibitors like 4-fluoro-N-acetyl-glucosamine (4-F-GlcNAc) are thought to be promising candidates. Antibodies against E-selectin or PSGL-1 are hypothesized to block the interaction between tumor cells and endothelial cells. Similarly, soluble PSGL-1 could quench

PSGL-1 on tumor cells, leukocytes, and platelets and prevent them from binding to activated endothelium. Glycosylation inhibitors like 4-F-GlcNAc have been shown to be incorporated into glycan structures and truncated their branching and elongation on PSGL-1, thereby preventing synthesis of sLe-x or sLe-a by fucosyltransferases. The above-mentioned selectin-targeting strategies have been applied with some success in treating diseases like psoriasis and offer attractive modes of interventions in cancer therapy (162).

Vascular Endothelial Growth Factor and Receptor Family

The vascular endothelial growth factor (VEGF) family consists of VEGF-A, VEGF-B, VEGF-C, VEGF-D, VEGF-E (viral), and placental growth factor (PlGF) (39;187). The term VEGF, by convention refers solely to VEGF-A, which is the predominant vascular endothelial growth factor. VEGF family members bind to four receptors with high affinity. Three of these receptors belong to the receptor tyrosine kinase (RTK) family: VEGFR1 (fms-like tyrosine kinase-1 / Flt-1), VEGFR2 (murine homologues of kinase insert domain-containing receptor (KDR) / fetal liver kinase (Flk-1)) and VEGFR3 (Flt-4). Neuropilin is the fourth receptor for the VEGF family. These receptors have seven extracellular immunoglobulin homology domains and two intracellular tyrosine kinase domains in their cytoplasmic tail region. VEGF initiates a cascade of events upon binding with their receptors: receptor dimerization and auto-phosphorylation of tyrosine domains followed by activation of numerous downstream proteins including phospholipase C-γ/protein (40;40;62;188-192).

Vascular Endothelial Growth Factor-A

VEGF-A or VEGF was first characterized as a vascular permeability factor (VPF) in 1983. Senger *et al.* reported that VPF / VEGF promoted extravasation of proteins from tumor-

associated blood vessels, and appeared to affect vessel permeability. Normal cell types, including macrophages, lung epithelial cells, kidney epithelial cells, follicular cells in the pituitary, corpus luteum cells, aortic smooth muscle cells and a numerous tumor cells and tumors, produce VEGF. Other functions of VEGF include anti-apoptosis modulation (159), lymphangiogensis, immune suppression, stimulation and recruitment of endothelial and hematopoietic precursor cells in vasculogenesis, and regulation of hematopoietic stem cell survival (40).

VEGF is one of the key regulators of tumor growth and metastases. It is a highly specific mitogen for vascular endothelial cells. Besides hypoxia, mutant ras, mutant p53 tumor suppressor, erbB-2/Her2, activated EGFR, and *bcr-abl* are associated with VEGF upregulation in tumors. VEGF mRNA was reported to be weakly expressed by naïve $CD34^+$ cells. The amount of VEGF released was substantially increased by incubating cells with a combination of cytokines IL-3, GM-CSF, and G-CSF (129). Although hypoxia is thought to be predominantly responsible for the expression of VEGF, it can be produced in tumor cells under normoxic conditions. This could explain elevated levels of VEGF at the tumor periphery, which is well vascularized and not devoid of oxygen (8;78). Stimulation of $VEGFR1^+$ and $VEGFR2^+$ endothelial cells by VEGF leads to their survival, proliferation, and increased mobility. More recently, an important role for VEGF has emerged in mobilization of endothelial progenitors from the bone marrow to distant sites of neo-vascularization (Table 1) (50;64;107).

VEGF has been strongly implicated in the progression of cancerous tumors (39). Several researchers have reported an increase in the systemic levels of VEGF in different types of tumors and cancers, namely glioma, neuroblastoma, colorectal, ovarian, breast, and prostate cancer. Elevation of VEGF in plasma in adult mice has been shown to mobilize $VEGFR2^+$ circulating endothelial progenitors. Monoclonal antibodies against VEGFR2 have a suppressive effect on

solid tumor growth in mice (190). Thus, VEGF and VEGFR2 are potential direct targets in the suppression of pathological angiogenesis. Avastin / Bevacizumab, anti-VEGF antibody was the first anti-angiogenic drug approved by the US Food and Drugs Administration (FDA) for the treatment of metastatic colorectal cancer. It is now used for the treatment of breast cancer and non-small cell lung carcinoma and is being evaluated in clinical trials for several different types of cancers.

Vascular Endothelial Growth Factor-B

VEGF-B is expressed in heart, skeletal muscle, and brown fat in adults and has two isoforms, VEGF-B_{167} and VEGF-B_{186}. The carboxy-terminal of VEGF-B_{167} has a heparin-binding domain whereas VEGF-B_{186} lacks the ability to bind to heparin. VEGF-B specifically binds to the soluble and membrane-bound forms of VEGFR1. Although VEGF-B is not critical in development, it might be important in inflammatory angiogenesis as demonstrated by reduced synovial angiogenesis in the arthritis model (Reviewed by (41). VEGF-B has been detected in several types of tumors; however, its role in tumor biology remains elusive (Reviewed by (193).

Vascular Endothelial Growth Factor-C and -D

VEGF-C is expressed prominently in heart, placenta, muscle, ovary, and small intestine; lower levels of VEGF-C are expressed in brain, liver and thymus. Post proteolytic maturation of VEGF-C generates multiple forms, which bind and activate VEGFR3 receptors. The fully processed form of VEGF-C can also bind and activate VEGFR2 receptor. VEGF-C plays an important role in lymphatic development. Deletion of *vegfc* in mice is reported to lead to the complete absence of lymph vessels and embryonic lethality, but did not affect the blood vasculature development (Reviewed by (41).

VEGF-D is structurally similar to VEGF-C, and is strongly expressed in heart, lung, skeletal muscle, colon, and small intestine. It is an activating ligand for the VEGFR2 and VEGFR3, but it does not bind to VEGFR1. VEGF-D is also a known mitogen for endothelial cells. It has been shown to induce tumor angiogenesis through VEGFR2 and tumor lymphangiogenesis through VEGFR3. VEGF-D is also reported to promote metastatic dissemination of tumor cells via the lymphatics. Elevated levels of VEGF-D have been detected in gastric tumors compared to healthy gastric mucosa (Reviewed by (41). Expression of VEGF-C and VEGF-D have been reported to correlate with lymph node metastasis and prognosis of patients with colorectal carcinoma (194). VEGF-D and VEGFR-3 are implicated in promoting nodal metastasis in human invasive lobular breast cancer (195).

Placental Growth Factor

Placental growth factor (PlGF) is expressed in placenta, heart, and lungs. Many cell types express PlGF, including EC, SMC, fibroblasts, leukocytes, BM progenitors, cardiomyocytes, epithelial, and tumor cells. It has four isoforms (PlGF1-4) in humans, of which only PlGF2 has a homologue in mice. It binds to VEGFR1, but not VEGFR2. It also binds to both neuropilin receptors. PlGF is upregulated in pathological conditions by various stimuli like hypoxia, nitric oxide, interleukins, TNFα, VEGF, and TGFβ etc. It serves several functions, including stimulation of vessel growth, as well as growth, migration, and survival of EC. PlGF stimulates angiogenesis by recruiting various cells that express VEGF, SDF-1α, FGF-2, PDGF-B, MMP, etc. It displaces VEGF from VEGFR1; the liberated VEGF then activates VEGFR2 and enhances VEGF-mediated angiogenesis (Reviewed by (41;193).

PlGF is considered to be a prognostic marker for cancer. It is reported to be significantly elevated in NSCLC, gastric, colorectal, and breast cancer. It is also correlated with lymph node

metastasis, tumor stage, and mortality in several types of cancer. Elevated plasma PlGF levels have also been correlated with tumor grade and survival in renal cell carcinoma. Furthermore, PlGF was reported to be elevated in patients undergoing anti-VEGF therapy and was thought to be responsible for drug resistance. Neutralizing anti-PlGF was reported to inhibit growth and metastases of tumor by inhibiting tumor angiogenesis, lymphangiogenesis and intratumor macrophage recruitment (Review by (86;193).

Vascular Endothelial Growth Factor Receptor 1 (VEGFR1)

An important feature of VEGFR-1 is that, unlike other VEGFR genes, it expresses two types of mRNA, one for a full-length receptor and another for a soluble short protein (lacks transmembrane and intracellular domains known as soluble VEGFR-1 (sFlt-1). The binding-affinity of VEGFR-1 for VEGF-A is higher than that of VEGFR-2, but the kinase activity of VEGFR-1 is weaker than that of VEGFR-2 (196). $VEGFR1^{-/-}$ mice die by embryonic day 9 (E8.5-9) due to excess EC and disorganized vasculature. However, mice expressing the VEGFR1 extracellular and transmembrane domains but lacking the tyrosine kinase domain intracellular domains of VEGFR1 are viable and have functional vasculature. This suggests that VEGFR1 acts as a negative regulator of angiogenesis during embryogenesis (188). Nonetheless, 50% of mice with homozygous deletion for both the intracellular and transmembrane domains die at E8.5-9 due to disorganization of blood vessels. Thus, membrane-bound form of VEGFR1 appears to regulate vascular development by trapping VEGF for the appropriate regulation of VEGF signaling in vascular endothelial cells during early embryogenesis {584, 388, 583}.

VEGFR1 is expressed by endothelial cells, monocytes, macrophages, hematopoietic cells, and pericytes express. VEGFR1 homodimerizes and binds VEGF, VEGF-B, VEGF-F, and PlGF. VEGFR1 has also been shown to dimerize with VEGFR2. Although, the tyrosine kinase

activity of VEGFR1 is weak and the downstream signaling pathway is poorly understood, the tyrosine kinase activity is thought to be important in hematopoietic cell migration in response to VEGF and PlGF (Reviewed by (41).

An increase in VEGFR1 is reported in several different cancers. Its expression is associated with poor prognosis, metastasis, and recurrence in breast and NSCLC (193). Recently, $VEGFR1^{+}$ BM-derived cells were implicated in formation of the pre-metastatic niche. It was also demonstrated that blocking VEGFR1 significantly reduced the metastatic burden (138). Thus, VEGFR1 appears to be important in tumor development.

Vascular Endothelial Growth Factor Receptor 2 (VEGFR2)

Endothelial cells and endothelial progenitors predominantly express VEGFR2. It binds VEGF, -C, -D and -E, however VEGF is the main ligand for VEGFR2. The mitogenic, angiogenic and permeabilizing effects of VEGF are mediated via VEGFR2 expressed on vascular, and lymphatic endothelium and has been strongly implicated in angiogenesis and vasculogenesis. The key role of VEGFR2 in developmental angiogenesis and hematopoiesis is indicated by the failure to form blood islands and develop vasculature in $VEGFR2^{-/-}$ mice (40).

VEGFR2 gene encodes only one message for the full-length receptor of 1357 amino acids. Within the cell, VEGFR2 protein is produced as a 150 kDa protein without significant glycosylation. This molecule is further glycosylated to a mature 230 kDa form and expressed on the cell surface. VEGF induces auto-phosphorylation of the 230 kDa molecule only.

In tumor cells, HIF-1α is stabilized which induces hypoxia-responsive genes such as VEGF. VEGF binds to VEGFR2 on VEC and via phospholipase C - protein kinase C - mitogen activated protein kinase (PLCγ-PKC-MAPK) pathway resulting in DNA synthesis, increased permeability, and cells survival. This leads to endothelial cell proliferation and tubular

formation (191). Significant inhibition of tumor growth, angiogenesis and vasculogenesis in tumors by administration of anti-VEGFR2 antibody has been reported by several groups (193;197).

Chemokines and Chemokine Receptors

Chemokines are structurally related, small (8-14 kDa) signaling polypeptides that bind and activate the seven trans-membrane G-protein coupled receptors. Bone marrow-derived cells, endothelial, smooth muscle, stromal, and epithelial cells secrete chemokines. Chemokines are important in leukocyte movement. The inducible chemokines recruit leukocytes in response to pathophysiological conditions, whereas the constitutively expressed chemokines are involved in basal leukocyte trafficking and maintenance of lymphoid organ architecture (198-201). Chemokines can be divided into four subgroups: CXC, CC, CX(3)C, and C chemokines, where C represents cysteine residues and X represents any other amino acid.

The CXC chemokines (α group) have two cysteine residues separated by a non-conserved amino acid (X) and are important in maintaining the delicate balance in angiogenesis (42). There are 17 different CXC chemokines known in the mammalian system. CXC chemokines are further subdivided into Glutamic acid-Leucine-Arginine (ELR)-positive and ELR-negative chemokines (Table 7). The ELR^+ CXC chemokines bind to chemokine receptors CXCR1 and CXCR2, are strong attractants for neutrophils, and are pro-anagiogenic. In contrast, most ELR^- CXC chemokines bind to receptor CXCR3, chemoattract lymphocytes, and are angiostatic in nature. The only exception is the pro-angiogenic ELR^- CXC chemokine stromal cell-derived factor-1 (CXCL12/SDF-1), which binds to receptors CXCR4 and CXCR7 (43). Similar to other members

Table 7: CXC Chemokines and Chemokine Receptors

Chemokine Receptor	Chemokine	Function
CXCR2	CXCL1 / Gro-α CXCL2 / Gro-β CXCL3 / Gro-γ CXCL5 / ENA-78 CXCL6 / GCP-2 CXCL7 / NAP-2 CXCL8 / IL-8	Angiogenic
CXCR4 CXCR7	CXCL12 / SDF-1	Angiogenic
CXCR3	CXCL9 / Mig CXCL10 / IP-10 CXCL11 / ITAC	Angiostatic
CXCR3B	CXCL4 / PF-4	Angiostatic
CXCR5	CXCL13 / BCA	Angiostatic

of the ELR^{-} CXC subgroup, SDF-1α attracts lymphocytes. In addition, it directs the migration of hematopoietic stem cells and the formation of blood vessels. It is suggested to be essential in tumor angiogenesis and vasculogenesis. Chemokine receptors CXCR2, 3 and 4 have been reported to be expressed on endothelial cells (42) and are considered as important modulators of tumor vascularization and metastasis (43;202-206).

CXCR2 and Ligands

CXCR2 (IL8-beta receptor or IL8Rb, IL8R1) is one of the seven known members of the CXC chemokine receptor group. ELR^{+} chemokines, such as CXCL1,2,3/GRO-α,β,γ, CXCL5/ENA-78, CXCL6/GCP-2, CXCL7/NAP-2, and CXCL8/IL-8 bind specifically to CXCR2. It is predominantly expressed by neutrophils. However, it has also been detected in some endothelial and tumor cells (42). CXCR2 is shown to be responsible for mediating the migration of neutrophils to sites of inflammation. Knockout studies in mice suggest that CXCR2 controlled the positioning of oligodendrocyte precursors in developing spinal cord by arresting their migration (43). Anti-CXCR2 antibodies were found to block CXCL8-induced stress fiber assembly and endothelial cell migration. The signaling pathways regulated by CXCR2 are essential in angiogenesis. CXCR2 has also been found to regulate angiogenesis *in vivo* (207).

The important role of CXCR2 in tumor growth and angiogenesis has been known for a few years (207-211). ELR^{+} CXC chemokine-mediated angiogenesis is inhibited in both $CXCR2^{-/-}$ mice and in mice homozygous for CXCR2 in the presence of CXCR2 neutralizing antibody. CXCR2 neutralizing antibody was also reported to reduce pancreatic cell supernatant-mediated neo-vascularization. A decrease in the tumor-associated angiogenesis and metastatic potential has been demonstrated in murine tumor model for lung cancer in $CXCR2^{-/-}$ compared

to wild-type mice. Taken together, these studies ascertain that CXCR2 is the receptor responsible for the angiogenic activity of the ELR^+ CXC chemokines (201).

Strieter *et al.* were the first to report that CXCR2 was the putative receptor for chemokine-induced angiogenesis involving ELR^+ CXC chemokines. They identified CXCR2 on human micro vascular endothelial cells (HMVEC) at the protein and RNA level. Chemotaxis of HMVEC in response to the ELR^+ CXC chemokines was also established; anti-CXCR2 neutralizing polyclonal antibody was shown to inhibit this chemotaxis (203). Our laboratory has investigated the expression of CXCR2 on primary cultures of murine cardiac vascular endothelial cells (VEC). In contrast to the above mentioned report, we did not detect CXCR2 mRNA or protein in these cultured VEC. Nonetheless, CXCR2 was detected in the endothelium of some blood vessels in Lewis lung tumors and bone marrow-derived neutrophils. Preliminary results indicate that neutrophils might be crucial for establishing a pre-metastatic niche (Verbanac laboratory, unpublished data). Thus, CXCR2 might be involved in vascularization in tumors and possibly in facilitating tumor cell metastases.

Stromal-Derived Factor (SDF-1α) and Receptor CXCR4

Three isoforms of SDF-1 have been identified: SDF-1α, SDF-1β, and SDF-1γ, arising from alternate splicing of a single gene. Among these, SDF-1α (CXCL12) is the most well studied isoform. SDF-1α is constitutively expressed in various organs including bone, lung, liver, brain, thymus, and lymph nodes (212). It is mainly produced by stromal cells, such as osteoblasts, fibroblasts, and endothelial cells in the bone marrow (212-215). *In vitro* and *in vivo* SDF-1α is shown to be chemotactic for lymphocytes, monocytes, bone marrow derived $CD34^+$ cells, but not neutrophils (135;216). It also plays an important role in development. Mice with

targeted disruption of the *sdf-1α* gene die perinatally due to defects in B-cell and myeloid progenitors and defective cardiac septa.

CXCR4, also called fusin, is an alpha-chemokine receptor specific for SDF-1α. It is expressed by peripheral mononuclear cells, monocytes, T-cells, B-cells, endothelial cells, neurons, astrocytes, tumor cells and a variety of stem cells including cancer stem cells (217). $CXCR4^{-/-}$ mice die perinatally where as $CXCR4^{+/-}$ mice are viable, fertile, and have normal vascularization, hematopoiesis and cerebral development (214). Besides the well known role of CXCR4 as a co-factor for human immunodeficiency virus infection of T lymphocytes (218), CXCL12/SDF-1α interaction with CXCR4 plays a prominent role in tumorigenesis (206;219-222).

Recently, there have been several reports suggesting that hematopoietic cells and T-cells harbor intracellular CXCR4. Several investigators have reported the constitutive intracellular expression of CXCR4. Additionally, CXCR4 has been shown to be internalized on binding to its ligand SDF-1α (223). Kollet reported that human $CD34^{+}CXCR4^{-}$ BMC had intracellular reserves of CXCR4 that could be rapidly mobilized to the cell surface in the presence of cytokine cocktail (SCF, FLT3-L, IL-6, IL-3, and G-CSF) or in serum-starved condition *in vitro* (223). The intracellular localization of CXCR4 has also been demonstrated in human trophoblasts and T-cells (224). This has been hypothesized to be a mechanism to prevent the activation of $CXCR4^{+}$ stem cells that predominantly reside in the bone marrow, which is a rich resource of SDF-1α (225;226). CXCR4 is also an important co-receptor in HIV infection. Thus, the predominant intracellular expression of CXCR4 is considered to be a natural adaptation to prevent viral infection (218).

SDF-1α and CXCR4 in Stem Cell Homing and Mobilization

Various research groups evaluating the mechanism of hematopoietic reconstitution (stem cells homing to the bone marrow post sub-lethal radiation) have indicated that SDF-1α played a crucial role in this phenomenon (223;227;228). SDF-1α has been reported to chemoattract HUVEC and $CD34^+$ human hematopoietic progenitor cell, and mediate trans-endothelial migration of HSC *in vitro* and *in vivo* (134;135). Thus, SDF-1α is important for mobilization of HSC, EPC, and differentiated EC.

SDF-1α upregulation in HUVEC in response to VEGF and bFGF has been demonstrated by RT-PCR, western blot analysis, and flow cytometry. It was suggested that VEGF- and bFGF-mediated autocrine signaling regulated the morphologic and angiogenic properties of SDF-1α and CXCR4 in EC (229). Gurtner *et al.* reported the expression of SDF-1α was regulated by HIF-1α in HUVEC. They have also made known that *in vivo* expression of SDF-1α is directly proportional to reduced oxygen tension. They observed that secreted SDF-1α in HUVEC culture medium increased by seven to nine folds when cell culture was maintained at 1% oxygen tension for 6 to 12 hours (109;131).

SDF-1α Expression in Tumor and Other Tissue

There is growing evidence that SDF-1α and its receptors are crucial in the growth and metastasis of tumors (13;205;217). It remains inconclusive whether SDF-1α is angiogenic or angiostatic because it has been reported to attenuate the angiogenic activity of ELR^+ CXC chemokines, bFGF, or VEGF {585, 378}, but Wang *et al.* demonstrated a link between SDF-1α and CXCR4-mediated pathways and angiogenesis modulation. Angiogenesis was reported to be stimulated by two separate pathways involving differential activation of the MEK/ERK and PI3K/AKT pathways, which resulted in differential secretion IL-6, and IL-8, and TIMP-2 and

VEGF in LNCaP and PC3 prostate cancer cell lines, respectively. This cytokine-mediated angiogenesis was inhibited due to the expression of angiostatin (endothelial angiogenesis inhibitor) when CXCR4 was knocked down in tumor cells. Stimulation by SDF-1α suppressed angiostatin expression and enabled angiogenesis (230). Subsequently, it was demonstrated that CXCR4-mediated expression of glyolytic enzyme phophoglycerate kinase 1 (PGK1) and angiostatin lead to a reduction in angiogenesis when SDF-1α was low. In contrast, in the presence of high concentrations of SDF-1, VEGF, IL-6 and IL-8 induced angiogenesis (231). Thus, the interaction of SDF-1α and CXCR-4 is critical in angiogenic modulation in context of tumorigenesis.

Aghi *et al.* reported that SDF-1α was expressed by the vasculogenic glioma cells but not by nonvasculogenic glioma cells, and was responsible for attracting endothelial progenitors to tumors. In addition they demonstrated that blocking CXCR4 reduced the homing and long-term engraftment of vascular progenitors by 80% in vasculogenic tumors (62).

SDF-1α has been linked to organ-specific metastasis of some tumor-types expressing CXCR4 and/or CXCR7 (204;212;232-236). The organ-specific pattern of breast and melanoma metastasis has been correlated with the expression of chemokine receptors, including CXCR4, CCR7, and CCR10, on tumor cells {77, 114}. Furthermore, the SDF-1α-mediated invasion of human basal carcinoma cells was reported to be influenced by the upregulation of matrix metalloproteinase MMP-13 (72). MMP have been suggested to play an important role in the invasion process because their proteolytic activities assist in degradation of the extracellular matrix and basement membranes. Thus, SDF-1α has been implicated in tumor vascularization and metastatic dissemination of tumor cells.

Endothelial Cell Surface-Associated SDF-1α

Peled *et al.* were the first to demonstrate the constitutive expression of SDF-1α on vascular endothelium in bone marrow. Using *in vitro* and *in vivo* assays, they showed that murine hematopoietic progenitors ($CD34^+$ BMC) established efficient rolling on P-$selectin^+$ and E-$selectin^+$ EC, but developed firm adhesion on EC surfaces only in the presence of immobilized-SDF-1α on EC. Additionally, in the absence of selectins, SDF-1α promoted VLA-4-mediated, G protein-dependent tethering, and VCAM-mediated adhesion under shear flow (227). Their results revealed that SDF-1α-activated lymphocyte function-associated antigen-1 (LFA-1), VLA-4 and VLA-5 on immature $CD34^+$ BMC (238).

Most chemokines, including SDF-1α, bind to heparan sulfates (HS) in the extracellular matrix and on the cell surface (239-242). HS are a family of sulfated glycosaminoglycans (GAG). The chemokine concentration gradient in tissue is important for directional migration of cells and is believed to be controlled by GAGs (239). GAGs are covalently attached to core proteins on all animal cells and ECM. The binding of SDF-1α to HS is reported to involve the amino acids lysine at positions 24 and 27 and arginine at position 41; the HS-binding sites are distinct from those required for CXCR4. The binding affinity of SDF-1α for HS has been calculated and is reported to range from 39-93 nM (243;244) compared to 1.67 nM for CXCR4 (243). The association of SDF-1α with HS is shown to prevent its inactivation by the serine protease CD26/DPP IV, which selectively removes the N-terminal dipeptide from SDF-1α (244-247). The constitutive expression of SDF-1α associated with heparan sulfate in cutaneous capillary endothelium was reported to trigger specific arrest of Kaposi Sarcoma-associated herpes virus-infected cells and dictated the preferential localization of Kaposi Sarcoma in the skin under physiologic shear flow (248).

Ceradini *et al.* detected a significant increase in endothelial cell surface-bound SDF-1α in hypoxic cell cultures by flow cytometry. They reported that greater numbers of $CXCR4^+$ EPC adhered to HUVEC pre-conditioned in hypoxic condition compared to HUVEC monolayers cultured under normoxic conditions. This effect was abolished by antibody-mediated blockage of SDF-1α and CXCR4 interaction. In addition, *in vivo* results demonstrated that $CXCR4^+$ progenitor cell localization to regenerating tissue was dependent on the hypoxia-induced SDF-1α gradient (109;131).

Similarly, it is likely that extracellular matrix-associated and endothelial cell-associated SDF-1α not only acts as an important chemotactic factor in recruiting EPC to tumors but also mediates the adhesion, retention, and incorporation of bone marrow-derived cells into the tumor vasculature, thereby contributing to tumor vasculogenesis.

CXCR4 Expression in Tumors

Several investigators have reported the involvement of CXCR4 and SDF-1α interaction in cancer progression (Reviewed by (217). This receptor-ligand interaction has been shown to promote angiogenesis and organ-specific migration of tumor cells in many cancers, like breast (249), (250), lung (233;251), ovarian (252), renal (13), and prostate (230) cancer, neuroblastomas (253) and glioblastomas (62). CXCR4 has also been strongly implicated in growth of several neuroectodermal tumors and small cell lung carcinoma (Reviewed by (254).

Muller *et al.* showed that the human breast cancer cell line MDA-MB-231 expressed CXCR4 and migrated in response to SDF-1α. They demonstrated that these cells migrated in response to protein extracts from lung, liver, bone marrow, lymph nodes, skin, and muscle. This chemotaxis was significantly inhibited by anti-CXCR4 antibody in the lung, liver, bone marrow, and lymph node protein extracts (212). Their results reinforced Paget's theory of "seed and soil"

and indicated the important function of SDF-1α and CXCR4 in determining the metastatic destination of tumor cells (255).

Hypoxia is an important mechanism that alters the metastatic behavior of tumor cells *in vivo*. It is reported to favor metastasis by up-regulating CXCR4 on tumor cells via the hypoxia-inducible factor-1α (HIF-1α) (256;257). Hypoxic conditions in the tumor mass promotes transcription and translation of HIF-1α, whereas under physiological conditions, the tumor suppressor protein von Hippel-Lindau negatively regulates CXCR4 expression by degradation of HIF-1α (258). A recent report by Maréchal *et al.* showed that CXCR4 expression in pancreatic tumors had a positive correlation with HIF-1α. They proposed that CXCR4 was a valuable prognostic factor and therapeutic target in pancreatic cancer. This study also reported the overexpression of CXCR4 in endometrial cancer. In a separate study, HEC1A human endometrial cancer cells were reported to be able to generate diffused metastases in nude mice. The number and size of these metastases was demonstrated to be dramatically reduced by simultaneous treatment with neutralizing anti-CXCR4 antibody (259). Another group reported a significant reduction in the growth of both colon and pancreatic tumors in mice that received intra-peritoneal injections of anti-CXCR4 antibody. Administration of anti-CXCR4 antibody lead to a significant reduction in capillary density but did not affect the expression of VEGF in tumors (215). Similarly, Aghi *et al.* reported that in the presence of AMD3100 (CXCR4 antagonist) the number of bone marrow-derived cells contributing to tumor endothelium was significantly reduced. Thus, the interaction between CXCR4 and SDF-1α has been established to be important for tumor angiogenesis and metastasis, and interrupting this association could be a valuable anti-cancer therapy.

A Second SDF-1α Receptor: CXCR7

CXCR7/RDC1 was subsequently identified in 2005 and 2006 as a novel receptor for SDF-1α and CXCL11/I-TAC (260-262). CXCR7 has been reported to be expressed on malignant cell types and fetal liver cells. High levels of CXCR7 mRNA were detected in healthy murine tissues: heart, lung, brain, kidney, testes, ovary, and 14 day-old fetus; thymus and liver had relatively lower expression.

Similar to the $CXCR4^{-/-}$ mice, mice with a homozygous deletion of CXCR7 died at birth with ventricular septal defects and semilunar heart valve malformation {367}. This report also confirmed that the principal chemokine ligand for CXCR7 was SDF-1α, but SDF-1α did not induce signaling through CXCR7; CXCR7 formed a functional heterodimer with CXCR4 and enhanced SDF-1α-induced signaling (263). Unlike many other chemokine receptors, ligand activation of CXCR7 did not cause calcium mobilization or cell migration. The interaction of SDF-1α with CXCR7 resulted in a proliferative effect, in contrast to CXCR4, which mediated chemotaxis (260).

Recently, Wang *et al.* (235) showed that CXCR7 expression was correlated with tumor aggressiveness in prostate cancer. CD44 and cadherin-11 were reported to be expressed downstream of CXCR7, and were suggested to contribute to the invasiveness of prostate cancer cells. CXCR7 was also demonstrated to regulate the expression of pro-angiogenic factors IL-8 and VEGF, which are known modulators of tumor angiogenesis.

Burns *et al.* (260) reported that more CXCR7-transfected MDA-MB-435S breast cancer cells adhered to HUVEC cultures stimulated by TNF-α and IL-1β. In addition, when HUVEC were stimulated with TNF-α and IL-1β, an increase in the expression of CXCR7 was observed. Based on these experiments they concluded that although the expression of CXCR7 on any one

cell type was sufficient to promote some cell-cell interactions, CXCR7 expression on both activated HUVEC and tumor cells concomitantly produced maximal adherence *in vitro*. They also reported that the administration of a CXCR7 antagonist resulted in a decrease in tumor growth in immunodeficient and syngeneic mice engrafted with human B lymphoma, human lung carcinoma, or mouse lung carcinoma. Each of these tumors was shown to express CXCR7. Thus, they proposed that CXCR7 was a viable target for development of novel cancer therapeutics.

Miao *et al.* (236) demonstrated the expression of CXCR7 on breast and lung tumor cell lines 4T1 and LLC, respectively. Furthermore, they reported that tumor growth was impaired when CXCR7 was knocked down in these tumor cells. Interestingly, they also observed specific expression of CXCR7 on tumor-associated blood vessels, but not on normal vasculature. They also reported that CXCR7 promoted the growth of breast and lung tumors and enhanced lung metastasis. Thus, suggesting that CXCR7 was important in promoting tumor development and progression (236). This premise was consistent with the clinical observation that higher expression of CXCR7 was linked to early and metastatic recurrence in pathological stage I non-small cell lung cancer (234).

Synopsis of Introduction

Tumors arise due to genetic and epigenetic changes that lead to transformation and uncontrolled proliferation of cells. These tumor cell clusters rely on diffusion of oxygen and nutrients for expansion; these become limiting factors as tumors reach 2-3 millimeters in size. For further propagation and progression, tumors must undergo an ‘angiogenic switch’ to develop tumor vasculature. Thus, inhibition to tumor vascularization is an important control point in tumor development and cancer progression. Several hypoxia-induced growth factors,

chemokines, and cell adhesion molecules have been shown to participate in tumor angiogenesis that is mediated by activated mature endothelial cells. In addition, there is growing evidence that some of these proteins are important in mediating tumor vasculogenesis by mobilizing and chemoattracting the bone marrow-derived endothelial progenitor to tumors. Stromal-derived factor (SDF-1α) is one of the well characterized hypoxia-induced, secreted proangiogenic chemokines. Several cell types, including endothelial cells, produce SDF-1α. Similar to other chemokines, secreted SDF-1α binds to proteglycans in the extracellular matrix and on cell surfaces. In addition, SDF-1α-mediated chemoattraction of $CXCR4^+$ endothelial cells and hematopoietic stem cells *in vitro* and to hypoxic regions in ischemic injuries *in vivo* has been demonstrated. SDF-1α is elevated in certain tumors, implicated in organ-specific metastasis of tumor cells, and involved in angiogenesis.

The literature in the field has thus led us to propose a specific role for SDF-1α in tumor vasculogenesis. These data are consistent with the proposal that tumor-derived stromal derived factor-1α (SDF-1α) binds to tumor endothelium and extracellular matrix and recruits and mediates the adhesion of circulating bone marrow-derived $CXCR4^+$ endothelial progenitors.

DISSERTATION HYPOTHESIS AND SYNOPSIS OF EXPERIMENTS

We hypothesize that stromal derived factor-1α mediates tumor vasculogenesis, recruiting bone marrow-derived endothelial progenitor cells to tumors.

LLCaB, a subclone of the murine Lewis lung adenocarcioma tumor cell line (LLC1), was used in this study. First, we evaluated the development of LLCaB subcutaneous tumor and metastases in syngeneic immunocompetent C57Bl/6 mice. Subsequently, subcutaneous and metastatic tumor tissue samples from experimental mice and healthy tissue samples from naïve

control mice were analyzed for the expression of SDF-1α and E-selectin. The expression of cognate receptor/ligands for SDF-1α and E-selectin and endothelial progenitor markers were evaluated on Lin^- BMC. The use of Lin^- BMC for *in vitro* and *in vivo* experiments was a practical alternative to endothelial progenitor cell purification. Dermal fibroblasts were used as a control cell type in both *in vitro* and *in vivo* experiments. Next, *in vitro* adhesion assays were conducted to evaluate the role of SDF-1α and E-selectin in mediating adhesion of Lin^- BMC with tumor-derived cells.

In the initial *in vivo* experiments, biolocalization of vascular endothelial cells (VEC), isolated from *EGFP*-transgenic mice, in tumor-bearing mice was evaluated by microscopy. Although *EGFP*-VEC were specifically detected in metastatic lesions, quantization of VEC homing was compromised by tissue autofluorescence and artifactual fluorescence. This prompted the development and standardization of a qPCR assay to detect tissue-localized *EGFP*-transgenic cells. Finally, the biolocalization of systemically administered *EGFP*-Lin^- BMC and *EGFP*-dermal fibroblasts, 3 days after cell injection, in subcutaneous and metastatic tumors, and other organs was evaluated by qPCR. Subsequently, long-term (7-day) retention of *EGFP*-Lin^- BMC in metastatic lesions was also assessed.

These data from *in vitro* and *in vivo* experiments lead to the development of a model suggestive of several functions that SDF-1α might be involved in tumor biology.

CHAPTER II: MATERIALS AND METHODS

Mice

Vascular endothelial cells (VEC) were isolated from neonatal C57Bl/6 mice that constitutively expressed the enhanced green fluorescent protein (*EGFP*) transgene (C57Bl/6-Tg(ACTb*EGFP*)10sb/J, #003291 and/or C57BL/6-Tg(UBC-GFP)30Scha/J, # 004353, The Jackson Laboratory). Strain #003291 is a heterozygous-bright, homozygous-lethal strain; the hemizygous mice used in this study were obtained by breeding transgenic male mice with C57Bl/6 wild-type females (#664, The Jackson Laboratory, Bar Harbor, ME). Strain #004353 is maintained as a homozygous strain. The above mentioned *EGFP*-transgenic mice strains were also used for harvesting bone marrow and purifying the lineage-negative bone marrow cells (*EGFP*-Lin$^-$ BMC). Two to six month-old wild-type C57BL/6 mice were used as recipients of syngeneic tumor cells and *EGFP*-VEC and *EGFP*-Lin$^-$ BMC. All mice strains were originally purchased from Jackson Laboratory and maintained in an in-house breeding colony. East Carolina University Animal Use and Care Committee approved all animal studies.

Isolation and Culture of Cell from Murine Tissue

Cardiac Vascular Endothelial Cells (VEC)

VEC were isolated from 2-5 day-old mouse pups (5-30 per preparation) and maintained in culture for 2-3 weeks as described (Figure 2A; (94)). A minimum of 5 pups were used for each preparation. The pups were euthanized using Isoflurane (Webster Veterinary, Sterling, MA), sterilized by a quick rinse in 70% ethanol, and followed by opening the chest cavity and removing the hearts using curved forceps. The hearts were placed in a 35 mm Petri dish containing Dulbecco's Modified Eagle Medium: Nutrient Mixture F-12 (DMEM-F12, Invitrogen,

Carlsbad, CA) at room temperature (RT). The hearts were minced with a sterile disposable scalpel with a no. 10 stainless steel blade. The tissue was then incubated in 0.1% DNase / 2 mg/mL Collagenase (Sigma, St. Louis, MO) in DMEM-F12 media containing 5% fetal calf serum (FCS) at 37°C in 5% carbon dioxide (CO_2) for 1 hour (3 mL DNase-Collagenase per 5-10 pups). The digested tissue was diluted in DMEM-F12 and collected in a 15 mL tube. Cell suspension was vortexed; the larger undigested tissue chunks were allowed to settle to the bottom of the tube and were removed using a sterile plastic transfer pipette. The cells in the remaining supernatant were pelleted by centrifugation at 300 × g for 10 minutes. The cell pellet was resuspended at 2 mL per 5 hearts in 38% Sterile Isotonic Percoll. Sterile Isotonic Percoll was a 90% Percoll (Pharmacia, Piscataway, NJ) solution in Hanks Buffered Salt Solution (HBSS, Gibco, Carlsbad, CA). The cells were pelleted by centrifugation at 800 × g for 20 minute at 25°C. The pellet containing the enriched VEC was resuspended in 5 mL VEC media, plated in a 35 mm tissue culture dish and incubated at 37°C for 1 hour. The VEC media consisted of DMEM-F12 high glucose (Gibco) with 2.438 g/L sodium bicarbonate (pH 7.0, 320±5 mOsm/L) supplemented with 5% FCS (Invitrogen), 15 μg/mL endothelial cell growth supplement (Sigma), 2 U/mL heparin (Sigma), 10 mM 4-(2-hydroxyethyl)-1-piperazineethanesulfonic acid (HEPES, Sigma), 1 mM sodium pyruvate, insulin transferrin-selenium (25 μg/mL, 25 μg/mL, 25 ng/mL; ITS, Sigma). The final pH was adjusted to 7.0 and osmolarity to 320±5 mOsm/L. Non-adherent cells were gently rinsed off using a plastic transfer pipette and transferred to gelatin-coated 6-well plates.

Cells from 5 hearts were plated per well. Next Day, the media was changed to remove the non-adherent red blood cells. Three to five days later, cells were purified by selective trypsinization with 0.25% trypsin-0.05% ethylenediaminetetraacetic acid (ETDA, Invitrogen)

after rinsing with Dulbecco's phosphate buffered saline (DPBS) without calcium (Ca^{2+}) and magnesium (Mg^{2+}). Cells were observed under the microscope, and at the first sign of detachment, cells were washed off the plate and re-plated in gelatin-coated plates or flasks. Cells were subsequently passaged when cultures reached 80% confluency. VEC were expanded in culture for up to 3 weeks.

VEC were routinely isolated from C57Bl/6-Tg(ACTb*EGFP*)10sb/J (Homozygous Actb-*EGFP*) transgenic mice as the homozygous Actb-*EGFP* mice are not viable. Nonetheless, the VEC isolated from both strains fluoresce with comparable brightness (Figure 2B).

Bone Marrow Cells (BMC)

Mice were euthanized by overdose of Isofluorane followed by cervical dislocation. The femur and tibia from the hind limbs were removed and attached muscle tissue was removed from the bones using clean gauze. The bones were placed in a 35 mm Petri dish containing 1X HBSS (without Ca^{2+} and Mg^{2+}) containing 0.1% Bovine Serum Albumin (BSA, Sigma) or Iscoves media (Gibco). The pH and osmolarilty of 1X HBSS and Iscoves were adjusted to 7.0 and 320±5 mOsm/L respectively. The ends of the bones were cut off. Using a 22-25 gauge needle and 10 cc syringe, the marrow from the bones were flushed with Iscoves or 1X HBSS with 0.1% BSA (HBSS/BSA). The cell suspension was triturated using a transfer pipette to break tissue chunks. The suspension was then centrifuged at 300 × g at 10°C for 10 minute. The bone marrow cell (BMC) pellet was resuspended in Iscoves or HBSS/BSA. RBCs were lysed on ice for 10 minutes using freshly prepared RBC lysis buffer [155 mM ammonium chloride (NH_4Cl) and 12 mM sodium bicarbonate ($NaHCO_3$)]. The volume was increased to 50 mL and the cell suspension was then passed though disposable 70 μm nylon cell strainer (BD Falcon, Franklin Lakes, NJ) to remove pieces of bones and debris. The cells suspension was centrifuged at 300 × g for 10

Figure 2: Isolation of Murine Cardiac Vascular Endothelial Cell

A) Protocol for isolating micro vascular endothelial cells from hearts of mouse neonates.

B) Histogram comparing the green fluorescence intensity of VEC isolated from C57Bl/6, hemizygous Actb*EGFP*, and homozygous Actb*EGFP*-transgenic mice. Although, the homozygous Actb*EGFP* mice have twice the number of *egfp*-transgene copies compared to the hemizygous Actb*EGFP*, the green fluorescent intensity was comparable in VEC isolated from both strains of mice.

A

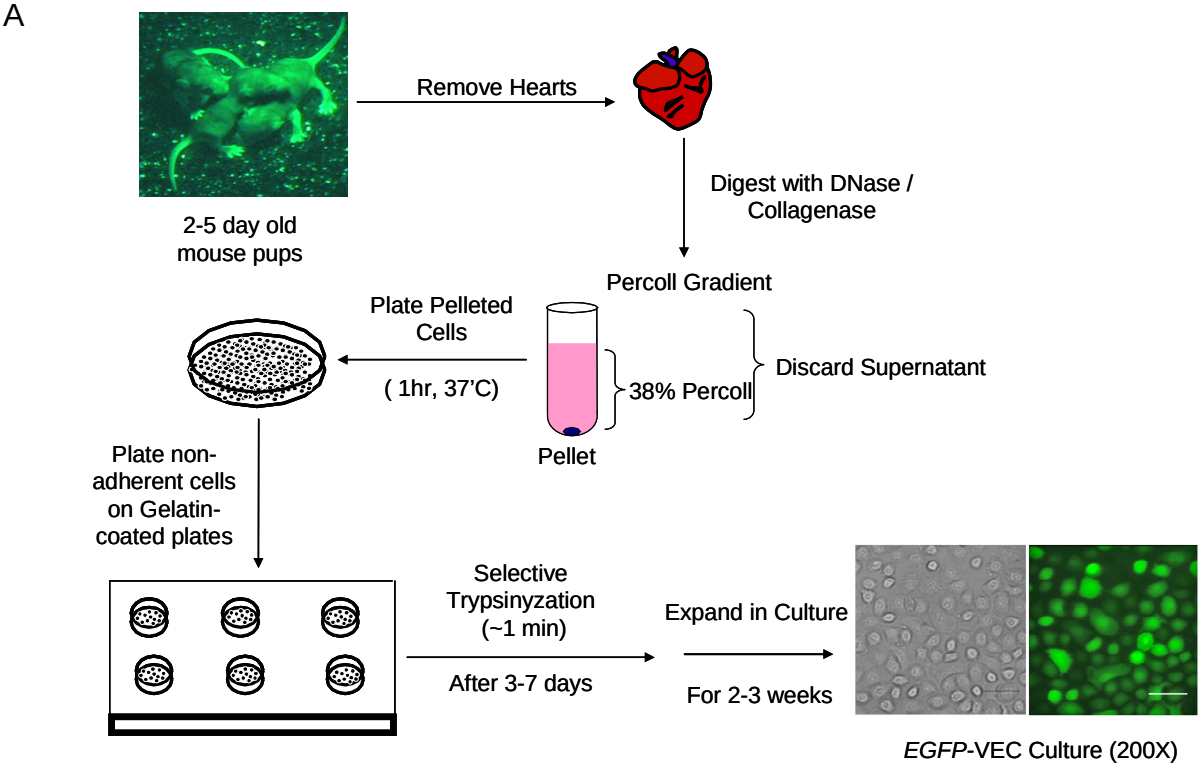
Remove Hearts
2-5 day old mouse pups
Digest with DNase / Collagenase
Percoll Gradient
Plate Pelleted Cells
(1hr, 37'C)
38% Percoll
Discard Supernatant
Pellet
Plate non-adherent cells on Gelatin-coated plates
Selective Trypsinyzation (~1 min)
After 3-7 days
Expand in Culture
For 2-3 weeks
EGFP-VEC Culture (200X)

B

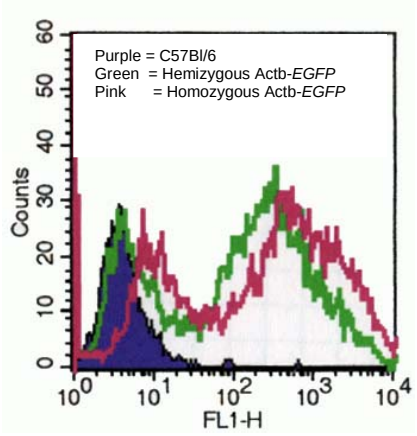
Purple = C57Bl/6
Green = Hemizygous Actb-EGFP
Pink = Homozygous Actb-EGFP
Counts
FL1-H

minutes at 10°C and cell count was done using 1% acetic acid and Trypan Blue (Gibco Invitrogen) on a hemocytometer.

Bone Marrow-derived Lineage-negative Cells (Lin^- BMC)

The lineage-positive cells were immunomagnetically depleted from the BMC with Dynabeads (Dynal Biotech, Oslo, Norway). Biotinylated anti-mouse antibodies were added to the BMC suspension in 1X HBSS containing 0.1% BSA and incubated on a rotator for 30-45 minutes at 4°C. Two microliters of each pre-diluted antibody, namely anti-CD3 (clone 145-2C11), anti-CD8, anti-CD11b (clone M1/70), anti-CD45R/B220 (clone RA3-6B2), anti-Gr-1 (clone RB6-8C5), and anti-Ly-76 (clone TER-119) (Biotin Mouse Lineage Panel, BD Biosciences), were added per 2×10^6 BMC. After centrifugation of the labeled cells, the cell pellet was resuspended at 1×10^7 cells per mL. Streptavidin-coated Dynabeads (DYNAL Cellection™ Biotin Binder, Dynal Biotech) were added to the cell suspension at a ratio of eight beads per cell and the cell suspension was incubated on a rotator for 45-60 minutes at 4°C. This cell-bead suspension was placed on a Dynal Magnetic Particle Concentrator (Dynal Biotech, Oslo, Norway) for 5 minutes to allow the cells coated with antibody and magnetic beads to bind to the magnet. The supernatant containing the Lin^- BMC were collected and washed with HBSS/BSA (Figure 3). Flow cytometric analysis of the enriched cells stained with biotinylated lineage panel antibodies and streptavidin-Fluorescein isothiocyanate (SAv-*FITC*) or SAv-Phycoerythrin (*PE*) confirmed the purity of the cell population. The Lin^- BMC were ~95% free of lineage-committed cells. The Lin^- BMC were used for *in vitro* and *in vivo* assays.

Dermal Fibroblasts

Fibroblasts were isolated from the dermis of 1-2 day-old mouse pup skin as schematically represented in Figure 4 (method adapted from (264). 1-3 day old pups were euthanized using

Figure 3: Protocol for Enriching Lineage-negative Bone Marrow Cells

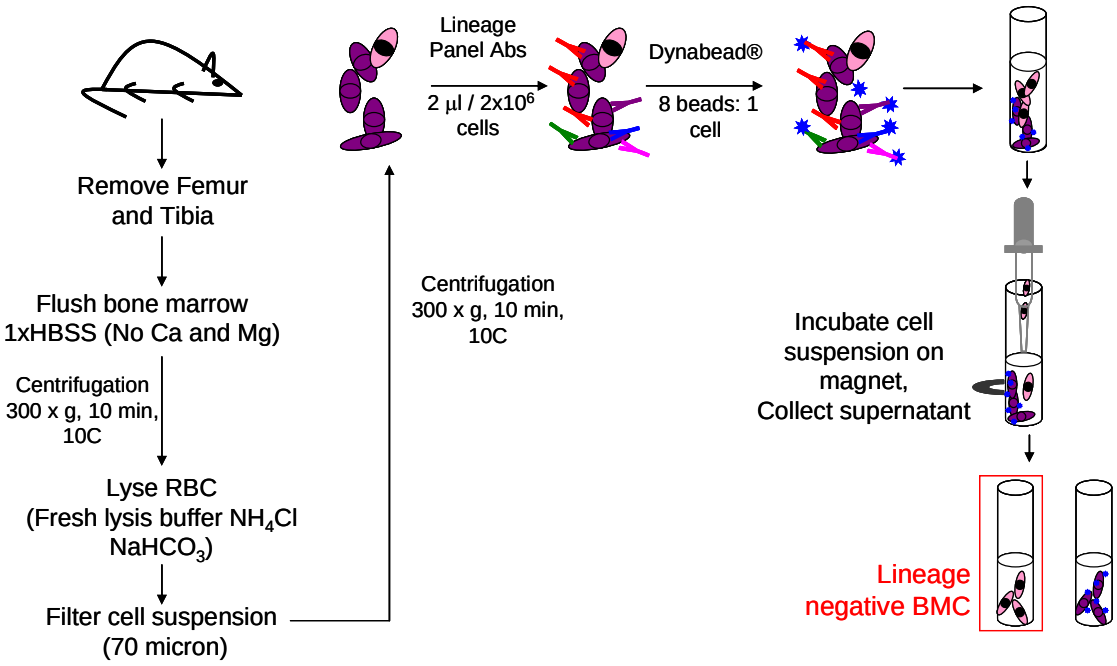
Remove Femur
and Tibia
Flush bone marrow
1xHBSS (No Ca and Mg)
Centrifugation
300 x g, 10 min,
10C
Lyse RBC
(Fresh lysis buffer NH_4Cl
$NaHCO_3$)
Filter cell suspension
(70 micron)
Centrifugation
300 x g, 10 min,
10C
Lineage
Panel Abs
2 µl / 2x10^6
cells
Dynabead®
8 beads: 1
cell
Incubate cell
suspension on
magnet,
Collect supernatant
Lineage
negative BMC

Isofluorane, sterilized with 70% ethanol, and the dorsal and ventral trunk skins were excised. Skins were incubated dermal side down in sterile 35 mm Petri dishes and incubated overnight at 4°C in 0.25% trypsin (Invitrogen). The epidermis was peeled off the dermis and discarded using two angled fine tip forceps. The epidermis was translucent white and the dermis was light brown to black in color. The dermal pieces were minced using sterile scissors and incubated at 37°C in 5 mL 0.1% Collagenase Type I (Worthington Biochemical, Freehood, NJ) per 3-5 skins. The dissociated dermis solution was diluted approximately 1:10 by increasing the volume to 50 mL with Dulbecco's Modified Eagles Medium (DMEM) containing high glucose (4500 mg/L D-glucose). This cell suspension was then filtered though sterile gauze and centrifuged at 200 x g for 7 minutes. The supernatant was carefully aspirated and the cell pellet was resuspended in DMEM containing 5% FCS and incubated in a humidified incubator with 5% CO_2 at 37°C. The next day, non-adherent cells and debris were removed and fresh media was added to the cell culture. Cells were detached from culture using 0.25% trypsin-0.05% EDTA and passaged when cultures reached 80% confluency. The dermal fibroblasts were kept in culture for a maximum of 10 days.

Dissociated Lewis Lung Subcutaneous Tumor Cell Culture

The protocol for culturing dissociated LLCaB subcutaneous tumor was adapted from our laboratory's previously established protocol to isolate endothelial cells from human tumors (265). Briefly, subcutaneous tumors were surgically removed and rinsed in cold DPBS (pH 7.0, 320±5 mOsm/L). Tumor tissue was then transferred into 20 mL of 10 mM EDTA in DPBS in 50 mL tubes and incubated on ice for 30 minutes. Next, the tumor tissue was minced using a scalpel and each 12 gm of tumor tissue was incubated in 15 mL of 0.1% DNase (Sigma) / 2 mg/mL Collagenase II (Sigma) in DMEM containing high glucose in 50 mL tubes.

Figure 4: Protocol for Isolating Dermal Fibroblasts from Mouse Neonates

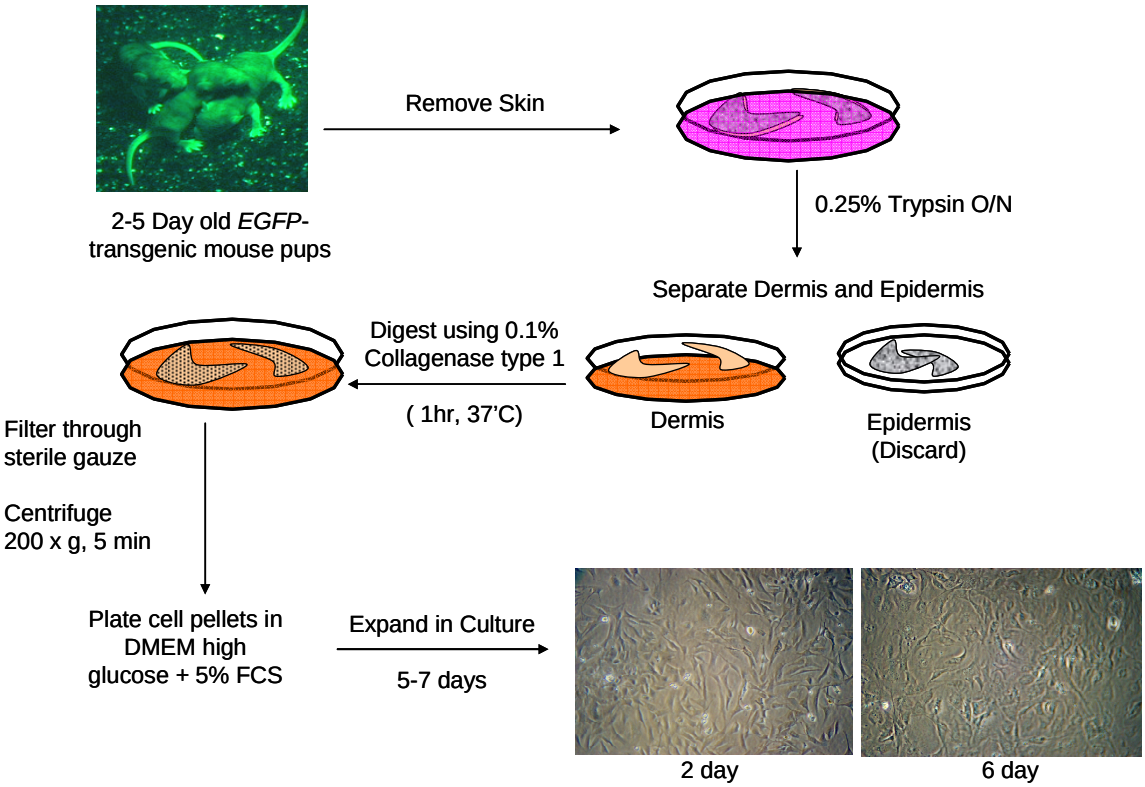
Remove Skin
2-5 Day old *EGFP*-transgenic mouse pups
0.25% Trypsin O/N
Separate Dermis and Epidermis
Digest using 0.1% Collagenase type 1
(1hr, 37'C)
Dermis
Epidermis (Discard)
Filter through sterile gauze
Centrifuge 200 x g, 5 min
Plate cell pellets in DMEM high glucose + 5% FCS
Expand in Culture
5-7 days
2 day
6 day

Tumor tissue was placed on a rotating shaker (150-200 rpm) for 1.5-2 hours at 37°C. The dissociated tumor tissue was then diluted 10 times in DMEM-high glucose and the suspension was filtered through 70 μm disposable cell strainers. The filtered cells were centrifuged at 300 x g for 10 minutes at 10°C. The cell pellet was resuspended in VEC media and cells were cultured in gelatin-coated flask. Cultures were rinsed to remove tissue debris and non-adherent cells and fresh media was added the next day. Cultures were passaged when cells reached 80% confluency; 0.25% trypsin-0.05% EDTA was used to detach cells from culture flasks.

Culture of Established Cell Lines

Lewis Lung Carcinoma Cells (LLCaB)

LLCaB is a subclone derived from a bone metastasis in a C57BL/6 mouse bearing a subcutaneous Lewis Lung Carcinoma (LLC1, ATCC #CRL-1642), and was provided to our laboratory by Dr. C. J. Kovacs and Mark Evans of the Department of Radiation Biology and Oncology at East Carolina University, Greenville, NC. LLCaB were cultured in DMEM containing high glucose (4500 mg/L D-glucose), sodium bicarbonate (3.7 mg/L) with 10% fetal calf serum in a humidified incubator at 37°C with 5% CO_2. The LLCaB culture medium was set to 320±5 mOsm/L and pH of 7.0. When the cell culture approached 80% confluency they were rinsed with DPBS, incubated with 500 μl of 0.25% trypsin for 2-5 minutes and collected using DMEM. The cell suspension was split 1:6-1:12 and placed in new flasks.

Brain Endothelioma Cells (bEnd.3)

The mouse brain endothelioma cell line (bEnd.3) express proteins that are specifically expressed by activated endothelial cells found in ischemic tissue and tumor. Thus, bEnd.3 cell line was purchased from ATCC (#CRL-2299) to use as a surrogate for tumor-derived endothelial

cells. The bEnd.3 cells were cultured in DMEM containing high glucose (4500 mg/L D-glucose), low sodium bicarbonate (1.5 mg/L) and 10% fetal calf serum, in a humidified incubator at 37°C with 5% CO_2. The bEnd.3 culture medium was set to 320±5 mOsm/L and had a pH of 7.0. When the cell culture approached 80% confluency they were rinsed with DPBS, incubated with 500 µl of 0.25% trypsin - 0.05% ETDA for 2-5 minutes and collected using DMEM.

3T3-L1 Pre-Adipocyte Cells

The 3T3-L1 (ATCC# CL-173) pre-adipocyte cell line was a gift from the laboratory of Philip Pekala in the Department of Biochemistry and Molecular Biology at East Carolina University. These cells were cultured in the recommended DMEM containing high glucose (4500 mg/L D-glucose), low sodium bicarbonate (1.5 mg/L) and 10% newborn calf serum (Invitrogen, Carlsbad, CA) in a humidified incubator at 37°C with 5% CO_2. The 3T3-L1 culture medium was set to 320±5 mOsm/L and a pH 7.0. These cells are a sub-strain from 3T3 cells from Swiss albino mice, which undergo a pre-adipose to adipose like conversion as they progress from a rapidly dividing to a confluent and contact-inhibited state.

Development of Lewis Lung Adenocarcinoma Tumors

Subcutaneous Tumors

Hair on the right flank of the C57Bl/6 mice was removed by shaving and application of Nair Hair Remover® at least two days prior to injecting tumor cells. LLCaB cells were harvested using 0.25% trypsin-0.01% EDTA and placed in DMEM for injection. C57Bl/6 mice were injected subcutaneously (s.c.) in the right flank with 5×10^5 LLCaB cells in 100 µl. Tumors became palpable in 7-10 days. Tumor growth was documented by measuring tumor size using digital calipers. Tumor volume was calculated as (width × width × length) / 2.

Pulmonary and Hepatic Tumors

Lung and liver metastases were induced in C57Bl/6 mice using a previously described method (4). Briefly, subcutaneous tumors were developed as described above. The subcutaneous tumors were surgically removed when they reached a volume of 1500 mm^3. Mice were closely monitored for weight loss and lethargy for two-three weeks following tumor removal. During this period the tumor cells that had seeded in the lung and liver developed into secondary pulmonary and/or hepatic tumors. The weight and diameter of each macroscopically visible lung and liver metastases was noted. Metastatic tumor volumes were calculated (assuming spherical shape) by $(4\pi r^3) / 3$ where r = radius. Tissue harvested were either flash frozen in liquid nitrogen or embedded in Tissue Tek® OCT (Optimum Cutting Temperature) compound (VWR Scientific Products, Suwannee, GA) and frozen using dry-ice and acetone (Sigma).

Hematoxylin and Eosin (H&E) Staining of Tissue Sections

Frozen cryostat sections were fixed by immersing slides in acetone for 20 minutes then rinsed with distilled water. Slides were serially dipped in Harris' hematoxylin (Sigma) for 1 minute, 3-10 quick dips in acid alcohol (1% hydrochloric acid in 70% ethanol), ammonium water (0.2% ammonium hydroxide in distilled water) for 1 minute, Eosin Y for 30 seconds with intermittent rinses in water (twice for 2 minutes each). Stock Eosin was prepared by dissolving 1 gm Eosin (Sigma) in 20 mL distilled water and 80 mL 95% Ethanol. Working Eosin solutions was prepared by combining 1 part stock Eosin with 3 parts 80% Ethanol; 0.5 mL acetic acid was added to 100 mL of working solution before use. The sections were dehydrated by sequential 2 minute changes in 95% ethanol (twice) and 100% ethanol (twice) to remove excess Eosin stain and finally in xylene. Coverslips were mounted on slides using Permount® (Fisher Scientific, Pittsburg, PA).

Analysis of RNA Expression

RNA Isolation

Ribonucleic acid (RNA) was isolated from cell pellets or frozen tissue specimens. Trizol® (Invitrogen) was added to pulverized tissue or cell pellets (1 ml / 2×10^6 cell). After incubation at RT for 5 minutes, chloroform was added and the suspension was thoroughly mixed by inversion. The tubes were centrifuged at 12,000 rpm for 15 minutes at 4°C. The aqueous layer was transferred into another tube and equal volume of 100% Isopropanol (Sigma) was added. These tubes were mixed and incubated at -20°C overnight to precipitate RNA. RNA was pelleted by centrifugation at 12,000 rpm for 15 minutes at 4°C. The RNA pellets were rinsed with 75% ethanol, allowed to air dry and resuspended in nuclease-free water (Ambion, Foster City, CA). RNA concentration was measured spectrophotometrically. The concentrations of all RNA samples were adjusted to 1 mg/mL.

cDNA Preparation

Complementary DNA (cDNA) was prepared using 5 μg RNA as previously described (266). Five microliters of RNA (1 μg/μl) was incubated with 0.5 μg of oligo (dT) primer at 65°C for 7 minutes and chilled on ice before adding a 20 μl reaction mixture containing 50 mM Tris-HCl (pH 8.3), 75 mM KCl, 3 mM $MgCl_2$, 10 mM DTT, 0.5 mM dNTP, 5 units of cloned placenta RNase inhibitor and 200 units of Maloney Murine Leukemia Virus Reverse Transcriptase (MLV-RT). For very dilute RNA samples a maximum volume of 10.5 μl RNA was used. All reagents were purchased from Gibco-Invitrogen. Samples were incubated for 1 hour at 37°C, followed by heating at 95°C for 5 minutes. cDNA samples were diluted 1:5 with water prior to freezing. All cDNA samples were stored at -20°C.

Reverse Transcriptase Polymerase Chain Reaction (RT-PCR)

Reverse transcriptase PCR Gene Expression Assays (Applied Biosystems, Foster City, CA) were used to evaluate the expression analysis of VEGF (Mm00437308_m1), SDF-1α (Mm00457276_m1), VEGFR2 (Mm00440111_m1), and CXCR4 (Mm01292123_m1). Beta-2-microglobulin (Mm00437762_m1) was used as the endogenous control. These are proprietary assays, detected with a FAM/MGB-labeled probe. 5 microliters of cDNA was used as the template in a 25 μl total reaction mixture containing 1X TaqMan® Universal Master Mix, nuclease free water and primer-probe. PCR was carried out under standard cycling condition: 2 minutes at 50˚C, 10 minutes at 95˚C followed by 40 cycles of 15 seconds at 95˚C and 1 minute at 60˚C in Applied Biosystems 7000 Thermocycler (Applied Biosystems, Inc).

Analysis of Protein Expression

Tissue Homogenization and Protein Quantitation

Protein samples were prepared by sonication of pulverized frozen tissue in DPBS containing the tissue-culture approved Protease Inhibitor Cocktail (Sigma) and 0.05% Triton X (Sigma) (2 mL / gram of tissue). Protein concentrations were determined using the Pierce Micro BCA Protein Assay (Thermo Scientific, Rockford, IL). Lysates (diluted 1:100), and standards (provided in the kit) were added to reagents on a 96-well flat-bottomed plate and incubated as according to manufacturers instructions. Plates were read at 562 nm on a Synergy HT Multi-Mode Microplate Reader (BioTek, Winoski, VT) and concentrations determined based on standard curve (polynomial equation).

Quantitation of Chemokines by Enzyme-Linked Immunosorbant Assay (ELISA)

Concentration of chemokine SDF-1α in tissue homogenates was determined using

Quantikine® ELISA kits (R&D Systems, Minneapolis, MN). Undiluted protein samples from cell and tissue lysates, and serum were assayed for SDF-1α expression. The amount of SDF-1α in each sample was calculated based on the standard curve (polynomial equation) from each assay. SDF-1α concentrations (pg/mL) in tissue homogenates were normalized to the protein concentration (mg/mL) of each sample; thus, the results are reported as picogram (pg) SDF-1α per milligram (mg) of protein.

Flow cytometric Analysis of Cell Surface and Intracellular Proteins

Flow cytometry was used to measure the cell surface and total (intracellular and cell surface) expression of specific proteins on cultured cell and bone marrow-derived cells. All adherent cell cultures were harvested using 0.25% trypsin-0.05% EDTA. Cell counts and percent viability was calculated using Trypan blue exclusion assay. Cells were washed with 1% bovine serum albumin (BSA, Sigma) and 0.05% sodium azide (Sigma) in DPBS (DPBS/BSA/Azide). 1×10^5 cells per 10 µl DPBS/BSA/Azide were aliquoted in 5 mL polystyrene tubes and primary labeled antibodies were added.. To measure both intra- and extracellular protein expression the cells were fixed using 0.5% paraformaldehyde and permeabilized using 0.5% saponin prior to addition of antibodies. Cells were washed with 4 mL DPBS/Azide, centrifuged at 300 × g for 10 minutes. Cell pellets were fixed using 200 µl of 1% paraformaldehyde (Electron Microscopy Sciences, Hatfield, PA) while vortexing. Cells were vortexed and incubated at RT for 15 minutes. Specific antibodies for flowcytometry from BD Pharmingen were used at 1 µg per 1×10^5 cells included PECAM-1 / CD31 (clone MEC13.3), CD34 (clone RAM34), VCAM-1 / CD106 (clone MVCAM.A), LAMP-1 / 107a (clone 1D4B), E-selectin / CD62E (clone 10E9.6), CXCR4 / CD184 (clone 2B11), cKit / CD117 (clone 2B8), Sca-1 (clone E13-161.7), VEGFR2 (clone

Avas12α1), and CD43 (clone S7). Specific antibodies purchased from R&D Systems included CXCR2 (clone Fab2164), and E-selectin (MAB575 and MAB5751).

Immunofluorescent Staining of Cell Cultures and Tissue Sections

For immunofluorescent studies, tissue was surgically removed post euthanasia and frozen in Tissue-TEK OCT compound using dry ice and acetone. Slides with tissue sections (10 μm for subcutaneous tumor and hepatic tissue and 16-18 μm for lung tissue) were prepared on a cryostat and stored in covered slide boxes at -70°C. Slides were brought to RT and fixed with cold acetone (-20°C) for 20 minutes. Individual sections were encircled using a PAP Pen (Invitrogen) prior to rinsing twice in DPBS (320±5 mOsm/L, pH 7.0).

For E-selectin and CD31 staining, the sections were then blocked for 1 hour at RT with blocking buffer: DPBS (320±5 mOsm/L, pH 7.0) containing 3% BSA (Sigma) and 10% goat serum (Sigma). Purified primary rat anti-mouse antibodies diluted 1:25 in blocking buffer were added to each section (100 μl / section), and incubated overnight in a humidified chamber at 4°C. Slides were rinsed twice with DPBS, and incubated with diluted 1:300 biotinylated goat anti-rat secondary antibody (BD Pharmingen) for 30 minutes at RT. The slides were rinsed with DPBS twice and incubated with diluted 1:300 Streptavidin-*PE* (BD Pharmingen) for 30 minutes at RT. Slides were rinsed in DPBS twice before mounting coverslips. Specific primary antibodies used were rat anti-mouse anti-E-selectin (clone 10E9.6, IgG2a), rat anti-mouse anti-CD31 (clone MEC13.3, IgG2a), and isotype control (clone R35-95, IgG2a).

For CD31 and SDF-1α double staining, the sections were rinsed twice with 1X Tris-Borate-Saline (TBS) and blocked with 10% horse serum in TBS for 1 hour at RT. Equal amounts (2 μg / mL) of both primary antibodies (anti-CD31 and anti-SDF-1 α) and both isotype-matched control antibodies were diluted 1:25 in the blocking buffer; 100 μl was added to each section and

slides were incubated overnight in a humidified chamber at 4°C. The slides were rinsed twice with 1X TBS and incubated with 1:400 diluted cocktail of both secondary antibodies for 30 minute at RT. The slides were finally rinsed in 1X TBS twice before mounting coverslips. Specific primary antibodies used were polyclonal goat anti-mouse anti-SDF-1α (clone C-19, Santa Cruz), polyclonal isotype control (Santa Cruz), rat anti-mouse anti-CD31 (clone MEC13.3, BD Pharmingen) and isotype control (BD Pharmingen). The secondary antibodies were purchased from Jackson ImmunoResearch Laboratories Inc (West Grove, PA): *PE*-labeled donkey anti-goat and *FITC*-labeled goat anti-mouse.

Aqua-Poly Mount (Polysciences, Inc., Warrington, PA) was used to mount coverslips on tissue sections on all slides. The slides were observed on Olympus LPS-220 or Olympus BX5 epifluorescence microscopes with a Texas Red and/or *FITC* filter. SPOT^{TM} (SPOT Imaging Solutions, Sterling Heights, MI) or DP Controller (Olympus) softwares were used to collect photographs from respective microscopes.

***In Vitro* Functional Assays**

Cell Adhesion Assay

Confluent monolayers of primary VEC and dissociated-tumor cell (DTC) cultures were established in gelatin-coated 12- or 24-well plates. Confluent cultures of bEnd.3, 3T3-L1, and LLCaB were established in uncoated 12 or 24-well plates. Cells were plated at various concentrations in duplicate and allowed to grow for 3-4 days. An empty plate was used as a control for non-specific adhesion of *EGFP*-Lin$^-$ BMC. Media was aspirated from all adherent cell cultures and 5×10^4 - 1×10^5 *EGFP*-Lin$^-$ BMC were added to each well and incubated for 30-45 minutes at RT. Non-adherent cells were removed by aspirating media using a 5 mL

Eppendorf pipettor. Each well was gently rinsed with 2 mL of complete medium for each respective cell type and careful aspirated. This process was repeated 5 times for each well. Finally, 500 µl 1X HBSS (containing Ca^{2+} and $Mg^{2+)}$ was added to each well and the plates were observed on an inverted phase contrast fluorescent microscope under bright light and fluorescent lamp. Images were collected using SPOT^{TM} imaging software. Next, the cells were harvested by trypsinization and fixed in 1% paraformaldehyde. The cell suspensions were enumerated using a hemocytometer on Olympus BX5 epifluorescent microscope and by flow cytometry (LSR II, Becton Dickenson, Franklin Lakes, NJ).

6- or 12-well plates were used to evaluate the adhesion of Lin^{-} $Sca1^{+}cKit^{+}$ (LSK) cells to different cell types and in presence of different blocking agents. Cells were pooled from 3-6 wells and split into 3 tubes; tube 1 was used for no staining control, cells in tube 2 were incubated with isotype control antibody, and cells in tube 3 were incubated with anti-Sca1-*PE* (Phycoerythrin, 488 nm-FL2) and anti-cKit-*APC* (Allophycocyanin, 633 nm-FL4) antibodies. Each tube was analyzed on the BD LSR II and 10^{5}-10^{7} events were processed to collect 500-10,000 fluorescent *EGFP* Lin^{-} BMC. The *PE-APC* double-labeled green-fluorescent cells were evaluated by three-color flow cytometry to estimate the percentage and total number of adhered LSK cells. In each experiment, Lin^{-} BMC were stained with anti-Sca1-*PE* and anti-cKit-*APC* to evaluate the preparatory $Sca1^{+}cKit^{+}$ (SK) population.

Cell Adhesion Blocking Assay

The adhesion of *EGFP*-Lin^{-} BMC was blocked using AMD3100, anti-CXCR4 (clone 247506, R&D Systems) and/or anti-E-selectin antibodies (clone MAB5751, R & D Systems). For blocking CXCR4, *EGFP*-Lin^{-} BMC were incubated in media containing AMD3100 at final concentration of 1, 0.1, 0.01 or 0.001 µM or blocking antibody: anti-CXCR4 antibody or isotype

control antibody at 12.5 or 25 μg/mL before adding to DTC, LLCaB, or bEnd.3 confluent cell cultures. For blocking E-selectin, the confluent cell cultures were incubated with anti-E-selectin antibody 12.5 or 25 μg/mL prior to addition of *EGFP*-Lin$^-$ BMC. As stated above, non-adherent cells were aspirated, cell cultures were gently rinsed, harvested by trypsinization, fixed with paraformaldehyde, and enumerated manually on a hemocytometer and by flow cytometry.

***In Vivo* Biolocalization of *EGFP*-Transgenic Cells**

***EGFP*-VEC Biolocalization in Metastatic Tumor Model**

Metastases in lung and liver tissues of C57Bl/6 mice were induced as described earlier. At this time, mice with metastases (n= 6) 2×10^6 *EGFP*-VEC were systemically administered via tail-vein or caudal artery. As control, healthy mice injected with 2×10^6 *EGFP*-VEC (n=5). Mice were sacrificed 24-72 hours after injection.

Localization of *EGFP*-Lin$^-$ BMC and *EGFP* Dermal Fibroblasts in Subcutaneous Tumor Model

Mice bearing small subcutaneous tumors (approximately 100 mm^3) were injected with 5 x 10^5 Lin$^-$ BMC isolated from *EGFP*-transgenic mice (n=7). Mice were sacrificed at 72 hours post *EGFP*-Lin$^-$ BMC injection. Subcutaneous tumors and other major organs were harvested and embedded in OCT compound (VWR Scientific Product) and frozen using dry-ice and acetone for tissue analysis. As control groups, subcutaneous tumor bearing mice were injected with either dermal fibroblasts (n=5) or media (n=3) that were isolated from *EGFP*-transgenic mice (Figure 6). The OCT-tissue blocks were sectioned and analyzed by qPCR, as described in Figure 8.

Figure 5: Diagrammatic Representation of the Experimental Design to Evaluate the Biolocalization of *EGFP*-Lin$^-$ BMC and Dermal Fibroblasts in the Subcutaneous Tumor Model

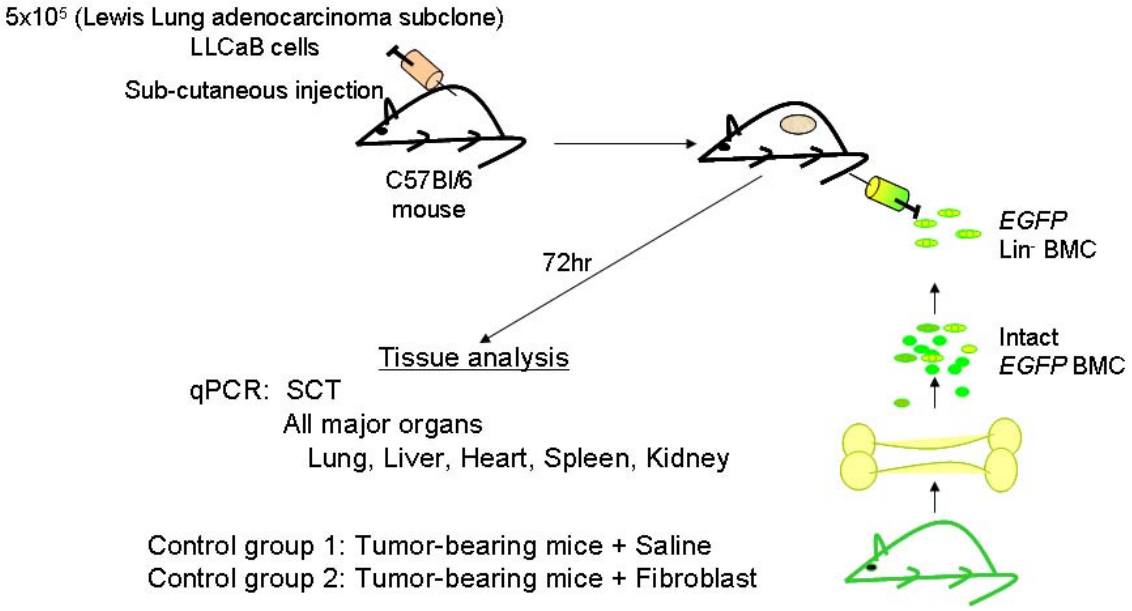
5x10⁵ (Lewis Lung adenocarcinoma subclone)
LLCaB cells
Sub-cutaneous injection
C57Bl/6
mouse
72hr
EGFP
Lin- BMC
Intact
EGFP BMC
Tissue analysis
qPCR: SCT
All major organs
Lung, Liver, Heart, Spleen, Kidney
Control group 1: Tumor-bearing mice + Saline
Control group 2: Tumor-bearing mice + Fibroblast

In vivo Localization of *EGFP*-Lin$^-$ BMC and *EGFP* Dermal Fibroblasts in Metastatic Tumor Model

Mice with metastatic tumors were injected with injected with 5×10^5 Lin$^-$ BMC (n=4) or dermal fibroblast (n=2) isolated from *EGFP*-transgenic mice (Figure 7). All experimental animals were sacrificed at 24-72 hours post *EGFP*-Lin$^-$ BMC injection. All samples were stored and analyzed as stated above. Similarly, 5×10^5 *EGFP*-Lin$^-$ BMC or *EGFP*-dermal fibroblasts systemically injected into s.c. tumor bearing mice or mice with the metastatic disease. Mice were euthanizes 24-72 hours or 7 days later. At euthanasia, blood was collected and metastatic tissue and all major organs were harvested and processed as described above.

Immunofluorescent Microscopy

EGFP-VEC homing was initially determined by visual enumeration of fluorescent cells. Fresh frozen tissue sections were prepared from all OCT-frozen tissues (10 μm for subcutaneous tumors, livers, hearts, spleens and kidneys and 16-18 μm for lung tissue). All slides were brought to RT, fixed in cold acetone (-20°C) for 20 minutes and rehydrated in 1X TBS or DPBS. AquaPolymount was used to mount coverslips on tissue sections. Slides were observed on Olympus LPS-220 or Olympus BX5 with a wide band *FITC* filter to view the tissue-localized fluorescent (*EGFP*) cells. Images were collected using digital cameras connected with the respective microscope and SPOT^{TM} Imaging or DP Controller software.

Figure 6: Diagrammatic Representation of the Experimental Design to Evaluate the Biolocalization of *EGFP*-Lin$^-$ BMC and Dermal Fibroblasts in the Metastatic Tumor Model

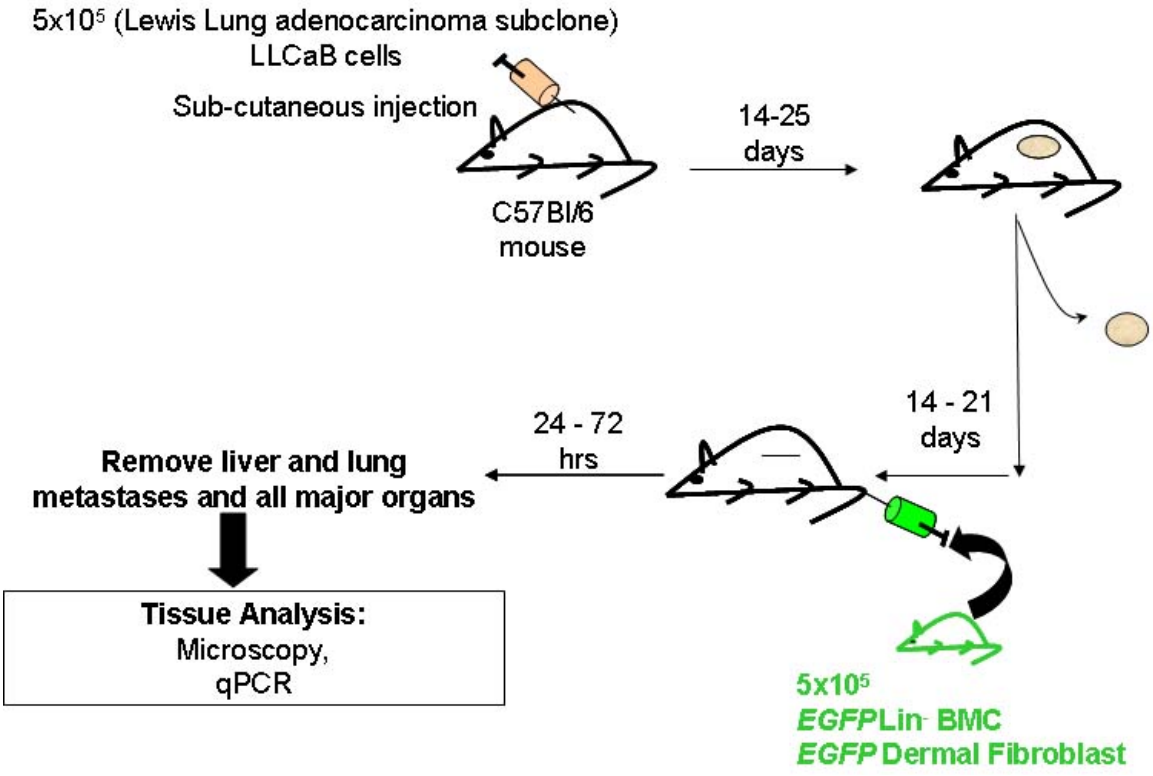
5x10⁵ (Lewis Lung adenocarcinoma subclone)
LLCaB cells
Sub-cutaneous injection
C57Bl/6
mouse
14-25
days
14 - 21
days
24 - 72
hrs
Remove liver and lung
metastases and all major organs
Tissue Analysis:
Microscopy,
qPCR
5x10⁵
EGFPLin- BMC
EGFP Dermal Fibroblast

Quantitative Real-time Polymerase Chain Reaction to Quantitate Tissue-Localized *EGFP*-Transgenic Cells

Isolation of Genomic DNA from Tissue

Genomic DNA was extracted from flash frozen or OCT-frozen murine tissue sections by the Phenol-Chloroform method (267). For the flash frozen tissue samples, an aluminum foil spatula and a foil pouch with 6 layers was prepared, chilled by immersing in liquid nitrogen. The frozen tissue was weighed (W1) in its original foil. The tissue was then quickly and completely transferred, to the chilled foil pouch, using the chilled foil spatula. The original foil was weighed once more (W2) and tissue weight was calculated (Wt = W1-W2). The pouch was folded tightly and immersed in liquid Nitrogen for about 30 seconds. The pouch was removed, placed on bench, and immediately the tissue was pulverized into powder using a hammer. The powdered tissue was transferred into a tube containing tissue lysis buffer (3 mL / 50-100 mg of tissue). For OCT-frozen tissues 10-50 μm sections of OCT-tissue block were cut, and using pre-chilled plastic tongs, the sections were collected in cold polypropylene tubes (Plastic tongs and 2 mL microfuge tubes were placed in the -20°C cryostat unit to pre-chill). The thickness and number of tissue sections varied from tissue to tissue to increase the *EGFP*-signal to background wild-type (noise) ratio (Figure 8A). For lung and liver specimens 5 × 50 μm sections / tube were routinely collected. These tubes were capped and stored at -70°C until ready to process. Tubes were brought to RT and sections were rinsed with DPBS to remove OCT, and were digested using Tissue Lysis Buffer (500 μl / tube) for at least 3 hour at 50-60°C. The Tissue Lysis Buffer contained 100 mM NaCl (Sigma), 10 mM Tris-EDTA (pH 8.0, Sigma), 25 mM EDTA (pH 8.0), 0.5% Sodium Dodecyle sulfate (SDS) and Proteinase K (100 μg/mL final concentration, Sigma) in MilliQ water. Tissue slurry was further incubated with RNase-A (Sigma, 25 μg/mL final

concentration) for 1 hour at RT. Equal volume of Phenol-Chloroform-Isoamly Alcohol (25:24:1) (Sigma) was added to tissue lysate, mixed by inversion (25 X), and centrifuged at 1500 × g for 15 minutes to separate the DNA-containing aqueous phase. The top aqueous phase was carefully transferred to a polypropylene tube, washed with equal volume of Chloroform-Isoamly Alcohol (49:1) (Sigma) and centrifuged at 1500 × g for 15 minute to remove phenol. Once again the top aqueous phase was carefully transferred into fresh polypropylene tube and DNA was precipitated using 0.5 times their volume of 7.5 M ammonium acetate and 2 times the volume of 100% ethanol. DNA was pelleted by centrifugation at 2000 × g for 20 minutes at 4°C. The DNA pellet was rinsed once with 70% ethanol, centrifuged at 2000 × g for 5 minutes followed by air-drying for 15 minutes. DNA was resuspended in 1X Tris-EDTA (Sigma) and heated at 50°C for 15 minutes to dissolve DNA. A rough estimate of DNA concentration was made by reading the samples spectrophotometrically on a NanoDrop®. Accurate DNA concentrations were determined with a fluorescence assay using SYBR-green dye (Invitrogen), which was more accurate than spectrophotometric determination (OD_{260}).

SYBR Green Assay for Quantitation of Genomic DNA

SYBR Green based fluorometric assay was the optimal method for quantitation of intact double-stranded DNA greater than 200 base pairs; the dye intercalates between AT-rich helices (268). DNA concentrations were estimated spectrophotometrically (e.g. using a NanoDrop®) to determine the dilution factor for the SYBR Green assay. Each 96-well plate-based SYBR Green assay to quantitate genomic DNA contained a standard curve: 8-10 points (8 ng/µl to 0.06 ng/µl) and two-fold dilutions of 1 Kb Plus DNA ladder (Invitrogen) in 1X TE. SYBR Green (269) was diluted 1:1250 in 1X TE (Tris-EDTA, Sigma) and always kept protect from light. All DNA samples were diluted in 1X TE (based on the spectrophotometric concentrations) such that the

dilutions approximately fell within the range of the standard curve. All samples were heated at 50°C for 10 minutes, vortexed for a few seconds in a microfuge to make a homogeneous solution. Appropriately diluted standards and samples (100 µl) were placed in each well of a 96-well plate and 100 µl diluted SYBR Green solution was added to each well with a multi-channel pipette. Each plate also included a blank sample (1X TE) and a positive control (mouse genomic DNA, Clonetech). The plates were covered with aluminum foil and incubated at RT for 10 minutes before reading on the automated fluorescent plate reader Synergy HT Multi-Mode Microplate Reader (BioTek, Winooski, VT) at 480/528 excitation/emission wavelengths. Fluorescent readings for standard curve dilutions were plotted on the y-axis, DNA concentrations were plotted on the x-axis, and a linear equation from the standard curve was obtained. Based on the standard curve, the concentrations of diluted DNA samples were calculated. The final concentrations of DNA from tissue samples were calculated by multiplying by the dilution factor.

Agarose Gel Electrophoresis of Genomic DNA

Agarose gel electrophoresis was performed on genomic DNA samples to determine DNA integrity and purity. 1X Tris-Acetate-EDTA (TAE) was used as the electrophoresis buffer; working buffer was prepared by diluting 10 X TAE in MilliQ water. Agarose gel (0.8-1.2%) was prepared by dissolving agarose powder (Pel-Freeze DNA Grade) to 1X TAE buffer. Ethidium bromide (0.5 µl, Sigma) was added to agarose gel solution. After cooling the solution to about 60°C, it was poured into a casting tray containing a sample comb and allowed to solidify at RT. DNA samples (200 ng DNA per well) were diluted in nuclease-free water and loading buffer containing glycerol (Gibco), EDTA (Gibco), Bromophenol blue (Sigma), and Xylene Cyanol FF (Sigma) in MilliQ water. DNA samples were carefully pipetted into each sample well in the gel,

the lid and power leads were placed on the apparatus, and current was applied. The voltage and run-time varied depending on the size of the gel: 90 volts for 45 minute for a Gibco Mini gel and 145 volts for 2 hours and 15 minute for a Bio-Rad double gel. The distance that DNA had migrated in the gel was judged by visually monitoring migration of the tracking dyes. Bromophenol blue and xylene cyanol dyes migrate through agarose gels at roughly the same rates as double-stranded DNA fragments of 300 and 4000 bp respectively. To examine DNA migration the gel was placed on an ultraviolet transilluminator. Digital photographs of gels were obtained using a Kodak DC290 Zoom camera and edited using Adobe Photoshop 7.0 software.

EGFP **Plasmid Standard Curve**

pEGFP-N3 plasmid contains the *egfp*-transgene, which was used to develop the *EGFP*-transgenic mice used as donors in the *in vivo* adoptive-cell transfer experiments. *pEGFP-N3* was a gift from Dr. Alexander Murashov (Department of Physiology, East Carolina University). DH5α cells transfected with *pEGFP-N3* using heat-shock technique and cultured on Kanamycin (10 mg/mL) agar plates. A single colony of successfully transfected cells was picked and expanded in LB broth. Large-scale purification of plasmid was carried out using QIAGEN Plasmid Mega kit (Qiagen, Valencia, CA). The plasmid concentration was measured spectrophotometrically on the NanoDrop® spectrophotometer. The mass of one copy (or molecule) of the plasmid *pEGFP-N3* was calculated from the following formula:

$\boldsymbol{m}$ *= mass of one copy =* $\boldsymbol{M / N_A}$ *where*

$\boldsymbol{M}$ *= the molecular weight (Dalton or gram/mole) of the plasmid (calculated using the base composition of the plasmid and MW of nucleotides) =* 3.09×10^6

$\boldsymbol{N_A}$ *= Avogadro's number =* 6.02×10^{23} *copies (or molecules) / mole.*

Number of plasmid copies / microliter = *concentration (*OD_{260}*) /* $\boldsymbol{m}$

Thus, it was calculated that each molecule or copy of *pEGFP-N3* has a mass of ~5.1 attograms (ag) and 1 ng of *pEGFP-N3* has approximately 1.95×10^8 copies of the *EGFP*-gene. A *pEGFP-N3* plasmid diluted in genomic DNA from wild-type mice was used to construct standard curve in each assay.

Quantitative Polymerase Chain Reaction (qPCR)

qPCR was conducted with 100 or 200 ng genomic DNA in duplicate in 20 or 25 µl reactions using the TaqMan® PCR Universal Master Mix (Applied Biosystems) in 96-well format in the Applied Biosystems 7000 Real-Time PCR System or 384-well format in the Applied Biosystems 7900 Real-Time PCR System. Primer and probe sequences for the *EGFP*-transgene were from The Jackson Laboratories and manufactured by Applied Biosystems: forward primer *5'-ccacatgaagcagcaggactt-3'*, reverse primer *5'-ggtgcgctcctggacgta-3'* and probe *6FAM-ttcaagtccgccatgcccgaa-TAMRA*. The final concentration of primers was 400 nM each and the probe was 150 nM. Gene Expression Assay Mm00607939_s1 (Applied Biosystems) was used for assaying *β-actin* (endogenous control) in separate reactions. This proprietary assay resulted in a 115 bp amplicon within exon 6, detected with a FAM/MGB-labeled probe. Aproteinin B (ApoB) was also used as an endogenous control: forward primer *5'-cacgtgggctccagcatt-3'*, reverse primer *5'-tcaccagtcatttctgcctttg-3'* and probe *Vic–ccaatggtcgggcactgctcaa–TAMRA*. Primer and probe sequences for ApoB were from The Jackson Laboratories and manufactured by Applied Biosystems. All reactions were 50 cycles using default Applied Biosystems cycling conditions (2 minute at 50ºC, 10 minute at 95ºC, and 50 cycles of 15 seconds denaturation at 95ºC and 1 minute annealing and extension at 60°C).

The number of *EGFP*-transgene copies in 100 or 200 ng DNA (from *EGFP*-transgenic mice or from wild-type mice transplanted with cells from *EGFP*-transgenic mice) was calculated

from their respective Ct (cycle threshold) using the linear equation derived from the respective plasmid standard curve. *EGFP* copy-number per diploid cell was calculated by dividing the number of *EGFP* copies in the DNA sample by the number of cells from which the DNA was isolated. Each diploid cell from a C57Bl/6 male has been reported to yield 6 pg DNA (270); thus 100 ng DNA ≈ 1.67×10^4 diploid cells. The schematic diagram for qPCR assay is represented in Figure 7B.

Association between Manual Cell Count using Fluorescence Microscopy and qPCR for Enumeration of *EGFP*-Transgenic Cells

To compare manual enumeration of tissue-localized *EGFP*-Transgenic Cells (*EGFP*-VEC) to the qPCR method, mice bearing small subcutaneous tumors (approximately 100 mm^3) were injected intra-tumor with *EGFP*-VEC. Mice were sacrificed after 2 hours and subcutaneous tumors were harvested. Ten micron thin sections were prepared and alternating 10 μm sections were examined by fluorescence microscopy or extracted for DNA.

Modification in qPCR

To increase the signal: noise ratio of *egfp*-transgene: background DNA of the qPCR assay five 50 μm thick tissue sections were collected in multiple tubes and DNA was extracted as schematically shown in Figure 7A. This generated multiple DNA samples per tissue and thus the qPCR assay was modified for a high throughput 384-well plate format which permitted a maximum reaction volume of 20 μl per well. Next, to increase the amount of DNA being analyzed in 20 μl reactions, dose-response assays were conducted using 100, 200, 400, and 600 nanogram of DNA.

Statistical Analysis

Data has been reported as average values and standard error means (SEM) from representative or all experiments. Statistical comparison between two groups in an experiment was performed using unpaired Student's t-test or Mann Whitney test. Comparison between multiple groups was performed using non-parametric one-way analysis of variance (ANOVA) with post-hoc Dunnett's test to compare with control samples and two-way ANOVA functions. For statistical tests, it was assumed that the data set was unpaired (or paired where applicable), non-parametric and lacked Gaussian distribution. The outliers were detected by plotting data set in box-whiskers plot and by the use of Tukey's analysis (GraphPad Prism 5.0 software); all outliers were excluded from data sets. For correlation studies, Pearson's and Spearman's coefficients were used. Microsoft Office Excel and GraphPad Prism 5.0 statistical software were used for data analysis.

Figure 7: Genomic DNA Isolation for qPCR Assay

A) Schematic representation of protocol used to isolate and analyze genomic DNA for *egfp*-transgene. To increase the sensitivity of the qPCR assay, each tissue block was sectioned and five 50 micron sections were collected in individual tubes. DNA was extracted from tissue sections in all tubes and analyzed in 384-well qPCR plates.

B) Schematic representation of qPCR assay to detect the tissue-localized adoptively-transferred *EGFP*-transgenic cells

A

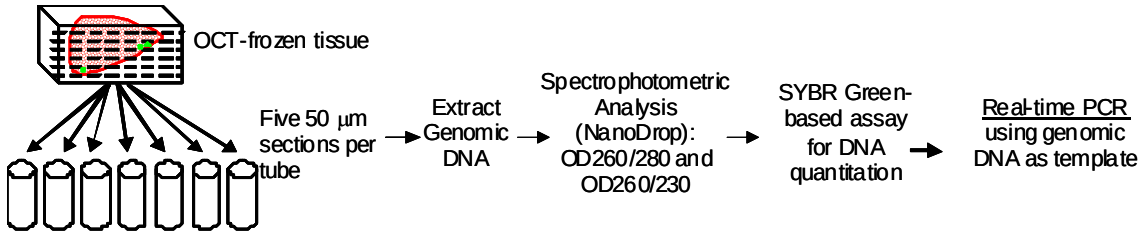
OCT-frozen tissue
Five 50 µm sections per tube
Extract Genomic DNA
Spectrophotometric Analysis (NanoDrop): OD260/280 and OD260/230
SYBR Green-based assay for DNA quantitation
Real-time PCR using genomic DNA as template

B

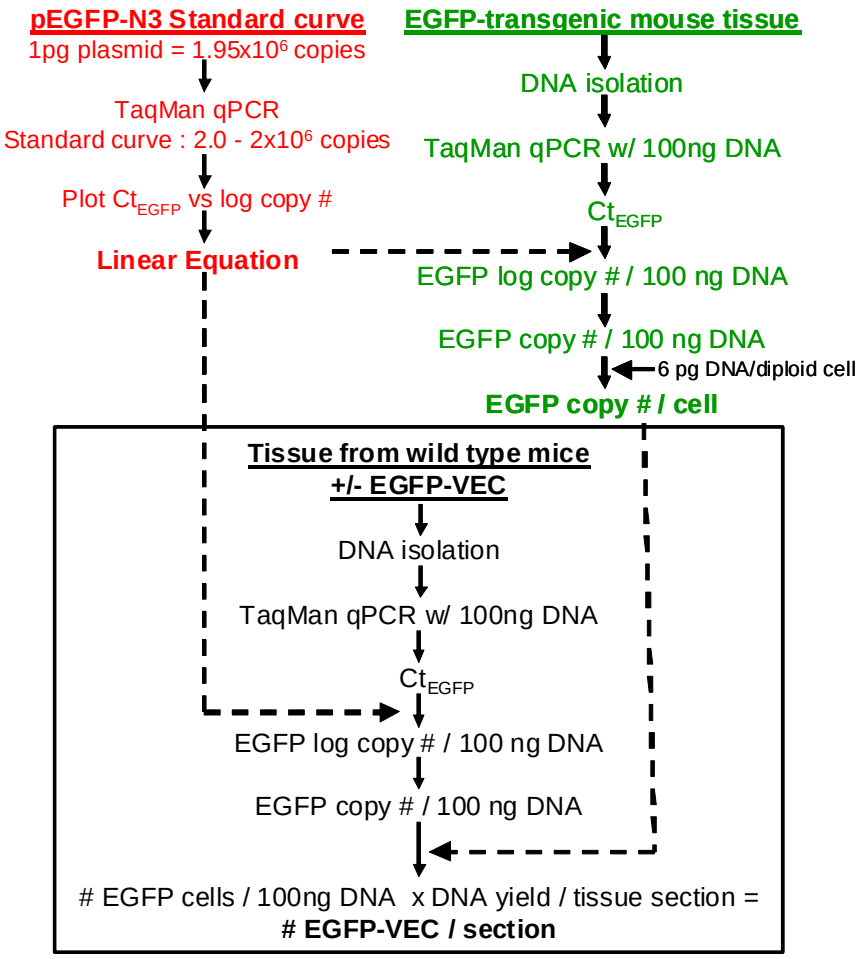
pEGFP-N3 Standard curve
1pg plasmid = 1.95x10⁶ copies
TaqMan qPCR
Standard curve : 2.0 - 2x10⁶ copies
Plot Ct EGFP vs log copy #
Linear Equation
EGFP-transgenic mouse tissue
DNA isolation
TaqMan qPCR w/ 100ng DNA
Ct EGFP
EGFP log copy # / 100 ng DNA
EGFP copy # / 100 ng DNA
6 pg DNA/diploid cell
EGFP copy # / cell
Tissue from wild type mice +/- EGFP-VEC
DNA isolation
TaqMan qPCR w/ 100ng DNA
Ct EGFP
EGFP log copy # / 100 ng DNA
EGFP copy # / 100 ng DNA
EGFP cells / 100ng DNA x DNA yield / tissue section =
EGFP-VEC / section

CHAPTER III: RESULTS

A: Description and Characterization of the Murine Lewis lung adenocarcinoma Model

Rationale:

The Lewis lung adenocarcinoma subclone LLCaB was used for developing subcutaneous (s.c.) tumors and subsequent metastases after surgical removal of s.c. tumors in syngeneic and immunocompetent C57Bl/6 mice (4). This cell line was chosen because the LLCaB tumors developed faster and produced greater number of metastatic lesions compared to the parental LLC1 line and the LLCC3 subclone (271). The s.c. tumor resection methodology produced robust metastatic disease and was deemed superior compared to the tail vein injection method (271). Nonetheless, due to substantial mortality (because of blood loss and anesthesia during the surgical procedure) and a wide variation in metastatic disease it was important to characterize the metastatic tumor model. The aim of this research project was to use this model to understand the role of the cell adhesion molecule E-selectin and chemokine SDF-1α in tumor biology.

This chapter describes the development of LLCaB tumors in a murine model, optimization of the conditions for development of metastatic disease and analysis of murine tissue for the expression of E-selectin and SDF-1α.

Results:

Lewis lung Adenocarcinoma Model

LLCaB cells (5×10^5) were injected subcutaneously and were visible as palpable tumors 10-14 days after injection. The average tumor growth curve from 11 separate experiments (n=173 mice) is shown in Figure 8A. Following the protocol developed by Folkman (4), primary s.c. tumors were surgically removed to promote the development of metastases. An average of 72% (30-95%) survived the s.c. tumor removal surgery, with death primarily due to anesthesia

and blood loss. Of the mice that survived through the end of the experiment (16±6 days after primary tumor removal) an average of 65% mice had visible metastases at euthanasia. Factors that influenced survival/euthanasia of mouse were s.c. tumor volume at resection, s.c. tumor recurrence and overall health. The majority of the mice at the end of the experiment had either both lung and liver metastases or had lung metastases only. A very small percentage of mice developed hepatic tumors only (Figure 8B). The metastatic burden varied between animals, which was evident on macroscopic examination of lungs and livers (Figure 8C). The metastases were visible as red lesions in the lungs (Figure 8C 1-3), and white lesions in the livers (Figure 8C 4-5). No such lesions were visible in lung and liver samples from healthy control mice (data not shown). The microscopic evaluation of ten-micron tissue sections after hematoxylin and eosin staining was used to visualize micrometastases. Tissue sections from healthy control mice showed normal lung and liver morphology (Figure 8D, 1 and 4). Hematoxylin-stained nucleus and eosin-stained cytoplasm were apparent in all cells, and uniformly distributed throughout the tissue section. In contrast, in tissue sections with metastases (Figure 8D, 2, 3, 5 and 6), tumor cells and metastatic lesions were stained dark blue-black and adjacent non-tumorous regions appear to be similar to control tissue sections (Figure 8D).

As expected, metastatic burden was related to the size of the primary tumor at resection and the number of days elapsed after s.c. tumor removal (Figure 9A-B). At euthanasia mice with visible lung or liver metastases had significantly larger s.c. tumors compared to the mice that had 'no visible metastases' (1618±1014 mm^3 vs. 1022±814 mm^3, $p<0.05$; Figure 9A). The mice that died during primary tumor removal surgery (n=18, day 0) were not included in this analysis.

Approximately 50% of mice with average s.c. tumor volume of 1500mm^3 that were euthanized by 10 days after tumor-removal surgery had significant numbers of visible metastases

Figure 8: Summary of LLCaB Tumor Growth and Metastasis

A) Average LLCaB subcutaneous tumor growth curve from 11 separate experiments (n=173).

B) Percentage of mice that developed pulmonary and/or hepatic metastases 16±6 days after primary tumor removal (n=173, 11 experiments).

C) Representative photographs showing the variation in metastatic burden in each tissue. Lung metastases are visible as the red lesions (1-3) and liver metastases are apparent as the white lesions (4-6).

D) Photomicrographs showing Hematoxylin and Eosin staining on (1) healthy lung, (2-3) lung metastases, (4) healthy liver, and (5-6) liver metastases (magnification 400×). The metastatic lesions were stained dark blue-black and are distinguishable from the adjacent relatively healthier tissue.

SEM = standard error of mean

A

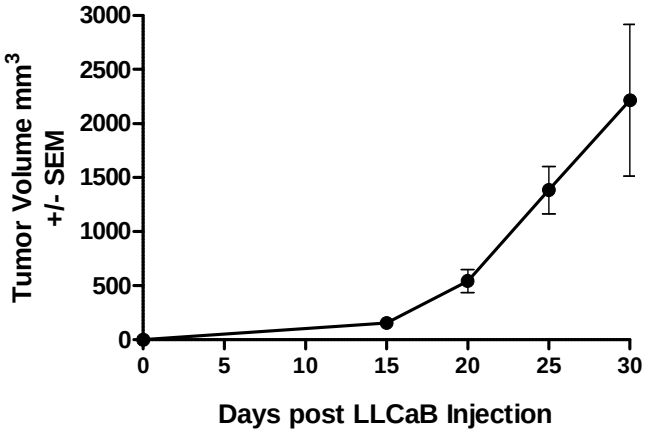
Tumor Volume mm3
+/- SEM
3000
2500
2000
1500
1000
500
0
0
5
10
15
20
25
30
Days post LLCaB Injection

B

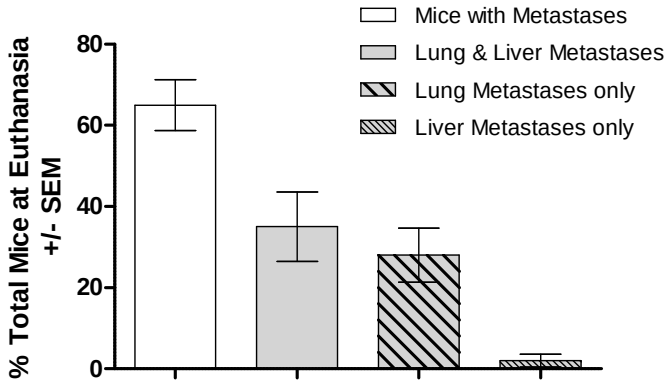
% Total Mice at Euthanasia
+/- SEM
80
60
40
20
0
Mice with Metastases
Lung & Liver Metastases
Lung Metastases only
Liver Metastases only

C

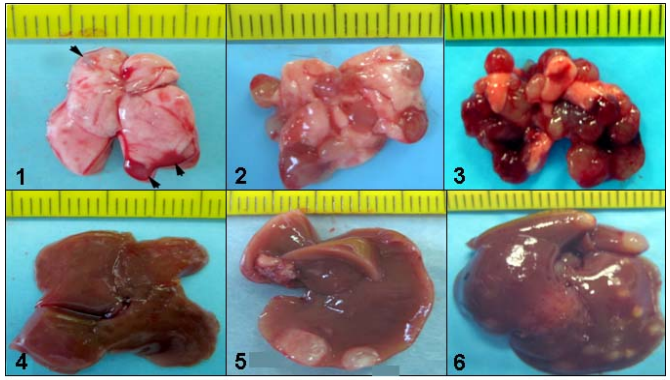
1
2
3
4
5
6

D

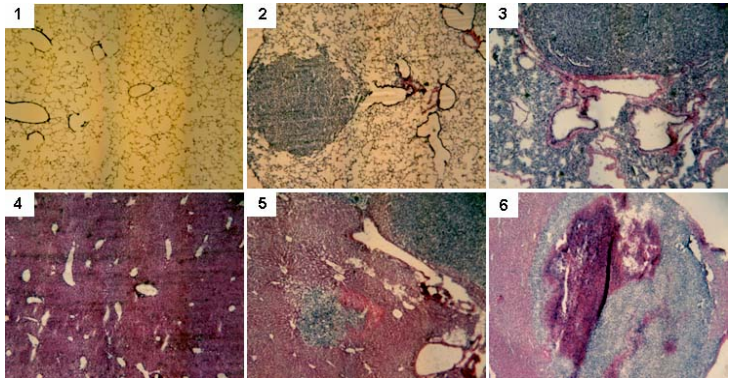
1
2
3
4
5
6

(Figure 9B). When mice with s.c. tumor volume of 1500 mm^3 were euthanized 11-20 days after tumor removal, about 77% of these mice had visible lung and/or liver metastases (Figure 9B). However, mice with tumor volume of approximately 1000 mm^3 were healthy for a longer time-period and approximately 75% of these mice had macroscopically detectable metastases (Figure 9B). These results suggested that s.c. tumor volume of approximately 1000-1500 mm^3 was optimal for mice to develop metastases but appear disease-free for 10-20 days post s.c. tumor resection.

At the time of euthanasia, in addition to macroscopic visualization for metastatic lesions, all major organs including heart, kidney, spleen, lung, and liver were weighed to estimate the metastatic burden. The weights of lungs from the mice with metastatic disease were significantly higher compared to control lungs from healthy mice. In one group (n=11), weights of the metastatic lungs were grouped according to number of days lapsed between tumor resection and euthanasia. There was no significant difference in the average s.c. tumor volume between these sub-groups. As reported in Figure 9C, metastatic burden, as estimated by lung weight, increased significantly with time. A substantial increase in the weights of spleens from mice with metastatic disease was also observed (data not shown). However, no metastatic lesions were visible on the spleens and thus the splenomegaly was most likely due to immune response.

These results were consistent with clinical observation. In human patients, the larger the primary tumor, the more likely there will be metastases and greater the extent of metastatic disease. Metastases also increased in size with time. It was also logical that smaller primary tumors would lead to smaller metastases that would take more time to produce visible lesions. Our LLCaB tumor model thus mimicked clinically relevant metastatic disease.

Figure 9: Association between Primary Tumor Volume and Metastases Development

A) Association between the average s.c. tumor volume (at resection) and metastatic burden in lung and/or liver was evaluated. Mice with s.c. tumors larger than 1500 mm^3 volume had macroscopically visible metastases compared to mice with s.c. tumors ≤ 1000 mm^3 at euthanasia (* $p< 0.05$, 2-tailed Student's-test).

B) The percentage of mice that developed macroscopically detectable metastases appeared to be a function of the s.c. tumor volume and the number of days after primary tumor removal. Metastases were apparent in 50% mice by day 10 (n=37) and 77% mice between 11-20 days (n=48) in mice with average tumor volume of 1500 mm^3, and 21-40 days in mice with tumor volume of 1000 mm^3 (n=22).

C) Metastatic burden estimated by measuring the tissue-wet weight at euthanasia suggested that there was a significant increase in weight in metastatic lungs (n=11) compared to healthy lungs (n=5). In addition, the extent of significantly metastatic burden increased with increase in number of days after primary tumor removal. (Data from one experiment; * $p< 0.05$ one-way ANOVA, Post-hoc Dunnett's test compared to control)

A

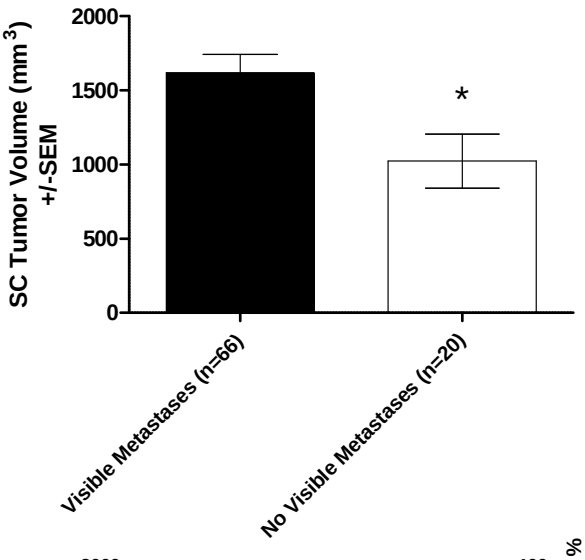
SC Tumor Volume (mm3) +/-SEM
2000
1500
1000
500
0
*
Visible Metastases (n=66)
No Visible Metastases (n=20)

B

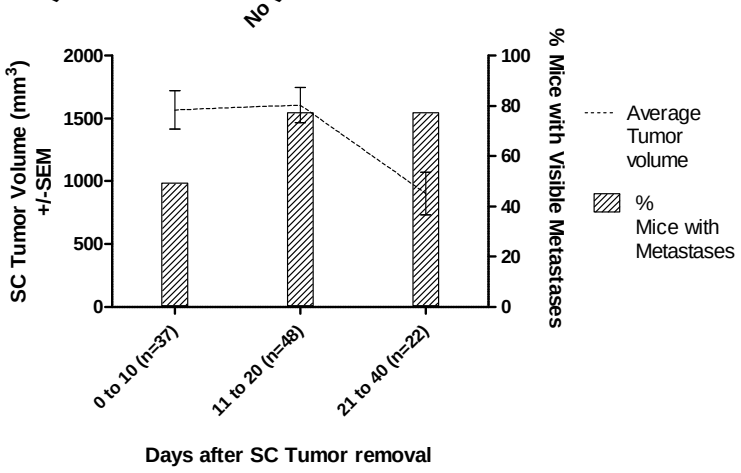
SC Tumor Volume (mm3) +/-SEM
% Mice with Visible Metastases
2000
1500
1000
500
0
100
80
60
40
20
0
Average Tumor volume
% Mice with Metastases
0 to 10 (n=37)
11 to 20 (n=48)
21 to 40 (n=22)
Days after SC Tumor removal

C

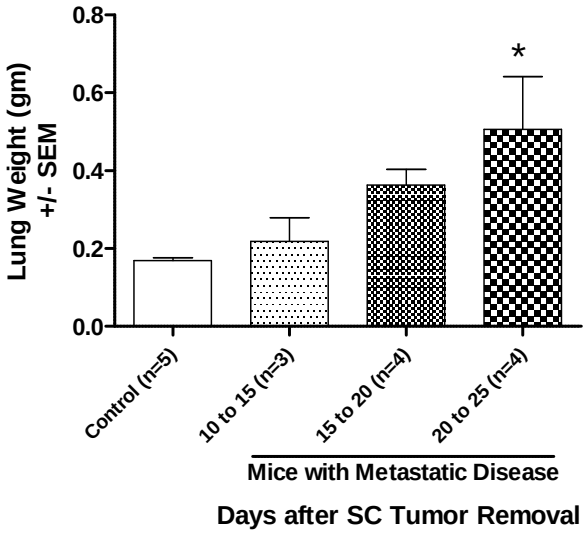
Lung Weight (gm) +/- SEM
0.8
0.6
0.4
0.2
0.0
*
Control (n=5)
10 to 15 (n=3)
15 to 20 (n=4)
20 to 25 (n=4)
Mice with Metastatic Disease
Days after SC Tumor Removal

E-selectin and SDF-1α Expression in LLCaB Tumors

The aim of this dissertation research was to understand the role of E-selectin and SDF-1α in tumor biology. We hypothesized that tumor endothelium expressed E-selectin and SDF-1α, and that the biolocalization and adhesion of bone marrow derived cells to LLCaB tumors were mediated by these factors. The expression of E-selectin and SDF-1α in naïve control tissues and in s.c. and metastatic tumors were evaluated.

Specific Upregulation of E-selectin on the LLCaB Tumor Endothelium

Our laboratory has previously shown that E-selectin was important for tumor growth and vascularization (170), Verbanac laboratory, unpublished data). It was also shown that E-selectin was expressed by the *ex vivo* cultured tumor-derived endothelial cells, but not by the endothelial cells isolated from normal healthy tissue. It was possible that E-selectin expression was simply being induced *in vitro*, after isolation and culture of tumor endothelial cells. To investigate if this was an *in vivo* phenomenon, we proceeded to analyze E-selectin expression in LLCaB tumor sections by immunohistochemistry. Ten-micron adjacent sections from s.c. tumors, lung and liver metastases, and healthy control tissues were stained with hematoxylin and eosin (H&E) or immunostained with anti-E-selectin antibody or anti-CD31 antibody (marker for endothelium). H&E staining helped in defining metastatic lesions within lung and liver samples. CD31-stained blood vessels were observed in all tissues whereas E-selectin staining was specifically observed within the tumors. Furthermore, expression of E-selectin was restricted to the blood vessels within tumors. This was seen in tissue sections stained with anti-E-selectin by the red staining pattern, which was similar to CD31 staining in adjacent tissue sections (Figure 10). The isotype-matched control antibody did not show any staining.

Figure 10: Expression of E-selectin in Healthy Controls, Subcutaneous and Metastatic Tumors

Adjacent tissue sections were stained with Hematoxylin and Eosin (H&E), isotype-matched control antibody, anti-CD31, or anti-E-selectin antibody. H&E staining was used to identify tumors and metastatic lesions in tissue sections. The blue staining pattern represents tumors. A rat anti-mouse CD31 antibody was used to identify blood vessels. Similarly, adjacent tissue sections were incubated with a rat anti-mouse anti E-selectin antibody. *PE*-labeled anti-rat secondary antibody was used to visualize antibody binding to tissue sections. E-selectin expression was restricted to blood vessels of tumorous tissue as noticeable by the similarity in staining pattern to the CD31 expression in adjacent tissue sections. The isotype-matched control antibody did not show any staining. Original magnification 400×, Scale 100 micron.

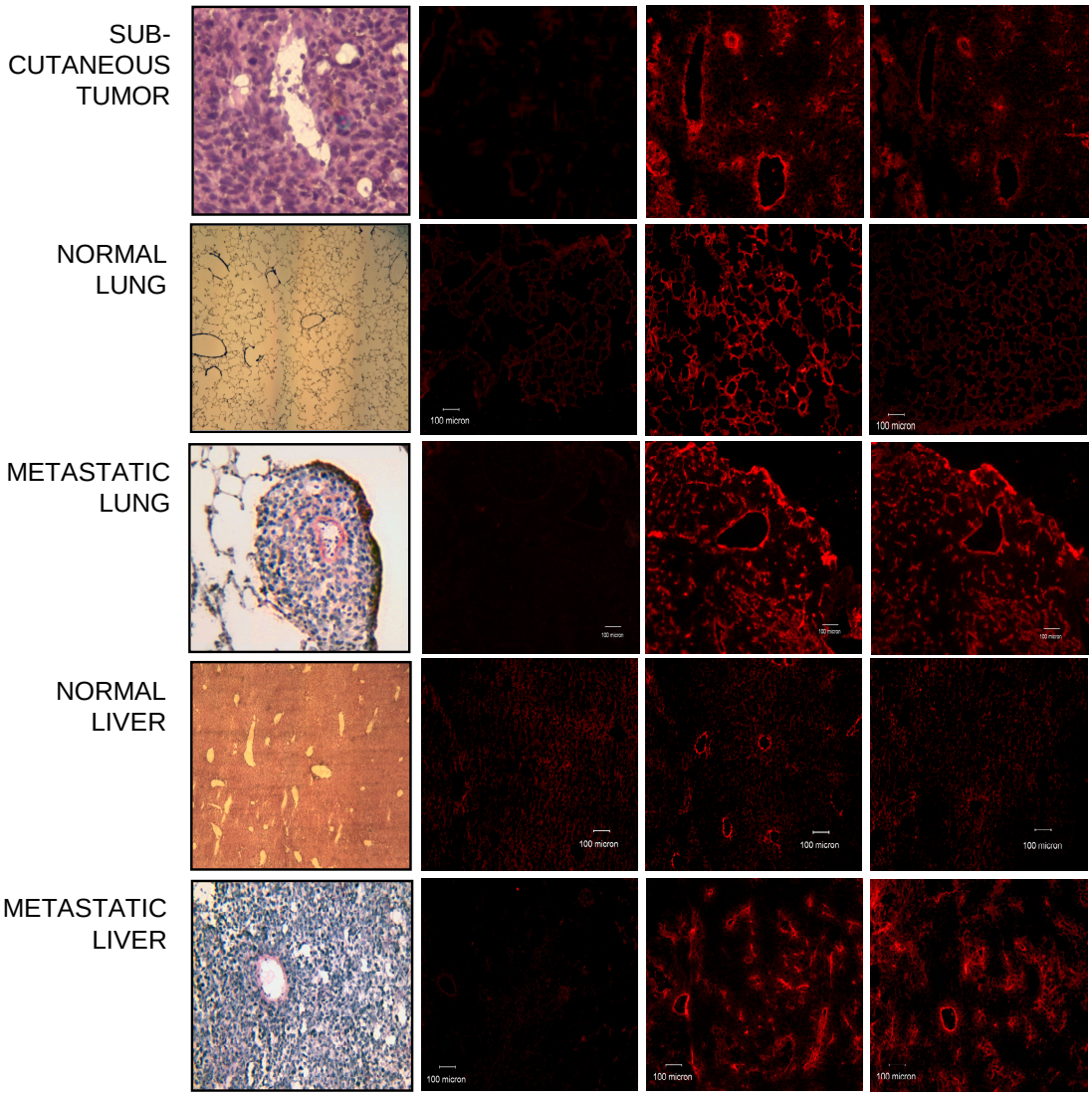
SUB-
CUTANEOUS
TUMOR
NORMAL
LUNG
METASTATIC
LUNG
NORMAL
LIVER
METASTATIC
LIVER
100 micron
H & E
Control
CD31
E-selectin

SDF-1α Expression in Murine Tissue

RNA from naïve healthy control tissues (n=7), s.c. tumors (n=11), and metastases (n=6) was assayed by quantitative RT-PCR for the expression of SDF-1α and an endogenous control gene Beta-2-microglobulin (*β2M*). Expression of *β2M* was highly consistent in all the samples analyzed (average Ct = 17.72±1). *Sdf-1α* gene transcript was detected in all tissue samples analyzed. The average Ct values for *sdf-1α* mRNA in healthy control tissues, s.c. tumors, and metastases were 23±2, 24.8±1 and 24.5±1, respectively. The relative gene expression between healthy control tissues, s.c. tumors and metastases was calculated as $2^{-\Delta\Delta Ct}$. Healthy lungs from naïve mice were used as 'calibrator'tissue.

$$Ct_{\beta 2M(s)} - Ct_{gene\ (s)} = \Delta Ct_{sample}$$

$$Ct_{\beta 2M(c)} - Ct_{gene\ (c)} = \Delta Ct_{calibrator}$$

$$\Delta Ct_{sample} - \Delta Ct_{calibrator} = \Delta\Delta Ct$$

$$Fold\ difference = 2^{-\Delta\Delta Ct}$$

The relative *sdf-1α* mRNA expression in s.c. tumors and lung metastases was found to be 0.6-fold and 0.2-fold that of healthy tissue samples (Figure 11A), respectively.

Consistent with previous studies, utilizing ELISA methodology, a substantial SDF-1α expression was observed in naïve healthy control lung and liver samples (n=12). SDF-1α protein was not significantly different in s.c. tumors (n=59) compared to healthy control tissue samples (60±4 pg/mg protein in s.c. tumors vs. 80±66 pg/mg protein in healthy tissue samples; Figure 11B). An overall three-fold increase in SDF-1α protein levels by ELISA in metastases (n=21) compared to healthy control samples (233±38 pg/mg vs. 80±66 pg/mg, $p<0.0001$; Figure 11B).

Using the Spearman's rank correlation test, a significant inverse correlation was determined between the tumor volumes of metastatic and s.c. tumors and their SDF-1α

concentration respectively (ρ = *-0.552* and *-0.36*; P-value *<0.01*; Figure 11 C-D). To our knowledge, this is the first report showing a correlation between tumor size and SDF-1α protein expression.

The *in situ* expression of SDF-1α in tissue sections from healthy and experimental mice was evaluated by immunohistochemical analysis. SDF-1 was distributed evenly throughout the specimen in healthy and tumor tissues (Figure 12A). In the lung and liver tissue sections with metastatic lesions, SDF-1 was observed to be concentrated within metastases compared to adjacent tissue (Figure 12A). This complemented our findings from ELISA assays that the increase in SDF-1α in the metastatic tissue samples was due to elevated SDF-1 expression in the metastatic lesions.

Metastases and s.c. tumor sections were co-incubated with rat anti-mouse anti-CD31 and goat anti-mouse anti-SDF-1 antibodies. Subsequently, tissue sections were co-incubated with donkey anti-rat-*FITC* and donkey anti-goat-*PE* secondary $F(ab')_2$ fragments to examine the colocalization of SDF-1 was associated with the tumor endothelium (Figure 12B). In 13 slides, co-localization of SDF-1 and CD31 was observed in approximately one-third of tumor vasculature. No staining was observed with the isotype matched control antibodies. This supported our hypothesis that Lewis lung tumors expressed SDF-1α and that SDF-1α was associated with tumor endothelium.

Blood from healthy control mice (n=9), and s.c. tumor-bearing mice (n=21), was collected from the inferior vena cava or retro-orbital sinus at euthanasia. By ELISA, serum from these samples was analyzed for circulating SDF-1α. No significant difference was observed in the levels of circulating SDF-1α in serum samples from s.c. tumor-bearing (Average tumor

Figure 11: SDF-1α Expression in Subcutaneous and Metastatic Tumors Compared to Healthy Tissue (RT-PCR and ELISA)

A) RNA from healthy control tissues (n=7), s.c. tumors (n=11) and lung/liver metastases (n=6) was evaluated for *sdf-1α* gene transcript by RT-PCR. P-value <0.0001 by one-way ANOVA; Post-hoc Dunnett's test compared to healthy tissue *** $p < 0.0001$; Average data from four separate RT-PCR assays

B) Protein homogenates from s.c. tumors (n=59), lung/liver metastases (n=21) and healthy control tissues (n=12) were evaluated for SDF-1α protein expression by ELISA. SDF-1α expression in lung/liver metastases was approximately 3-folds higher than naïve tissue. P-value <0.0001 by one-way ANOVA; Post-hoc Dunnett's test compared to healthy tissue *** $p < 0.0001$; Average data from four separate ELISA assays

B-C) An inverse non-linear/exponential relationship was observed between SDF-1α protein expression in s.c. tumors (B) and in metastases (C) and their respective tumor volumes. Spearman rank correlation value $\rho = -0.36$ and -0.55 with P-value <0.01 for s.c. tumors and metastases respectively.

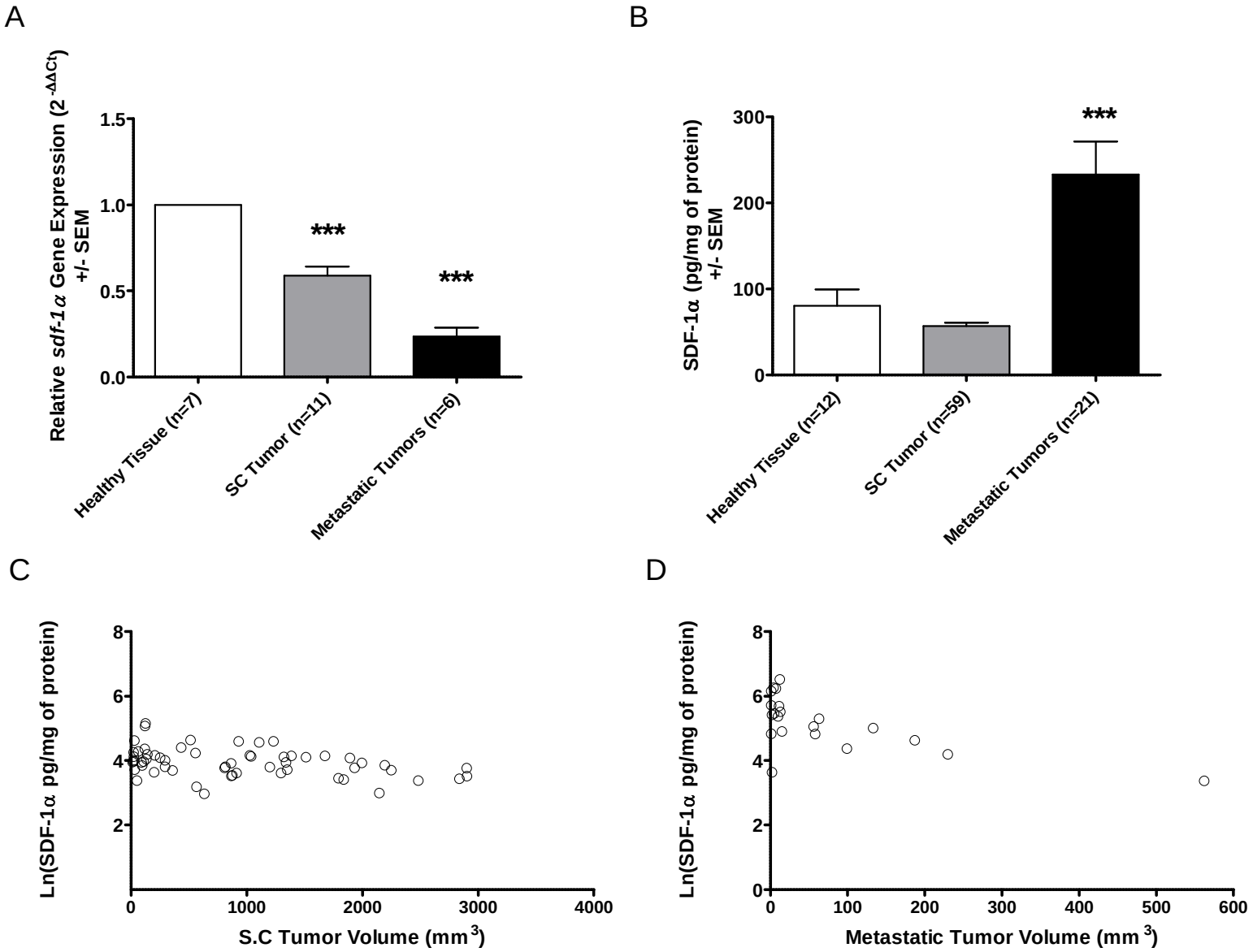
A
Relative sdf-1α Gene Expression (2-ΔΔCt) +/- SEM
1.5
1.0
0.5
0.0
***
***
Healthy Tissue (n=7)
SC Tumor (n=11)
Metastatic Tumors (n=6)
B
SDF-1α (pg/mg of protein) +/- SEM
300
200
100
0
***
Healthy Tissue (n=12)
SC Tumor (n=59)
Metastatic Tumors (n=21)
C
Ln(SDF-1α pg/mg of protein)
8
6
4
2
0
1000
2000
3000
4000
S.C Tumor Volume (mm3)
D
Ln(SDF-1α pg/mg of protein)
8
6
4
2
0
0
100
200
300
400
500
600
Metastatic Tumor Volume (mm3)

Figure 12: SDF-1α Expression in Subcutaneous and Metastatic Tumor Compared to Healthy Tissue (Immunohistochemistry)

A) Tissue sections were stained with anti-SDF-1 (orange-yellow). SDF-1 was detected throughout healthy lung and liver sections, and in areas adjacent to sections from metastatic tissue. Metastatic lesion (T) and the edge demarking the lesion and adjacent tissue appeared to be more concentrated with SDF-1. Due to settings on the microscope, SDF-1 staining appears to be yellowish in these photomicrographs.

B) Tissue sections were co-incubated with rat anti-mouse anti-CD31 and goat anti-mouse anti-SDF-1. Donkey anti-rat-*FITC* and donkey anti-goat-*PE* were used to visualize primary antibody binding. Co-localization (yellow) of SDF-1 (red) with the endothelial marker CD31 (green) was observed in about one-third of the blood vessels in s.c. and metastatic tumors. Representative of 13 slides. Original magnification 400×.

A

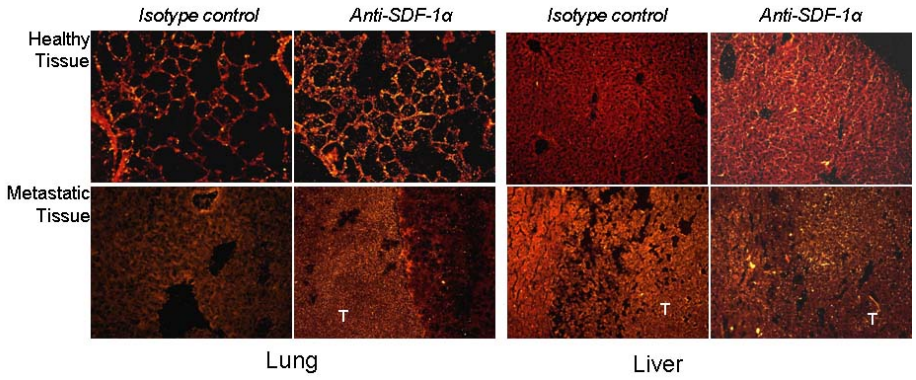
Isotype control
Anti-SDF-1α
Isotype control
Anti-SDF-1α
Healthy Tissue
Metastatic Tissue
T
T
T
Lung
Liver

B

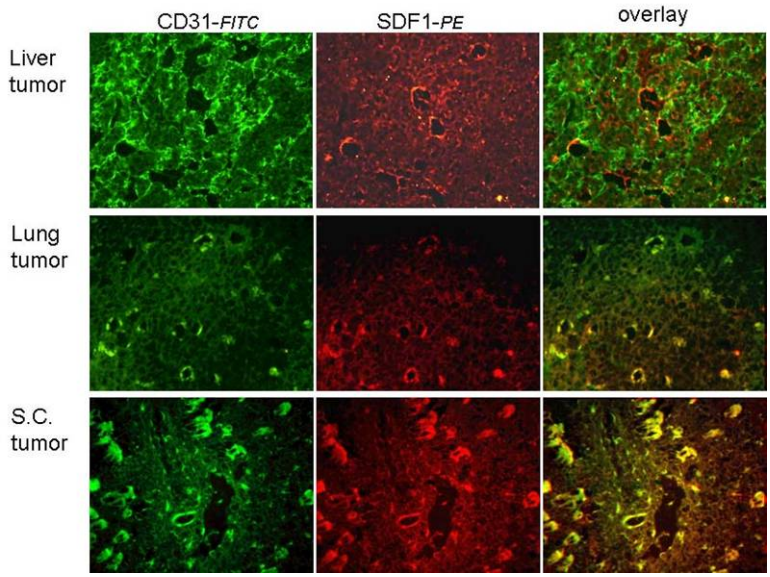
CD31-FITC
SDF1-PE
overlay
Liver tumor
Lung tumor
S.C. tumor

volume = 2865 ± 696 mm^3) and healthy mice (Figure 13A). However, it was intriguing to note a consistently lower amount of circulating SDF-1α in serum from female mice compared to male mice in both healthy and s.c. tumor-bearing mice (Figure 13B). To the best of our knowledge, this is a novel observation indicating a sex-based difference in circulating SDF-1α. This information might be relevant in treating estrogen-dependent malignancies.

Synopsis:

These data have validated that the LLCaB tumor model accurately mimicked cancer progression in humans and was thus a clinically relevant murine model. We have also demonstrated that E-selectin was specifically upregulated in tumor endothelium whereas it was undetectable in naïve tissues from healthy mice. In contrast, tissue samples from healthy mice expressed basal levels of SDF-1α. SDF-1α protein levels were significantly increased in the metastatic tumors, but not in the s.c. tumors. In addition, these data showed a significant inverse relationship between SDF-1α levels and tumor size in both s.c. and metastatic tumors. This novel information supports the premise that SDF-1α might be important in the early stages of tumor development. In addition, approximately one-fifth of SDF-1α in tumors was observed to be colocalized with tumor endothelium, and might be important in the adhesion of bone marrow-derived progenitors to tumors. These events could contribute to vasculogenesis and growth of tumors. E-selectin may be important in retarding the circulating bone marrow-derived cells in tumors. In addition, it might be involved in strengthening the adhesion of infiltrating cells within the proliferating tumor endothelium.

Figure 13: Circulating SDF-1α (ELISA)

A) Serum samples from healthy mice (n=9) and s.c. tumor-bearing mice (n=21) was assayed for circulating SDF-1α by ELISA. No difference was observed in the circulating SDF-1α levels between the two groups.

B) Circulating SDF-1α was compared in the female (triangle) and male (circle) mice in both healthy (filled) and s.c. tumor-bearing (open) groups. Data not significant by two-way ANOVA

A

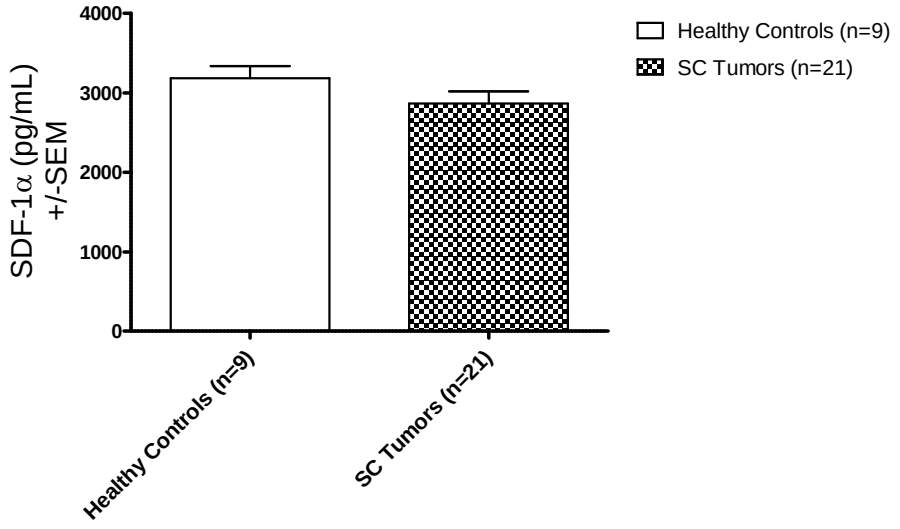
4000
3000
2000
1000
0
SDF-1α (pg/mL)
+/-SEM
Healthy Controls (n=9)
SC Tumors (n=21)
Healthy Controls (n=9)
SC Tumors (n=21)

B

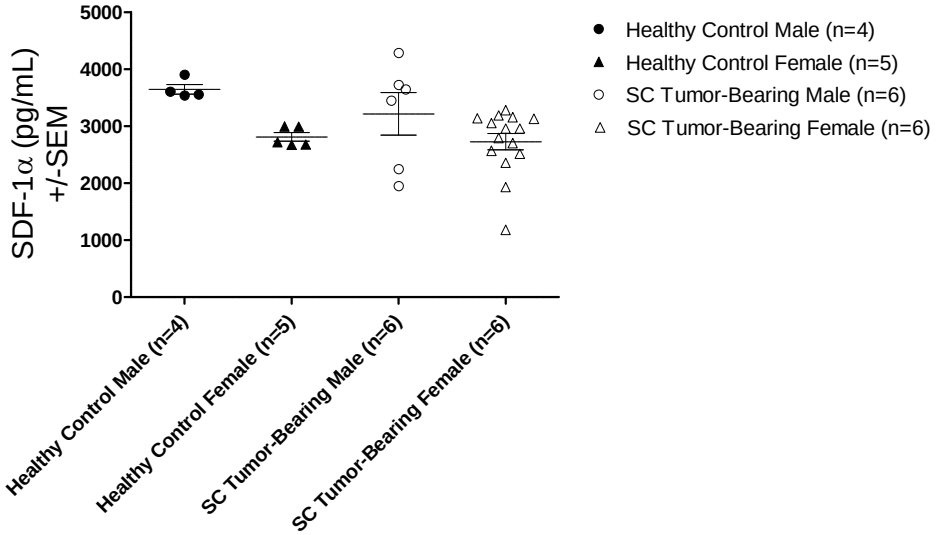
5000
4000
3000
2000
1000
0
SDF-1α (pg/mL)
+/-SEM
Healthy Control Male (n=4)
Healthy Control Female (n=5)
SC Tumor-Bearing Male (n=6)
SC Tumor-Bearing Female (n=6)
Healthy Control Male (n=4)
Healthy Control Female (n=5)
SC Tumor-Bearing Male (n=6)
SC Tumor-Bearing Female (n=6)

B: The Role of E-selectin and SDF-1α in the *In Vitro* Adhesion of Bone Marrow-derived Lineage-negative Cells to Tumors

Rationale:

The second aim of this research project was to evaluate the role of SDF-1α and E-selectin as a cell adhesion molecule on tumor-derived cells. It is widely accepted that SDF-1α acted as a chemoattractant for $CXCR4^{+}$ endothelial and bone marrow-derived cells. We hypothesized that SDF-1α was associated with tumor endothelium and acted as a potential cell adhesion molecule, and circulating bone marrow-derived endothelial progenitors that localized to tumors could bound to tumor endothelium-associated SDF-1α and incorporated into the proliferating blood vessel, thereby contributing to the growth of tumors. In the previous chapter, it was demonstrated that metastatic tumors had elevated levels of SDF-1α compared to naïve tissue samples. In addition, it was illustrated that *in situ* SDF-1α co-localized with the tumor endothelium. In this chapter, using *in vitro* assays, we tested if SDF-1α mediated the adhesion of bone marrow-derived cells to tumors. The role of E-selectin in this interaction was also evaluated.

The first part of this chapter describes the three cell populations used for *in vitro* adhesion experiments: murine lineage-negative bone marrow cells (Lin^{-} BMC), Dissociated LLCaB Tumor Cells (DTC) and control dermal fibroblasts. Because endothelial progenitors (EPC) are a subset of Lin^{-} BMC and constitute a tiny proportion of total bone marrow cells, the use of Lin^{-} BMC for adhesion experiments was thought to be most practical. DTC were chosen for *in vitro* adhesion assays because they represented the heterogeneous cell populations in tumors more accurately than any one cell-line. Results of *in vitro* assays to evaluate the adhesion of Lin^{-} BMC to monolayers of DTC and other control cell types (LLCaB, bEnd.3, VEC, and 3T3-L1)

are subsequently presented. LLCaB was used to measure of Lin^- BMC to tumor cells. bEnd.3 (mouse brain tumor endothelioma) cell line shares properties with activated endothelium, and was used as a surrogate for tumor endothelial cells. Primary cultures of vascular endothelial cell (VEC) were used as a negative control (resting endothelial cells). The pre-adipocyte cell line 3T3-L1 was a negative control for non-specific adhesion. In addition, the adhesion of control dermal fibroblast cells to DTC and bEnd.3 monolayers was also evaluated. Finally, to assess the roles of E-selectin and SDF-1α in the binding of Lin^- BMC to various cell monolayers, we attempted to inhibit adhesion by blocking CXCR4 (a receptor for SDF-1α) and E-selectin.

Results:

Isolation and Characterization of Lineage-negative BMC

Bone marrow cells are comprised of lineage-negative (pluripotent) cells and lineage-committed cells, i.e. cells that are committed to a specific cell lineage such as erythrocytes, monocytes, macrophages, dendritic, natural killer, and B- and T-cells. The Lin^- BMC were isolated by immunomagnetic depletion of lineage-committed cells from intact bone marrow (Figure 4) that was harvested from femurs and tibias of wild-type C57Bl/6 or *EGFP*-transgenic (C57Bl/6-Tg(ACTb*EGFP*)10sb/J) mice. The Lin^- BMC was found to constitute 3-5% of the intact BMC and contained only about 5% lineage-committed cells after negative purification. Intact BMC and Lin^- BMC were assayed for the expression of a variety of growth factor ligands and receptors (Figure 14A).

Lin^- BMC that express cKit and Sca1 (also known as LSK cells) comprise an enriched population of EPC (115;120). Intact BMC were indirectly labeled with *FITC*-labeled lineage panel antibodies, anti-cKit-*APC,* and anti-Sca1-*PE*. To quantitate the percentage of LSK cells, the $FITC^-$ BMC were gated and evaluated for cells positive for both red ($Sca1^+$) and blue ($cKit^+$)

fluorescence. An average of 42±12 % (n=7) and 19±4 % (n=6) Lin^- BMC expressed cKit and Sca1 respectively. However, only 3-9% of Lin^- BMC expressed both cKit and Sca1. As reported, Lin^- BMC constituted 3-5% of total BMC and $Sca1^+cKit^+$ (SK) were 3-9% of Lin^- BMC, thus the $Lin^-Sca1^+cKit^+$ (LSK) subset was calculated to constitute only about 0.3% of intact BMC.

The expression of several proteins that defined specific cell populations on intact and Lin^- BMC were compared: 1) stem/progenitor cells (cKit and Sca-1), 2) cells expressing E-selectin ligands (Lamp-1 and CD43), 3) cells expressing chemokine receptors (CXCR4, CXCR2), 4) cells expressing receptors for vascular endothelial growth factors (VEGFR1 and VEGFR2), and 5) endothelial cells (VCAM, CD31 and CD34) (Figure 14B). Lin^- BMC were enriched for cells of endothelial cell lineage and for cells that expressed cognate ligands/receptors for E-selectin and CXCR4. Lin^- BMC contained significantly enriched populations of $CD31^+$, $LAMP1^+$, $CXCR4^+$, $cKit^+$, and $cKit^+Sca1^+$ cells compared to intact BMC. Although, only about 10% of Lin^- BMC were $VEGFR2^+$, almost 35 % of the Lin^- BMC expressed VEGFR1. VEGFR1 is reported to be closely related to VEGFR2, and shared common and specific ligands, and regulated angiogenesis (9). The $Lin^-Sca1^+cKit^+$ (LSK) cells that expressed $VEGFR2^+$ have been reported to be EPC. Our data showed that almost 90% of LSK-BMC expressed VEGFR2 (Figure 15), suggesting that LSK cells were predominantly endothelial progenitors. Moreover, approximately 85% LSK cells were also $CXCR4^+$ (Figure 15, data from one experiment). These data indicated that Lin^- BMC were enriched for $Sca1^+cKit^+$ progenitors, and that LSK-BMC predominantly contained endothelial progenitors, and expressed CXCR4.

Figure 14: Characterization of Lineage-negative BMC

A) Magnetic depletion of lineage-committed cells from total bone marrow cells was used to enrich the lineage-negative (Lin^-) BMC. After the depletion protocol, approximately 95% BMC were Lin^- BMC. Lin^- BMC were double labeled with anti-cKit*APC* and anti-Sca-1-*PE* antibodies. The green box in the dot-plot in the upper right quadrant side shows the LSK cells, that is, the $Sca1^+cKit^+$ (SK) cells of Lin^- BMC population. Lin^- BMC were also labeled with *PE*-conjugated antibodies for E-selectin ligands (LAMP1 and CD43) and SDF-1α receptor (CXCR4) and analyzed by flow cytometry.

B) Expression of cell surface proteins in intact BMC and Lin^- BMC were incubated with *PE*-conjugated antibodies and analyzed by flow cytometry (* $p < 0.05$ Intact BMC vs. Lin^- BMC by 2-tailed Student's t-test).

A

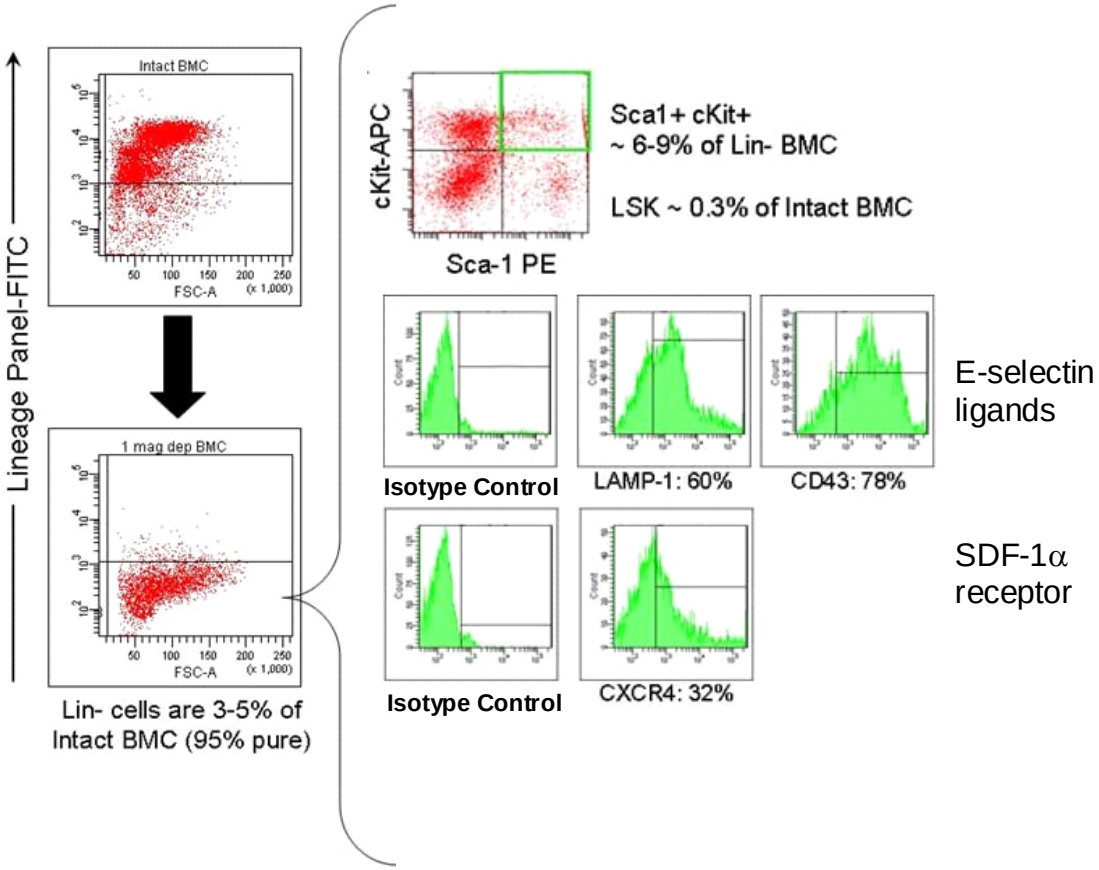
Intact BMC
FSC-A
Lineage Panel-FITC
1 mag dep BMC
Lin- cells are 3-5% of Intact BMC (95% pure)
cKit-APC
Sca-1 PE
Sca1+ cKit+
~ 6-9% of Lin- BMC
LSK ~ 0.3% of Intact BMC
Isotype Control
LAMP-1: 60%
CD43: 78%
E-selectin ligands
Isotype Control
CXCR4: 32%
SDF-1α receptor

B

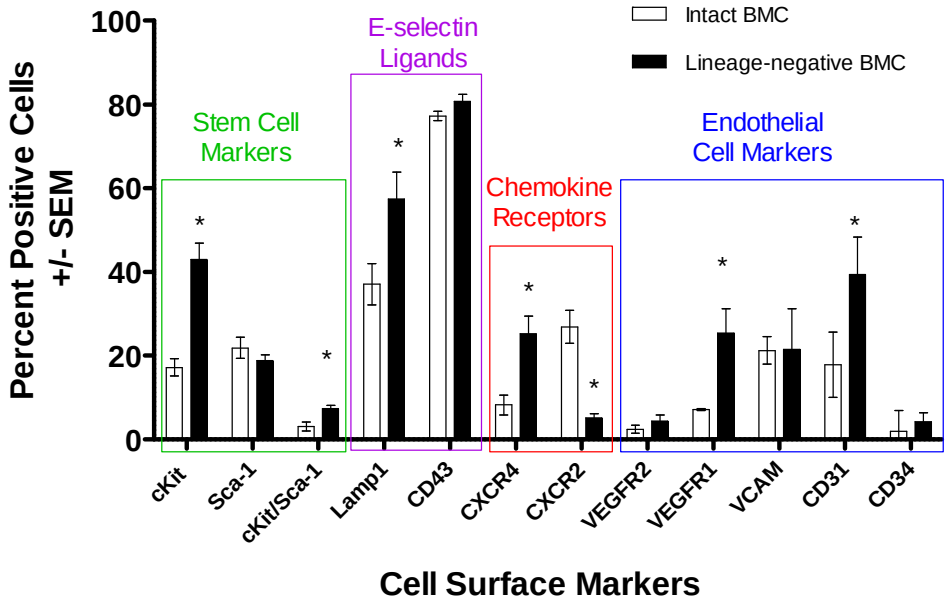
Intact BMC
Lineage-negative BMC
Percent Positive Cells +/- SEM
Stem Cell Markers
E-selectin Ligands
Chemokine Receptors
Endothelial Cell Markers
cKit
Sca-1
cKit/Sca-1
Lamp1
CD43
CXCR4
CXCR2
VEGFR2
VEGFR1
VCAM
CD31
CD34
Cell Surface Markers

Figure 15: Lin^{-} $Sca1^{+}cKit^{+}$ BMC are highly Enriched for Endothelial Progenitor Cells

Lin^{-} BMC isolated by immunomagnetic depletion of lineage-committed bone marrow cells were incubated with anti-cKit-*APC*, anti-Sca1-*PE*/*FITC*, and anti-CD31-*FITC*, anti-VEGFR2-*PE* or anti-CXCR4-*PE* and analyzed by three-color flow cytometry. LSK subset was significantly enriched for $VEGFR2^{+}$ cells, and expressed CXCR4.

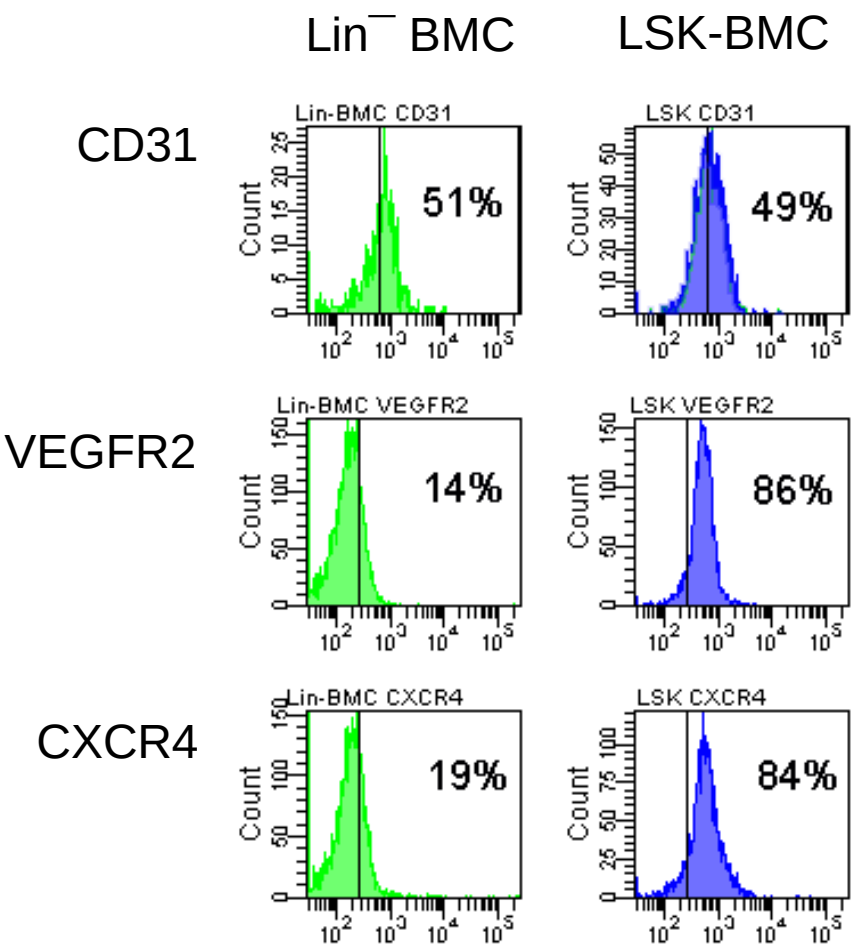
Lin⁻ BMC
LSK-BMC
CD31
VEGFR2
CXCR4
Lin-BMC CD31
51%
LSK CD31
49%
Lin-BMC VEGFR2
14%
LSK VEGFR2
86%
Lin-BMC CXCR4
19%
LSK CXCR4
84%
Count

Characterization of Cultured Dissociated-LLCaB Tumors

Subcutaneous tumors (average tumor volume 1081±456 mm^3, average days post cell injection 23±3) were harvested and dissociated, as described, and adherent cell cultured. These adherent cells were designated as Dissociated Tumor Cells (DTC).

Confluent adherent DTC cultures were collected over time in culture using Trypsin-EDTA and monitored for the of tumor endothelial cell markers E-selectin and VEGFR2 by flow cytometry. Cell surface levels of both E-selectin and VEGFR2 gradually increased over time, peaked by day 9-15 of culture, and then declined (Figure 16A). Similar results were obtained from all DTC cultures evaluated (n=4).

DTC cultures were analyzed for the expression of SDF-1α by quantitative RT-PCR; expression of SDF-1α gene transcript was compared to the expression of endogenous control Beta-2 microglobulin (*β2M*). As graphically represented in Figure 16B, SDF-1α was expressed at moderate levels and the expression of both SDF-1α (n=16, average Ct = 28.7 ± 2.99) and *β2M* (n=16, average Ct = 16.4 ± 1.0) was consistent in all DTC cultures over time. Some of the samples (n=7) with $Ct_{\beta 2M}$ = 24.2 ± 4.7 were excluded from the analysis; high $Ct_{\beta 2M}$ was most likely due sub-optimal quality of RNA and/or cDNA. SDF-1α gene transcript was detected at higher levels in both VEC (n=6; $Ct_{SDF\text{-}1\alpha}$ = 24.3 ± 5.6, $Ct_{\beta 2M}$ = 16.7 ± 2.5) and bEnd. 3 (n=5; $Ct_{SDF\text{-}1\alpha}$ = 20.5 ±1.3, $Ct_{\beta 2M}$ = 17.7 ± 0.6) cultures compared to DTC. Using $2^{-\Delta\Delta Ct}$ method for calculating relative gene expression, we observed that bEnd.3 and VEC expressed 4X and 1X folds higher levels SDF-1α, compared to calibrator 3T3-L1 cells. Additionally, SDF-1α mRNA in DTC was calculated to be 0.01X that in 3T3-L1 cells.

The association of SDF-1α protein with DTC was analyzed by immunohistochemical staining of DTC cultures in chamber slides. Cell cultures were fixed, incubated with unlabeled

anti-E-selectin and anti-SDF-1α, followed by additions of *FITC*- or *PE*-labeled secondary antibodies. DAPI was used to stain the cell nuclei. Some wells received only isotype-matched control antibodies and/or secondary antibodies to test for non-specific staining. Overall, compared to control wells, a substantial staining was observed on DTC with anti-SDF-1α and E-selectin antibodies (Figure 16C). Cells positive for E-selectin were most likely tumor endothelial cells. SDF-1α was observed to be associated with numerous E-selectin expressing endothelial cells, in agreement with our hypothesis.

Isolation and Characterization of Control Cell Type (Dermal Fibroblast)

Fibroblasts were isolated from dorsal and ventral trunk skins of 1-3 day-old mouse pups. The cell surface and total expression of LAMP1, CD43, and CXCR4 by dermal fibroblasts was evaluated by flow cytometry using five separate cell preparations (Figure 17). Only LAMP1 was detected on the cell surface. More than 70% of dermal fibroblasts appeared to have intracellular reserves of LAMP1 and CD43, as evaluated by total staining of permeabilized cells. However, CXCR4 expression was not detected on the cell surface or within the cells in these cultured dermal fibroblasts (Figure 17 A and B).

Adhesion Assay and Quantitation of Adhered Cells

Confluent monolayer cultures of 3T3-L1, VEC, bEnd.3, LLCaB and DTC in 24- or 12-well plates were used for the adhesion assays. Lin^- BMC (0.5×10^5 or 1×10^5) isolated from adult *EGFP*-transgenic mice were added to the above mentioned cell cultures. *EGFP*-Lin^- BMC were used because these cells fluoresced green and could be visualized and enumerated by fluorescence microscopy and flow cytometry. The non-adherent cells were washed after 30 min.

Figure 16: Characterization of Dissociated Tumor Cell Culture

A) DTC cultures were analyzed over time for expression of E-selectin and VEGFR2 by flow cytometry. The number of cells positive for E-selectin and VEGFR2 increased in culture by 9-12 days and then started declining in all DTC cultures tested. Similar results were observed in four separate experiments.

B) SDF-1α gene transcript expression in DTC from six different tumors was evaluated by quantitative RT-PCR in duplicate (n=1 for days 2, 5 and 7, and n=3 days 4, 6, 9, 13, and 14). Beta-2-microglobulin (*β2M*) was used as the endogenous control (qRT-PCR). SDF-1α expression was reasonably consistent over time and between different DTC cultures.

C) Representative photomicrographs of DTC cultured in chamber slides that were stained with *FITC*-labeled E-selectin (green) and *PE*-labeled SDF-1α (red) or isotype controls. DAPI (blue), a nuclear stain, was used to delineate cells. Cells that stained for both E-selectin and SDF-1α are yellow. The arrowhead indicated where SDF-1α staining appears membrane-associated.

A

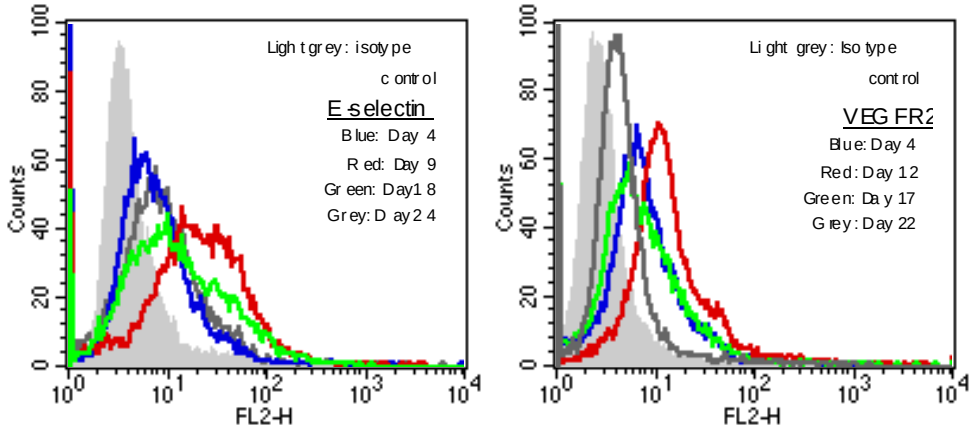
Light grey: isotype control
E-selectin
Blue: Day 4
Red: Day 9
Green: Day18
Grey: Day24
Counts
FL2-H
Light grey: Isotype control
VEGFR2
Blue: Day 4
Red: Day 12
Green: Day 17
Grey: Day 22
Counts
FL2-H

B

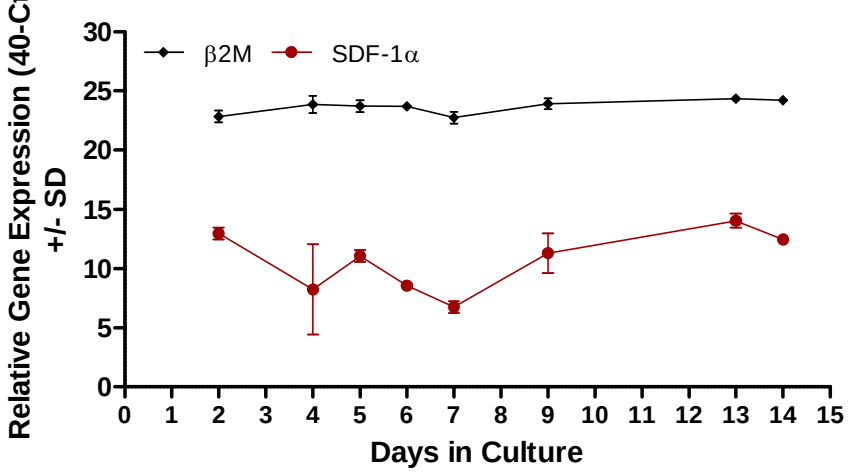
β2M
SDF-1α
Relative Gene Expression (40-Ct) +/- SD
Days in Culture

C

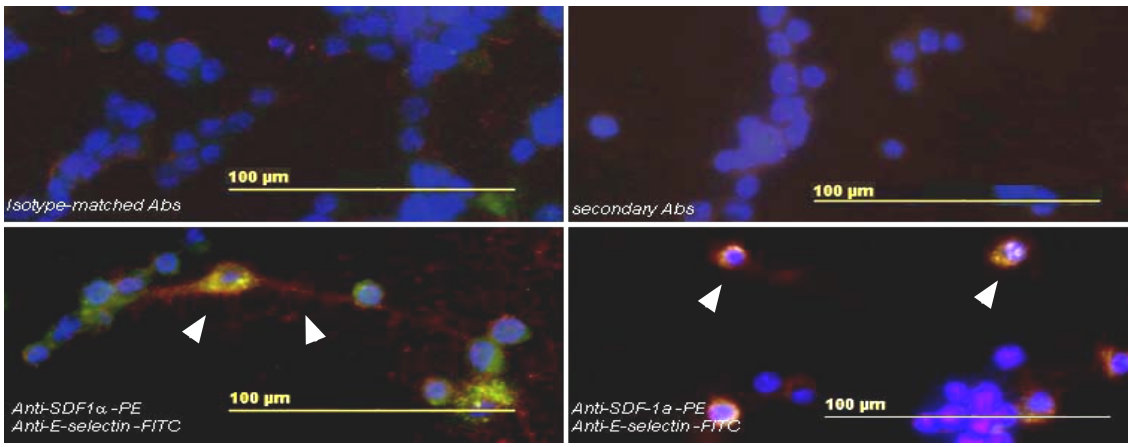
Isotype-matched Abs
100 μm
secondary Abs
100 μm
Anti-SDF1α-PE
Anti-E-selectin-FITC
100 μm
Anti-SDF-1a-PE
Anti-E-selectin-FITC
100 μm

Figure 17: Characterization of Dermal Fibroblasts

A) Representative histogram overlay from flow cytometric analysis of cell surface and total protein expression by murine dermal fibroblasts (n=4). Only LAMP1 was detected on the cell surface of 46% dermal fibroblasts. 73% dermal fibroblasts had intracellular reserves of CD43. No CXCR4 was detected in these cells.

B) Average percentage of dermal fibroblasts positive for the expression of cell surface and total LAMP1, CD43, and CXCR4 from five separate cell preparations (Average of five separate assays).

A

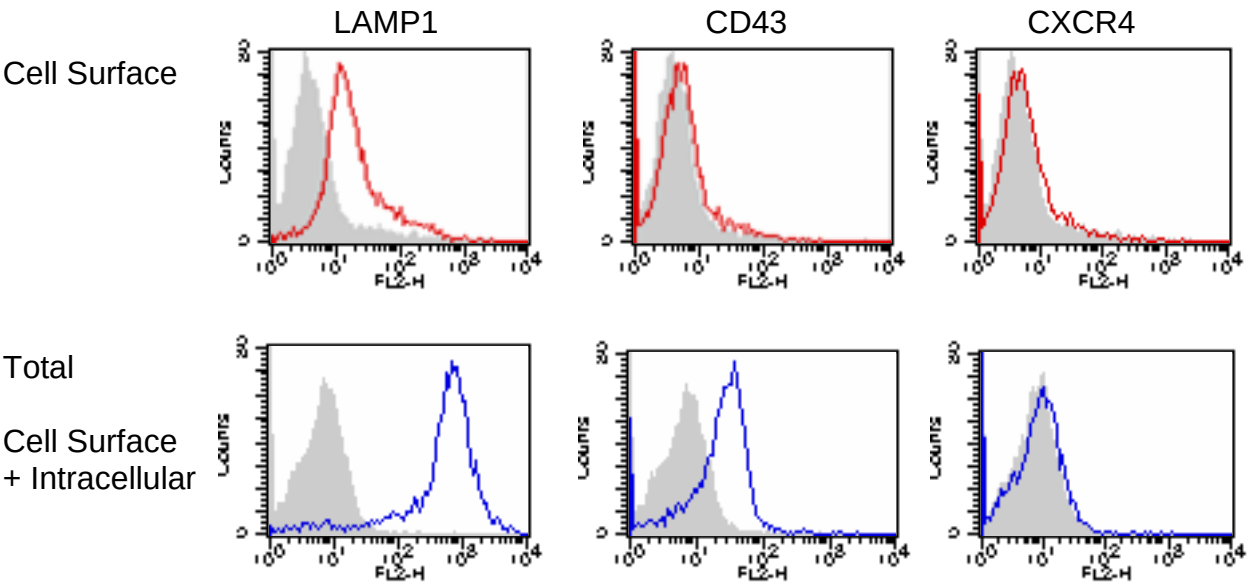
LAMP1
CD43
CXCR4
Cell Surface
Total
Cell Surface
+ Intracellular
Counts
FL2-H

B

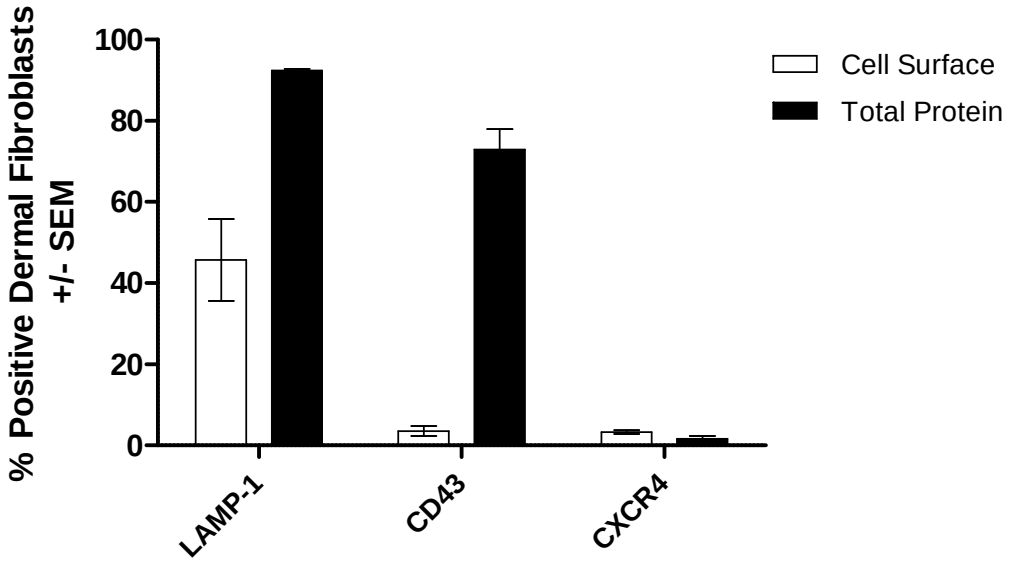
% Positive Dermal Fibroblasts
+/- SEM
100
80
60
40
20
0
Cell Surface
Total Protein
LAMP-1
CD43
CXCR4

All plates were observed on an inverted fluorescent microscope and representative photographs were obtained (Figure 18A). Next, cell monolayers and adherent BMC were harvested using trypsin-EDTA and *EGFP*-Lin$^-$ BMC were enumerated by manual counting on an upright fluorescent microscope using a hemocytometer. Additionally, cell suspensions were also analyzed by flow cytometry (Figure 18B). These assays were performed twice.

During adhesion experiments, a separate tube containing 0.5×10^5 or 1×10^5 *EGFP*-Lin$^-$ BMC was set aside as a control (i.e. not added to culture wells) to determine the accuracy of the two methods used to enumerate adherent fluorescent cells. This control tube was treated the same with respect to washes, and centrifugation and enumeration, as all other cell cultures. The manual counting method using fluorescent microscopy, in 3 experiments, ranged from 55-143% (i.e. control cells that were counted under white light on a phase contrast microscope could be visualized under fluorescent light). This was most likely because the fluorescent light intensity on the microscope was set so that the hemocytometer grid could be visualized; thus dimmer *EGFP*-cells were not apparent. This problem was exacerbated by the small size of Lin$^-$ BMC. It was not practical to set the light intensity to a setting that enabled visualization of even dim *EGFP* cells, because either the grid was not visible or non-specific autofluorescence of non-*EGFP* cells in experimental samples would then hinder enumeration of *EGFP*-cells. When the control tube of *EGFP*-Lin$^-$ BMC was analyzed by flow cytometry, only 36% (range of 23-51% in 5 assays) of cells were detected. The low efficiency with the flow cytometer was apparently because *EGFP*-Lin$^-$ BMC has cells with varying fluorescent intensity and small cell size. In addition, there was a significant overlap in the fluorescence between *EGFP*-Lin$^-$ BMC and the autofluorescence of the non-fluorescent adherent cells.

Adhesion of Lin$^-$ BMC and Lin$^-$ Sca1$^+$cKit$^+$ (LSK) BMC

More *EGFP*-Lin$^-$ BMC adhered to DTC cultures than to other cell types (Figures 18). Data was evaluated as the total number and percent Lin$^-$ BMC that adhered to cultured cells. The adhesion assays was conducted in either 12-well or 24-well format, and although different, but proportional, numbers of *EGFP*-Lin$^-$ BMC were added to all plates. Thus, reporting the data as the percentage of Lin$^-$ BMC adhered was most favorable. Greatest percentage of Lin$^-$ BMC adhered to DTC cultures compared to other cell types assayed (Figure 18 A and B).

The Lin$^-$ BMC contained progenitors of many different cell types. As mentioned earlier, endothelial progenitor cells (EPC) are a subset of Lin$^-$ BMC that expressed both cKit and Sca1 (also known as LSK cells). To quantitate the number of adherent LSK cells, the cells harvested from adhesion assays were incubated with anti-cKit-*APC* and anti-Sca1-*PE* antibodies. Samples were analyzed by three-color flow cytometry by gating on the green *EGFP*-Lin$^-$ BMC. Although, significantly fewer Lin$^-$ BMC adhered to the surrogate tumor endothelial cell line (bEnd.3), the average percentage of Sca1$^+$cKit$^+$ (SK) cells that bound to bEnd.3 cells was 2.4-times higher than the %SK that bound to DTC (data not shown). Additionally, 1.6-times greater %SK adhered to VEC compared to DTC (data not shown). This suggested that the LSK population preferentially bound to activated endothelial cells. Because the percent Sca1$^+$cKit$^+$ (SK) cells in Lin$^-$ BMC varied between experiments, reporting the data as the percentage of LSK cells adhered to the total LSK cells in each Lin$^-$ BMC isolation was optimum. The %LSK cells adhered was a ratio of total LSK cells adhered (%SK × Total *EGFP*-Lin$^-$ BMC adhered per well) to total LSK cells incubated with adherent monolayers in each well (%SK × Total *EGFP*-Lin$^-$ BMC added per well). Overall, a significantly higher percentage of LSK subset adhered to DTC cultures compared to other cell types (Figure 18C).

Figure 18: Analysis of Adhesion of Lin$^-$ BMC to Different Cell Types

A) *EGFP*-Lin$^-$ BMC were added to confluent cell cultures (DTC, LLCaB, bEnd.3, VEC and 3T3-L1) or blank plates for about 30 min. The non-adherent *EGFP*-Lin$^-$ BMC were washed and adhesion was reviewed on fluorescent microscope. Representative photomicrographs from adhesion assay showed that significantly greater number of *EGFP*-Lin$^-$ BMC adhered to DTC cultures compared to other cell types.

B) *EGFP*-Lin$^-$ BMC, in cell suspensions from adhesion assays, were enumerated manually, and by flow cytometric analysis. A significantly higher percentage of Lin$^-$ BMC adhered to DTC cultured compared to other cell types. Average data from two separate assays.

C) Percentage of Sca1$^+$cKit$^+$ in adhered Lin$^-$ BMC, i.e. LSK cells, were evaluated by three-color flow cytometry. %LSK cells adhered was calculated as (%SK × Total *EGFP*-Lin$^-$ BMC adhered per well) / (%SK × Total *EGFP*-Lin$^-$ BMC added per well). By FACS analysis, a significantly greater %LSK cells was observed to adhere to DTC cultured compared to other cell types. When data was compared based on manual enumeration, no difference was detected between the adhesion of LSK cells to DTC, LLCaB and bEnd.3. Average data from two separate assays. P-value < 0.0001 by one-way ANOVA; Post-hoc Dunnett's test comparing adhesion to each cell-type to adhesion to DTC * $p < 0.05$ and *** $p < 0.001$.

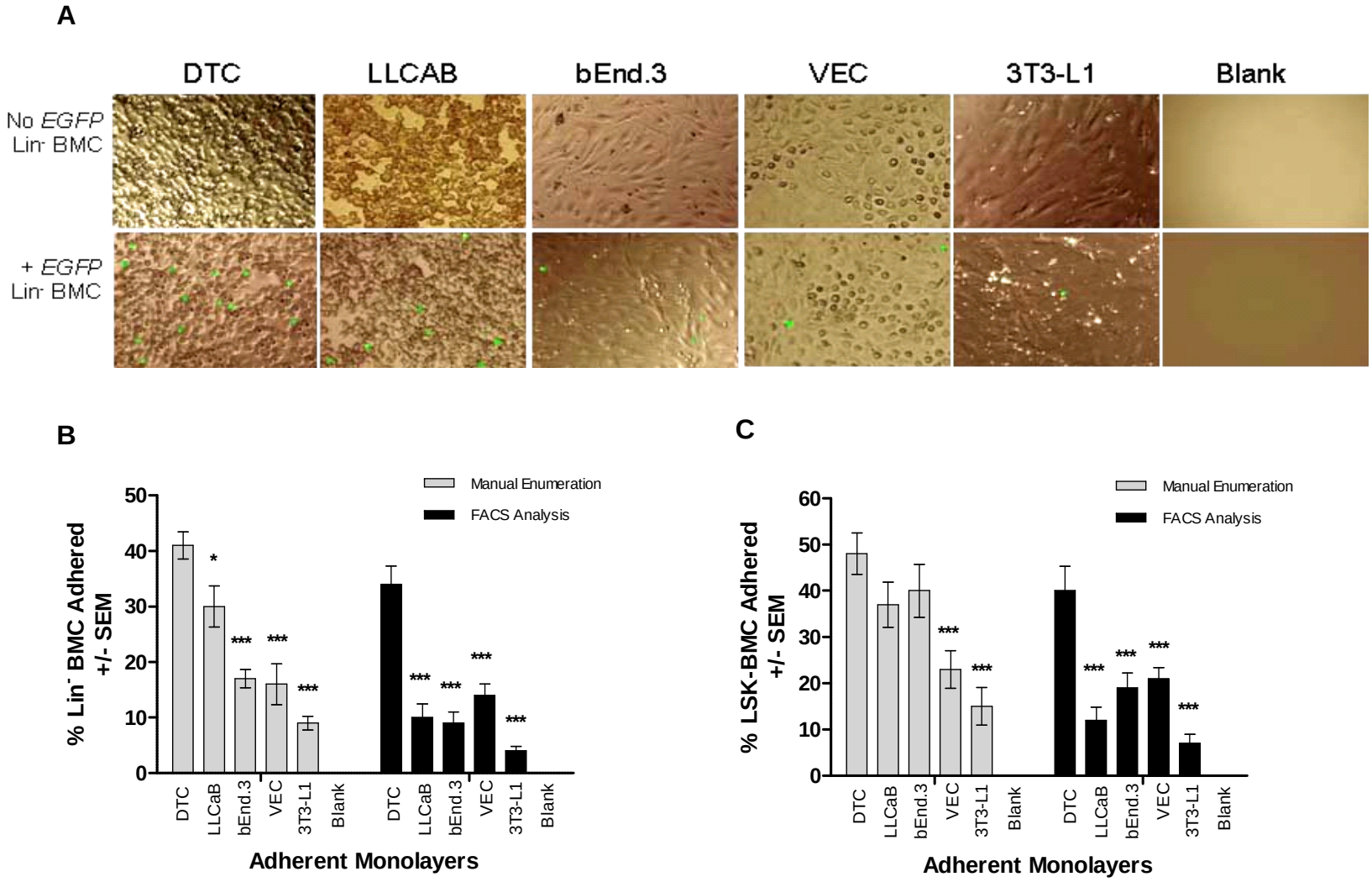
A
DTC
LLCAB
bEnd.3
VEC
3T3-L1
Blank
No EGFP Lin- BMC
+ EGFP Lin- BMC
B
Manual Enumeration
FACS Analysis
% Lin- BMC Adhered +/- SEM
Adherent Monolayers
C
Manual Enumeration
FACS Analysis
% LSK-BMC Adhered +/- SEM
Adherent Monolayers

Role of CXCR4 and E-selectin in Adhesion of Lin$^-$ BMC and LSK Cells

The role of CXCR4 and SDF-1α in the adhesion of Lin$^-$ BMC and LSK subset to DTC cultures was evaluated in the presence of two CXCR4-blocking agents: AMD3100 and anti-CXCR4 antibody (Figure 19). AMD3100 (Plerixafor) is a bicyclic compound that is a specific antagonist for CXCR4 (272-274).

Lin$^-$ BMC were incubated with 0.001, 0.01, 0.1, or 1μM AMD3100 for 15 min prior to adding these cells to adherent monolayers of different cell cultures. Viability of Lin$^-$ BMC incubated in different concentrations of AMD3100 was evaluated at the end of each assay by Trypan Blue exclusion assay. AMD3100 did not affect the viability of cells at any of the above-mentioned concentrations (data not shown). There was a significant decrease in the number of Lin$^-$ BMC and LSK cells that adhered to DTC cultures in the presence of AMD3100 at all concentrations tested (Figures 19 A and B). Similarly, a significant decrease was observed in the adhesion of total number of Lin$^-$ BMC and %LSK cells to DTC in the presence of anti-CXCR4 antibody (Ab) at 12.5 μg/ml and anti-E-selectin Ab at 25 μg/ml (Figures 19 C-F). Overall, there was maximum decrease of 60, 50, and 30% in the adhesion of the total number of Lin$^-$ BMC to DTC in the presence of AMD3100, anti-CXCR4 Ab, and anti-E-selectin Ab (Figures 19 A, C and E). The total number of LSK cells that adhered to DTC also decreased in the presence of AMD3100, anti-CXCR4, and anti-E-selectin by 40, 50, and 30% respectively (Figure 19 B, D and F).

Adhesion of Lin$^-$ BMC to bEnd.3 cells in the presence of AMD3100 was evaluated. There was only a modest decrease in adhesion of Lin$^-$ BMC to bEnd.3 (Figure 20A). Nonetheless, the percentage of LSK cells that adhered to bEnd.3 in presence of AMD3100 decreased considerably. When this data was extrapolated to calculate the total number of LSK

cells that adhered to bEnd.3, 82% fewer LSK cells had adhered to bEnd.3 monolayers in the presence of all concentrations of AMD3100 tested (Figure 20B). The binding of Lin^- BMC and LSK cells to LLCaB tumor cell monolayers in the presence of AMD3100 was comparable to control wells with media only or to isotype-matched antibody (Figure 20 C and D).

The adhesion of control cell type (*EGFP*-dermal fibroblasts) with DTC and bEnd.3 monolayers in the absence and presence of AMD3100 was evaluated in 2-3 separate assays. A significant number of dermal fibroblasts adhered to both DTC and bEnd.3 cell cultures, but this adhesion was relatively less compared to the adhered Lin^- BMC. Furthermore, this adhesion was not mediated by the interaction of SDF-1α and CXCR4 (Figure 21 A and B).

Synopsis:

These data demonstrated that DTC cultures expressed SDF-1α and E-selectin. The *in vitro* adhesion assays suggested that Lin^- BMC cell preferentially bound to cultures of dissociated tumor cell. In addition, LSK cells preferentially appeared to adhere to cells of endothelial lineage. This adhesion was mediated by the interaction of CXCR4 on Lin^- BMC/LSK cells and SDF-1α associated with the cell monolayers. E-selectin also appeared to be instrumental in the adhesion of Lin^- BMC and LSK cell. To our knowledge, this is the first report showing that SDF-1α acted as an adhesion molecule *in vitro* on tumor-derived cells.

Figure 19: Investigation of Blocking Adhesion of Lin$^-$ BMC to Confluent DTC Cultures

EGFP-Lin$^-$ BMC were incubated in increasing concentrations of AMD3100 or media only before adding to the DTC monolayers. Adhesion of *EGFP*-Lin$^-$ BMC and LSK cells was evaluated by flow cytometry.

A) A significant decrease was observed in the % Lin$^-$ BMC adhered to DTC in presence of increasing concentrations of AMD3100 (Average of 3 separate assays). P-value <0.05 by one-way ANOVA; Post-hoc Dunnett's test comparing each treatment to media control * $p<0.05$ in individual assays

B) A significant decrease in %LSK subset that adhered to DTC cultures was observed at all AMD3100 concentrations tested (Average from 2 separate assays). P-value $=0.01$ by one-way ANOVA; Post-hoc Dunnett's test comparing each treatment to media control * $p<0.05$ in individual assays.

C-D) *EGFP*-Lin$^-$ BMC were incubated with media only, isotype-matched Ab (Ig) or anti-CXCR4 Ab only before addition to DTC monolayers. Approximately 50% decrease in adhesion of Lin$^-$ BMC (C) and % LSK population (D) was observed in the presence of anti-CXCR4 Ab at 12.5 μg/mL (Average data from 3 separate experiments). P-value <0.0001 by Students t-test compared to isotype-matched control antibody.

E-F) DTC cultures were incubated with unlabeled anti-E-selectin Ab, isotype-matched Ab (Ig) or media only before addition of *EGFP*-Lin$^-$ BMC. About 30% inhibition in adhesion of Lin$^-$ BMC (E) and LSK cells (F) was observed in the presence of 25 μg/mL anti-E-selectin Ab. (Average data from 2 separate experiments). P-value <0.001 by Students t-test to isotype-matched control antibody.

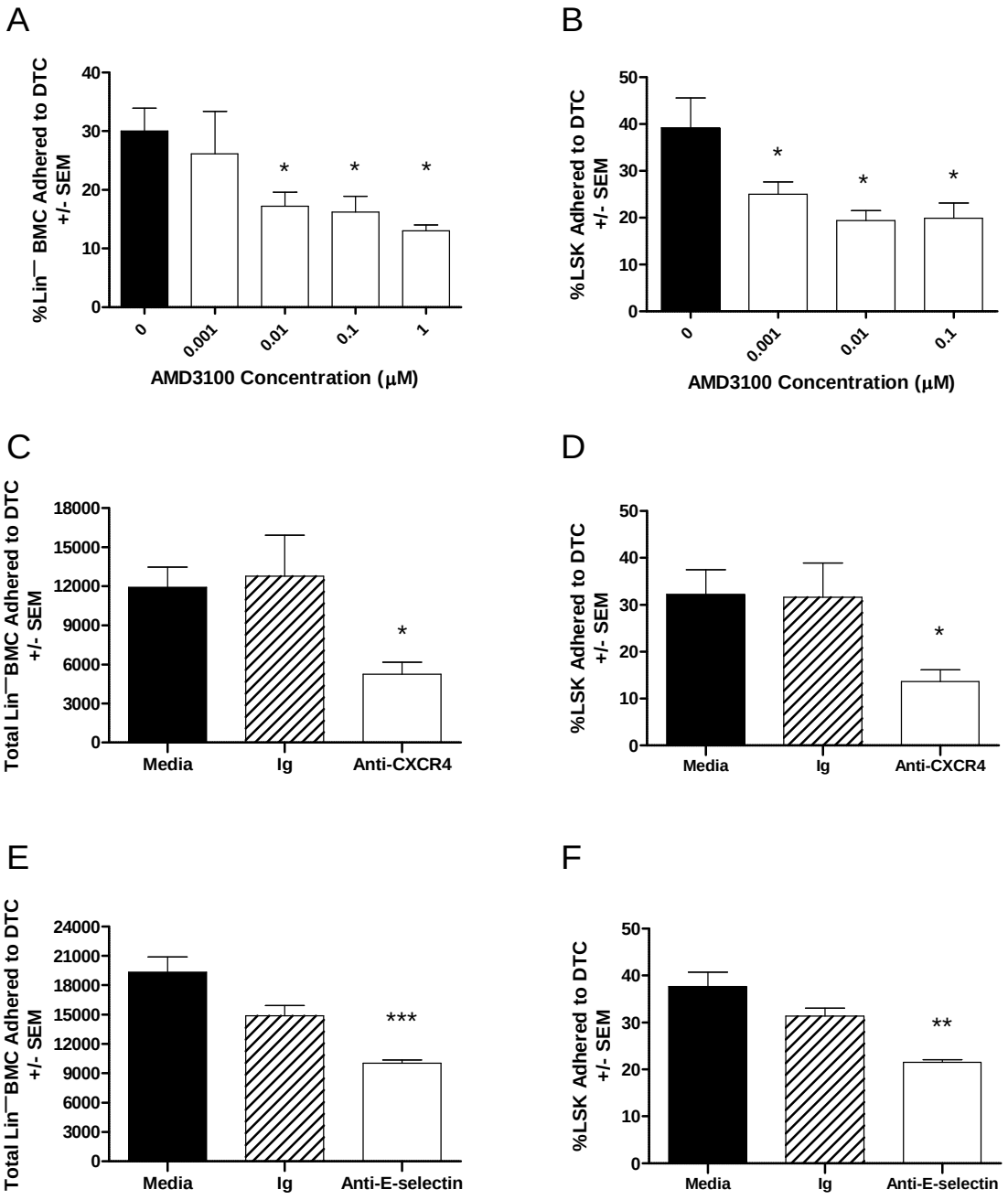
A
%Lin⁻ BMC Adhered to DTC +/- SEM
40
30
20
10
0
*
*
*
0
0.001
0.01
0.1
1
AMD3100 Concentration (μM)
B
%LSK Adhered to DTC +/- SEM
50
40
30
20
10
0
*
*
*
0
0.001
0.01
0.1
AMD3100 Concentration (μM)
C
Total Lin⁻ BMC Adhered to DTC +/- SEM
18000
15000
12000
9000
6000
3000
0
*
Media
Ig
Anti-CXCR4
D
%LSK Adhered to DTC +/- SEM
50
40
30
20
10
0
*
Media
Ig
Anti-CXCR4
E
Total Lin⁻ BMC Adhered to DTC +/- SEM
24000
21000
18000
15000
12000
9000
6000
3000
0
***
Media
Ig
Anti-E-selectin
F
%LSK Adhered to DTC +/- SEM
50
40
30
20
10
0
**
Media
Ig
Anti-E-selectin

Figure 20: Study of Blocking Adhesion of Lin$^-$ BMC to bEnd.3 and LLCaB Monolayers

A) *EGFP*-Lin$^-$ BMC were incubated with media only or different concentrations of AMD3100 before adding to bEnd.3 monolayers. P-value = ns by one-way ANOVA, Average of 2 assays.

B) The total number of LSK cells that adhered to bEnd.3 in the presence of AMD3100 decreased up to 80%. P-value *<0.001* by one-way ANOVA; Post-hoc Dunnett's test comparing each treatment to media control *** *p<0.0001*, Average of 4 assays.

C-D) *EGFP*-Lin$^-$ BMC were incubated in media only or different concentrations of AMD3100 were added to LLCaB monolayers. No significant difference was observed in the adhesion of Lin$^-$ BMC or LSK cells to LLCaB monolayers. P-value = ns by one-way ANOVA.

A

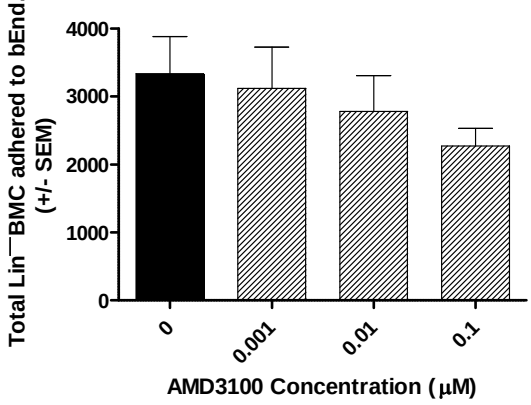
Total Lin⁻BMC adhered to bEnd.3 (+/- SEM)
4000
3000
2000
1000
0
0
0.001
0.01
0.1
AMD3100 Concentration (μM)

B

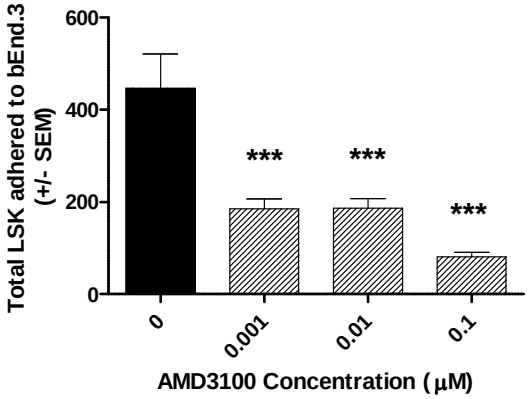
Total LSK adhered to bEnd.3 (+/- SEM)
600
400
200
0
***
***
***
0
0.001
0.01
0.1
AMD3100 Concentration (μM)

C

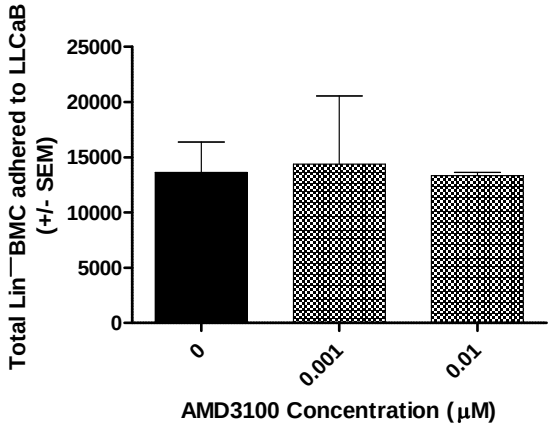
Total Lin⁻BMC adhered to LLCaB (+/- SEM)
25000
20000
15000
10000
5000
0
0
0.001
0.01
AMD3100 Concentration (μM)

D

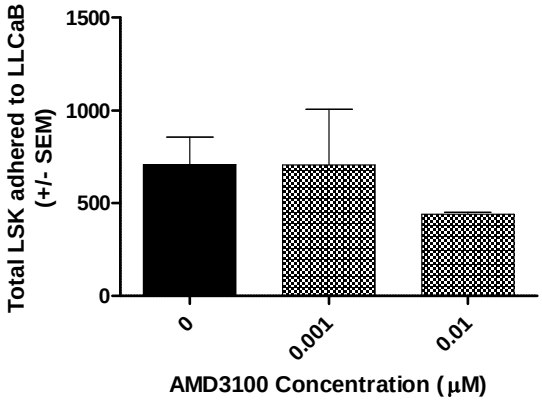
Total LSK adhered to LLCaB (+/- SEM)
1500
1000
500
0
0
0.001
0.01
AMD3100 Concentration (μM)

Figure 21: Evaluation of Dermal Fibroblast Adhesion to DTC and bEnd.3 Monolayers

EGFP-dermal fibroblasts were pretreated with increasing concentrations of AMD3100 before incubating with cultured DTC or bEnd.3. *EGFP*-dermal fibroblasts adhesion was quantitated by flow cytometry.

A) AMD3100 treatment did not affect the adhesion of dermal fibroblasts with DTC cultures (Average data from 3 assays).

B) No significant difference was observed in the adhesion of dermal fibroblasts with bEnd.3 cells in presence of AMD3100 (Representative data from 2 assays).

A

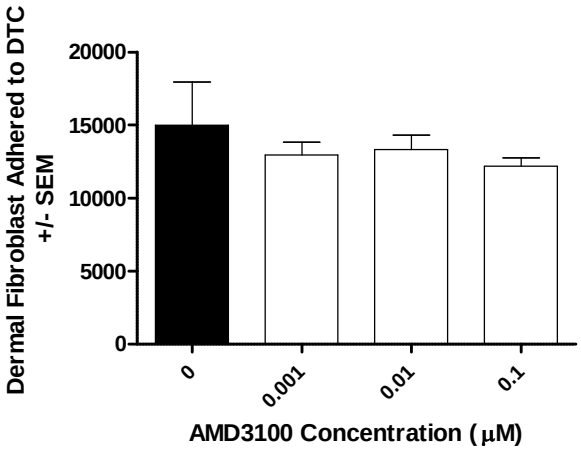
Dermal Fibroblast Adhered to DTC
+/- SEM
20000
15000
10000
5000
0
0
0.001
0.01
0.1
AMD3100 Concentration (μM)

B

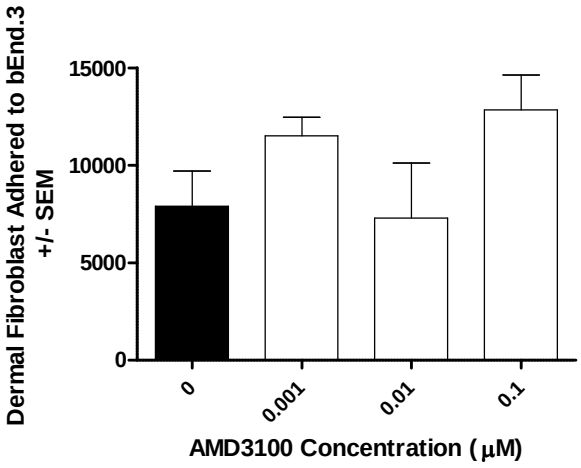
Dermal Fibroblast Adhered to bEnd.3
+/- SEM
15000
10000
5000
0
0
0.001
0.01
0.1
AMD3100 Concentration (μM)

C: Real-time PCR to Determine the Transgene Copy Number and to Quantitate the Biolocalization of Adoptively-transferred *EGFP*-Transgenic Cells

Rationale:

The third aim of this project was to evaluate the *in vivo* localization of Lin^- BMC in adoptive transfer experiments in the previously described metastatic model. In past, our laboratory assessed the biolocalization of adoptively-transferred vascular endothelial cells (VEC) in this same model. In these experiments, mice with metastatic disease were injected with *EGFP*-VEC, euthanized 24-72 hours later, and the harvested pulmonary and hepatic tumors and other major organs were frozen in OCT. Tissue sections were evaluated by fluorescent microscopy. Although *EGFP*-VEC were specifically observed in metastatic tissue, (Figure 22) this analysis was severely compromised by tissue autofluorescence and tissue artifacts. Often fluorescent cell-like structures were visible in sections from mice that did not receive any *EGFP*-VEC (data not shown). This prompted the development of an alternate, objective, and accurate method for quantitation of tissue-localized *EGFP*-cells.

Quantitative real-time PCR (qPCR) methodology has not been widely utilized to quantitate *egfp*-transgene-bearing cells in biodistribution studies. A qPCR assay was developed to quantitate *egfp*-transgene in the genomic DNA isolated from various tissues in this syngeneic murine tumor model. The development and standardization of the qPCR methodology is discussed in this chapter.

Results:

Accurate Quantitation of Genomic DNA

DNA was extracted from tissue as described in the Materials and Methods section. In the initial qPCR experiments, the amount of DNA used for qPCR was determined

Figure 22: Biolocalization of Adoptively-transferred *EGFP*-VEC in Mice with Metastatic Disease

Tissue sections from control mice (+/- *EGFP*-VEC), and mice with metastatic disease (+/- *EGFP*-VEC) were visualized on a fluorescent microscope. *EGFP*-VEC are visible as a bright punctuate pattern, specifically in metastatic lungs from mice that were injected with *EGFP*-VEC (Lungs 7, 8 and 9) compared to lungs from healthy mice that received *EGFP*-VEC (Lungs 4, 5 and 6). No *EGFP*-VEC were detected in heart, spleen, or kidney by microscopy.

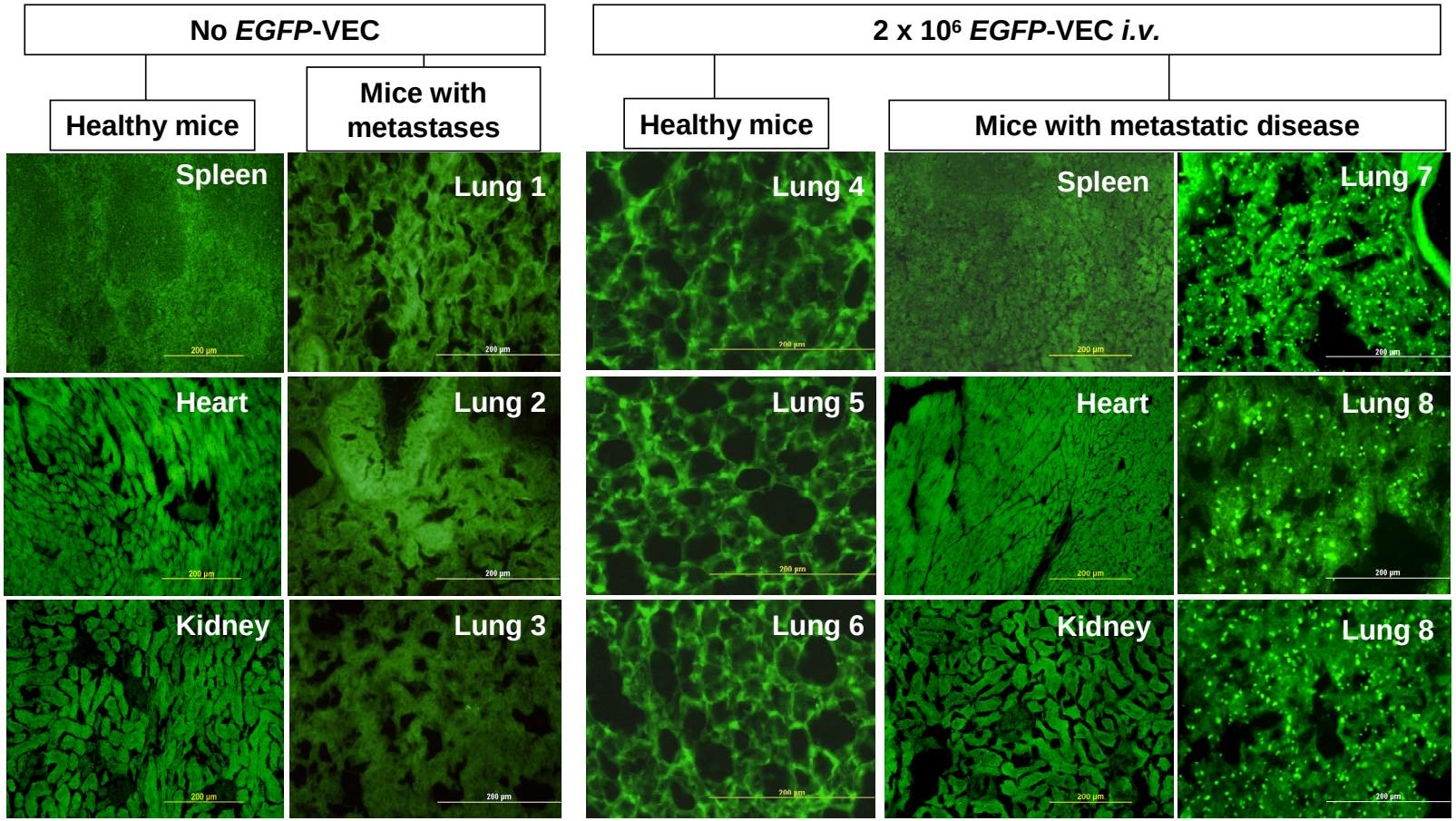

Representative sections: 18µm lung sections 400X, 10µm heart, spleen, kidney sections 200X

spectrophotometrically (OD_{260}). Beta-actin (*β-actin*) was used as an endogenous control for qPCR. Consistently higher *β-actin* cycle threshold (Ct) values were observed in both C57Bl/6 wild-type and *EGFP*-transgenic mice with genomic DNA (gDNA) isolated from liver tissue compared to lung tissue (25.3± 0.2 vs. 23.6± 0.2, respectively; n=9, $p<0.0001$). Liver samples from transgenic mice also exhibited higher Ct values for the *egfp*-transgene, corresponding to a 2-fold difference in *EGFP* copy number between lung and liver. It was hypothesized that gDNA from liver samples may have a high degree of contamination by proteins or organic compounds, undetected by $OD_{260/280}$ ratios(267) , which were comparable for DNA isolated from lung and liver samples. Thus, a SYBR green-based 96-well assay was used to determine the gDNA concentrations accurately (268). The concentration of gDNA was calculated based on the standard curve built using serial dilutions of DNA of known concentration. After diluting the gDNA, the isolates were analyzed by agarose gel and SYBR Green fluorescence and results indicated that the amount of gDNA in liver samples was 27% of that indicated by spectrophotometric measurement (Figure 23). No significant differences were observed in lung DNA concentrations determined by the two methods. The SYBR Green method was thus the optimal method for gDNA quantitation.

Plasmid Standard Curve for Absolute Quantitation of *EGFP*-transgene in qPCR Assay

In the initial qPCR assays, plasmid *pEGFP*-N3 (Figure 24A) dilutions were prepared in nuclease-free water. However, these standard curves showed significant variation between assays (Figure 24B). Since a very low amount (picogram-attogram) of plasmid was used for the standard curve, the inconsistency was probably due to the plasmid sticking to the polypropylene plastic tube. This was overcome by preparing the plasmid (p*EGFP*-N3) dilutions in carrier DNA,

Figure 23: Comparison between Spectrophotometric Method and SYBR-green Assay to Quantitate Genomic DNA Concentration

A) Genomic DNA (250 ng based on OD_{260}) from liver (lanes 1-5) and lung (lanes 6-10) tissue of five different mice shows significant difference in band intensity on agarose gel. Lane 11 shows the 1 Kb Plus DNA ladder.

B) The concentration of genomic DNA (100 ng based on OD_{260}) from liver and lung were measured spectrophotometrically (OD_{260}) and using the 96-well SYBR-Green assay. Mean concentration of gDNA by SYBR-green fluorescent assay (Liver = 26.5±1.37, Lung = 96.6±20.3).

A

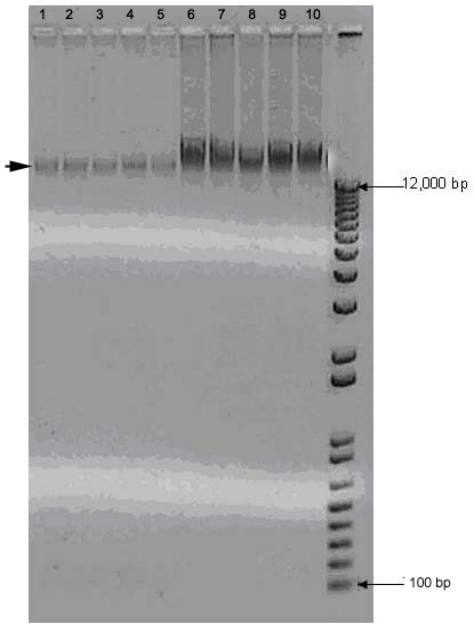
1 2 3 4 5 6 7 8 9 10
12,000 bp
100 bp

B

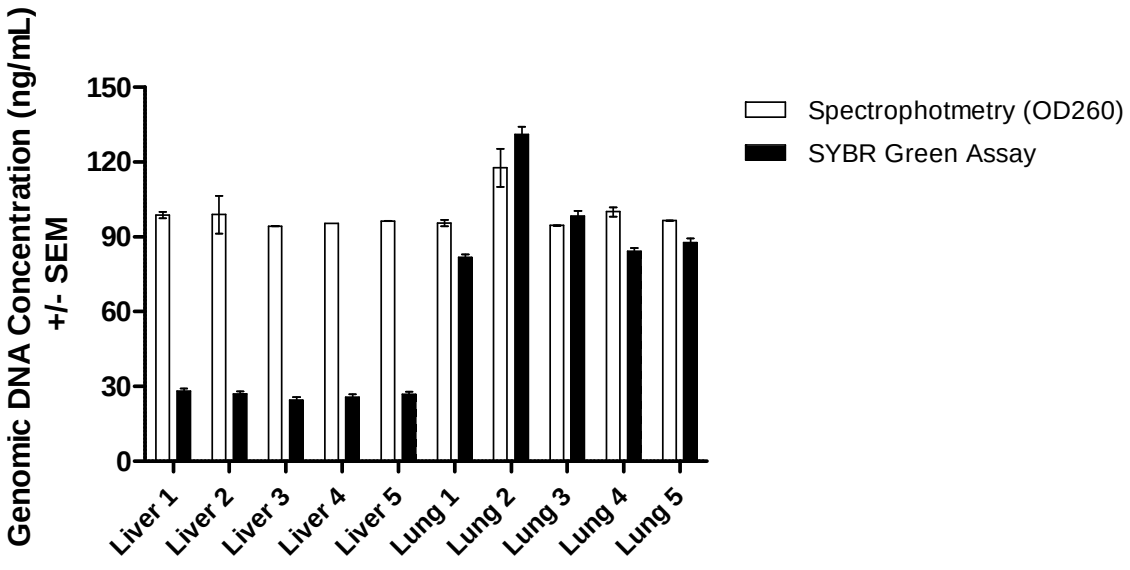
Genomic DNA Concentration (ng/mL)
+/- SEM
150
120
90
60
30
0
Liver 1
Liver 2
Liver 3
Liver 4
Liver 5
Lung 1
Lung 2
Lung 3
Lung 4
Lung 5
Spectrophotmetry (OD260)
SYBR Green Assay

which was genomic DNA isolated from either lung or liver of C57Bl/6 wild-type mice. This, subsequently, gave standard curves that were consistent between assays (Figure 23C). When the plasmid was diluted in carrier DNA from lung or liver, no significant difference in amplification was observed (data not shown).

***EGFP*-Transgene Copy Number**

To understand how the *egfp*-transgene copy number from experimental samples correlated to the number of transplanted *EGFP*-cells in biolocalization studies, the *egfp*-transgene copy number in the genome of C57Bl/6-Tg(Actb*EGFP*)10sb/J mice was determined. When the *pEGFP*-N3 plasmid was used to construct a standard curve, TaqMan® qPCR detected as few as two copies of the *egfp*-transgene; this assay was repeated with high reproducibility. qPCR analysis of DNA from hemizygous Actb*EGFP*- transgenic mice was subsequently repeated using 100 ng gDNA template as determined by SYBR Green. No *egfp* amplification was observed with gDNA from lungs and livers of C57Bl/6 wild-type mice (negative controls) included in each assay. Replicates were consistent, the Ct values and copy number determinants did not differ significantly between lung and liver samples (Table 8). Overall, gDNA (100 ng) from hemizygous mice was found to contain about 33,300 copies of the transgene, which corresponded to two copies of the *egfp*-transgene per cell. Previously, another group had determined that the *egfp*-transgene was inserted at a single site in the mouse genome of C57Bl/6-Tg(ACTb*EGFP*)10sb/J mice by FISH analysis (http://kumikae01.gen-info.osaka-u.ac.jp/tg/TGFISHresult1.cfm). However, transgenic mice often have tandem copies of the transgene at one insertion site (270). Thus, the hemizygous C57Bl/6-Tg(ACTb*EGFP*)10sb/J (Actb*EGFP*) mice have two copies of *egfp*-transgene inserted in tandem. This method compared

Figure 24: Standardization of Plasmid Standard Curve

A) Plasmid p*EGFP*-N3 containing the *egfp*-transgene

B) Representative standard curve from five separate experiments using plasmid dilutions prepared in nuclease free water resulted in erratic standard curve

C) Representative standard curve from seven separate experiments prepared by diluting the plasmid in carrier DNA (genomic DNA from lung or liver DNA from C57Bl/7 mouse) were consistently reproducible and were used for making standard curves in all subsequently assays.

A

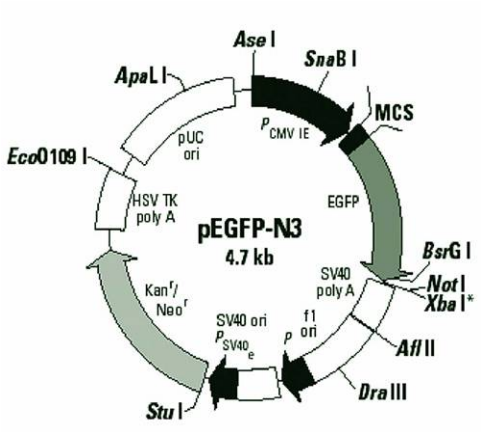
Ase I
SnaB I
ApaL I
MCS
P CMV IE
pUC ori
Eco0109 I
HSV TK poly A
EGFP
pEGFP-N3
4.7 kb
BsrG I
Not I
Xba I*
SV40 poly A
Kanr/ Neor
SV40 ori
P SV40e
f1 ori
P
AflII
DraIII
StuI

B

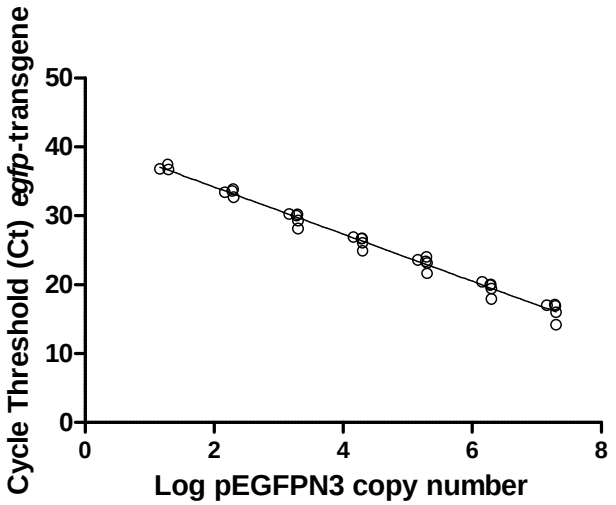
Cycle Threshold (Ct) egfp-transgene
50
40
30
20
10
0
0
2
4
6
8
Log pEGFPN3 copy number

C

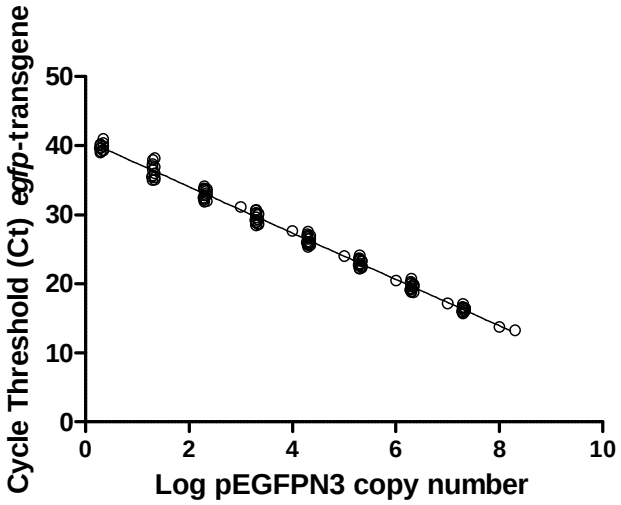
Cycle Threshold (Ct) egfp-transgene
50
40
30
20
10
0
0
2
4
6
8
10
Log pEGFPN3 copy number

Table 8: Two copies of *EGFP*-transgene per cell calculated from genomic DNA from the hemizygous mouse strain C57Bl/6-Tg(ACTb*EGFP*)10sb/J

Tissue	Sample ID*	Average Ct *EGFP***	Average Ct B-actin**	*EGFP* copy number per cell***	AVG copy number per cell
Lung	201	24.82 ± 0.11	23.09 ± 0.11	2.1	**1.8 ± 0.26**
	203	24.95 ± 0.13	23.48 ± 0.03	2	
	205	25.31 ± 0.14	23.58 ± 0.09	1.5	
	207	25.09 ± 0.07	23.28 ± 0.09	1.8	
	209	25.29 ± 0.12	23.37 ± 0.05	1.6	
Liver	200	24.81 ± 0.01	23.48 ± 0.1	2.2	**1.92 ± 0.25**
	202	25.11 ± 0.31	23.5 ± 0.1	1.8	
	204	24.76 ± 0.16	23.36 ± 0.1	2.2	
	206	25.08 ± 0.07	23.57 ± 0.17	1.8	
	208	25.18 ± 0.16	23.48 ± 0.16	1.7	

** Tissue samples from five different transgenic mice*

*** Average Ct values from duplicate samples assayed in two separate experiments (n=4)*

**** EGFP copy number based on average standard curve equation from two assays (y =-3.4x + 40.3)*

favorably with the $2^{-\Delta\Delta Ct}$ qPCR method for determining transgene copy number, especially when a transgenic animal with a known copy number was unavailable for comparison.

In one series, we analyzed DNA (lung, liver, and VEC) from the Actb*EGFP*-transgenic mice along with DNA from the homozygous transgenic C57Bl/6Tg(UBC_GFP)30/Scha/J strain (Ubq*EGFP*). Using *β-actin* as endogenous control and the $2^{-\Delta\Delta Ct}$ method, we found that both strains contained the same number of copies of the transgene (Figure 25). Thus, Ubq*EGFP*-transgenic mice have a single transgene at a single insertion site per haploid cell and thus had two copies per diploid (somatic) cell. Although the homozygous C57Bl/6-Tg(ACTb*EGFP*)10sb/J (Actb$EGFP^{+}$)-transgenic mice die within the first month of birth, we bred these mice to confirm the *egfp*-copy number. qPCR results show that these mice have four copies of the *egfp*-transgene compared to two copies in hemizygous Actb*EGFP*-transgenic strain (Figure 3B). Thus, the *egfp*-transgene copy number in both hemizygous C57Bl/6-Tg(ACTb*EGFP*)10sb/J and homozygous C57Bl/6Tg(UBC_GFP)30/Scha/J mouse strains was calculated to be two.

Association between Manual Cell Count and qPCR to Enumerate Tissue-Localized *EGFP*-Transgenic Cells

As stated above, using fluorescent microscopy, systemically administered *EGFP*-VEC were visualized in metastases, but were not detected in healthy organs. However, high tissue autofluorescence often prohibited the analysis of specimens, particularly in lung tissue. For the development of the qPCR assay to quantitate tissue localized *EGFP*-cells, three control groups: (1) healthy, (2) metastases-bearing mice not injected with *EGFP*-VEC, and (3) healthy mice injected with *EGFP*-VEC, were used along with test group: metastases-bearing mice injected

Figure 25: *EGFP* Copy Number in Transgenic Mouse Strains

Egfp-transgene copy number in hemizygous C57Bl/6-Tg(Actb*EGFP*)10sb/J (n=4) was calculated using the plasmid stand curve in qPCR assays. The *egfp*-transgene copy number in homozygous C57Bl/6-Tg(Actb*EGFP*)10sb/J (n=5) and C57BL/6-Tg(UBC-GFP)30Scha/J (Ub-*EGFP*) (n=3) were calculated by $2^{-\Delta\Delta Ct}$ methods.

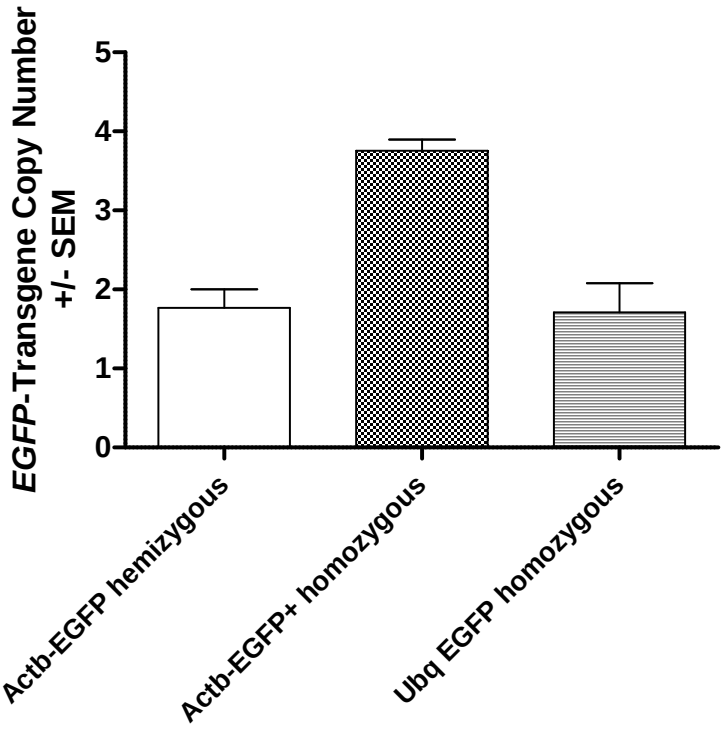
EGFP-Transgene Copy Number
+/- SEM
5
4
3
2
1
0
Actb-EGFP hemizygous
Actb-EGFP+ homozygous
Ubq EGFP homozygous

with *EGFP*-VEC. *EGFP*-VEC were manually enumerated by examining 10 μm liver sections by fluorescent microscopy (an average of 21 sections examined/group). No *EGFP*-VEC were found in liver sections from control groups 1 and 2 (healthy and metastases-bearing mice not injected with *EGFP*-VEC). A few apparent *EGFP*-VEC were detected in liver sections from a single mouse in control group 3 (healthy mice injected with *EGFP*-VEC) (Figure 26 A and B). In contrast, a significant number of *EGFP*-VEC were detected in metastases-bearing mice injected with *EGFP*-VEC (33±7 *EGFP*-VEC/mm^2 vs. 3±5 in controls, $p<0.001$). In order to compare directly with manual enumeration, liver tissue was scraped from the same slides enumerated (Figure 26A) and gDNA was extracted and analyzed by qPCR. Replicates within each assay were consistent (average Ct standard deviation=0.24). The transgene was undetected in livers from control groups. In contrast, *EGFP* was detected in 100% (4/4) of metastatic liver tissue from mice injected with *EGFP*-VEC. A Pearson correlation coefficient of 0.81 indicated a strong positive correlation between the two methods (275), although the actual number of *EGFP*-VEC per section differed (Figure 26C). Quantitative differences were most likely due to a culmination of things: underestimation by PCR, poor DNA recovery from the slides (170 ng per section), and pooling of sections causing dilution of transgene signal.

Due to the low overall number of tumor-localized VEC in the former experiment, intra-tumor (*i.t.*) injection of *EGFP*-VEC into subcutaneous (s.c.) tumor model was used for further assay validation. C57Bl/6 mice bearing approximately 150 mm^3 s.c. LLCaB tumors were injected *i.t.* with saline (n=4) or *EGFP*-VEC (n=8). Tumors were harvested 2 hours later and alternating 10 μm sections were assayed for *EGFP*-VEC by manual enumeration or qPCR. A total of 39-77 sections were assayed per tumor. The average values per section for every 80 μm segment of tissue (5 sections for qPCR and 3 intervening sections for microscopy) were plotted

Figure 26: Localization and Enumeration of *EGFP*-VEC to Liver Metastases

A) Representative fluorescent microscopy pictures of 10 µm liver sections from: 1) normal animal not injected with *EGFP*-VEC (n= 5); 2) normal animal injected with *EGFP*-VEC (n=5); 3-6) four metastases-bearing animals that received *EGFP*-VEC.

B) Manual enumeration of *EGFP*-VEC in liver metastases compared to control group 3 (healthy mice injected with *EGFP*-VEC) suggests that VEC specifically localized to tumor-bearing tissue.

C) Correlation of manual enumeration and qPCR. PCR analysis of tissue sections scraped from a subset of slides from normal mice injected with *EGFP*-VEC and metastases-bearing animals that received *EGFP*-VEC that were previously enumerated manually. Although DNA recovery was low, these results correlated strongly with *EGFP*-VEC enumeration determined by manual counting (Pearson correlation $\rho = 0.81$).

A

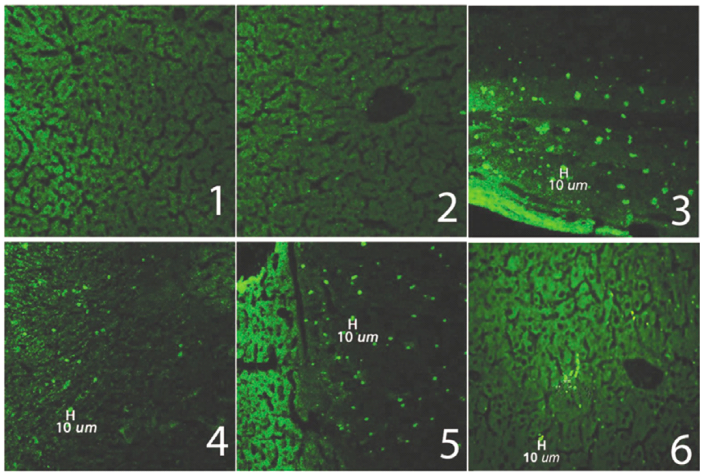
1
2
3
10 um
4
10 um
5
10 um
6
10 um

B

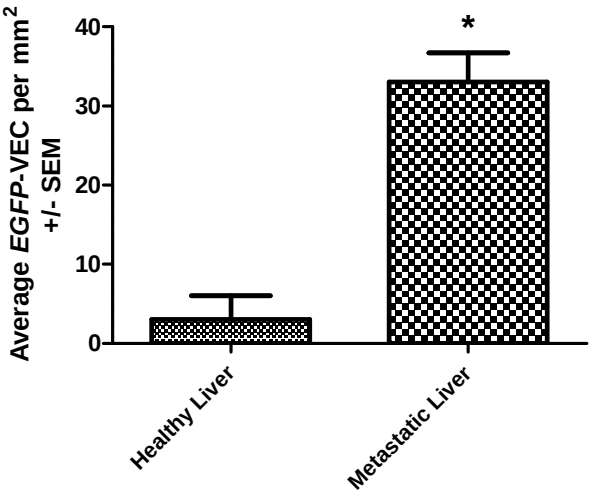
Average EGFP-VEC per mm2 +/- SEM
40
30
20
10
0
*
Healthy Liver
Metastatic Liver

C

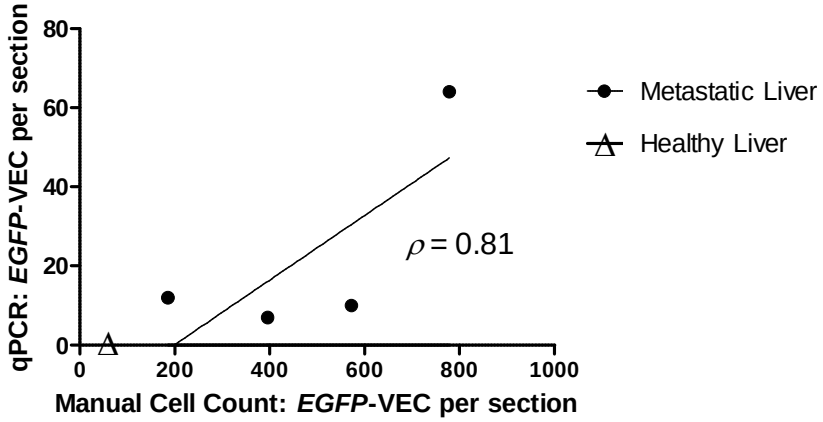
qPCR: EGFP-VEC per section
80
60
40
20
0
0
200
400
600
800
1000
Manual Cell Count: EGFP-VEC per section
ρ = 0.81
Metastatic Liver
Healthy Liver

for all tumors in all animals. Alternating 10 μm s.c. tumor sections were analyzed by fluorescent microscopy and qPCR as described above. PCR values were converted to the number of *EGFP*-VEC per section as described in Figure 7B. *EGFP*-VEC were detected, by both microscopy and PCR, in all eight s.c. tumors injected with *EGFP*-VEC. qPCR quantitation again correlated with enumeration by manual cell count, both when assayed sections from all tumors were plotted (positive Pearson correlation of *0.61*; Figure 27A) and when average *EGFP*-VEC per section per mouse were compared (strong positive Pearson correlation $\rho = 0.82$; Figure 27B). Although 85% of the sections from saline-injected tumors showed bright green apparent cell-like structures by microscopy, no *egfp* amplification was detected by qPCR in any saline control sample assayed. This was also true in some sections from *EGFP*-VEC-injected tumors.

All s.c. tumor sections were further analyzed by optical Z-stacks using confocal microscopy. Confocal microscopy was used to distinguish *EGFP*-VEC from artifactual fluorescence. Four 100 μm^2 areas of s.c. tumor sections, each containing an apparent fluorescent cell, were randomly selected and corresponding Z-stacks containing ten 1 μm optical sections were generated. Average intensities from 4 sections were plotted, starting at the tissue surface (confocal Z-stack section #1) through each descending 1 μm plane to confocal Z stack section #10. The average mean and maximum fluorescent intensities of sections of tumors injected with *EGFP*-VEC (n=8) were elevated throughout and were significantly higher than saline controls (n=4). The fluorescence intensity of each section as well as four 100 μm^2 areas per tumor, each containing an apparent fluorescent cell, was measured. Blinded analysis showed that the mean and maximum fluorescence intensity of sections (data not shown) and cell-like structures (Figure 27C) were significantly higher for tumors injected with *EGFP*-VEC compared to saline-injected

tumors ($p<0.005$). Fluorescent signals apparent by conventional microscopy (on a single plane) were thus sometimes due to tissue artifacts, not *EGFP*-VEC, leading to false positive results.

The biolocalization of adoptively-transferred *EGFP*-VEC in the metastatic model was analyzed by qPCR (Figure 28). The *egfp*-transgene was specifically detected in significantly higher quantities in lung and liver compared to other organs from mice with metastatic disease that were injected with *EGFP*-VEC. This data substantiated our earlier findings using fluorescent microscopy (Figure 22).

In conclusion, the qPCR assay for the *egfp*-transgene described here enabled the rapid, objective, and accurate quantitation of biolocalized transgenic cells and was superior to the microscopic examination of histological specimens.

Modification of qPCR Method to Assay Large Number of Samples

To increase the sensitivity of the qPCR assay to detect the *egfp*-transgene, five 50 μm thick tissue sections were collected in multiple tubes and DNA was extracted (Figure 5A). This generated several DNA samples per tissue and thus the qPCR assay was modified for a high throughput 384-well plate format. The qPCR assay efficiently translated from a 96-well plate format where reaction volume was 25 μl to a 384-well format where the reaction volume was 20 μl, using 100 ng DNA as template (Figure 29A and B). The Ct_{EGFP} and $Ct_{\beta\text{-}actin}$ were comparable between assays for the negative control DNA from C57Bl/6 mice (Blk 1-3, n=3), positive control DNA from Actb *EGFP*-transgenic mice (Actb*EGFP* 1-3, n=3), and test DNA samples from mice with metastatic disease injected with *EGFP*-VEC (n=12).

To increase the amount of genomic DNA to be assayed in 20 μl qPCR reaction a dose-response experiment was conducted using 100, 200, 400, and 600 ng DNA. Although *egfp* amplification was proportional to increasing amounts of DNA extracted from *EGFP*-transgenic

Figure 27: Comparison of Manual Enumeration and qPCR Method to Quantitate Tissue-Localized *EGFP*-Transgenic Cells

A) A positive correlation (Pearson correlation ρ = 0.61; range 0.2-1.0) was observed between the two methods i.e. manual enumeration and qPCR for quantitation of *EGFP*-VEC.

B) The overall average values per section per tumor plotted for each animal. There was a strongly positive correlation (Pearson correlation coefficient ρ = 0.82) between the two methods.

C) Confocal microscopy analysis was used to distinguish *EGFP*-VEC from artifactual fluorescence. The average mean and maximum fluorescent intensities of sections of tumors injected with *EGFP*-VEC (n=8) were elevated throughout the section and were significantly higher than saline controls (n=4).

A

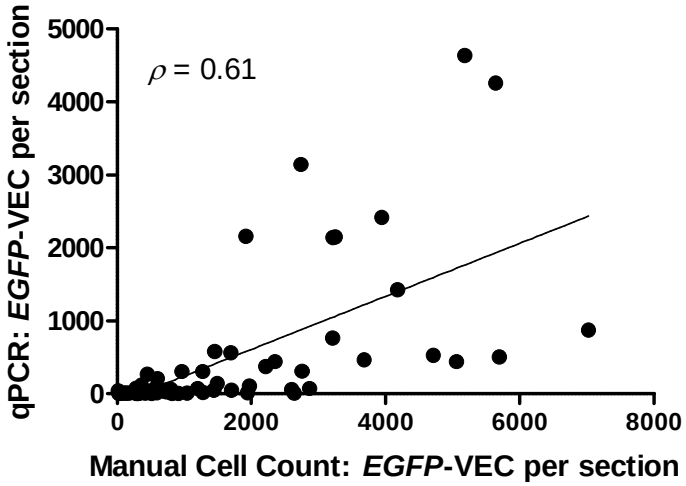
ρ = 0.61
qPCR: EGFP-VEC per section
Manual Cell Count: EGFP-VEC per section
0
1000
2000
3000
4000
5000
6000
8000

B

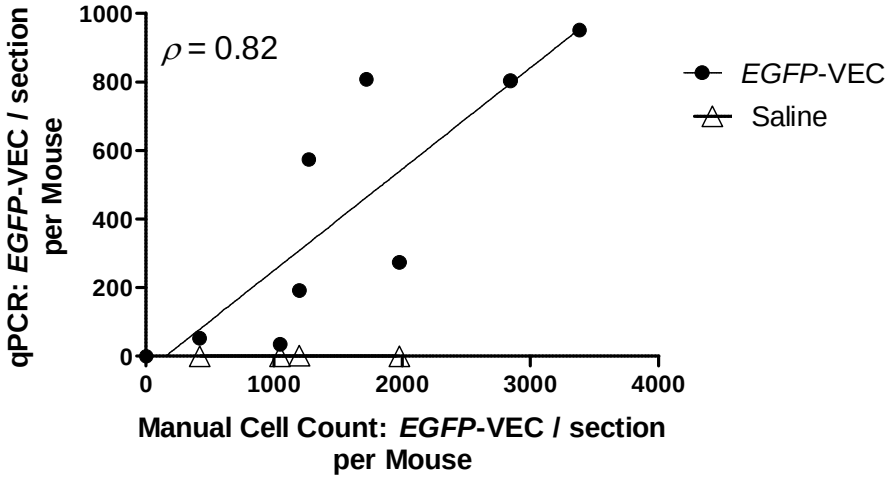
ρ = 0.82
qPCR: EGFP-VEC / section per Mouse
Manual Cell Count: EGFP-VEC / section per Mouse
EGFP-VEC
Saline
0
200
400
600
800
1000
1000
2000
3000
4000

C

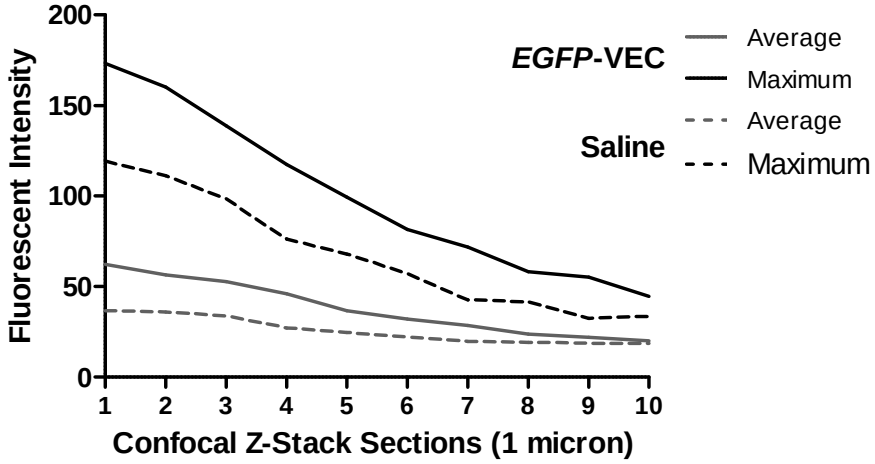
Fluorescent Intensity
Confocal Z-Stack Sections (1 micron)
EGFP-VEC
Average
Maximum
Saline
Average
Maximum
0
50
100
150
200
1
2
3
4
5
6
7
8
9
10

Figure 28: Quantitation by qPCR of Biolocalization of Systemically Injected *EGFP*-VEC in Mice with Metastatic Disease

DNA from lung and liver metastases and other major organs from control groups (Healthy mice not injected with *EGFP*-VEC, Mice with metastases not injected with *EGFP*-VEC and healthy mice injected with *EGFP*-VEC), and experimental group (mice with metastases injected with *EGFP*-VEC) were analyzed for *egfp*-transgene by qPCR. The specific localization of *EGFP*-VEC was predominantly detected in the lung metastases.

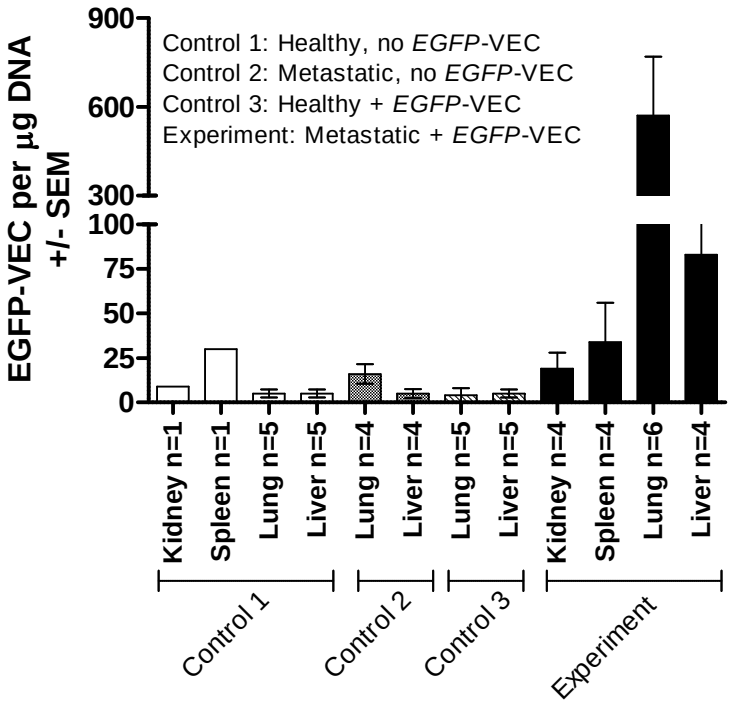
EGFP-VEC per µg DNA
+/- SEM
900
600
300
100
75
50
25
0
Control 1: Healthy, no EGFP-VEC
Control 2: Metastatic, no EGFP-VEC
Control 3: Healthy + EGFP-VEC
Experiment: Metastatic + EGFP-VEC
Kidney n=1
Spleen n=1
Lung n=5
Liver n=5
Lung n=4
Liver n=4
Lung n=5
Liver n=5
Kidney n=4
Spleen n=4
Lung n=6
Liver n=4
Control 1
Control 2
Control 3
Experiment

mice (Figure 29C, black filled), the amplification efficiency for experimental DNA samples did not increase proportionally when more than 200 ng DNA was used (Figure 29C, open triangles). Thus, subsequent qPCR assays were run using 200 ng DNA in 20 μl reactions in 384-well format on AB7900.

Synopsis:

These data suggested that the qPCR methodology offered specific, objective, and rapid quantitation of *EGFP*-transgenic cells. This qPCR-based quantitation was uncomplicated by tissue autofluorescence. This method should be readily transferable to other *in vivo* models to quantitate the biolocalization of transplanted transgenic cells.

Figure 29: Modification of qPCR Assay for High-Throughput 384-Well Analysis.

A-B) The two graphs compare the qPCR assays in 25 μl reaction mix in 96-well (filled circles and squares) format and the qPCR assays in 20 μl reaction mix in 384-well format (open circles and squares) using 100 ng genomic DNA. In the first graph (A) shows the Ct values corresponding to *β-actin* amplification (squares) in negative (Blk 1-3) and positive (Actb*EGFP* 1-3) control samples. Amplification of *egfp*-transgene (circles) was not detected in the negative control samples. The second graph (B) shows the Ct values corresponding to *β-actin* and *egfp* amplification in DNA from metastatic mice injected with *EGFP*-VEC. The values on the x-axis represent the identification number for each mouse. The Ct values between the 25 μl and 20 μl reactions are similar.

C) The qPCR amplification efficiency was compared to the increasing amount of genomic DNA in 20 μl qPCR reaction. The average fold-change in *egfp*-transgene detection was not proportional to the amounts of genomic DNA when more than 200 ng DNA from experimental tissue was used (table of right and open triangles in the graph). The *egfp* amplification appeared more proportional for DNA extracted from *EGFP*-transgenic mice (filled box in the graph).

A

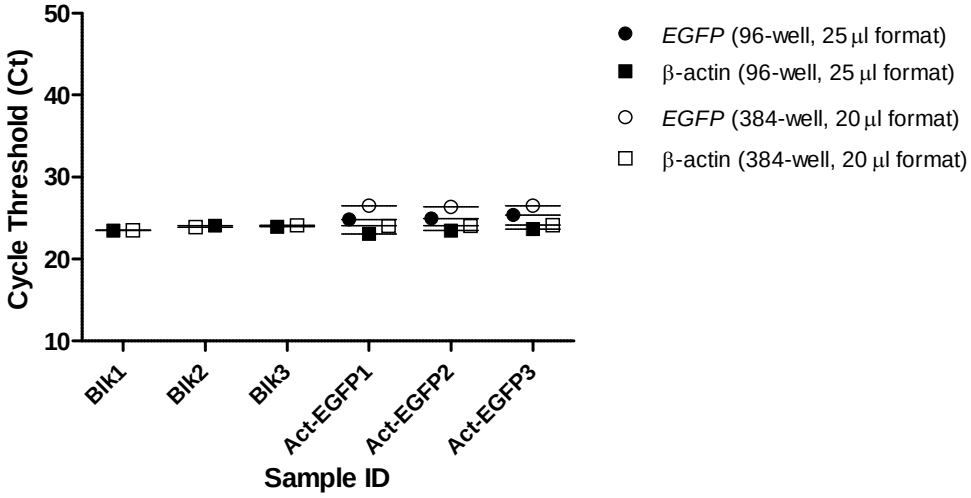

B

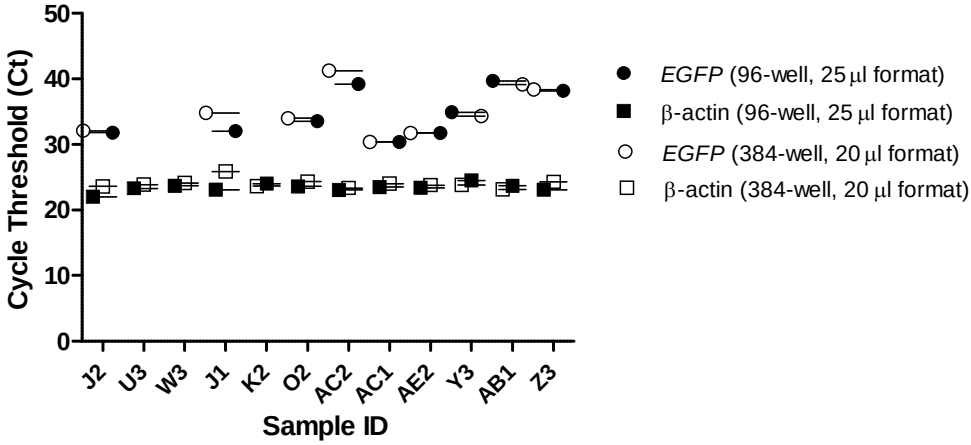

C

Input DNA	EGFP transgene detection ratio compared to EGFP detection at 100ng
100	**1 ± 0.0**
200	**1.6 ± 0.4**
400	**2.7 ± 1.3**
600	**4.15 ± 2.4**

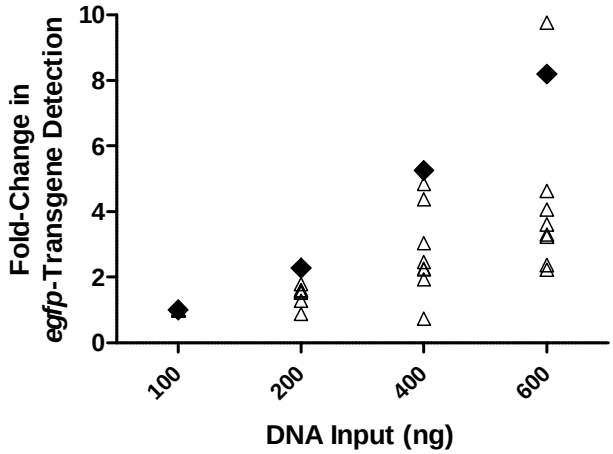

D: The Role of E-selectin and SDF-1α in the Biolocalization of Bone Marrow-Derived Cells to Tumors

Rationale:

The hypothesis for this research project was that SDF-1α associated with tumor endothelium, was an important mediator for biolocalization and adhesion of bone marrow-derived endothelial progenitors (EPC) to LLCaB tumors. Bone marrow-derived lineage-negative cells (Lin^- BMC) which are enriched for EPC (125;126) were selected for the *in vitro* adhesion assay. For the *in vivo* experiments, dermal fibroblasts (from a non-endothelial lineage) were used as control cells to evaluate if biodistribution of the systemically administered cells was specific for endothelial progenitors (i.e. Lin^- BMC). This chapter describes the biolocalization of dermal fibroblasts and Lin^- BMC to s.c. and metastatic LLCaB tumors.

Results:

In vivo Biolocalization of Lin^- BMC and Dermal Fibroblast

The *in vivo* experiments were conducted as described in the Methods and Materials sections, and as schematically represented in Figures 5 and 6. Briefly, mice with either s.c. tumors or metastatic disease were systemically injected with Lin^- BMC or dermal fibroblasts that were isolated from *EGFP*-transgenic mice. As diagrammatically represented in Figure 8B, 50 μm-thick sections of the tissue harvested from the *in vivo* experiments were collected (5 per individual tube) and genomic DNA was extracted, quantified, and used for qPCR. From each tube, 200 ng of DNA was assayed for the *egfp*-transgene in duplicate.

The data set was obtained from three separate qPCR assays run in 384-well plate format. Cycle threshold (Ct) values greater than 37 appeared unreliable and were occasionally detected in negative controls, and thus were deemed negative. Overall data obtained from *in vivo*

experiments is summarized in box-and-whisker plots in Figures 30-31 A and C, and 32A (GraphPad Prism 5.0 software). The box-plot rectangle graphically depicted Q1 and Q3 quartiles, the line within the box-plot indicated the median value, and the I-bar ("whiskers") extended to the minimum and maximum values in the data set. Box-plots are programmed to identify outlier cutoff or fences according to Tukey's rule; outliers thus detected were excluded from data set prior to analysis. Higher Ct values represented fewer copies of *egfp*-transgene. As described in the previous chapter, Ct values were translated into *egfp*-transgene numbers based on the plasmid standard curve in individual plates. It must be noted that PCR amplification is exponential and a difference of one Ct is equal to a 2X difference in gene copy number. The total amount of DNA extracted and the total number of *egfp*-transgene detected per tube per tissue block was calculated and used to derive a single value and reported as *egfp*-transgene per microgram per tissue. These values were used for one-way ANOVA and post-hoc Dunnett's analysis for determining statistical difference between groups and tissues. For statistical tests, it was assumed that the data set was unpaired, non-parametric and lacked Gaussian distribution.

Subcutaneous Tumor Model

Mice with small s.c. tumors (average tumor volume = 200 ± 43 mm^3) were injected with 5×10^5 *EGFP*-Lin^- BMC (n=7),*EGFP* dermal fibroblasts (n=5), or media (n=3). There was no significant difference in the *in vivo* tumor growth curves from the three groups (data not shown). Animals were euthanized 72 hours post injection and s.c. tumors and the other major organs were frozen in OCT. Each s.c. tumor was frozen in two tissue blocks; one block was completely sectioned for analysis. DNA from an average of eight tubes per tumor from each group was analyzed. *Egfp*-transgene amplification was not observed in any DNA samples from tumors from three control mice that were injected with media only (Figure 30 A and C). *Egfp*-transgene

amplification in tumor DNA from mice injected with fibroblasts (n=5) was weak and erratic. None of the tumor DNA samples tested from two of these mice showed amplification for *egfp*-transgene and were deemed negative. The remaining three mice in the fibroblast group had only 1 or 2 samples that were deemed weakly positive (4/25 tubes, Ct = 38.7- 45.5).

Similarly, the *egfp*-transgene was not detected in any of the tumor DNA samples from 4 of the 7 mice that were injected with Lin^- BMC. Weak and erratic amplification was observed in 2 mice in this group (DNA from 4/16 samples had detectable *egfp*-transgene amplification Ct = 37.2- 46.9). However, the majority of samples from one tumor in this group had substantial *egfp*-transgene amplification (DNA from 7/10 tubes were positive Ct 34.7-36.96; Figure 30A). When data was averaged for all tumor samples in each group, a higher number of total *egfp*-transgene was detected in the group that was injected with Lin^- BMC, but this difference was statistically insignificant (Figure 30B).

All major organs from the mouse that showed the highest biolocalization of Lin^- BMC to s.c. tumors were assayed for expression of the *egfp*-transgene (Figure 30C). When Ct_{EGFP} were transformed to the total number of *egfp*-transgene per μg DNA, substantially higher values were detected in all of these organs (Figure 30D). Thus, although higher number of Lin^- BMC compared to fibroblasts localized to s.c. tumors at 72 hours, the Lin^- BMC did not preferentially or specifically localize to s.c. tumors.

Figure 30: Biolocalization of *EGFP*-Lin$^-$ BMC in Subcutaneous Tumor Model

DNA from tissue samples from s.c. tumor-bearing mice that were injected with media, *EGFP* fibroblasts or *EGFP*-Lin$^-$ BMC were analyzed for *egfp*-transgene by qPCR.

A) Cycle threshold (Ct) values for *egfp*-transgene amplification for all positive samples from all mice are plotted. *Egfp*-transgene amplification was detected in 1 of 7 tumors from the group that were injected with *EGFP*-Lin$^-$ BMC. No *egfp* amplification was observed in any tumors from mice injected with media or *EGFP*-dermal fibroblast. The reported n represents the number of tubes of DNA positive for *egfp*-amplification / total number of DNA tubes assayed.

B) The *egfp*-transgene was detected in s.c. tumors in the group of mice injected with Lin$^-$ BMC.

C) Ct_{EGFP} for all positive samples from the one positive s.c. tumor and other major organs for the same mouse are plotted. Compared to s.c. tumor, more *egfp*-transgene amplification was observed in the other major organs from the one positive mouse injected with *EGFP*-Lin$^-$ BMC.

D) Higher amounts of *egfp*-transgene per organ were detected in the lungs, livers, hearts, spleens, and kidneys when compared to the s.c. tumor in the mouse that had the most *EGFP*-Lin$^-$ BMC.

A

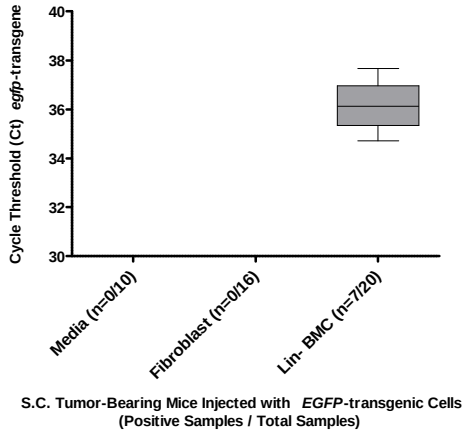
Cycle Threshold (Ct) egfp-transgene
40
38
36
34
32
30
Media (n=0/10)
Fibroblast (n=0/16)
Lin- BMC (n=7/20)
S.C. Tumor-Bearing Mice Injected with EGFP-transgenic Cells
(Positive Samples / Total Samples)

B

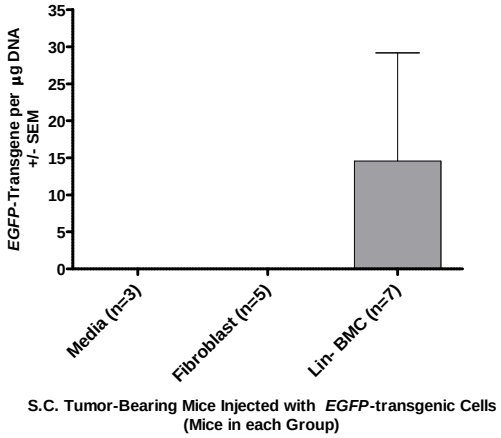
EGFP-Transgene per µg DNA
+/- SEM
35
30
25
20
15
10
5
0
Media (n=3)
Fibroblast (n=5)
Lin- BMC (n=7)
S.C. Tumor-Bearing Mice Injected with EGFP-transgenic Cells
(Mice in each Group)

C

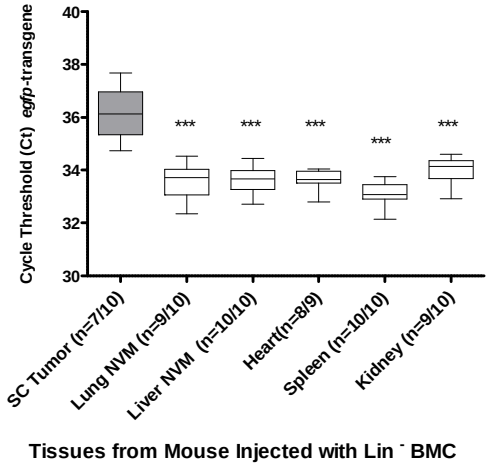
Cycle Threshold (Ct) egfp-transgene
40
38
36
34
32
30
***
***
***
***
***
SC Tumor (n=7/10)
Lung NVM (n=9/10)
Liver NVM (n=10/10)
Heart(n=8/9)
Spleen (n=10/10)
Kidney (n=9/10)
Tissues from Mouse Injected with Lin - BMC

D

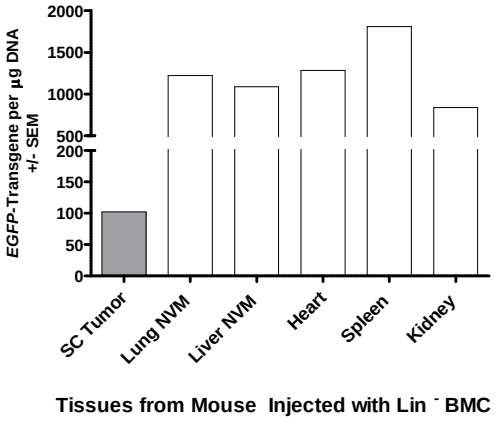
EGFP-Transgene per µg DNA
+/- SEM
2000
1500
1000
500
200
150
100
50
0
SC Tumor
Lung NVM
Liver NVM
Heart
Spleen
Kidney
Tissues from Mouse Injected with Lin - BMC

Metastatic Tumor Model

Mice with metastatic disease were injected *i.v.* with 5×10^5 *EGFP*-Lin$^-$ BMC (n=4 mice) and were euthanized at 48-72 hours post-injection. The biolocalization of *EGFP*-Lin$^-$ BMC in metastatic lung/liver tumors (n=7 metastases), as well as other control organs (heart, spleen, and kidney, n=4 mice) were analyzed by qPCR. Two mice with metastatic disease were injected *i.v.* with 5×10^5 *EGFP* dermal fibroblast as controls. These mice were euthanized at 24 hours after *EGFP* dermal fibroblast injection due to their moribund condition. The lung/liver with visible metastases (n=4 metastases) were evaluated for biolocalization of *EGFP* dermal fibroblasts by qPCR.

The control group injected with dermal fibroblasts had a significantly higher median Ct_{EGFP} and lower number of *egfp*-transgene per mg of tissue weight compared to mice with metastatic disease that were injected with *EGFP*-Lin$^-$ BMC (Figure 31 A and B). A total of 37 tubes of DNA from 4 metastatic lesions from n = 2 mice and 80 tubes of DNA from 7 metastatic lesions from n = 4 mice were evaluated from mice with metastatic disease injected with dermal fibroblasts or *EGFP*-Lin$^-$ BMC, respectively. In addition, all four mice injected with Lin$^-$ BMC had median Ct_{EGFP} in metastases was significantly lower compared to other organs analyzed (Figure 31C). This translated to the detection of significantly greater numbers of *EGFP*-Lin$^-$ BMC in metastatic lesions compared to lungs/livers with 'no visible metastases' (NVM), hearts and spleens, but not kidneys (Figure 31 D and E).

Data was also analyzed as total *egfp*-transgene per tissue based on DNA isolated from individual samples. This analysis indicated that significantly higher numbers of *EGFP*-Lin$^-$ BMC were detected in metastases compared to dermal fibroblasts and all other major organs (data not shown).

Figure 31: Biolocalization of *EGFP*-Lin$^-$ BMC in Metastatic Tumor Model

Mice with metastatic disease were injected with *EGFP*-Lin$^-$ BMC or*EGFP* fibroblasts. DNA isolated in multiple tubes from tissues blocks containing lung/liver metastases, lung/liver tissue with no visible metastases or other organs was analyzed for *egfp*-transgene by qPCR.

A) Cycle threshold values (Ct). Significantly lower median Ct_{EGFP} was observed in mice with metastases injected with *EGFP*-Lin$^-$ BMC (Ct range 27.4-37) compared to mice with metastases that received dermal fibroblasts (Ct range 27-36.9); lower Ct values indicated higher amounts of *egfp*-transgene. n = positive samples / total samples analyzed per group.

B) A significantly higher number of *egfp*-transgene per mg tissue wet-weight was calculated in metastases from the mice injected with *EGFP*-Lin$^-$ BMC compared to metastases from mice injected with dermal fibroblasts.

C) Cycle threshold values (Ct). Mean Ct_{EGFP} for metastatic tissues was significantly lower than Ct_{EGFP} from lung/liver tissues with no visible metastases (NVM, Ct range 28.7-36.8), hearts (Ct range 30.1-36.4) and spleen (Ct range 36.9-32.1), but not kidney (Ct range 27.6-33.4) in the group of mice injected with Lin$^-$ BMC (3 days after injection). P-value <0.0001 by one-way ANOVA; Post-hoc Dunnett's test compared to metastases *** $p<0.0001$.

D) Significantly greater number of *egfp*-transgene per mg tissue wet-weight were detected in metastatic tissues compared to adjacent tissues with no visible metastases (NVM) in mice injected with Lin$^-$ BMC. Two-tailed unpaired Student's t-test ** $p<0.01$.

E) Compared to metastases, significantly lower amounts of *egfp*-transgene per μg DNA were detected in hearts and spleens. P-value = 0.001 by one-way ANOVA; Post-hoc Dunnett's test compared to metastases ** $p<0.001$.

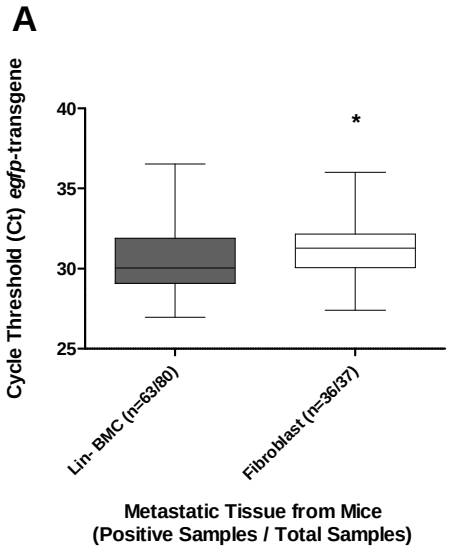
A
Cycle Threshold (Ct) egfp-transgene
40
35
30
25
*
Lin- BMC (n=63/80)
Fibroblast (n=36/37)
Metastatic Tissue from Mice
(Positive Samples / Total Samples)

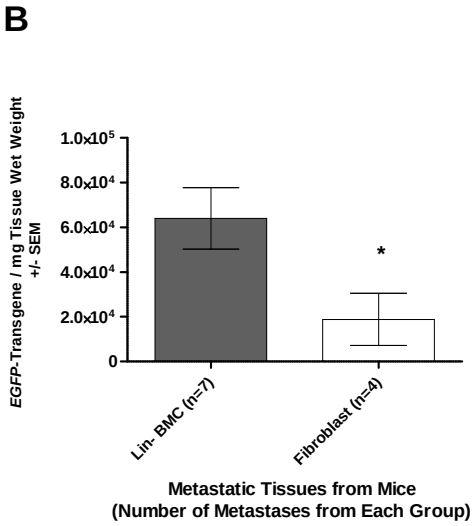
B
EGFP-Transgene / mg Tissue Wet Weight
+/- SEM
1.0x10^5
8.0x10^4
6.0x10^4
4.0x10^4
2.0x10^4
0
*
Lin- BMC (n=7)
Fibroblast (n=4)
Metastatic Tissues from Mice
(Number of Metastases from Each Group)

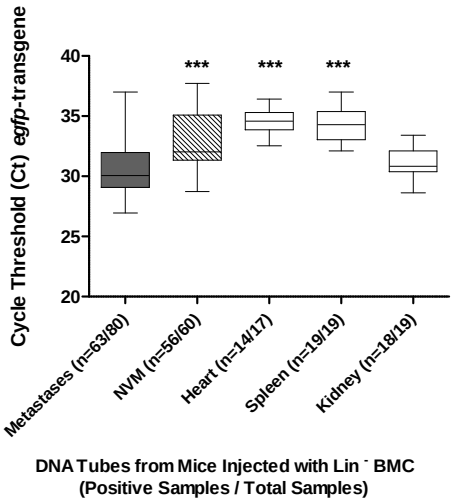
C
Cycle Threshold (Ct) egfp-transgene
40
35
30
25
20
***
***
***
Metastases (n=63/80)
NVM (n=56/60)
Heart (n=14/17)
Spleen (n=19/19)
Kidney (n=18/19)
DNA Tubes from Mice Injected with Lin - BMC
(Positive Samples / Total Samples)

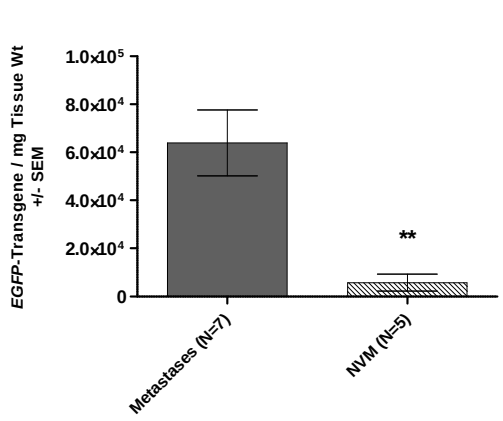
D
EGFP-Transgene / mg Tissue Wt
+/- SEM
1.0x10^5
8.0x10^4
6.0x10^4
4.0x10^4
2.0x10^4
0
**
Metastases (N=7)
NVM (N=5)
Lung and Liver Tissues from Mice Injected with Lin - BMC
(Number of Tissues from 4 Mice)

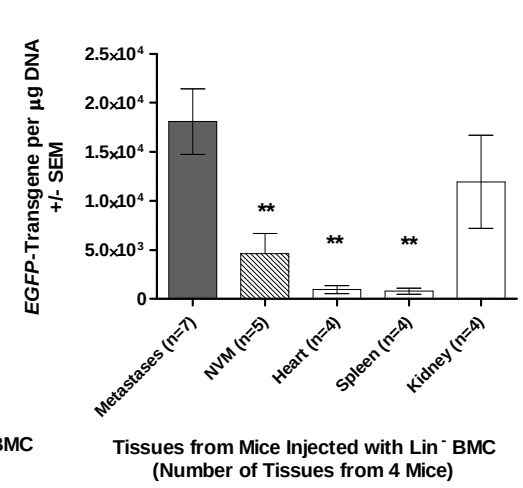
E
EGFP-Transgene per µg DNA
+/- SEM
2.5x10^4
2.0x10^4
1.5x10^4
1.0x10^4
5.0x10^3
0
**
**
**
Metastases (n=7)
NVM (n=5)
Heart (n=4)
Spleen (n=4)
Kidney (n=4)
Tissues from Mice Injected with Lin - BMC
(Number of Tissues from 4 Mice)

The relationship between *EGFP*-Lin$^-$ BMC homing (*EGFP*-Lin$^-$ BMC per metastases per mm^3) and metastatic tumor volumes (Average metastatic tumor volume = 24 ± 25 mm^3) was also evaluated. Overall, an inverse correlation was apparent between biolocalization of *EGFP*-Lin$^-$ BMC and metastatic tumor volumes by Spearman's correlation (ρ = -0.59), however the P-value for this analysis was not significant.

In a subsequent experiment, a total of 10 metastatic lesions from 4 mice were evaluated for long-term (7 days post *EGFP*-Lin$^-$ BMC administration) retention of Lin$^-$ BMC in metastases. DNA from an average of 11 tubes per metastatic lesion was assayed by qPCR for *egfp*-transgene. All tubes showed amplification of *egfp*-transgene with Ct ranging from 23 to 35.5. Overall, twice as many *EGFP*-Lin$^-$ BMC were detected in metastases on day 7 compared day 3 after *EGFP*-Lin$^-$ BMC administration; however, this difference was not statistically significant (Figure 32). Nonetheless, Lin$^-$ BMC appeared to be retained long-term in metastatic lesions.

Synopsis:

These *in vivo* experiments have demonstrated that a substantial number of Lin$^-$ BMC localized to metastatic tumors compared to s.c. tumors and other non-metastatic tissues and organs. In addition, a significantly greater number of CXCR4$^+$ Lin$^-$ BMC localized to metastatic tissues compared to CXCR4$^-$ dermal fibroblasts. The metastases expressed significantly elevated levels of SDF-1α compared to s.c. tumors. Thus, the data *en bloc* suggested that the biolocalization of Lin$^-$ BMC to metastases was most likely due to the interaction of tissue-derived SDF-1α and the CXCR4$^+$ Lin$^-$ BMC.

Figure 32: Long-term Retention of *EGFP*-Lin$^-$ BMC in Metastatic Tumors

Mice with metastases were euthanized 3 and 7 days after injecting *EGFP*-Lin$^-$ BMC. Multiple tubes of DNA from metastatic lung/liver tissue sections from frozen tissue blocks were analyzed for *egfp*-transgene by qPCR.

A) Cycle threshold values (Ct). No significant difference in median Ct_{EGFP} was observed between the 3-day (Ct range 27.4-37) and 7-day (Ct range 23-35.5) groups. The reported n indicates positive samples / total samples analyzed per group.

B) *EGFP*-transgene per μg DNA in metastatic lesions was higher on day 7 compared to day 3 after intravenous injection of *EGFP*-Lin$^-$ BMC, indicating cell retention and/or replication.

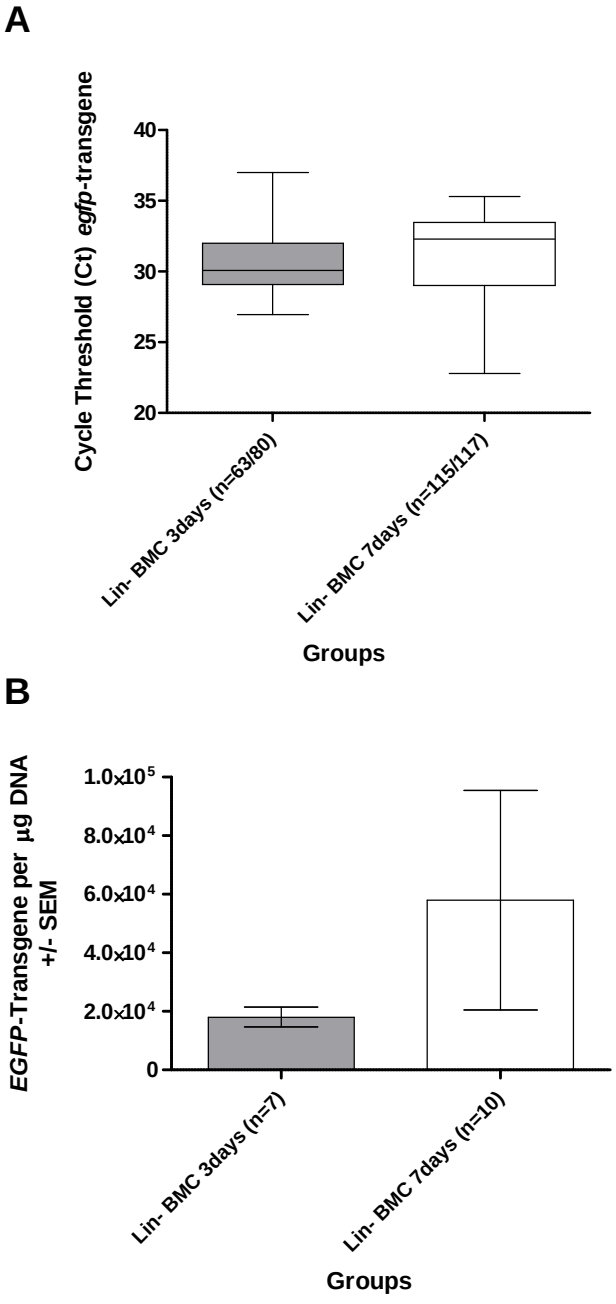
A
Cycle Threshold (Ct) egfp-transgene
40
35
30
25
20
Lin- BMC 3days (n=63/80)
Lin- BMC 7days (n=115/117)
Groups
B
EGFP-Transgene per µg DNA +/- SEM
1.0x10^5
8.0x10^4
6.0x10^4
4.0x10^4
2.0x10^4
0
Lin- BMC 3days (n=7)
Lin- BMC 7days (n=10)
Groups

CHAPTER IV: MODEL

A suggested model for an SDF-1α-mediated mechanism of tumor biolocalization and adhesion of bone marrow-derived progenitors is shown in Figure 33. This is based on our accumulated data in a mouse model and the use of systemically-administered, adoptively-transferred bone marrow-derived EPC as surrogates for *in vivo*-mobilized EPC during tumor vasculogenesis.

In vitro and *in vivo* experiments have shown that both E-selectin and SDF-1α were expressed in LLCaB subcutaneous and metastatic tumors. E-selectin was selectively expressed in tumor endothelium, but not in normal healthy tissue. SDF-1α was significantly upregulated in metastatic tumors compared to normal tissues and orthotopic subcutaneous tumors. SDF-1α protein levels in tumors were most likely regulated by hypoxia, necrosis, and proteases. SDF-1α was not only found dispersed through out the extracellular matrix, but also found to be associated with tumor endothelium suggesting its possible role as a cell adhesion molecule. The association of SDF-1α with the ECM and cell membranes was most likely via heparan sulphates. *In vitro* adhesion assays demonstrated that Lin^- BMC and endothelial progenitors ($Lin^-Sca1^+cKit^+$ BMC) adhered to the tumor-derived cells, and that their adhesion to tumor-derived cells was mediated by the interaction of SDF-1α and CXCR4. A significantly greater number of Lin^- BMC localized to metastases compared to adjacent healthy tissues and organs and subcutaneous tumors. Thus, it appeared that SDF-1α was one of the permissive triggers of tumor vasculogenesis that regulated the recruitment and adhesion of BMC to tumors.

Figure 33: SDF-1α-Mediated Mechanism for Tumor Biolocalization and Adhesion of Lineage-negative BMC

Greater numbers of adoptively-transferred $CXCR4^{+}Lin^{-}$ BMC localized to LLCaB metastases (mouse on right), which had significantly elevated levels of SDF-1α protein, compared to LLCaB subcutaneous tumors (mouse on left) and adjacent healthier tissues. SDF-1α was associated with the extracellular matrix (ECM) and with tumor endothelium (EC) and this adhesion most likely occurred via heparan sulphates. *In vitro* assays demonstrated that the adhesion of Lin^{-} BMC and endothelial progenitor to tumor endothelial cells was mediated by the interaction of SDF-1α and CXCR4. Together these data suggested in our model that tumor-derived SDF-1α bound to tumor endothelial cells may recruit and facilitate adhesion of circulating bone marrow-derived $CXCR4^{+}$ progenitor cells to SDF-1α-rich tumors.

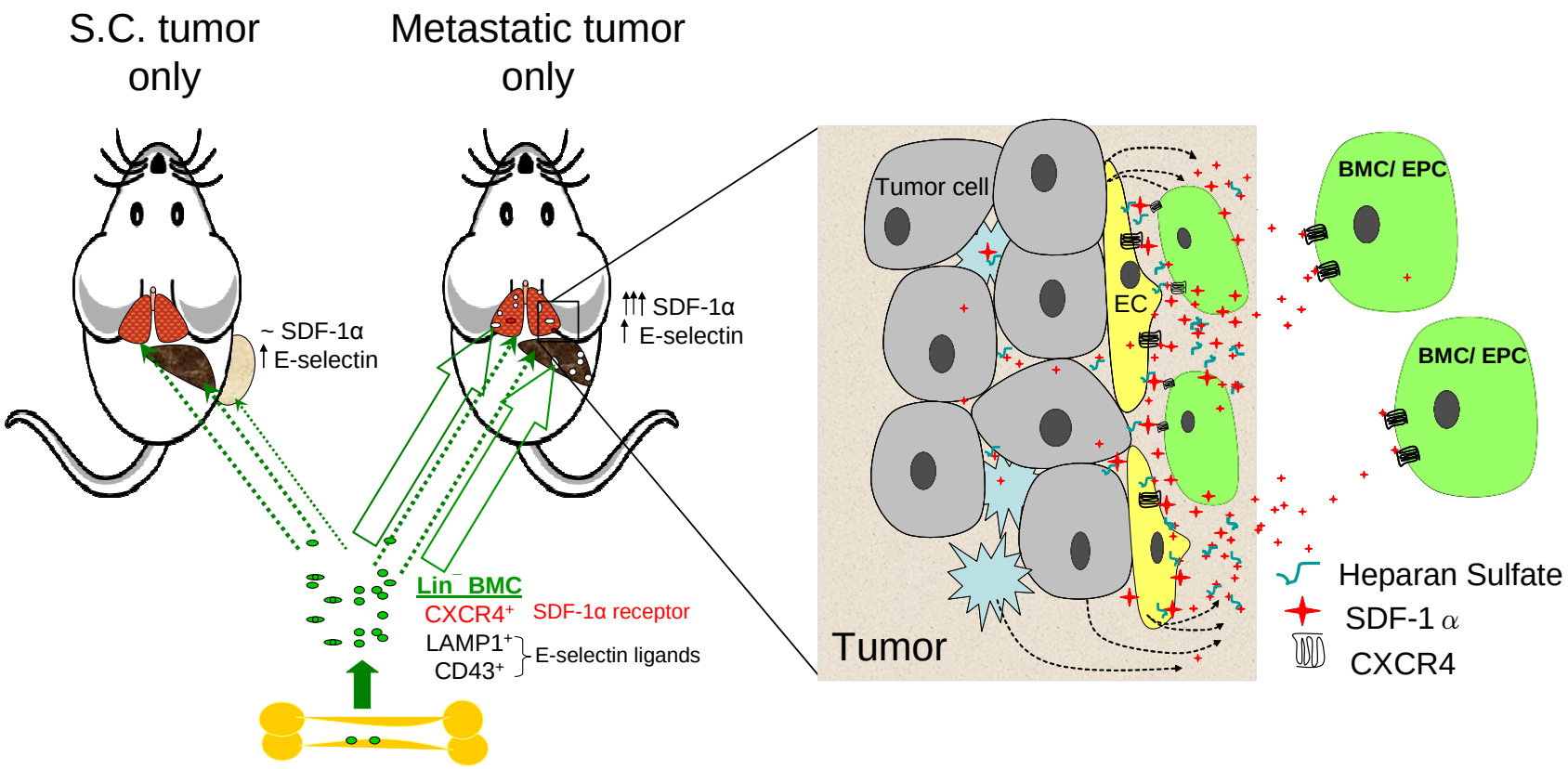
S.C. tumor only
Metastatic tumor only
~ SDF-1α
E-selectin
SDF-1α
E-selectin
Lin⁻ BMC
CXCR4⁺ SDF-1α receptor
LAMP1⁺
CD43⁺
E-selectin ligands
Tumor cell
EC
Tumor
BMC/ EPC
BMC/ EPC
Heparan Sulfate
SDF-1 α
CXCR4

CHAPTER V: DISCUSSION

The formation of new blood vessels by angiogenesis and/or vasculogenesis is predominantly observed in embryonic development, and vascularization in healthy adults is observed during the menstrual cycle, pregnancy, and wound healing. It was in the early 1970's that it was first demonstrated that tumor growth was angiogenesis-dependent. Dr. Judah Folkman proposed that targeting the developing tumor vasculature would be a valuable intervention in controlling tumor growth and cancer progression. In addition, it was suggested that specific targeting of the tumor vasculature would have advantages such as easy accessibility, specificity, and low toxicity, overcome limitations like drug resistance of tumor cell, and be applicable to a wide array of tumors. Lal *et al.* were the first to report the implantation and survival of systemically injected endothelial cells (EC) within tumors (31). Subsequently, Zwiebel *et al.* reported a significant reduction in metastatic burden by systemic administration of EC that were genetically modified to overexpress the cytotoxic cytokine IL-2 (89). This initial account opened the door for potential EC-mediated therapeutic strategies: the use of EC to deliver specific treatment to tumors. This approach has not been vigorously pursued, due to setbacks in clinical gene therapy and limited availability of syngeneic endothelial cells. However, other anti-angiogenic strategies targeting specific steps in tumor vascularization have been established as important in restricting cancer progression, and are being developed as new approaches in cancer therapy (4;5).

In 1997, Asahara's group isolated a unique cell fraction from peripheral blood mononuclear cells mobilized from bone marrow (BM) that possessed properties similar to that of an embryonic angioblast; these were designated endothelial progenitor cells (EPC). This group demonstrated that *in vitro*, EPC proliferated and/or migrated in response to angiogenic growth

factors and differentiated into mature EC, and *in vivo* were mobilized in response to ischemic injury and contributed to the re-vascularization of ischemic tissue (48;49). This led to the exploration of the role of BM-derived EPC in tumor vascularization (vasculogenesis). At the advent of this dissertation research, in 2005, EPC-mediated tumor vascularization was a novel concept with only a handful of reports with inconsistent findings (Table 1). Lyden *et al.* were the first to report the recruitment of hematopoietic and circulating endothelial precursor cells (CEPs) and their importance in tumor growth. They reported that BMC-mediated tumor vascularization was driven by vascular endothelial growth factor (VEGF), and that blocking the mobilization of both $VEGFR2^{+}$ CEPs and $VEGFR1^{+}$ bone marrow-derived cells was necessary to completely ablate tumor growth (197). On the contrary, Vajkoczy had *et al.* reported that P- and E-selectin and their ligand PSGL-1 mediated the localization and incorporation of embryonic endothelial progenitors to tumor vasculature (51). Later, in 2004 Wei *et al.* demonstrated that systemically-injected embryonic EPC that were transfected with a suicide construct led to improvement in the survival of mice that received the substrate for the suicide gene (78).

Early reports suggested that, like the mature endothelial cells, endothelial progenitors might be important in tumor vascularization and tumor targeting. Thus, understanding the mechanism by which EPC contributed to the process of vascularization could help in developing drugs to control vasculogenesis and arrest tumor growth. Additionally, genetically modified EPC could be developed as a therapeutic Trojan horse to specifically deliver therapy to tumors.

In 2005, we proposed that SDF-1α was important in recruitment and adhesion of bone marrow-derived progenitors to tumors. Since then there have been about 20 reports that have demonstrated the tumor-localization of EPC from adult bone marrow and the role of hypoxia-

induced proteins. Five of these reports have demonstrated the role of SDF-1α in tumor vasculogenesis.

The metastatic tumor model was characterized in the first part of this dissertation. The LLCaB cell line was suitable for use in immunocompetent C57Bl/6 mice and was syngeneic to the host. Additionally, previous *in vivo* experiments in our laboratory showed that the LLCaB cell line, compared to the parental cell line LLC1 and LLCC3 subclone, developed primary tumors more rapidly and produced larger metastases. Subcutaneous (s.c.) tumor resection was used to promote development of metastatic tumor cells seeded in the lungs and livers. Although lungs appeared to be the predominant site of metastases, liver metastases were frequently observed. This was in agreement with the clinically observation that lung tumors metastasized to livers. In addition, we have demonstrated that the primary tumor volumes and the number of days after surgical excision of s.c. tumors were critical for consistent development of metastases (Figure 9). These data were in alignment with earlier studies and the current concept of tumor development in the human population. The larger primary tumors gave rise to a greater number of metastases, which developed rapidly after primary tumor removal. In contrast, the smaller primary tumors led to fewer metastases and took a longer time to develop. Ohizumi *et al.* observed similar relationship between the frequency of metastases and the primary tumor volumes in 1987 (276;277). Their model was similar to ours, although they used a different and apparently more aggressive Lewis lung tumor subclone, injected it intramuscularly in the hind limb, and studied the metastatic development without resection of the primary tumors. These data suggested that the LLCaB tumor model was a clinically relevant murine model.

The expression of E-selectin and SDF-1α in s.c. and metastatic tumors was evaluated by RT-PCR, ELISA and immunohistochemistry in Chapter III A. E-selectin was specifically

expressed on activated endothelium in tumors and absent from healthy control tissue, supporting our and others earlier findings (Figure 10). In contrast to E-selectin, SDF-1α protein was detected at basal levels in healthy control lung and liver samples. This observation was in agreement with other published reports (249;278). Although, no difference in the amounts of SDF-1α protein in s.c. tumors and healthy control samples was observed, SDF-1α protein was significantly elevated in metastases (Figure 11). In addition, smaller tumors appeared to express higher amounts of SDF-1α protein per milligrams of total protein compared to the larger tumors. These data might imply that SDF-1α was critical in the early phases of tumor development and was replaced by other growth factors, as the tumor progressed. However, even when comparably sized tumors were compared, the s.c. tumor had significantly lower expression of SDF-1α protein. This could suggest that the expression of SDF-1α was influenced by the physiologic location of tumors. It was also possible that SDF-1α expression was dependent to the nature of tumor initiation (growth of tumor cell bolus in s.c. tumors in heterotopic environment versus proliferations of localized single tumor cell to produce metastases in orthotopic environment). In addition, this could be attributed to the difference in the ratio of blood vasculature to tumor cells in larger tumors compared to smaller tumors. There are several reports that have associated elevated levels of SDF-1α with the more aggressive and advanced phenotype in glioma (279), colorectal cancer (280), and pituitary adenoma (281). It must be noted that LLCaB is an aggressive adenocarcinoma cell line, and that tumor size must not be confused with tumor biology/stage. Nevertheless, to our knowledge this is the first report that describes a relationship between tumor size and SDF-1α protein expression.

Substantial levels of *sdf-1α* gene transcripts were detected in s.c. tumors and metastases, but these were significantly less than *sdf-1α* transcripts in healthy tissues. The inconsistency in

the levels of *sdf-1α* gene transcript and SDF-1α protein could be attributed to the fact that regulation of SDF-1α expression occurs primarily at the protein level. *Sdf-1α* mRNA has been reported to have a long half-life (282;282). The half-life of SDF-1α protein in circulation has been demonstrated to be less than one minute (246), its half-life in tissue is not known.

It has been reported that the association of secreted SDF-1α with proteoglycans like heparan sulfate in extracellular matrix protected SDF-1α protein from degradation by proteases such as dipeptidyl peptidase IV (246;247). Dipeptidyl peptidase IV (DPP IV/CD26) is thought to be important in tumor biology (283;284). Human DPP IV has been shown to be ubiquitously expressed in epithelial and endothelial cells (285), and certain tumor cells (286-288). It must be noted that proteolytic enzymes are plentiful in necrotic areas of tumor (289), and that necrosis increases with tumor size. Most subcutaneous tumors are considerably larger than metastases, contain larger areas of necrosis, and contain greater amounts of certain proteases. Indeed, increase in dipeptidyl peptidases II and IV paralleling the increase in size of the subcutaneous tumors in tumor-bearing animals and in blood and solid cancers patients has been reported (290). Additionally, several matrix metalloproteinases (MMP) have also been reported to cleave SDF-1α, rendering it unable to bind to CXCR4 (291). Elevated levels of MMPs have been associated with tumor progression (292) and shown to indirectly modulate vasculogenesis (69;293). This increase in necrosis and proteolytic enzymes in large tumors could have possibly resulted in the increased degradation of SDF-1α protein, resulting in the reduction of detectable SDF-1α protein in larger tumors. This data is partially supported by the fact that relatively higher amounts of *sdf-1α* gene transcript were detected in s.c. tumors compared to metastases. Taken together, SDF-1α protein levels in tumors appear to be modulated by proteolytic enzymes, and likely correlate with hypoxia and/or necrosis.

The tumor endothelium is the first point of attachment for circulating endothelial progenitors (EPC) and lineage-negative bone marrow cells (Lin^- BMC) in our model. Evaluating the differentially expressed/upregulated proteins on activated tumor endothelium would be important to understand the mechanism by which EPC/Lin^- BMC adhered and incorporated into the tumor vasculature. We hypothesized that SDF-1α was associated with the tumor-derived endothelial cell *in vivo*. By indirect immunofluorescent staining method, SDF-1α protein was observed throughout lung and liver sections from naïve control mice. In metastatic tissue sections, SDF-1α protein appeared to be concentrated within the metastatic lesions. In addition, SDF-1α protein was found to often colocalize with the vasculature in s.c. tumors and metastases (Figure 12). The association of SDF-1α with endothelial cells and extracellular matrix was most likely via heparan sulphates, which have been reported to be present on EC surface and ECM (243). Several investigators have provided evidence that SDF-1α played an important role in the reconstitution of bone marrow after sub-lethal radiation. Lapidot *et al.* reported that SDF-1α adhered to bone marrow endothelium via heparan sulfate, and was critical for stem cells to be localized, arrested, and maintained within the marrow niche (294). E-selectin was also shown to be important for these events. If vasculogenesis was involved in tumor growth, the developing tumors would most likely need to provide a similar microenvironment for attracting the progenitor cells or Lin^- BMC. Our results indicated that metastases were rich in SDF-1α, and that E-selectin and SDF-1α were present on tumor endothelium, thus creating a microenvironment for Lin^- BMC to be recruited, retained, and incorporated into neovasculature.

Tumor cells, stromal cells, infiltrating cells or activated endothelial cells could be the source of secreted SDF-1α protein that was associated with tumor endothelium. Quantitative RT-PCR results suggested that endothelioma cells (surrogate for activated tumor endothelial cells)

expressed higher levels of *sdf-1α* gene transcripts compared to other cell types (3T3-L1 preadipocytes, unstimulated vascular endothelial cells from healthy tissue, BMC and LLCaB tumor cells) tested. Overall, these data showed that SDF-1α was elevated in tumors and it was associated with the endothelium.

SDF-1α has been demonstrated to be a chemoattractant for lymphocytes and human $CD34^+$ progenitors *in vitro* and *in vivo* (295;296). In addition, circulating SDF-1α has been implicated as a prognostic marker for cancer progression (231;297-301). However, we did not observe any difference in serum SDF-1α protein between healthy controls and s.c. tumor bearing mice (Figure 13). This is most likely due to the short half-life of circulating SDF-1α (246). We did not test for circulating $CXCR4^+$ cells in naïve healthy mice and/or tumor-bearing mice, thus the putative role of SDF-1α in mobilizing $CXCR4^+$ BMC in our model remains unclear.

Aghi *et al.* did not observe any increase in circulating $CXCR4^+$ BMC in mice implanted with SDF-1α expressing glioma (62;302). In addition, no difference was observed in the plasma SDF-1α levels from mice implanted with tumors that expressed or did not express SDF-1α. Similarly, we have demonstrated the lack of increase in circulating serum SDF-1α in a lung adenocarcinoma model. It is also possible that there was indeed a transient increase in tumor-derived SDF-1α and circulating $CXCR4^+$ cells, and the $CXCR4^+$ cells bound the circulating SDF-1α. CXCR4 has been reported to be rapidly internalized on binding SDF-1α (223), thus neither the increase in $CXCR4^+$ cells nor the elevated SDF-1α levels were detected. In contrast, Madlambayan *et al.* (76) reported more than 2-fold increase in serum SDF-1α by day 7 post intramuscular injections of LLC tumor cells; serum SDF-1α was reported to decrease to basal levels by day 13 with the tumor still intact. They did not report any parallel data about change in circulating $CXCR4^+$ BM-derived cells. Since most of our blood samples were collected at least

15 days after subcutaneous injection of LLCaB tumors, we may have missed increased serum levels associated with early phases of tumor development.

One of our novel observations was that SDF-1α in serum samples from the female mice was consistently lower compared to the male mice. This might be due to the fact that SDF-1α is a target for estrogen (303). This novel observation indicating a sex-based distinction in SDF-1α expression might be relevant in treating estrogen-dependent malignancies.

In Chapter III B, a series of *in vitro* adhesion assays were conducted to test our hypothesis that SDF-1α could act as a cell-cell adhesion molecule and was instrumental to the association of $CXCR4^+$ Lin^- BMC and endothelium in tumors. Before initiating these experiments, the protocol to isolate Lin^- BMC was standardized. Endothelial progenitor cells (EPC) have been shown to be a subset of Lin^- $Sca1^+cKit^+$ (LSK) population. Our data showed that LSK cells constituted less than 0.5% of total BMC (Figure 14) and predominantly (~85%) contained cells with phenotype consistent with endothelial progenitor cells, i.e. $\underline{Lin^- Sca1^+cKit^+ VEGFR2^+}$ (Figure 15). This data was consistent with a previously published report (304). Additionally, we observed that ~80% LSK-BMC expressed CXCR4, a receptor for SDF-1α.

Endothelial progenitor cells (EPC) /LSK cells could have been purified by positive selection of $Sca1^+cKit^+$ from Lin^- BMC using antibodies as an alternative method. However, this would render the LSK cells coated with anti-cKit and anti-Sca-1 antibodies, which could cause stearic hindrance, interfere with cell-cell adhesion and complicate the interpretation of results. This could also alter the *in vivo* biodistribution of cells. Alternatively, it would be possible to culture Lin^- BMC *in vitro* with growth factors to promote EPC differentiation. Several groups have successfully cultured Lin^- BMC and have reported the expression of endothelial cell-specific markers on these cells. However, progenitor cell culture is expensive and difficult, there

is a lack of standardized protocol for culturing Lin^- BMC, and *ex vivo*-expanded cells might not accurately reflect the *in vivo* biology of mobilized Lin^- BMC. It was also possible to use a chimeric mouse model for studying *in vivo* mobilization and biodistribution of bone marrow derived cells. In the chimeric mouse model, bone marrow in host mice is depleted by radiation, and reconstituted by transplanting intact bone marrow from a transgenic mouse strain. This model would prove useful for understanding the role of different BM-derived cell lineages in tumor development. Often transgenic BMC detected in tumors have been reported to belong to a committed lineage *i.e.* $CD11b^+$ cells that belonged to the granulocytic lineage (71;76;77) making it difficult to interpret if progenitor cells localized to tumors prior to differentiation or if differentiated cells from bone marrow were recruited to tumors. In contrast, the detection of systemically injected stem cell populations in tumors ensures the progenitor phenotype of tumor-localized cells.

Because of these concerns, the use of Lin^- BMC as EPC surrogates for *in vitro* and *in vivo* experiments was considered most practical. Additionally, in order to develop a cell-based vehicle to deliver site-specific therapy, it is important that cells satisfied certain basic criteria like 1) simple harvesting procedure, 2) tolerance to *ex vivo* culture, 3) low risk of non-specific differentiation *in vitro*, 4) high transfectability, 5) adequate *in vivo* tropism, and 6) inability to generate a graft versus host immune response. Thus, exploring biolocalization of syngeneic stem cells in an immunocompetent animal model was essential. We chose to evaluate the mechanism by which adoptively-transferred syngeneic Lin^- BMC localized to orthotopic and heterotopic tumors in a clinically relevant immunocompetent C57Bl/6 mouse tumor model.

As discussed earlier, SDF-1α was expressed by a variety of cell types within tumors. To best reproduce the heterogeneous cell population in the tumor microenvironment, we dissociated

LLCaB tumors and cultured them *in vitro*. These tumor-derived cell cultures were designated Dissociated Tumor Cells (DTC). Expression of E-selectin and VEGFR2 were used to determine the percentage of tumor endothelial cells in cultured DTC, which gradually increased, peaked between 9-15 days in culture, and declined thereafter (Figure 16A). We predict that LLCaB-derived VEGF might be responsible for the stimulation and proliferation of tumor endothelial cells in DTC cultures. Additionally, the commercial endothelial cell growth supplement in culture media could be responsible for the increase in endothelial cells. The ultimate decline in E-selectin$^+$ and VEGFR2$^+$ cells was most likely due to the fact that these endothelial cells were capable of only limited *in vitro* growth. The expression of SDF-1α gene transcript in all DTC cultures was found to be constant by RT-PCR (Figure 16B). In addition, by immunofluorescent staining, SDF-1α protein was observed to be co-localized with the cell membrane of DTC. In addition, approximately 35% E-selectin$^+$ SDF-1α$^+$ cells were observed in DTC cultures indicating that SDF-1α bound to tumor-derived endothelial cells (Figure 16C).

For *in vitro* adhesion assays, monolayers of DTC, LLCaB (tumor cell line), bEnd.3 (endothelioma cell line), VEC (unstimulated murine cardiac vascular endothelial cells), and 3T3-L1 (pre-adipocyte cell line) were incubated with *EGFP*-Lin$^-$ BMC. The number and percentage of *EGFP*-Lin$^-$ BMC that adhered to each cell type was evaluated by manual enumeration on a fluorescent microscope and by flow cytometry. Results indicated that Lin$^-$ BMC preferentially adhered to DTC compared to all other monolayer cultures tested (Figure 17). Three-color flow cytometric evaluation for adhesion of Lin$^-$Sca1$^+$cKit$^+$ (LSK) cells revealed that, although sizeable percentage of LSK cells adhered to naïve endothelial and endothelioma cells, the largest percentage of LSK cells bound to DTC (Figure 17). Blocking E-selectin on DTC cultures decreased the number of adhered Lin$^-$ BMC and LSK cells by 30%. When CXCR4 was blocked

on the Lin^- BMC by either AMD3100 or anti-CXCR4 antibody, the adhesion of Lin^- BMC decreased by an average of 50%. CXCR4 blocking by AMD3100 and anti-CXCR4 antibody reduced the adhesion of the LSK population by approximately 30% and 60% respectively (Figure 18). A significant number of control cell-type, $CXCR4^-$ dermal fibroblast, adhered to DTC and bEnd.3 monolayers. However, as expected, this adhesion of $CXCR4^-$ dermal fibroblasts to DTC cultures was not influenced by the presence of AMD3100. These experiments demonstrated that SDF-1α acted as an adhesion molecule for Lin^- BMC and LSK cells in tumors.

As already mentioned, a significantly high percentage of LSK cells bound to bEnd.3 cells. In the presence of CXCR4 blocking drug AMD3100, there was an 80% decrease in the number of LSK cells that adhered to bEnd.3 cultures (Figure 19). These data suggested that LSK cells preferentially adhered to cells of endothelial lineage. The affect of blocking CXCR4 on the adhesion of Lin^- BMC to unstimulated resting vascular endothelial cells was not evaluated. Thus, no comment can made about preferential adhesion of Lin^- BMC and/or LSK cells to activated tumor endothelial cells compared to normal endothelial cells.

The Lin^- BMC and LSK cell adhesion to DTC was not completely inhibited in presence of CXCR4 or E-selectin blocking agents for most cell types tested. It must be noted that blocking would only be as efficient as the percentage of cells expressing E-selectin and CXCR4. On average about 45% of cells in DTC cultures expressed E-selectin. Approximately 30% of Lin^- BMC expressed CXCR4 and ~80% of LSK cells expressed CXCR4. LSK population and in presence of AMD3100 the adhesion of LSK cells to endothelioma cells decreased by 80%, indicating an almost complete inhibition of the interaction between CXCR4 and SDF-1α. In addition, CXCR7, a second receptor for SDF-1α, could be playing a role in adhesion of bone

marrow-derived cells to tumor-derived cells. Although, AMD3100 has been reported to bind CXCR7, it appears to act agonist of CXCR7 {586}. Due to the lack of a commercially available anti-mouse anti-CXCR7 antibody and/or CXCR7-antagonist, we have not been able to evaluate the role of CXCR7 in adhesion of Lin- BMC or LSK to DTC. In addition, it was possible that E-selectin and SDF-1α acted together in a complementary fashion. However, we did not simultaneously block both CXCR4 and E-selectin in the same experiment, primarily due to the possible stearic hindrance that could interfere in cell-cell adhesion. It is also plausible that other cell adhesion molecules were involved in the adhesion of Lin- BMC and/or LSK to tumors. Nonetheless, taken together, these data suggested that Lin^{-} BMC had a tendency to adhere to several cell types in tumors, and both SDF-1α and E-selectin mediated this interaction with DTC.

Finally, in Chapter IV, data from *in vivo* studies were reported. For *in vivo* experiments, mice transgenic for the *egfp*-transgene were used as donors in adoptive transfer experiments because: 1) post-harvest biochemical labeling of cells would not be required, 2) bright fluorescent signals would help in detecting tissue-localized cells, and 3) the *egfp*-transgene would be inherited by all progeny cells, thus making long-term studies more feasible. In the early *in vivo* experiments, biolocalization of vascular endothelial cells (VEC) isolated from *EGFP*-transgenic mice in wild-type C57Bl/6 mice with metastatic disease was evaluated by fluorescent microscopy (Figure 20). Although *EGFP*-VEC were specifically detected in metastases, evaluation of tissue sections was compromised by tissue autofluorescence and artifactual fluorescence. This prompted the development of a qPCR method to detect the *egfp*-transgene to quantitate the tissue-localized *EGFP*-transgenic cells (Figure 20). Overall, this methodology was accurate, objective and efficient, and detected as low as two *egfp*-transgenes (1 cell) in 200 ng of genomic DNA (~35,000 cells).

Earlier studies in our laboratory have shown that adoptively-transferred vascular endothelial cells (VEC) specifically localized to primary and metastatic tumors. This homing of VEC to tumors was mediated by E-selectin (Storey and Verbanac, unpublished data). It was proposed that Lin^- BMC, which were enriched for EPC might localize to tumors using a similar mechanism, with SDF-1α playing crucial roles in their recruitment and adhesion. Additionally we sought to test an "irrelevant" cell type (dermal fibroblast) as a control cell to evaluate if tumor-localization was specific to bone marrow-derived Lin^- BMC.

No *EGFP*-dermal fibroblast were detected in any subcutaneous tumors at 72 hours after systemic injection. *EGFP*-Lin^- BMC were detected in only 1 of 7 s.c. tumors. However, in this mouse greater numbers of *EGFP*-Lin^- BMC were detected in normal organs like lung, liver, heart, spleen, and kidney, compared to the s.c. tumor. Shinde et al. (60) have reported similar whole body biodistribution results, based on the detection of tissue-localized radioactively-labeled Lin^- BMC on a gamma counter. They concluded that stem cells were recruited in low levels to subcutaneously implanted LLC in syngeneic animals, but did not contribute directly to vasculogenesis. In our study, the low biolocalization of Lin^- BMC to s.c. tumors could also be attributed to the fact that cells were injected into the caudal artery instead of the caudal vein. However, this theory could be disputed by the fact that *EGFP*-Lin^- BMC were detected in other organs. Additionally, in earlier experiments *EGFP*-VEC injected via caudal artery were successfully detected in s.c. tumors.

In contrast, in the metastatic model a significantly greater number of *EGFP*-Lin^- BMC localized to metastatic tissues compared to adjacent tissue with no visible metastatic lesions and other normal organs like heart, and spleen. In addition, a significantly greater number of *EGFP*-Lin^- BMC were detected in metastases compared mice injected with *EGFP*-dermal fibroblast. In

this experiment, cells were administered via the caudal vein, and the lungs would be the first major organ that cells would encounter. To summarize, it is possible that the disparity in *EGFP*-Lin^- BMC localization to metastases compared to s.c. tumors data is partially due to the physiology and anatomy of the circulatory system. It is perhaps more likely that $CXCR4^+$ Lin^- BMC preferentially localize to metastases that expressed higher levels of SDF-1α protein, but not the heterotopically implanted primary tumors with lower SDF-1α expression.

Although a significantly high number of *EGFP*-Lin^- BMC were detected in metastatic lesions 48-72 hours after injection, we also detected a substantial number of *EGFP*-Lin^- BMC in other major organs that did not have visible metastases, particularly in kidneys (Figure 30 and 31). Detection of *EGFP*-Lin^- BMC in kidney samples could be because kidneys receive about 20% of the total cardiac output (305;306) and are involved in blood clearance function. When Shinde *et al.* systemically injected stem cells into tumor-bearing mice, they did not detect any cells in the kidneys at 24 hours post-injection but identified about 5% of the injected cells at 72 hours post-injection (60), suggesting that the increase of Lin^- BMC in kidneys could be due to blood clearance. A time-course study must be conducted to evaluate the non-specific retention of Lin^- BMC in healthy tissue. We are currently analyzing normal organs from the experiment where tissue samples were collected 7 days after administration of Lin^- BMC.

Bone marrow is one of the tissues that we have not evaluated for localized Lin^- BMC after adoptive transfer. Bone marrow localization of adoptively-transferred BMC has been reported in many radiation chimera models, however Xie *et al.* have demonstrated that the transplanted BMC did not localize to the hematopoietic stem cell niche in bone marrow in mice whose bone marrow was not depleted by irradiation (304).

The calculated total number of *EGFP*-cells detected from all organs analyzed from each mouse exceeded the number of *EGFP*-Lin$^-$ BMC that was injected. This could be due to the highly proliferative nature of stem cells. Murine stem cells have been reported to be have a doubling time that ranges from 12 to 41 hours (307;307-309;309). Thus, in 72 hours the cell number could multiply at least 2-64 fold. In a subsequent study, just completed, mice with metastatic disease were injected with *EGFP*-Lin$^-$ BMC, and tumor-localization of adoptively-transferred cells was evaluated 7 days later. In this group, the number of *egfp*-transgenes/μg DNA detected at 7 day was ~3X greater than that detected by 3 day (Figure 32). This increase in number of Lin$^-$ BMC at 7 day indicates retained and/or proliferating cells.

While this dissertation was in preparation, Madlambayan *et al.* published a similar report showing that BM-derived stem and progenitor cells contributed to neovasculogenesis, and that "SDF-1α was a permissive trigger for BM recruitment to sites of neovascularization" (76). Their studies were conducted in a single mouse model with multiple neovascularization (Ischemic retinal injury, Lewis lung carcinoma, and B16 melanomas tumors). Although, this model was intriguing, it must be noted that tumor is a systemic disease and could potentially influence the BM-mediated ischemic repair and tumor growth in such a dual model system, and/or create competing sites. Nonetheless, they illustrated that the greatest BMC homing was detected in ischemic retinas, compared to intra-muscular Lewis lung carcinoma and B16 melanomas. This BMC recruitment was demonstrated to be dependent on site-specific expression of SDF-1α and CD133$^+$CXCR4$^+$ myeloid progenitor cells were reported to directly participate in new blood vessel formation. The abrogation of BM-derived neo-vascularization in heterotopic LLC and retinopathy by blocking SDF-1α activity with neutralizing antibodies was also demonstrated by immunohistochemistry. Thus, they concluded that active sites, which expressed SDF-1α, were

prone to BM involvement and underwent vasculogenesis whereas vascularization was mediated by a non-BM-derived mechanism in the other sites.

Our results reiterate similar findings. We observed that tumor localization of Lin^- BMC was greater in mice with only metastatic lesions (with high SDF-1α levels), than in mice bearing only primary subcutaneous tumors. A greater number of Lin^- BMC localized to metastatic tissues compared to adjacent tissue with no visible metastatic lesion and other normal organs like heart, spleen, and kidney. Moreover, significantly fewer $CXCR4^-$ *EGFP*-dermal fibroblasts localized to the metastases. Furthermore, data from *in vitro* experiments showed that adhesion of Lin^- BMC and endothelial progenitors to the tumor microenvironment was mediated by SDF-1α. Thus, it appears that SDF-1α might be a key regulator in facilitating adhesion and retention of Lin^- BMC in metastases.

A 2010 report by Kioi *et al.* demonstrated that irradiation caused a HIF-1-dependent increase in SDF-1α expression, and influx of bone marrow-derived cells in murine glioblastomas (77). This mechanism was shown to be responsible for tumor recurrence. $CD11b^+Tie2^+$ bone marrow-derived cells, also known as Tie2-expressing monocytes (TEM), were the predominantly detected cells in tumors and tumor vasculature. Endothelial progenitors were not involved in tumor vasculogenesis, and there was no difference in tumor recurrence in the presence of VEGFR2-blocking antibody treatment. However, pharmacological inhibition of HIF-1 or SDF-1α/CXCR4 interaction prevented the influx of bone marrow-derived $CD11b^+$ myelomonocytes, inhibited post-radiation vascularization, and abrogated tumor re-growth. Similarly, Ahn *et al.* had reported earlier that tumor-infiltrating bone marrow cells were predominantly MMP9-expressing $CD11b^+$ and contributed to vasculogenesis. Genetic ablation of MMP-9 reduced tumor growth and vascularization in B16 melanoma, Lewis lung, and mammary carcinoma

models (69). Our data showed the biolocalization of bone marrow-derived cells that were depleted of lineage-committed cells, including $CD11b^+$ cells. Nonetheless, it is possible that lineage-negative progenitors could differentiate into $CD11b^+$ cells and participate in vasculogenesis in mechanism similar to that described by Kioi and Ahn.

In summary, this research was conducted in a clinically relevant metastatic murine model. Quantitative PCR assay was used to objectively enumerate the biodistribution of transgenic cells and it enabled comprehensive analysis of tissue samples. A distinction of our study is the use of dermal fibroblast cells as a control cell type in the *in vitro* and the *in vivo* experiments. As fibroblasts are considerably more adherent compared to bone marrow-derived cells, they acted as a more stringent control. We have also addressed the mechanistic interaction between the bone marrow-derived cells and tumor cells in a series of *in vitro* assays, which appears to corroborate with *in vivo* data. Nonetheless, interpretation of results from the *in vivo* experiments was limited due to the use of heterogeneous lineage-negative bone marrow and small sample sizes. In addition, experiments with *in vivo* blocking of CXCR4 remain to be performed. Subsequently, the phenotype of the tumor-localized lineage-negative BMC needs to be analyzed. Additionally, evaluation of the incorporation of these adoptively-transferred bone marrow cells into the developing tumor blood vessels will help understand their role in vascularization, and analysis of proliferation markers would help in evaluating their long-term retention potential.

CHAPTER VI: SIGNIFICANCE

The mechanism by which tumor cells colonize, vascularize, and metastasize must be understood to aid in the design of effective anti-cancer therapies. It is also important to identify the proteins that might participate in this process. Moreover, evaluating these mechanisms in a model that mimics clinical scenario is essential. We have shown that the murine LLCaB tumor model recapitulated human cancer development closely. A novel tumor size-specific role for SDF-1α has been proposed in this dissertation. If SDF-1α was important for the development of vascularized metastases, early intervention to block SDF-1α could prove to be an effective therapy in controlling tumor proliferation. In addition, there is a growing body of evidence that bone marrow-derived cells might be recruited to tumors in a SDF-1α-modulated manner. Results from our group and others suggest that SDF-1α could be an important trigger for a tumor-recruited endothelial progenitor-mediated "angiogenic switch". Inhibiting the tumor localization of BM-derived cells could be utilized to restrict tumor proliferation and this strategy could be developed into a cancer-restricting therapy. As with the current anti-angiogenic strategies found to be effective clinically to date, strategies to block vasculogenesis via SDF-1α/CXCR4 targeting are almost certain to be used as adjuvant therapy to standard chemotherapy or hormonal therapy drugs that directly target the tumor cells.

Understanding the phenotype of progenitor cells that preferentially localize to specific tumor types and techniques to efficiently deplete these cells could be used as anti-cancer treatments. If $CXCR4^{+}Lin^{-}$ BMC preferentially localized to SDF-1α-expressing tumors, then these cells could be used to deliver specific therapy to tumors that are otherwise inaccessible. In addition, the interaction between SDF-1α in certain organs and $CXCR4^{+}$ tumor cells has been revealed crucial for organ-specific metastasis in animal models. Currently there are two clinical

trials evaluating the role of SDF-1α/CXCR4 in cancer patients; both these trials are investigating the role of SDF-1α/CXCR4 in the metastatic process. Nonetheless, with the emerging multifaceted functions of SDF-1α in tumor biology it appears that inhibition of SDF-1α could be used to not only restrict the metastatic process per se, but to tumor vasculogenesis and angiogenesis.

CHAPTER VII: REFERENCES

1. Singhal S, Vachani A, ntin-Ozerkis D, Kaiser L, Albelda S. Prognostic implications of cell cycle, apoptosis, and angiogenesis biomarkers in non-small cell lung cancer: a review. *Clinical Cancer Research* 2005;11:3974-86.

2. Opdenakker G VDJ. The countercurrent principle in invasion and metastasis of cancer cells. Recent insights on the roles of chemokines. *Int.J.Dev.Biol* 2004.

3. Hanahan D, Weinberg RA. The hallmarks of cancer. *Cell* 2000;100:57-70.

4. Holmgren L, O'Reilly M, Folkman J. Dormancy of micrometastases: balanced proliferation and apoptosis in the presence of angiogenesis suppression. *Nature Medicine* 1995;1:149-53.

5. Folkman J. Role of angiogenesis in tumor growth and metastasis. *Semin Oncol* 2002;29:15-8.

6. Furuya M, Nishiyama M, Kasuya Y, Kimura S, Ishikura H. Pathophysiology of tumor neovascularization. *Vascular health and risk management* 2005;1:277-90.

7. Vaupel P. The role of hypoxia-induced factors in tumor progression. *The Oncologist* 2004;9 Suppl 5:10-7.

8. Ziemer LS, Koch CJ, Maity A, Magarelli DP, Horan AM, Evans SM. Hypoxia and VEGF mRNA expression in human tumors. *Neoplasia (New York, NY)* 2001;3:500-8.

9. Brahimi-Horn C, Pouysségur J. The role of the hypoxia-inducible factor in tumor metabolism growth and invasion. *Bulletin du cancer* 2006;93:E73-E80.

10. Theodoropoulos VE, Lazaris AC, Kastriotis I, Spiliadi C, Theodoropoulos GE, Tsoukala V et al. Evaluation of hypoxia-inducible factor 1alpha overexpression as a predictor of tumour recurrence and progression in superficial urothelial bladder carcinoma. *BJU.Int* 2005;95:425-31.

11. Theodoropoulos GE, Lazaris AC, Theodoropoulos VE, Papatheodosiou K, Gazouli M, Bramis J et al. Hypoxia, angiogenesis and apoptosis markers in locally advanced rectal cancer. *Int J Colorectal Dis* 2006;21:248-57.

12. Theodoropoulos VE, Lazaris AC, Sofras F, Gerzelis I, Tsoukala V, Ghikonti I et al. Hypoxia-inducible factor 1 alpha expression correlates with angiogenesis and unfavorable prognosis in bladder cancer. *Eur Urol.* 2004;46:200-8.

13. Pan J, Mestas J, Burdick MD, Phillips RJ, Thomas GV, Reckamp K et al. Stromal derived factor-1 (SDF-1/CXCL12) and CXCR4 in renal cell carcinoma metastasis. *Molecular cancer* 2006;5:56.

14. Zagzag D, Lukyanov Y, Lan L, Ali MA, Esencay M, Mendez O et al. Hypoxia-inducible factor 1 and VEGF upregulate CXCR4 in glioblastoma: implications for angiogenesis and glioma cell invasion. *Laboratory investigation; a journal of technical methods and pathology* 2006;86:1221-32.

15. Ke Q, Costa M. Hypoxia-inducible factor-1 (HIF-1). *Mol Pharmacol* 2006;70:1469-80.

16. Ma WW, Adjei AA. Novel agents on the horizon for cancer therapy. *CA: A Cancer Journal for Clinicians* 2009;59:111-37.

17. Hong X, Jiang F, Kalkanis S, Zhang Z, Zhang X, decarvalho A et al. SDF-1 and CXCR4 are up-regulated by VEGF and contribute to glioma cell invasion. *Cancer letters* 2006;236:39-45.

18. Bach F, Uddin FJ, Burke D. Angiopoietins in malignancy. *European journal of surgical oncology : the journal of the European Society of Surgical Oncology and the British Association of Surgical Oncology* 2007;33:7-15.

19. Shim WS, Ho IA, Wong PE. Angiopoietin: a TIE(d) balance in tumor angiogenesis. *Molecular cancer research : MCR* 2007;5:655-65.

20. Suzuma K, Takagi H, Otani A, Honda Y. Hypoxia and vascular endothelial growth factor stimulate angiogenic integrin expression in bovine retinal microvascular endothelial cells. *Invest Ophthalmol.Vis.Sci* 1998;39:1028-35.

21. Yamashita T, Ohneda K, Nagano M, Miyoshi C, Kaneko N, Miwa Y et al. Hypoxia-inducible transcription factor-2alpha in endothelial cells regulates tumor neovascularization through activation of ephrin A1. *The Journal of biological chemistry* 2008;283:18926-36.

22. Vihanto MM, Plock J, Erni D, Frey BM, Frey FJ, Huynh-Do U. Hypoxia up-regulates expression of Eph receptors and ephrins in mouse skin. *FASEB J* 2005;19:1689-91.

23. Mosch B, Reissenweber B, Neuber C, Pietzsch J. Eph receptors and ephrin ligands: important players in angiogenesis and tumor angiogenesis. *J Oncol* 2010;2010:135285.

24. Merlos-Suarez A, Batlle E. Eph-ephrin signalling in adult tissues and cancer. *Curr Opin Cell Biol* 2008;20:194-200.

25. Zund G, Nelson DP, Neufeld EJ, Dzus AL, Bischoff J, Mayer JE et al. Hypoxia enhances stimulus-dependent induction of E-selectin on aortic endothelial cells. *Proceedings of the National Academy of Sciences of the United States of America* 1996;93:7075-80.

26. Kannagi R, Izawa M, Koike T, Miyazaki K, Kimura N. Carbohydrate-mediated cell adhesion in cancer metastasis and angiogenesis. *Cancer science* 2004;95:377-84.

27. Kannagi R. Carbohydrate antigen sialyl Lewis a--its pathophysiological significance and induction mechanism in cancer progression. *Chang Gung medical journal* 2007;30:189-209.

28. Gao D, Nolan DJ, Mellick AS, Bambino K, McDonnell K, Mittal V. Endothelial progenitor cells control the angiogenic switch in mouse lung metastasis. *Science (New York, NY)* 2008;319:195-8.

29. Patan S. Vasculogenesis and angiogenesis as mechanisms of vascular network formation, growth and remodeling. *Journal of neuro-oncology* 2000;50:1-15.

30. Ribatti D, Nico B, Crivellato E, Vacca A. The structure of the vascular network of tumors. *Cancer letters* 2007;248:18-23.

31. Lal B, Indurti R, Couraud P, Goldstein G, Laterra J. Endothelial cell implantation and survival within experimental gliomas. *Proceedings of the National Academy of Sciences* 1994;91:9695-9.

32. Tei K, Kawakami-Kimura N, Taguchi O, Kumamoto K, Higashiyama S, Taniguchi N et al. Roles of cell adhesion molecules in tumor angiogenesis induced by cotransplantation of cancer and endothelial cells to nude rats. *Cancer research* 2002;62:6289-96.

33. Silva R, D'Amico G, Hodivala-Dilke KM, Reynolds LE. Integrins: the keys to unlocking angiogenesis. *Arteriosclerosis, Thrombosis, and Vascular Biology* 2008;28:1703-13.

34. Kerbel RS. Tumor angiogenesis. *The New England journal of medicine* 2008;358:2039-49.

35. Folkman J. Angiogenesis. *Annual review of medicine* 2006;57:1-18.

36. Carmeliet P. Angiogenesis in health and disease. *Nature Medicine* 2003;9:653-60.

37. Carmeliet P. Angiogenesis in life, disease and medicine. *Nature* 2005;438:932-6.

38. Young MR. Tumor skewing of CD34+ progenitor cell differentiation into endothelial cells. *International journal of cancer Journal international du cancer* 2004;109:516-24.

39. Terman B, Stoletov K. VEGF and tumor angiogenesis. *J Biol and Med* 2001;18:59-66.

40. Cross MJ, Dixelius J, Matsumoto T, Claesson-Welsh L. VEGF-receptor signal transduction. *Trends Biochem Sci* 2003;28:488-94.

41. Lohela M, Bry M, Tammela T, Alitalo K. VEGFs and receptors involved in angiogenesis versus lymphangiogenesis. *Curr Opin Cell Biol* 2009;21:154-65.

42. Strieter RM, Burdick MD, Gomperts BN, Belperio JA, Keane MP. CXC chemokines in angiogenesis. *Cytokine Growth Factor Rev* 2005;16:593-609.

43. Vandercappellen J, Van Damme J, Struyf S. The role of CXC chemokines and their receptors in cancer. *Cancer letters* 2008;267:226-44.

44. Nishiyama K, Takaji K, Kataoka K, Kurihara Y, Yoshimura M, Kato A et al. Id1 gene transfer confers angiogenic property on fully differentiated endothelial cells and contributes to therapeutic angiogenesis. *Circulation* 2005;112:2840-50.

45. Volpert OV, Pili R, Sikder HA, Nelius T, Zaichuk T, Morris C et al. Id1 regulates angiogenesis through transcriptional repression of thrombospondin-1. *Cancer Cell* 2002;2:473-83.

46. Hillen F, Griffioen AW. Tumour vascularization: sprouting angiogenesis and beyond. *Cancer metastasis reviews* 2007;26:489-502.

47. Shojaei F, Ferrara N. Antiangiogenic therapy for cancer: an update. *Cancer J* 2007;13:345-8.

48. Asahara T, Kawamoto A. Endothelial progenitor cells for postnatal vasculogenesis. *Am J Physiol Cell Physiol* 2004;287:C572-C579.

49. Asahara T, Murohara T, Sullivan A, Silver M, van der Zee R, Li T et al. Isolation of putative progenitor endothelial cells for angiogenesis. *Science (New York, NY)* 1997;275:964-7.

50. Lyden D, Hattori K, Dias S, Costa C, Blaikie P, Butros L et al. Impaired recruitment of bone-marrow-derived endothelial and hematopoietic precursor cells blocks tumor angiogenesis and growth. *Nature Medicine* 2001;7:1194-201.

51. Vajkoczy P, Blum S, Lamparter M, Mailhammer R, Erber R, Engelhardt B et al. Multistep nature of microvascular recruitment of ex vivo-expanded embryonic endothelial progenitor cells during tumor angiogenesis. *The Journal of experimental medicine* 2003;197:1755-65.

52. Li H, Gerald WL, Benezra R. Utilization of bone marrow-derived endothelial cell precursors in spontaneous prostate tumors varies with tumor grade. *Cancer research* 2004;64:6137-43.

53. Nolan DJ, Ciarrocchi A, Mellick AS, Jaggi JS, Bambino K, Gupta S et al. Bone marrow-derived endothelial progenitor cells are a major determinant of nascent tumor neovascularization. *Genes Dev.* 2007;21:1546-58.

54. Gao D, Mittal V. The role of bone-marrow-derived cells in tumor growth, metastasis initiation and progression. *Trends in molecular medicine* 2009;15:333-43.

55. De Palma M, Venneri MA, Roca C, Naldini L. Targeting exogenous genes to tumor angiogenesis by transplantation of genetically modified hematopoietic stem cells. *Nature Medicine* 2003;9:789-95.

56. Capillo M, Mancuso P, Gobbi A, Monestiroli S, Pruneri G, Dell'Agnola C et al. Continuous infusion of endostatin inhibits differentiation, mobilization, and clonogenic potential of endothelial cell progenitors. *Clinical cancer research : an official journal of the American Association for Cancer Research* 2003;9:377-82.

57. Gothert JR, Gustin SE, van Eekelen JA, Schmidt U, Hall MA, Jane SM et al. Genetically tagging endothelial cells in vivo: bone marrow-derived cells do not contribute to tumor endothelium. *Blood* 2004;104:1769-77.

58. Bagley RG, Walter-Yohrling J, Cao X, Weber W, Simons B, Cook BP et al. Endothelial precursor cells as a model of tumor endothelium: characterization and comparison with mature endothelial cells. *Cancer research* 2003;63:5866-73.

59. Jodele S, Chantrain CF, Blavier L, Lutzko C, Crooks GM, Shimada H et al. The contribution of bone marrow-derived cells to the tumor vasculature in neuroblastoma is matrix metalloproteinase-9 dependent. *Cancer research* 2005;65:3200-8.

60. Shinde Patil VR, Friedrich EB, Wolley AE, Gerszten RE, Allport JR, Weissleder R. Bone marrow-derived lin(-)c-kit(+)Sca-1+ stem cells do not contribute to vasculogenesis in Lewis lung carcinoma. *Neoplasia (New York, NY)* 2005;7:234-40.

61. Santarelli J, Udani V, Yung Y, Cheshier S, Wagers A, Brekken R et al. Incorporation of Bone Marrow-derived Flk-1-expressing CD34+ Cells in the Endothelium of Tumor Vessels in the Mouse Brain. *Neurosurgery* 2006;59:374-82.

62. Aghi M, Cohen KS, Klein RJ, Scadden DT, Chiocca EA. Tumor stromal-derived factor-1 recruits vascular progenitors to mitotic neovasculature, where microenvironment influences their differentiated phenotypes. *Cancer research* 2006;66:9054-64.

63. Jin H. A homing mechanism for bone marrow-derived progenitor cell recruitment to the neovasculature. *The Journal of clinical investigation* 2006;116:652-62.

64. Li B, Sharpe EE, Maupin AB, Teleron AA, Pyle AL, Carmeliet P et al. VEGF and PlGF promote adult vasculogenesis by enhancing EPC recruitment and vessel formation at the site of tumor neovascularization. *FASEB J* 2006;20:1495-7.

65. Tabatabai G, Herrmann C, von KÃ¼rthy G, Mittelbronn M, Grau S, Frank B et al. VEGF-dependent induction of CD62E on endothelial cells mediates glioma tropism of adult haematopoietic progenitor cells. *Brain* 2008;131:2579-95.

66. Mahller YY, Vaikunth SS, Ripberger MC, Baird WH, Saeki Y, Cancelas JA et al. Tissue inhibitor of metalloproteinase-3 via oncolytic herpesvirus inhibits tumor growth and vascular progenitors. *Cancer research* 2008;68:1170-9.

67. Suriano R, Chaudhuri D, Johnson RS, Lambers E, Ashok BT, Kishore R et al. 17Beta-estradiol mobilizes bone marrow-derived endothelial progenitor cells to tumors. *Cancer research* 2008;68:6038-42.

68. Purhonen S, Palm J, Rossi D, Kaskenpaa N, Rajantie I, Yla-Herttuala S et al. Bone marrow-derived circulating endothelial precursors do not contribute to vascular endothelium and are not needed for tumor growth. *Proc Natl Acad Sci U.S.A* 2008;105:6620-5.

69. Ahn GO, Brown JM. Matrix metalloproteinase-9 is required for tumor vasculogenesis but not for angiogenesis: role of bone marrow-derived myelomonocytic cells. *Cancer Cell* 2008;13:193-205.

70. Reddy K, Zhou Z, Jia S, Lee T, Morales-Arias J, Cao Y et al. Stromal cell-derived factor-1 stimulates vasculogenesis and enhances Ewing's sarcoma tumor growth in the absence of vascular endothelial growth factor. *International journal of cancer Journal international du cancer* 2008;123:831-7.

71. Du R, Lu KV, Petritsch C, Liu P, Ganss R, PasseguÃ© E et al. HIF1alpha induces the recruitment of bone marrow-derived vascular modulatory cells to regulate tumor angiogenesis and invasion. *Cancer Cell* 2008;13:206-20.

72. Chu CY, Cha ST, Lin WC, Lu PH, Tan CT, Chang CC et al. Stromal cell-derived factor-1alpha (SDF-1alpha/CXCL12)-enhanced angiogenesis of human basal cell carcinoma cells involves ERK1/2-NF-kappaB/interleukin-6 pathway. *Carcinogenesis* 2009;30:205-13.

73. Wickersheim A, Kerber M, de Miguel LS, Plate KH, Machein MR. Endothelial progenitor cells do not contribute to tumor endothelium in primary and metastatic tumors. *International journal of cancer Journal international du cancer* 2009;125:1771-7.

74. Folkins C, Shaked Y, Man S, Tang T, Lee CR, Zhu Z et al. Glioma tumor stem-like cells promote tumor angiogenesis and vasculogenesis via vascular endothelial growth factor and stromal-derived factor 1. *Cancer research* 2009;69:7243-51.

75. Murakami J, Li TS, Ueda K, Tanaka T, Hamano K. Inhibition of accelerated tumor growth by blocking the recruitment of mobilized endothelial progenitor cells after chemotherapy. *International journal of cancer Journal international du cancer* 2009;124:1685-92.

76. Madlambayan GJ, Butler JM, Hosaka K, Jorgensen M, Fu D, Guthrie SM et al. Bone marrow stem and progenitor cell contribution to neovasculogenesis is dependent on model system with SDF-1 as a permissive trigger. *Blood* 2009;114:4310-9.

77. Kioi M, Vogel H, Schultz G, Hoffman RM, Harsh GR, Brown JM. Inhibition of vasculogenesis, but not angiogenesis, prevents the recurrence of glioblastoma after irradiation in mice. *The Journal of clinical investigation* 2010;120:694-705.

78. Wei J, Blum S, Unger M, Jarmy G, Lamparter M, Geishauser A et al. Embryonic endothelial progenitor cells armed with a suicide gene target hypoxic lung metastases after intravenous delivery. *Cancer Cell* 2004;5:477-88.

79. Tilki D, Hohn HP, Ergun B, Rafii S, Ergun S. Emerging biology of vascular wall progenitor cells in health and disease. *Trends Mol Med* 2009;15:501-9.

80. Kopp H, Ramos CA, Rafii S. Contribution of endothelial progenitors and proangiogenic hematopoietic cells to vascularization of tumor and ischemic tissue. *Current opinion in hematology* 2006;13:175-81.

81. Ruzinova MB, Benezra R. Id proteins in development, cell cycle and cancer. *Trends Cell Biol* 2003;13:410-8.

82. Ruzinova MB, Schoer RA, Gerald W, Egan JE, Pandolfi PP, Rafii S et al. Effect of angiogenesis inhibition by Id loss and the contribution of bone-marrow-derived endothelial cells in spontaneous murine tumors. *Cancer Cell* 2003;4:277-89.

83. Ribatti D. The involvement of endothelial progenitor cells in tumor angiogenesis. *Journal of cellular and molecular medicine* 2004;8:294-300.

84. McDonald DM, Foss AJ. Endothelial cells of tumor vessels: abnormal but not absent. *Cancer metastasis reviews* 2000;19:109-20.

85. di Tomaso E, Capen D, Haskell A, Hart J, Logie JJ, Jain RK et al. Mosaic tumor vessels: cellular basis and ultrastructure of focal regions lacking endothelial cell markers. *Cancer research* 2005;65:5740-9.

86. Cao Y. Antiangiogenic cancer therapy. *Seminars in cancer biology* 2004;14:139-45.

87. Tandle A, Blazer DG, Libutti SK. Antiangiogenic gene therapy of cancer: recent developments. *Journal of translational medicine* 2004;2:22.

88. Ojeifo JO, Forough R, Paik S, Maciag T, Zwiebel JA. Angiogenesis-directed implantation of genetically modified endothelial cells in mice. *Cancer research* 1995;55:2240-4.

89. Ojeifo JO, Lee HR, Rezza P, Su N, Zwiebel JA. Endothelial cell-based systemic gene therapy of metastatic melanoma. *Cancer gene therapy* 2001;8:636-48.

90. Ferrari N, Glod J, Lee J, Kobiler D, Fine H. Bone marrow-derived, endothelial progenitor-like cells as angiogenesis-selective gene-targeting vectors. *Gene Therapy* 2003;10:647-56.

91. Deng W, Jia J. Endothelial progenitor cells as cellular vehicles to deliver oncolytic virus therapies to metastatic tumors: the "Trojan horse" approach. *Med Hypotheses* 2008;70:842-4.

92. Michael H.Ross, Gordon I.Kaye, Wojciech MDP. Histology. Lippincott Williams & Wilkins, 2003.

93. Yamashita JK. Differentiation of arterial, venous, and lymphatic endothelial cells from vascular progenitors. *Trends Cardiovasc Med* 2007;17:59-63.

94. Lodge PA, Haisch CE, Thomas FT. A simple method of vascular endothelial cell isolation. *Transplant.Proc* 1992;24:2816-7.

95. Magee JC, Stone AE, Oldham KT, Guice KS. Isolation, culture, and characterization of rat lung microvascular endothelial cells. *The American journal of physiology* 1994;267:L433-L441.

96. Yan Q, Vernon RB, Hendrickson AE, Sage EH. Primary culture and characterization of microvascular endothelial cells from Macaca monkey retina. *Invest Ophthalmol.Vis.Sci* 1996;37:2185-94.

97. Garlanda C, Dejana E. Heterogeneity of endothelial cells. Specific markers. *Arterioscler.Thromb Vasc Biol* 1997;17:1193-202.

98. Woywodt A, Kirsch T, Haubitz M. Circulating endothelial cells in renal disease: markers and mediators of vascular damage. *Nephrol.Dial.Transplant.* 2008;23:7-10.

99. Goon PK, Boos CJ, Stonelake PS, Lip GY. Circulating endothelial cells in malignant disease. *Future.Oncol* 2005;1:813-20.

100. Goon PK, Boos CJ, Lip GY. Circulating endothelial cells: markers of vascular dysfunction. *Clin Lab* 2005;51:531-8.

101. Steurer M, Kern J, Zitt M, Amberger A, Bauer M, Gastl G et al. Quantification of circulating endothelial and progenitor cells: comparison of quantitative PCR and four-channel flow cytometry. *BMC Res Notes* 2008;1:71.

102. Urbich C, Dimmeler S. Endothelial progenitor cells: characterization and role in vascular biology. *Circ.Res* 2004;95:343-53.

103. Hristov M, Weber C. Endothelial progenitor cells: characterization, pathophysiology, and possible clinical relevance. *Journal of cellular and molecular medicine* 2004;8:498-508.

104. Urbich C, Dimmeler S. Endothelial progenitor cells functional characterization. *Trends in Cardiovascular Medicine* 2004;14:318-22.

105. Timmermans F, Plum J, Yoder MC, Ingram DA, Vandekerckhove B, Case J. Endothelial progenitor cells: identity defined? *Journal of cellular and molecular medicine* 2009;13:87-102.

106. Rumpold H, Wolf D, Koeck R, Gunsilius E. Endothelial progenitor cells: a source for therapeutic vasculogenesis? *Journal of cellular and molecular medicine* 2004;8:509-18.

107. Asahara T, Takahashi T, Masuda H, Kalka C, Chen D, Iwaguro H et al. VEGF contributes to postnatal neovascularization by mobilizing bone marrow-derived endothelial progenitor cells. *EMBO J* 1999;18:3964-72.

108. Otani A, Kinder K, Ewalt K, Otero FJ, Schimmel P, Friedlander M. Bone marrow-derived stem cells target retinal astrocytes and can promote or inhibit retinal angiogenesis. *Nat Med* 2002;8:1004-10.

109. Ceradini DJ, Gurtner GC. Homing to hypoxia: HIF-1 as a mediator of progenitor cell recruitment to injured tissue. *Trends Cardiovasc Med* 2005;15:57-63.

110. Otani A. Rescue of retinal degeneration by intravitreally injected adult bone marrow-derived lineage-negative hematopoietic stem cells. *The Journal of clinical investigation* 2004;114:765-74.

111. Burger PE, Coetzee S, McKeehan WL, Kan M, Cook P, Fan Y et al. Fibroblast growth factor receptor-1 is expressed by endothelial progenitor cells. *Blood* 2002;100:3527-35.

112. Peichev M, Naiyer AJ, Pereira D, Zhu Z, Lane WJ, Williams M et al. Expression of VEGFR-2 and AC133 by circulating human CD34(+) cells identifies a population of functional endothelial precursors. *Blood* 2000;95:952-8.

113. Gehling UM, Ergun S, Schumacher U, Wagener C, Pantel K, Otte M et al. In vitro differentiation of endothelial cells from AC133-positive progenitor cells. *Blood* 2000;95:3106-12.

114. Hunting CB, Noort WA, Zwaginga JJ. Circulating endothelial (progenitor) cells reflect the state of the endothelium: vascular injury, repair and neovascularization. *Vox Sang.* 2005;88:1-9.

115. Rafii S, Lyden D. Therapeutic stem and progenitor cell transplantation for organ vascularization and regeneration. *Nat Med* 2003;9:702-12.

116. Yoder MC. Defining human endothelial progenitor cells. *Journal of thrombosis and haemostasis : JTH* 2009;7 Suppl 1:49-52.

117. Yoder MC, Ingram DA. The definition of EPCs and other bone marrow cells contributing to neoangiogenesis and tumor growth: is there common ground for understanding the roles of numerous marrow-derived cells in the neoangiogenic process? *Biochimica et biophysica acta* 2009;1796:50-4.

118. Yoder MC, Ingram DA. Endothelial progenitor cell: ongoing controversy for defining these cells and their role in neoangiogenesis in the murine system. *Current opinion in hematology* 2009;16:269-73.

119. Ribatti D. The discovery of endothelial progenitor cells. An historical review. *Leuk.Res* 2007;31:439-44.

120. Zhang Y, Adachi Y, Iwasaki M, Minamino K, Suzuki Y, Nakano K et al. G-CSF and/or M-CSF accelerate differentiation of bone marrow cells into endothelial progenitor cells in vitro. *Oncol Rep.* 2006;15:1523-7.

121. Gan B, Sahin E, Jiang S, Sanchez-Aguilera A, Scott KL, Chin L et al. mTORC1-dependent and -independent regulation of stem cell renewal, differentiation, and mobilization. *Proc Natl Acad Sci U.S.A* 2008;105:19384-9.

122. Zeng H, Yucel R, Kosan C, Klein-Hitpass L, Moroy T. Transcription factor Gfi1 regulates self-renewal and engraftment of hematopoietic stem cells. *EMBO J* 2004;23:4116-25.

123. Kiuru M, Hidaka C, Hubner RH, Solomon J, Krause A, Leopold PL et al. Sonic hedgehog expands diaphyseal trabecular bone altering bone marrow niche and lymphocyte compartment. *Mol Ther* 2009;17:1442-52.

124. Morales M, Liu Y, Laiakis EC, Morgan WF, Nimer SD, Petrini JH. DNA damage signaling in hematopoietic cells: a role for Mre11 complex repair of topoisomerase lesions. *Cancer research* 2008;68:2186-93.

125. Zhang Y, Harada A, Bluethmann H, Wang JB, Nakao S, Mukaida N et al. Tumor necrosis factor (TNF) is a physiologic regulator of hematopoietic progenitor cells: increase of early hematopoietic progenitor cells in TNF receptor p55-deficient mice in vivo and potent inhibition of progenitor cell proliferation by TNF alpha in vitro. *Blood* 1995;86:2930-7.

126. Zhang F, Tsai S, Kato K, Yamanouchi D, Wang C, Rafii S et al. Transforming growth factor-beta promotes recruitment of bone marrow cells and bone marrow-derived mesenchymal stem cells through stimulation of MCP-1 production in vascular smooth muscle cells. *J.Biol.Chem.* 2009;284:17564-74.

127. Robertson P, Means TK, Luster AD, Scadden DT. CXCR4 and CCR5 mediate homing of primitive bone marrow-derived hematopoietic cells to the postnatal thymus. *Experimental hematology* 2006;34:308-19.

128. Hristov M, Weber C. Progenitor cell trafficking in the vascular wall. *Journal of thrombosis and haemostasis : JTH* 2009;7 Suppl 1:31-4.

129. Bautz F, Rafii S, Kanz L, MÃ¶hle R. Expression and secretion of vascular endothelial growth factor-A by cytokine-stimulated hematopoietic progenitor cells Possible role in the hematopoietic microenvironment. *Experimental hematology* 2000;28:700-6.

130. Petit I, Jin D, Rafii S. The SDF-1-CXCR4 signaling pathway: a molecular hub modulating neo-angiogenesis. *Trends in immunology* 2007;28:299-307.

131. Ceradini D, Kulkarni A, Callaghan M, Tepper O, Bastidas N, Kleinman M et al. Progenitor cell trafficking is regulated by hypoxic gradients through HIF-1 induction of SDF-1. *Nature Medicine* 2004;10:858-64.

132. van Buul JD, Voermans C, van dB, V, Anthony EC, Mul FP, van WS et al. Migration of human hematopoietic progenitor cells across bone marrow endothelium is regulated by vascular endothelial cadherin. *Journal of immunology (Baltimore, Md : 1950)* 2002;168:588-96.

133. Liesveld JL, Rosell K, Panoskaltsis N, Belanger T, Harbol A, Abboud CN. Response of human CD34+ cells to CXC, CC, and CX3C chemokines: implications for cell migration and activation. *J Hematother.Stem Cell Res* 2001;10:643-55.

134. Mohle R, Bautz F, Rafii S, Moore MA, Brugger W, Kanz L. The chemokine receptor CXCR-4 is expressed on CD34+ hematopoietic progenitors and leukemic cells and mediates transendothelial migration induced by stromal cell-derived factor-1. *Blood* 1998;91:4523-30.

135. Mohle R, Moore MA, Nachman RL, Rafii S. Transendothelial migration of CD34+ and mature hematopoietic cells: an in vitro study using a human bone marrow endothelial cell line. *Blood* 1997;89:72-80.

136. Ciarrocchi A, Jankovic V, Shaked Y, Nolan DJ, Mittal V, Kerbel RS et al. Id1 restrains p21 expression to control endothelial progenitor cell formation. *PloS one* 2007;2:e1338.

137. Garcia-Barros M, Paris F, Cordon-Cardo C, Lyden D, Rafii S, Haimovitz-Friedman A et al. Tumor response to radiotherapy regulated by endothelial cell apoptosis. *Science (New York, NY)* 2003;300:1155-9.

138. Kaplan R, Riba R, Zacharoulis S, Bramley A, Vincent L, Costa C et al. VEGFR1-positive haematopoietic bone marrow progenitors initiate the pre-metastatic niche. *Nature* 2005;438:820-7.

139. Garmy-Susini B, Jin H, Zhu Y, Sung RJ, Hwang R, Varner J. Integrin alpha4beta1-VCAM-1-mediated adhesion between endothelial and mural cells is required for blood vessel maturation. *The Journal of clinical investigation* 2005;115:1542-51.

140. Singh Jaggi J, Henke E, Seshan SV, Kappel BJ, Chattopadhyay D, May C et al. Selective alpha-particle mediated depletion of tumor vasculature with vascular normalization. *PloS one* 2007;2:e267.

141. Barczyk M, Carracedo S, Gullberg D. Integrins. *Cell Tissue Res* 2010;339:269-80.

142. Avraamides CJ, Garmy-Susini B, Varner JA. Integrins in angiogenesis and lymphangiogenesis. *Nature reviews Cancer* 2008;8:604-17.

143. Desgrosellier JS, Cheresh DA. Integrins in cancer: biological implications and therapeutic opportunities. *Nature reviews Cancer* 2010;10:9-22.

144. Schwartz MA. Integrins, oncogenes, and anchorage independence. *The Journal of cell biology* 1997;139:575-8.

145. Wyble CW, Hynes KL, Kuchibhotla J, Marcus BC, Hallahan D, Gewertz BL. TNF-alpha and IL-1 upregulate membrane-bound and soluble E-selectin through a common pathway. *The Journal of surgical research* 1997;73:107-12.

146. Ding YB, Chen GY, Xia JG, Zang XW, Yang HY, Yang L. Association of VCAM-1 overexpression with oncogenesis, tumor angiogenesis and metastasis of gastric carcinoma. *World J Gastroenterol.* 2003;9:1409-14.

147. Cavallaro U, Liebner S, Dejana E. Endothelial cadherins and tumor angiogenesis. *Experimental cell research* 2006;312:659-67.

148. Bischoff J. Cell adhesion and angiogenesis. *The Journal of clinical investigation* 1997;100:S37-S39.

149. Kneuer C, Ehrhardt C, Radomski MW, Bakowsky U. Selectins--potential pharmacological targets? *Drug Discov.Today* 2006;11:1034-40.

150. McEver RP. Selectin-carbohydrate interactions during inflammation and metastasis. *Glycoconjugate journal* 1997;14:585-91.

151. Borsig L, Wong R, Hynes RO, Varki NM, Varki A. Synergistic effects of L- and P-selectin in facilitating tumor metastasis can involve non-mucin ligands and implicate leukocytes as enhancers of metastasis. *Proc Natl Acad Sci U.S.A* 2002;99:2193-8.

152. Garcia J, Callewaert N, Borsig L. P-selectin mediates metastatic progression through binding to sulfatides on tumor cells. *Glycobiology* 2007;17:185-96.

153. Hahne M, JÃ¤ger U, Isenmann S, Hallmann R, Vestweber D. Five tumor necrosis factor-inducible cell adhesion mechanisms on the surface of mouse endothelioma cells mediate the binding of leukocytes. *The Journal of cell biology* 1993;121:655-64.

154. Ye C, Kiriyama K, Mistuoka C, Kannagi R, Ito K, Watanabe T et al. Expression of E-selectin on endothelial cells of small veins in human colorectal cancer. *International journal of cancer Journal international du cancer* 1995;61:455-60.

155. Nguyen M. Angiogenic factors as tumor markers. *Investigational new drugs* 1997;15:29-37.

156. Ghersa P, Hooft van HR, Whelan J, DeLamarter JF. Labile proteins play a dual role in the control of endothelial leukocyte adhesion molecule-1 (ELAM-1) gene regulation. *The Journal of biological chemistry* 1992;267:19226-32.

157. Subramaniam M, Koedam JA, Wagner DD. Divergent fates of P- and E-selectins after their expression on the plasma membrane. *Mol Biol Cell* 1993;4:791-801.

158. Haraldsen G, Kvale D, Lien B, Farstad IN, Brandtzaeg P. Cytokine-regulated expression of E-selectin, intercellular adhesion molecule-1 (ICAM-1), and vascular cell adhesion

molecule-1 (VCAM-1) in human microvascular endothelial cells. *Journal of immunology (Baltimore, Md : 1950)* 1996;156:2558-65.

159. Li ZD, Bork JP, Krueger B, Patsenker E, Schulze-Krebs A, Hahn EG et al. VEGF induces proliferation, migration, and TGF-beta1 expression in mouse glomerular endothelial cells via mitogen-activated protein kinase and phosphatidylinositol 3-kinase. *Biochemical and biophysical research communications* 2005;334:1049-60.

160. LAFERRIERE J, HOULE F, HUOT J. Regulation of the metastatic process by E-selectin and stress-activated protein kinase-2/p38. *Annals of the New York Academy of Sciences* 2002;973:562-72.

161. Matsuo Y, Amano S, Furuya M, Namiki K, Sakurai K, Nishiyama M et al. Involvement of p38alpha mitogen-activated protein kinase in lung metastasis of tumor cells. *The Journal of biological chemistry* 2006;281:36767-75.

162. Barthel SR, Gavino JD, Descheny L, Dimitroff CJ. Targeting selectins and selectin ligands in inflammation and cancer. *Expert opinion on therapeutic targets* 2007;11:1473-91.

163. Sueyoshi S, Sawada R, Fukuda M. Carbohydrate structures of recombinant soluble lamp-1 and leukosialin containing sialyl Le(x) terminus. *Bioorganic & medicinal chemistry* 1994;2:1331-8.

164. Uotani H, Yamashita I, Nagata T, Kishimoto H, Kashii Y, Tsukada K. Induction of E-selectin after partial hepatectomy promotes metastases to liver in mice. *The Journal of surgical research* 2001;96:197-203.

165. Insug O, Kieber-Emmons T, OTVOS JR L, Blaszczyk-Thurin M. Peptides mimicking sialyl-Lewis A isolated from a random peptide library and peptide array.

166. Monzavi-Karbassi B, Whitehead TL, Jousheghany F, Artaud C, Hennings L, Shaaf S et al. Deficiency in surface expression of E-selectin ligand promotes lung colonization in a mouse model of breast cancer. *International journal of cancer Journal international du cancer* 2005;117:398-408.

167. O I, Otvos L, Kieber-Emmons T, Blaszczyk-Thurin M. Role of SA-Le(a) and E-selectin in metastasis assessed with peptide antagonist. *Peptides* 2002;23:999-1010.

168. Thurin M, Kieber-Emmons T. SA-Lea and tumor metastasis: the old prediction and recent findings. *Hybridoma and hybridomics* 2002;21:111-6.

169. Otvos L, Kieber-Emmons T, Blaszczyk-Thurin M. Role of SA-Lea and E-selectin in metastasis assessed with peptide antagonist. *Peptides* 2002.

170. Storey, B. T., Pittman, H. K., Haisch, C. E., and Verbanac, K. E-selectin mediates *in vitro* and *in vivo* adhesion of exogenous endothelial cells to tumor vasculature. Proceedings of

American Association of Cancer Research 44(1434). 2003.
Ref Type: Abstract

171. Storey, B. T., Pittman, H. K., Min, C. J., Haisch, C. E., and Verbanac, K. M. Murine Vascular Endothelial Cells Specifically Home to Syngeneic Lung Adenocarcinomas and Incorporate into Tumor Vasculature. Angiogenesis and Cancer Book of Abstracts . 2000.
Ref Type: Abstract

172. Kraling BM, Razon MJ, Boon LM, Zurakowski D, Seachord C, Darveau RP et al. E-selectin is present in proliferating endothelial cells in human hemangiomas. *Am J Pathol* 1996;148:1181-91.

173. Mayer B, Spatz H, Funke I, Johnson JP, Schildberg FW. De novo expression of the cell adhesion molecule E-selectin on gastric cancer endothelium. *Langenbeck's archives of surgery / Deutsche Gesellschaft fÃ¼r Chirurgie* 1998;383:81-6.

174. Banks RE, Gearing AJ, Hemingway IK, Norfolk DR, Perren TJ, Selby PJ. Circulating intercellular adhesion molecule-1 (ICAM-1), E-selectin and vascular cell adhesion molecule-1 (VCAM-1) in human malignancies. *British journal of cancer* 1993;68:122-4.

175. Aychek T, Miller K, Sagi-Assif O, Levy-Nissenbaum O, Israeli-Amit M, Pasmanik-Chor M et al. E-selectin regulates gene expression in metastatic colorectal carcinoma cells and enhances HMGB1 release. *International journal of cancer Journal international du cancer* 2008;123:1741-50.

176. Velikova G, Banks RE, Gearing A, Hemingway I, Forbes MA, Preston SR et al. Circulating soluble adhesion molecules E-cadherin, E-selectin, intercellular adhesion molecule-1 (ICAM-1) and vascular cell adhesion molecule-1 (VCAM-1) in patients with gastric cancer. *British journal of cancer* 1997;76:1398-404.

177. Velikova G, Banks RE, Gearing A, Hemingway I, Forbes MA, Preston SR et al. Serum concentrations of soluble adhesion molecules in patients with colorectal cancer. *British journal of cancer* 1998;77:1857-63.

178. Hebbar M, Révillion F, Louchez MM, Vilain MO, Fournier C, Bonneterre J et al. The relationship between concentrations of circulating soluble E-selectin and clinical, pathological, and biological features in patients with breast cancer. *Clinical cancer research : an official journal of the American Association for Cancer Research* 1998;4:373-80.

179. Liu CM, Sheen TS, Ko JY, Shun CT. Circulating intercellular adhesion molecule 1 (ICAM-1), E-selectin and vascular cell adhesion molecule 1 (VCAM-1) in head and neck cancer. *British journal of cancer* 1999;79:360-2.

180. Sawada R, Lowe JB, Fukuda M. E-selectin-dependent adhesion efficiency of colonic carcinoma cells is increased by genetic manipulation of their cell surface lysosomal membrane glycoprotein-1 expression levels. *The Journal of biological chemistry* 1993;268:12675-81.

181. Saitoh O, Wang WC, Lotan R, Fukuda M. Differential glycosylation and cell surface expression of lysosomal membrane glycoproteins in sublines of a human colon cancer exhibiting distinct metastatic potentials. *The Journal of biological chemistry* 1992;267:5700-11.

182. Sawada R, Tsuboi S, Fukuda M. Differential E-selectin-dependent adhesion efficiency in sublines of a human colon cancer exhibiting distinct metastatic potentials. *The Journal of biological chemistry* 1994;269:1425-31.

183. Woynarowska B, Skrincosky DM, Haag A, Sharma M, Matta K, Bernacki RJ. Inhibition of lectin-mediated ovarian tumor cell adhesion by sugar analogs. *The Journal of biological chemistry* 1994;269:22797-803.

184. Sarafian V, Jadot M, Foidart J, Letesson J, Van den Brule F, Castronovo V et al. Expression of Lamp-1 and Lamp-2 and their interactions with galectin-3 in human tumor cells. *International Journal of Cancer* 1998;75.

185. Fuzii HT, Travassos LR. Transient resistance to B16F10 melanoma growth and metastasis in CD43-/- mice. *Melanoma Res* 2002;12:9-16.

186. Dimitroff CJ, Descheny L, Trujillo N, Kim R, Nguyen V, Huang W et al. Identification of leukocyte E-selectin ligands, P-selectin glycoprotein ligand-1 and E-selectin ligand-1, on human metastatic prostate tumor cells. *Cancer research* 2005;65:5750-60.

187. Judith H.Harmey. VEGF and Cancer. 2004.

188. Takahashi H, Shibuya M. The vascular endothelial growth factor (VEGF)/VEGF receptor system and its role under physiological and pathological conditions. *Clin Sci (Lond)* 2005;109:227-41.

189. Ferrara N. Molecular and biological properties of vascular endothelial growth factor. *Journal of molecular medicine (Berlin, Germany)* 1999;77:527-43.

190. Ferrara N. Vascular endothelial growth factor: basic science and clinical progress. *Endocr.Rev* 2004;25:581-611.

191. Hicklin DJ, Ellis LM. Role of the vascular endothelial growth factor pathway in tumor growth and angiogenesis. *J Clin Oncol* 2005;23:1011-27.

192. Xie K, Wei D, Shi Q, Huang S. Constitutive and inducible expression and regulation of vascular endothelial growth factor. *Cytokine Growth Factor Rev* 2004;15:297-324.

193. Fischer C, Mazzone M, Jonckx B, Carmeliet P. FLT1 and its ligands VEGFB and PlGF: drug targets for anti-angiogenic therapy? *Nature reviews Cancer* 2008;8:942-56.

194. Onogawa S, Kitadai Y, Tanaka S, Kuwai T, Kimura S, Chayama K. Expression of VEGF-C and VEGF-D at the invasive edge correlates with lymph node metastasis and prognosis of patients with colorectal carcinoma. *Cancer science* 2004;95:32-9.

195. van I, V, Leidenius M, von SK, Bono P, Heikkila P. VEGF-D in association with VEGFR-3 promotes nodal metastasis in human invasive lobular breast cancer. *Am J Clin Pathol* 2007;128:759-66.

196. Shibuya M. Vascular endothelial growth factor receptor-1 (VEGFR-1/Flt-1): a dual regulator for angiogenesis. *Angiogenesis* 2006;9:225-30.

197. Lyden D, Hattori K, Dias S, Costa C, Blaikie P, Butros L et al. Impaired recruitment of bone-marrow-derived endothelial and hematopoietic precursor cells blocks tumor angiogenesis and growth. *Nat Med* 2001;7:1194-201.

198. Christopherson K, Hromas R. Chemokine regulation of normal and pathologic immune responses. *Stem Cells* 2001;19:388-96.

199. Keeley EC, Mehrad B, Strieter RM. Chemokines as mediators of neovascularization. *Arteriosclerosis, Thrombosis, and Vascular Biology* 2008;28:1928-36.

200. Schober A. Chemokines in Vascular Dysfunction and Remodeling. *Arteriosclerosis, Thrombosis, and Vascular Biology* 2008;28:1950-9.

201. Raman D, Baugher PJ, Thu YM, Richmond A. Role of chemokines in tumor growth. *Cancer letters* 2007;256:137-65.

202. Dias S, Choy M, Rafii S. The role of CXC chemokines in the regulation of tumor angiogenesis. *Cancer investigation* 2001;19:732-8.

203. Strieter RM, Belperio JA, Phillips RJ, Keane MP. CXC chemokines in angiogenesis of cancer. *Seminars in cancer biology* 2004;14:195-200.

204. Strieter RM, Belperio JA, Burdick MD, SHARMA S, Dubinett SM, Keane MP. CXC chemokines: angiogenesis, immunoangiostasis, and metastases in lung cancer. *Ann.N Y.Acad Sci* 2004;1028:351-60.

205. Wang J, Loberg R, Taichman RS. The pivotal role of CXCL12 (SDF-1)/CXCR4 axis in bone metastasis. *Cancer metastasis reviews* 2006;25:573-87.

206. Kollmar O, Rupertus K, Scheuer C, Junker B, Tilton B, Schilling MK et al. Stromal cell-derived factor-1 promotes cell migration and tumor growth of colorectal metastasis. *Neoplasia (New York, NY)* 2007;9:862-70.

207. Keane MP, Belperio JA, Xue YY, Burdick MD, Strieter RM. Depletion of CXCR2 inhibits tumor growth and angiogenesis in a murine model of lung cancer. *Journal of immunology (Baltimore, Md : 1950)* 2004;172:2853-60.

208. Matsuo Y, Raimondo M, Woodward TA, Wallace MB, Gill KR, Tong Z et al. CXC-chemokine/CXCR2 biological axis promotes angiogenesis in vitro and in vivo in pancreatic cancer. *Int.J.Cancer* 2009;125:1027-37.

209. Mestas J, BURDICK M, Reckamp K, Pantuck A, Figlin R, STRIETER R. The Role of CXCR2/CXCR2 Ligand Biological Axis in Renal Cell Carcinoma 1. *The Journal of Immunology* 2005;175:5351-7.

210. Shen H, Schuster R, Lu B, Waltz SE, Lentsch AB. Critical and opposing roles of the chemokine receptors CXCR2 and CXCR3 in prostate tumor growth. *The Prostate* 2006;66:1721-8.

211. Singh S, Sadanandam A, Nannuru KC, Varney ML, Mayer-Ezell R, Bond R et al. Small-molecule antagonists for CXCR2 and CXCR1 inhibit human melanoma growth by decreasing tumor cell proliferation, survival, and angiogenesis. *Clinical cancer research : an official journal of the American Association for Cancer Research* 2009;15:2380-6.

212. Muller A, Homey B, Soto H, Ge N, Catron D, Buchanan M et al. Involvement of chemokine receptors in breast cancer metastasis. *Nature* 2001;410:50-6.

213. Yun HJ, Jo DY. Production of stromal cell-derived factor-1 (SDF-1)and expression of CXCR4 in human bone marrow endothelial cells. *J Korean Med Sci* 2003;18:679-85.

214. Ma Q, Jones D, Borghesani PR, Segal RA, Nagasawa T, Kishimoto T et al. Impaired B-lymphopoiesis, myelopoiesis, and derailed cerebellar neuron migration in CXCR4- and SDF-1-deficient mice. *Proceedings of the National Academy of Sciences of the United States of America* 1998;95:9448-53.

215. Guleng B, Tateishi K, Ohta M, Kanai F, Jazag A, Ijichi H et al. Blockade of the stromal cell-derived factor-1/CXCR4 axis attenuates in vivo tumor growth by inhibiting angiogenesis in a vascular endothelial growth factor-independent manner. *Cancer research* 2005;65:5864-71.

216. Salcedo R, Oppenheim JJ. Role of chemokines in angiogenesis: CXCL12/SDF-1 and CXCR4 interaction, a key regulator of endothelial cell responses. *Microcirculation.* 2003;10:359-70.

217. Kucia M, Reca R, Miekus K, Wanzeck J, Wojakowski W, Janowska-Wieczorek A et al. Trafficking of normal stem cells and metastasis of cancer stem cells involve similar mechanisms: pivotal role of the SDF-1-CXCR4 axis. *Stem Cells* 2005;23:879-94.

218. Feng Y, Broder CC, Kennedy PE, Berger EA. HIV-1 entry cofactor: functional cDNA cloning of a seven-transmembrane, G protein-coupled receptor. *Science (New York, NY)* 1996;272:872-7.

219. Shim H, Oishi S, Fujii N. Chemokine receptor CXCR4 as a therapeutic target for neuroectodermal tumors. *Seminars in cancer biology* 2009;19:123-34.

220. Huang EH, Singh B, Cristofanilli M, Gelovani J, Wei C, Vincent L et al. A CXCR4 Antagonist CTCE-9908 Inhibits Primary Tumor Growth and Metastasis of Breast Cancer. *The Journal of surgical research* 2008.

221. Yoon Y, Liang Z, Zhang X, Choe M, Zhu A, Cho HT et al. CXC chemokine receptor-4 antagonist blocks both growth of primary tumor and metastasis of head and neck cancer in xenograft mouse models. *Cancer research* 2007;67:7518-24.

222. Burger JA, Kipps TJ. CXCR4: a key receptor in the crosstalk between tumor cells and their microenvironment. *Blood* 2006;107:1761-7.

223. Dar A, Goichberg P, Shinder V, Kalinkovich A, Kollet O, Netzer N et al. Chemokine receptor CXCR4-dependent internalization and resecretion of functional chemokine SDF-1 by bone marrow endothelial and stromal cells. *Nat Immunol* 2005;6:1038-46.

224. Maldonado-Estrada J, Menu E, Roques P, Vaslin B, utry-Varsat A, Barre-Sinoussi F et al. Predominant intracellular expression of CXCR4 and CCR5 in purified primary trophoblast cells from first trimester and term human placentae. *Am J Reprod.Immunol* 2003;50:291-301.

225. Kollet O, Petit I, Kahn J, Samira S, Dar A, Peled A et al. Human CD34(+)CXCR4(-) sorted cells harbor intracellular CXCR4, which can be functionally expressed and provide NOD/SCID repopulation. *Blood* 2002;100:2778-86.

226. Zhang Y, Foudi A, Geay JF, Berthebaud M, Buet D, Jarrier P et al. Intracellular localization and constitutive endocytosis of CXCR4 in human CD34+ hematopoietic progenitor cells. *Stem Cells* 2004;22:1015-29.

227. Peled A, Grabovsky V, Habler L, Sandbank J, renzana-Seisdedos F, Petit I et al. The chemokine SDF-1 stimulates integrin-mediated arrest of CD34(+) cells on vascular endothelium under shear flow. *The Journal of clinical investigation* 1999;104:1199-211.

228. Lapidot T, Dar A, Kollet O. How do stem cells find their way home? *Blood* 2005;106:1901-10.

229. Salcedo R, Wasserman K, Young HA, Grimm MC, Howard OM, Anver MR et al. Vascular endothelial growth factor and basic fibroblast growth factor induce expression of CXCR4 on human endothelial cells: In vivo neovascularization induced by stromal-derived factor-1alpha. *Am J Pathol* 1999;154:1125-35.

230. Wang J, Wang J, Sun Y, Song W, Nor J, Wang C et al. Diverse signaling pathways through the SDF-1/CXCR4 chemokine axis in prostate cancer cell lines leads to altered patterns of cytokine secretion and angiogenesis. *Cellular signalling* 2005;17:1578-92.

231. Wang DF, Lou N, Zeng CG, Zhang X, Chen FJ. Expression of CXCL12/CXCR4 and its correlation to prognosis in esophageal squamous cell carcinoma. *Chin J Cancer* 2009;28:154-8.

232. Opdenakker G, Van DJ. The countercurrent principle in invasion and metastasis of cancer cells. Recent insights on the roles of chemokines. *Int J Dev Biol* 2004;48:519-27.

233. Phillips RJ, Burdick MD, Lutz M, Belperio JA, Keane MP, Strieter RM. The stromal derived factor-1/CXCL12-CXC chemokine receptor 4 biological axis in non-small cell lung cancer metastases. *American journal of respiratory and critical care medicine* 2003;167:1676-86.

234. Iwakiri S, Mino N, Takahashi T, Sonobe M, Nagai S, Okubo K et al. Higher expression of chemokine receptor CXCR7 is linked to early and metastatic recurrence in pathological stage I nonsmall cell lung cancer. *Cancer* 2009;115:2580-93.

235. Wang J, Shiozawa Y, Wang J, Wang Y, Jung Y, Pienta KJ et al. The role of CXCR7/RDC1 as a chemokine receptor for CXCL12/SDF-1 in prostate cancer. *The Journal of biological chemistry* 2008;283:4283-94.

236. Miao Z, Luker KE, Summers BC, Berahovich R, Bhojani MS, Rehemtulla A et al. CXCR7 (RDC1) promotes breast and lung tumor growth in vivo and is expressed on tumor-associated vasculature. *Proceedings of the National Academy of Sciences of the United States of America* 2007;104:15735-40.

237. Payne AS, Cornelius LA. The role of chemokines in melanoma tumor growth and metastasis. *The Journal of investigative dermatology* 2002;118:915-22.

238. Peled A, Kollet O, Ponomaryov T, Petit I, Franitza S, Grabovsky V et al. The chemokine SDF-1 activates the integrins LFA-1, VLA-4, and VLA-5 on immature human CD34(+) cells: role in transendothelial/stromal migration and engraftment of NOD/SCID mice. *Blood* 2000;95:3289-96.

239. Hamel DJ, Sielaff I, Proudfoot AE, Handel TM. Chapter 4. Interactions of chemokines with glycosaminoglycans. *Methods Enzymol.* 2009;461:71-102.

240. Hoogewerf AJ, Kuschert GS, Proudfoot AE, Borlat F, Clark-Lewis I, Power CA et al. Glycosaminoglycans mediate cell surface oligomerization of chemokines. *Biochemistry* 1997;36:13570-8.

241. Netelenbos T, Van Den BJ, Kessler FL, Zweegman S, Merle PA, van Oostveen JW et al. Proteoglycans on bone marrow endothelial cells bind and present SDF-1 towards hematopoietic progenitor cells. *Leukemia : official journal of the Leukemia Society of America, Leukemia Research Fund, UK* 2003;17:175-84.

242. Netelenbos T, Zuijderduijn S, Van Den BJ, Kessler FL, Zweegman S, Huijgens PC et al. Proteoglycans guide SDF-1-induced migration of hematopoietic progenitor cells. *Journal of leukocyte biology* 2002;72:353-62.

243. Amara A, Lorthioir O, Valenzuela A, Magerus A, Thelen M, Montes M et al. Stromal cell-derived factor-1alpha associates with heparan sulfates through the first beta-strand of the chemokine. *The Journal of biological chemistry* 1999;274:23916-25.

244. Laguri C, renzana-Seisdedos F, Lortat-Jacob H. Relationships between glycosaminoglycan and receptor binding sites in chemokines-the CXCL12 example. *Carbohydr.Res* 2008;343:2018-23.

245. Sadir R, Imberty A, Baleux F, Lortat-Jacob H. Heparan sulfate/heparin oligosaccharides protect stromal cell-derived factor-1 (SDF-1)/CXCL12 against proteolysis induced by CD26/dipeptidyl peptidase IV. *The Journal of biological chemistry* 2004;279:43854-60.

246. Lambeir AM, Proost P, Durinx C, Bal G, Senten K, Augustyns K et al. Kinetic investigation of chemokine truncation by CD26/dipeptidyl peptidase IV reveals a striking selectivity within the chemokine family. *The Journal of biological chemistry* 2001;276:29839-45.

247. Sadir R. Heparan Sulfate/Heparin Oligosaccharides Protect Stromal Cell-derived Factor-1 (SDF-1)/CXCL12 against Proteolysis Induced by CD26/Dipeptidyl Peptidase IV. *Journal of Biological Chemistry* 2004;279:43854-60.

248. Yao L, Salvucci O, Cardones AR, Hwang ST, Aoki Y, De La Luz SM et al. Selective expression of stromal-derived factor-1 in the capillary vascular endothelium plays a role in Kaposi sarcoma pathogenesis. *Blood* 2003;102:3900-5.

249. Gassmann P, Haier J, Schluter K, Domikowsky B, Wendel C, Wiesner U et al. CXCR4 regulates the early extravasation of metastatic tumor cells in vivo. *Neoplasia.* 2009;11:651-61.

250. Smith MC, Luker KE, Garbow JR, Prior JL, Jackson E, Piwnica-Worms D et al. CXCR4 regulates growth of both primary and metastatic breast cancer. *Cancer research* 2004;64:8604-12.

251. Arenberg DA, Polverini PJ, Kunkel SL, Shanafelt A, Hesselgesser J, Horuk R et al. The role of CXC chemokines in the regulation of angiogenesis in non-small cell lung cancer. *Journal of leukocyte biology* 1997;62:554-62.

252. Scotton CJ, Wilson JL, Scott K, Stamp G, Wilbanks GD, Fricker S et al. Multiple actions of the chemokine CXCL12 on epithelial tumor cells in human ovarian cancer. *Cancer research* 2002;62:5930-8.

253. Geminder H, Sagi-Assif O, Goldberg L, Meshel T, Rechavi G, Witz IP et al. A possible role for CXCR4 and its ligand, the CXC chemokine stromal cell-derived factor-1, in the development of bone marrow metastases in neuroblastoma. *Journal of immunology (Baltimore, Md : 1950)* 2001;167:4747-57.

254. Gross N, Meier R. Chemokines in neuroectodermal cancers: the crucial growth signal from the soil. *Seminars in cancer biology* 2009;19:103-10.

255. Ribatti D, Mangialardi G, Vacca A. Stephen Paget and the 'seed and soil' theory of metastatic dissemination. *Clinical and experimental medicine* 2006;6:145-9.

256. Schioppa T, Uranchimeg B, Saccani A, Biswas SK, Doni A, Rapisarda A et al. Regulation of the chemokine receptor CXCR4 by hypoxia. *The Journal of experimental medicine* 2003;198:1391-402.

257. Schutyser E, Su Y, Yu Y, Gouwy M, Zaja-Milatovic S, Van DJ et al. Hypoxia enhances CXCR4 expression in human microvascular endothelial cells and human melanoma cells. *Eur Cytokine Netw.* 2007;18:59-70.

258. Staller P, Sulitkova J, Lisztwan J, Moch H, Oakeley EJ, Krek W. Chemokine receptor CXCR4 downregulated by von Hippel-Lindau tumour suppressor pVHL. *Nature* 2003;425:307-11.

259. Gelmini S, Mangoni M, Castiglione F, Beltrami C, Pieralli A, Andersson KL et al. The CXCR4/CXCL12 axis in endometrial cancer. *Clinical & experimental metastasis* 2009;26:261-8.

260. Burns J, Summers B, Wang Y, Melikian A, Berahovich R, Miao Z et al. A novel chemokine receptor for SDF-1 and I-TAC involved in cell survival, cell adhesion, and tumor development. *Journal of Experimental Medicine* 2006;203:2201.

261. Balabanian K, Lagane B, Infantino S, Chow KY, Harriague J, Moepps B et al. The chemokine SDF-1/CXCL12 binds to and signals through the orphan receptor RDC1 in T lymphocytes. *The Journal of biological chemistry* 2005;280:35760-6.

262. Levoye A, Balabanian K, Baleux F, Bachelerie F, Lagane B. CXCR7 heterodimerizes with CXCR4 and regulates CXCL12-mediated G protein signaling. *Blood* 2009;113:6085-93.

263. Sierro F, Biben C, Martinez-Munoz L, Mellado M, Ransohoff RM, Li M et al. Disrupted cardiac development but normal hematopoiesis in mice deficient in the second CXCL12/SDF-1 receptor, CXCR7. *Proc Natl Acad Sci U.S.A* 2007;104:14759-64.

264. Hager B, Bickenbach JR, Fleckman P. Long-term culture of murine epidermal keratinocytes. *The Journal of investigative dermatology* 1999;112:971-6.

265. Carson-Walter E, Watkins D, Nanda A, Vogelstein B, Kinzler K, Croix B. Cell Surface Tumor Endothelial Markers Are Conserved in Mice and Humans 1. *Cancer research* 2001;61:6649-55.

266. Min CJ, Tafra L, Verbanac KM. Identification of superior markers for polymerase chain reaction detection of breast cancer metastases in sentinel lymph nodes. *Cancer research* 1998;58:4581-4.

267. Strauss WM. Preparation of genomic DNA from mammalian tissue. *Curr Protoc.Mol Biol* 2001;Chapter 2:Unit2.

268. Leggate J, Allain R, Isaac L, Blais BW. Microplate fluorescence assay for the quantification of double stranded DNA using SYBR Green I dye. *Biotechnol Lett* 2006;28:1587-94.

269. Joshi M, Keith Pittman H, Haisch C, Verbanac K. Real-time PCR to determine transgene copy number and to quantitate the biolocalization of adoptively-transferred cells from EGFP-transgenic mice. *BioTechniques* 2008;45:247-58.

270. Nakanishi T, Kuroiwa A, Yamada S, Isotani A, Yamashita A, Tairaka A et al. FISH analysis of 142 EGFP transgene integration sites into the mouse genome. *Genomics* 2002;80:564-74.

271. Storey BT, Pittman HK, Christian JF, Haisch CE, Verbanac KM. Characterization of Lewis lung clonal variants in a model of syngeneic pulmonary murine metastases. *Clinical & experimental metastasis* 2004;21:265-73.

272. Fricker SP, Anastassov V, Cox J, Darkes MC, Grujic O, Idzan SR et al. Characterization of the molecular pharmacology of AMD3100: a specific antagonist of the G-protein coupled chemokine receptor, CXCR4. *Biochemical pharmacology* 2006;72:588-96.

273. Rosenkilde MM, Gerlach LO, Jakobsen JS, Skerlj RT, Bridger GJ, Schwartz TW. Molecular mechanism of AMD3100 antagonism in the CXCR4 receptor: transfer of binding site to the CXCR3 receptor. *The Journal of biological chemistry* 2004;279:3033-41.

274. Gupta SK, Pillarisetti K, Thomas RA, Aiyar N. Pharmacological evidence for complex and multiple site interaction of CXCR4 with SDF-1alpha: implications for development of selective CXCR4 antagonists. *Immunol Lett* 2001;78:29-34.

275. Zou KH, Tuncali K, Silverman SG. Correlation and simple linear regression. *Radiology* 2003;227:617-22.

276. Ohizumi Y, Maezawa H, Mori T. Relationship between primary tumor volume and lung metastasis in Lewis lung carcinoma (1). Assay for time course of development of metastasis. *Tokai J Exp Clin Med* 1987;12:229-35.

277. Ohizumi Y, Maezawa H, Mori T. Relationship between primary tumor volume and lung metastasis in Lewis lung carcinoma (II). Tumor bed effect. *Tokai J Exp Clin Med* 1987;12:237-42.

278. Kryczek I, Wei S, Keller E, Liu R, Zou W. Stroma-derived factor (SDF-1/CXCL12) and human tumor pathogenesis. *American journal of physiology Cell physiology* 2007;292:C987-C995.

279. Rempel SA, Dudas S, Ge S, Gutierrez JA. Identification and localization of the cytokine SDF1 and its receptor, CXC chemokine receptor 4, to regions of necrosis and angiogenesis in human glioblastoma. *Clinical cancer research : an official journal of the American Association for Cancer Research* 2000;6:102-11.

280. Akishima-Fukasawa Y, Nakanishi Y, Ino Y, Moriya Y, Kanai Y, and Hirohashi S. Prognostic significance of CXCL12 expression in patients with colorectal carcinoma. Am J Clin Pathol. 132(2), 202-210. 2010.
Ref Type: Abstract

281. Nomura R, Yoshida D, Teramoto A. Stromal cell-derived factor-1 expression in pituitary adenoma tissues and upregulation in hypoxia. *Journal of neuro-oncology* 2009;94:173-81.

282. Nakayama T, Mutsuga N, Tosato G. FGF2 posttranscriptionally down-regulates expression of SDF1 in bone marrow stromal cells through FGFR1 IIIc. *Blood* 2007;109:1363-72.

283. Havre PA, Abe M, Urasaki Y, Ohnuma K, Morimoto C, Dang NH. The role of CD26/dipeptidyl peptidase IV in cancer. *Front Biosci.* 2008;13:1634-45.

284. Pro B, Dang NH. CD26/dipeptidyl peptidase IV and its role in cancer. *Histol.Histopathol.* 2004;19:1345-51.

285. Ghersi G, Zhao Q, Salamone M, Yeh Y, Zucker S, Chen WT. The protease complex consisting of dipeptidyl peptidase IV and seprase plays a role in the migration and invasion of human endothelial cells in collagenous matrices. *Cancer research* 2006;66:4652-61.

286. Wesley UV, Albino AP, Tiwari S, Houghton AN. A role for dipeptidyl peptidase IV in suppressing the malignant phenotype of melanocytic cells. *The Journal of experimental medicine* 1999;190:311-22.

287. Gonzalez-Gronow M, Hershfield MS, rredondo-Vega FX, Pizzo SV. Cell surface adenosine deaminase binds and stimulates plasminogen activation on 1-LN human prostate cancer cells. *The Journal of biological chemistry* 2004;279:20993-8.

288. Kehlen A, Lendeckel U, Dralle H, Langner J, Hoang-Vu C. Biological significance of aminopeptidase N/CD13 in thyroid carcinomas. *Cancer research* 2003;63:8500-6.

289. Bonfil RD, Medina PA, Gomez DE, Farias E, Lazarowski A, Lucero Gritti MF et al. Expression of gelatinase/type IV collagenase in tumor necrosis correlates with cell detachment and tumor invasion. *Clinical & experimental metastasis* 1992;10:211-20.

290. Kojima K, Mihara R, Sakai T, Togari A, Matsui T, Shinpo K et al. Serum activities of dipeptidyl-aminopeptidase II and dipeptidyl-aminopeptidase IV in tumor-bearing animals and in cancer patients. *Biochem Med Metab Biol* 1987;37:35-41.

291. McQuibban GA, Butler GS, Gong JH, Bendall L, Power C, Clark-Lewis I et al. Matrix metalloproteinase activity inactivates the CXC chemokine stromal cell-derived factor-1. *The Journal of biological chemistry* 2001;276:43503-8.

292. Eck SM, Blackburn JS, Schmucker AC, Burrage PS, Brinckerhoff CE. Matrix metalloproteinase and G protein coupled receptors: co-conspirators in the pathogenesis of autoimmune disease and cancer. *J Autoimmun.* 2009;33:214-21.

293. Heissig B, Hattori K, Dias S, Friedrich M, Ferris B, Hackett N et al. Recruitment of stem and progenitor cells from the bone marrow niche requires MMP-9 mediated release of kit-ligand. *Cell* 2002;109:625-37.

294. Spiegel A, Zcharia E, Vagima Y, Itkin T, Kalinkovich A, Dar A et al. Heparanase regulates retention and proliferation of primitive Sca-1+/c-Kit+/Lin- cells via modulation of the bone marrow microenvironment. *Blood* 2008;111:4934-43.

295. Bleul CC, Fuhlbrigge RC, Casasnovas JM, Aiuti A, Springer TA. A highly efficacious lymphocyte chemoattractant, stromal cell-derived factor 1 (SDF-1). *The Journal of experimental medicine* 1996;184:1101-9.

296. Aiuti A, Webb IJ, Bleul C, Springer T, Gutierrez-Ramos JC. The chemokine SDF-1 is a chemoattractant for human CD34+ hematopoietic progenitor cells and provides a new mechanism to explain the mobilization of CD34+ progenitors to peripheral blood. *The Journal of experimental medicine* 1997;185:111-20.

297. Mirisola V, Zuccarino A, Bachmeier BE, Sormani MP, Falter J, Nerlich A et al. CXCL12/SDF1 expression by breast cancers is an independent prognostic marker of disease-free and overall survival. *Eur J Cancer* 2009;45:2579-87.

298. kishima-Fukasawa Y, Nakanishi Y, Ino Y, Moriya Y, Kanai Y, Hirohashi S. Prognostic significance of CXCL12 expression in patients with colorectal carcinoma. *Am J Clin Pathol* 2009;132:202-10.

299. Wagner PL, Hyjek E, Vazquez MF, Meherally D, Liu YF, Chadwick PA et al. CXCL12 and CXCR4 in adenocarcinoma of the lung: association with metastasis and survival. *J Thorac.Cardiovasc Surg* 2009;137:615-21.

300. Suzuki M, Mohamed S, Nakajima T, Kubo R, Tian L, Fujiwara T et al. Aberrant methylation of CXCL12 in non-small cell lung cancer is associated with an unfavorable prognosis. *Int J Oncol* 2008;33:113-9.

301. Ishigami S, Natsugoe S, Okumura H, Matsumoto M, Nakajo A, Uenosono Y et al. Clinical implication of CXCL12 expression in gastric cancer. *Ann.Surg Oncol* 2007;14:3154-8.

302. Tate MC, Aghi MK. Biology of angiogenesis and invasion in glioma. *Neurotherapeutics.* 2009;6:447-57.

303. Sauve K, Lepage J, Sanchez M, Heveker N, Tremblay A. Positive feedback activation of estrogen receptors by the CXCL12-CXCR4 pathway. *Cancer Res.* 2009;69:5793-800.

304. Xie Y, Yin T, Wiegraebe W, He XC, Miller D, Stark D et al. Detection of functional haematopoietic stem cell niche using real-time imaging. *Nature* 2009;457:97-101.

305. Boron WF, Boulpaep EL. *Medical Physiology: A Cellular and Molecular Approach*. Elsevier/Saunders, 2005.

306. Eaton DC, Pooler JP. *Vander's Renal Physiology* (8th edition ed.). Lange Medical Books/McGraw-Hill, 2004.

307. Peleraux A, Eliason JF. Proliferation of single hemopoietic progenitor cells in the absence of colony-stimulating factors and serum. *Experimental hematology* 1989;17:1032-7.

308. Hoyer M, Nielsen OS. Influence of dose on regeneration of murine hematopoietic stem cells after total body irradiation and 5-fluorouracil. *Oncology* 1992;49:166-72.

309. Cheshier SH, Morrison SJ, Liao X, Weissman IL. In vivo proliferation and cell cycle kinetics of long-term self-renewing hematopoietic stem cells. *Proc Natl Acad Sci U.S.A* 1999;96:3120-5.

CHAPTER VII: APPENDIX: ANIMAL USE APPROVAL LETTERS

EAST CAROLINA UNIVERSITY

Animal Care and Use Committee
East Carolina University
212 Ed Warren Life Sciences Building
Greenville, NC 27834
252-744-2436 office • 252-744-2355 fax

November 13, 2007

Kathryn Verbanac, Ph.D.
Department of Surgery
Brody 4S-10
ECU Brody School of Medicine

Dear Dr. Verbanac:

Your Animal Use Protocol entitled, "Mice as Bone Marrow Cell Donors," (AUP #T233) was reviewed by this institution's Animal Care and Use Committee on 11/13/07. The following action was taken by the Committee:

"Approved as submitted"

A copy is enclosed for your laboratory files. Please be reminded that all animal procedures must be conducted as described in the approved Animal Use Protocol. Modifications of these procedures cannot be performed without prior approval of the ACUC. The Animal Welfare Act and Public Health Service Guidelines require the ACUC to suspend activities not in accordance with approved procedures and report such activities to the responsible University Official (Vice Chancellor for Health Sciences or Vice Chancellor for Academic Affairs) and appropriate federal Agencies.

Sincerely yours,

Robert G. Carroll, Ph.D.
Chairman, Animal Care and Use Committee

RGC/jd

enclosure

EAST CAROLINA UNIVERSITY

Animal Care and Use Committee
East Carolina University
212 Ed Warren Life Sciences Building
Greenville, NC 27834
252-744-2436 office • 252-744-2355 fax

October 3, 2007

Kathryn Verbanac, Ph.D.
Department of Surgery
Brody 4S-10
ECU Brody School of Medicine

Dear Dr. Verbanac:

Your Animal Use Protocol entitled, "Migration of Endothelial Cells and Progenitors to Murine Tumors," (AUP #T219a) was reviewed by this institution's Animal Care and Use Committee on October 3, 2007. The following action was taken by the Committee:

"Approved as submitted"

****Note: Please contact EH&S to perform testing to verify safety of isoflurane via benchtop method. Please notify us of results when testing has been completed.****

A copy is enclosed for your laboratory files. Please be reminded that all animal procedures must be conducted as described in the approved Animal Use Protocol. Modifications of these procedures cannot be performed without prior approval of the ACUC. The Animal Welfare Act and Public Health Service Guidelines require the ACUC to suspend activities not in accordance with approved procedures and report such activities to the responsible University Official (Vice Chancellor for Health Sciences or Vice Chancellor for Academic Affairs) and appropriate federal Agencies.

Sincerely yours,

Robert G Carroll, Ph.D

Robert G. Carroll, Ph.D.
Chairman, Animal Care and Use Committee

RGC/jd

enclosure

EAST CAROLINA UNIVERSITY

Animal Care and Use Committee
East Carolina University
212 Ed Warren Life Sciences Building
Greenville, NC 27834
252-744-2436 office • 252-744-2355 fax

October 8, 2007

Kathryn Verbanac, Ph.D.
Department of Surgery
Brody 4S-10
ECU Brody School of Medicine

Dear Dr. Verbanac:

Your Animal Use Protocol entitled, "Isolation of the Vascular Endothelial Cell," (AUP #T141d) was reviewed by this institution's Animal Care and Use Committee on October 8, 2007. The following action was taken by the Committee:

"Approved as submitted"

A copy is enclosed for your laboratory files. Please be reminded that all animal procedures must be conducted as described in the approved Animal Use Protocol. Modifications of these procedures cannot be performed without prior approval of the ACUC. The Animal Welfare Act and Public Health Service Guidelines require the ACUC to suspend activities not in accordance with approved procedures and report such activities to the responsible University Official (Vice Chancellor for Health Sciences or Vice Chancellor for Academic Affairs) and appropriate federal Agencies.

Sincerely yours,

Robert G. Carroll, Ph.D.
Chairman, Animal Care and Use Committee

RGC/jd

enclosure

East Carolina University

Animal Care and Use Commitee
212 Ed Warren Life Sciences Building
East Carolina University
Greenville, NC 27834

252-744-2436 office
252-744-2355 fax

June 16, 2010

Kathryn Verbanac, Ph.D.
Department of Surgery
Brody 4S-10
ECU Brody School of Medicine

Dear Dr. Verbanac:

The Amendment to your Animal Use Protocol entitled, "Migration of Endothelial Cells and Progenitors to Murine Tumors", (AUP #T219a) was reviewed by this institution's Animal Care and Use Committee on 6/16/10. The following action was taken by the Committee:

"Approved as amended"

A copy of the Amendment is enclosed for your laboratory files. Please be reminded that all animal procedures must be conducted as described in the approved Animal Use Protocol. Modifications of these procedures cannot be performed without prior approval of the ACUC. The Animal Welfare Act and Public Health Service Guidelines require the ACUC to suspend activities not in accordance with approved procedures and report such activities to the responsible University Official (Vice Chancellor for Health Sciences or Vice Chancellor for Academic Affairs) and appropriate federal Agencies.

Sincerely yours,

Robert G. Carroll, Ph.D.
Chairman, Animal Care and Use Committee

RGC/jd

enclosure

APPENDIX: PERMISSION LETTER FROM BIOTECHNIQUES®

BioTechniques
Informa Healthcare
52 Vanderbilt Avenue
New York, NY 10017

Date: May 18, 2009

Dear Mallikarjun Joshi,

In response to your request of May 7, 2009, we are pleased to grant you permission to reproduce the following Material.

Verbanac et al.,"Real Time PCR to Determine Transgene Copy Number and to Quantitate the Biolocalization of Adoptively-transferred Cells from EGFP-Transgenic Mice" *BioTechniques* 45 (3), p 247-55, data and supplementary protocol to be reproduced in:

Publication: doctoral dissertation at East Carolina University
Publisher:
Publication Date: August 2009
Region: World/North America/ Europe
Language: English
Format: Print and Electronic

This permission is subject to the following conditions:

1. Permission is granted as a one-time, non-exclusive, non-transferable license, and refers only to original Material owned or controlled by Informa Healthcare or Eaton Associates.
2. The Work will fully cite the article to which the Material originally appeared.
3. The Work will include a copyright notice of the form "© 2008 BioTechniques. Used by Permission."
4. BioTechniques and Informa Healthcare may request and receive one copy of the published Work free of charge.

Yours Sincerely,

Natalie Goode
Editorial Assistant